

# **Lubricant Transport by Misting and the Link to Degradation in the Piston Assembly of Fired Engines**

Christopher James Dyson

MEng (Hons)

Submitted in accordance with the requirements of the degree of:  
Doctor of Philosophy

The University of Leeds  
Institute of Engineering Thermofluids, Surfaces and Interfaces  
School of Mechanical Engineering

August 2011



The candidate confirms that the work submitted is his own and that appropriate credit has been given where reference has been made to the work of others.

This copy has been supplied on the understanding that it is copyright material and that no quotation from the thesis may be published without proper acknowledgement.

© 2011 The University of Leeds and Christopher James Dyson.





## **Abstract**

The presence of lubricant mist in the piston assembly of an automotive engine has been known of for many years, but has not been specifically investigated. This study, therefore, focuses on understanding the lubricant misting process and its effect on the engine in terms of lubricant degradation. Informed by existing literature, it was hypothesised that mist is formed in the piston ring gaps. A laboratory rig was designed and built to simulate this environment, producing and measuring representative mist flows. Using this rig, the contribution of the components of a commercial lubricant to its misting properties was studied. Base oil viscosity and molecular weight, and the presence of polymeric viscosity modifiers were identified as being the key parameters controlling the tendency of an oil to form mist. Further investigation using viscosity modifiers of varying size and molecular structure was performed, indicating differences between the behaviour of linear and star polymers.

Measurements of the droplet flows in the crankcase of an engine were made using a particle sizer. These confirmed the dependency of misting properties on viscosity, and validated the hypothesis that lubricant mist in the crankcase is formed in the piston assembly by a similar mechanism to that produced in the laboratory rig. Longer engine tests were used to investigate the effect of lubricants with varying misting tendency on lubricant degradation. A range of chemical and rheological analyses were performed to compare fresh and used lubricant samples in different flows and positions in the engine. These tests were not able to differentiate between the degradation of the different lubricants tested, though the degradation of lubricant in different positions in the engine varied significantly. It was shown that lubricant mist is formed in the piston assembly and that lubricant misting is a significant lubricant transport mechanism.



## Acknowledgements

Thanks to Professor Martin Priest and Dr Peter Lee for their supervision, wisdom, guidance and patience. Thanks too for giving me this opportunity in the first place.

Thanks to BP for funding this project. Thanks to all who have supported and guided it from Pangbourne: Dr Kevin West, Gareth Dowd and Dr Ammer Jadoon. Thanks to Sam Whitmarsh for his time and effort doing chemical analysis.

Thanks to all those at the University of Leeds who have given ideas, encouraged, asked tricky questions, shown me how to use the lab, and been good friends and travel companions. In particular: Professor Dick Coy, Prashan De Silva, Dr Richard Chittenden, Rai Singh Notay, Dr Rupesh Roshan.

Thanks to the technical staff in the School of Mechanical Engineering for their help and expertise: Paul Banks, Ron Cellier, John Groves, Brian Leach and Mark Batchelor.

Thanks to the EPSRC Loan Pool for the use of the Malvern Spraytec and their support of this equipment.

Thanks to my family for their love, encouragement, support and example: Mum, Dad, Helen, Grandpa, Grandma.

Thanks to my friends who have been an encouragement and support through all this.

Thanks to God who has kept everything together by his grace.

...I am grateful to all of you. I would not have been able to do any of this without you. Thank you.



## Contents

Abstract.....	v
Acknowledgements.....	vii
Contents .....	ix
List of Figures .....	xiv
List of Tables .....	xxi
Abbreviations.....	xxii
Chapter 1: Introduction.....	1
1.1 Introduction .....	1
1.2 The Piston Assembly.....	3
1.3 Piston Assembly Tribology.....	5
1.3.1 Piston Assembly.....	5
1.3.2 Lubricant Transport Mechanisms .....	7
1.3.3 Lubricant Misting.....	8
1.4 Outline of the Study .....	9
Chapter 2: Piston Assembly Tribology and Lubricant Chemistry.....	10
2.1 Introduction .....	10
2.2 Blow-By .....	10
2.3 Modelling .....	16
2.3.1 Variation with Temperature and Pressure.....	21
2.3.2 Piston Assembly Models.....	22
2.4 Friction and Power Loss.....	24
2.4.1 Other Oil Transport Mechanisms.....	25
2.5 Oil Consumption .....	32
2.6 Automotive Lubricant Formulation .....	33
2.6.1 Base Oil.....	33
2.6.2 Mineral Oil.....	33
2.6.3 Synthetic Oil .....	34
2.6.4 Base Oil Classification.....	34
2.6.5 Tribofilm-Forming Lubricant Additives.....	36

2.6.6	Surface-Active Lubricant Additives .....	37
2.6.7	Detergent.....	37
2.6.8	Dispersant .....	38
2.6.9	Anti-Foam.....	39
2.7	Viscosity Modifier or Viscosity Index Improvers.....	39
2.7.1	Linear Chain Polymers .....	41
2.7.2	Star Polymers .....	44
2.7.3	Polymer Degradation .....	45
2.8	Lubricant Degradation.....	47
2.8.1	Thermal Degradation .....	47
2.8.2	Evaporation Loss .....	49
2.8.3	Additive Depletion.....	49
2.8.4	Low Temperature Oxidation.....	49
2.8.5	High Temperature Oxidation .....	51
2.8.6	Anti-Oxidant .....	52
2.8.7	Nitration .....	53
2.8.8	Fuel Dilution .....	53
2.8.9	Particulates and Sludge .....	53
2.9	Summary .....	54
<b>Chapter 3: Review of Relevant Studies on Two Phase Flow and Hydrocarbon</b>		
<b>Misting 55</b>		
3.1	Introduction .....	55
3.2	Two Phase Flow .....	55
3.2.1	Classification.....	55
3.3	Annular Mist Flow .....	56
3.3.1	Film Behaviour .....	56
3.3.2	Droplet Behaviour.....	58
3.3.3	Droplet Coalescence and Destruction.....	60
3.3.4	Droplet Formation.....	62
3.3.5	Droplet Formation from a Surface Film .....	62
3.3.6	Droplet Formation by Inertia .....	64
3.4	Industrial Droplet Formation.....	65

3.5	Hydrocarbon Mists .....	68
3.5.1	Oil Mist Lubrication .....	68
3.5.2	Marine Crankcase Mists .....	70
3.5.3	Metalworking Fluids .....	71
3.6	The Effect of Polymers on Misting .....	73
3.7	Polymer Rheology .....	74
3.7.1	Viscoelasticity .....	77
3.7.2	Molecular Dynamics of Polymers .....	82
3.8	Summary .....	87
Chapter 4: Simulation of Misting in the Piston Ring Gap and Considering the		
Components of a Commercial Lubricant .....		
4.1	Introduction .....	89
4.2	Mist Generator .....	89
4.3	Measurement .....	96
4.3.1	Droplet Size Distribution .....	96
4.3.2	Oil to Air Ratio and Other Flow Rate Data .....	101
4.4	Parametric Testing .....	103
4.5	Test Matrix .....	108
4.6	Results .....	109
4.7	Statistical Analysis .....	117
4.7.1	Principal Component Analysis .....	117
4.7.2	Outcomes .....	120
4.8	Summary .....	123
Chapter 5: Simulation of Misting in the Piston Ring Gap and Considering the		
Effects of Viscosity Modifying Polymers .....		
5.1	Introduction .....	125
5.2	Method .....	125
5.3	Polymer Molecular Weight Characterisation .....	125
5.4	Oil Matrix .....	129
5.5	Rheological Testing .....	133
5.6	Results .....	136
5.6.1	Rheological Analysis .....	136

5.6.2	Misting Tendency .....	141
5.7	Summary .....	154
Chapter 6:	Measurement of the Lubricant Mist Formed in a Fired Engine.....	155
6.1	Introduction .....	155
6.2	Method .....	156
6.2.1	Engine .....	156
6.2.2	Mist Extraction and Measurement .....	157
6.2.3	Procedure .....	160
6.3	Test Matrix .....	162
6.4	Simulation .....	163
6.5	Results .....	164
6.6	Statistical Analysis .....	171
6.7	Summary .....	181
Chapter 7:	Measurement of Lubricant Degradation in a Fired Engine with Varying Viscosity Modifier Structure.....	183
7.1	Introduction .....	183
7.2	Method .....	183
7.2.1	Apparatus .....	183
7.2.2	Procedure .....	188
7.3	Chemical and Physical Analysis .....	190
7.3.1	Chemical Degradation .....	190
7.3.2	Fuel Dilution .....	193
7.3.3	Polymer Degradation .....	194
7.4	Oil Matrix .....	195
7.5	Results .....	197
7.5.1	FTIR Analysis .....	198
7.5.2	Fuel Dilution .....	202
7.5.3	Polymer Degradation .....	204
7.5.4	Rheological Analysis .....	208
7.6	Polymer Concentration Change .....	211
7.7	Summary .....	215
Chapter 8:	Conclusions.....	217



8.1	Introduction .....	217
8.2	Review of Relevant Studies on Two Phase Flow and Hydrocarbon Misting 218	
8.3	Simulation of Misting in the Piston Ring Gap .....	219
8.3.1	Considering the Components of a Commercial Lubricant .....	219
8.3.2	Considering the Effects of Viscosity Modifying Polymers .....	219
8.4	Measurement of the Lubricant Mist Formed in a Fired Engine .....	220
8.5	Measurement of Lubricant Degradation in a Fired Engine with Varying Viscosity Modifier Structure.....	221
8.6	Suggestions for Future Work .....	222
8.7	Recommendations for Future Research .....	223
Chapter 9:	References.....	225
Appendix 1:	.....	241

## List of Figures

Figure 1.1: The Progression of CO <sub>2</sub> Emission Regulations in Automobiles (Gunsel, 2009) .....	2
Figure 1.2: Engine Power Distribution and Friction Power Loss, after Tung (2004) ...	3
Figure 1.3: Engine Friction Power Loss Breakdown, after Mufti (2009).....	4
Figure 1.4: A Typical Automotive Three-Ring Piston Assembly .....	5
Figure 2.1: Orifice Model of Piston Assembly Gas Flow from Furuhama (1961).....	11
Figure 2.2: Piston Assembly Gas Flow Properties from Furuhama (1961); a) Gas Pressures, b) Gas Flow Rates. 0 = Combustion Chamber, 1 = Below Top Ring, 2 = Below 2nd Ring .....	12
Figure 2.3: Top Ring Axial Movement from Thirouard (1998) .....	13
Figure 2.4: Observation of Ring Collapse from Usui (2008) .....	14
Figure 2.5: Piston Ring Gap Phase (Nakashima et al., 1995): a) In Phase b) Out of Phase .....	15
Figure 2.6: Modelled Piston Ring Friction Force from Furuhama (1959) .....	16
Figure 2.7: LIF Film Thickness Trace of Piston Assembly, from Taylor (2004).....	18
Figure 2.8: Modelled a) Friction Force and b) Power Loss, Including EHL and Boundary Conditions, from Keribar (1991).....	19
Figure 2.9: Modelled Piston Ring Film Thickness with Lubricant Starvation, from Ma (1996).....	20
Figure 2.10: Generalised Geometry of Bore Distortion from Ma (1996).....	21
Figure 2.11: Modified Minimum Oil Film Thickness on the Thrust Side Including Ring Dynamics, from Tian (2002 II) .....	23
Figure 2.12: Piston Ring Running Face Profiles a) Barrel-Faced b) Napier .....	23
Figure 2.13: Measured Piston Assembly Friction using the IMEP Method, from Mufti (2005).....	25
Figure 2.14: Inertial Movement of Oil on Piston, from Thirouard (1998) .....	26
Figure 2.15: Oil Pumping from Ring Groove from Thirouard (2003 II).....	26
Figure 2.16: Oil Dragged Along the Piston Lands by Blow-By Gas, from Thirouard (2003 I).....	27

Figure 2.17: Relationship between Ring Gap Position and Oil Consumption, from Min (1998) .....	28
Figure 2.18: Entrainment of Droplets from a Film on a Surface .....	29
Figure 2.19: Formation of Droplets at Component Edge .....	29
Figure 2.20: Interaction between Blow-By Gas and Oil at Ring Gap, from Thirouard (1998).....	29
Figure 2.21: Particulate Emissions from the Crankcase of a Large Diesel Engine, ....	31
Figure 2.22: Schematic of a Tribofilm.....	37
Figure 2.23: Schematic of a Sludge and Dispersant Micelle .....	39
Figure 2.24: Temperature Response of Linear Viscosity Modifier Molecules .....	40
Figure 2.25: Repeating Units in Common Linear Viscosity Modifiers (Taylor, 1993) .....	41
Figure 2.26: Schematic Ordering of Copolymers .....	42
Figure 2.27: Extension Mechanisms of DNA, Representative of Long Chain Polymer Viscosity Modifiers (Nguyen et al., 1999).....	43
Figure 2.28: Extension of Star Polymers .....	44
Figure 2.29: FISST Rig for Measuring Shear Stability of Polymeric Fluids, ASTM 6278-07 (2010).....	46
Figure 2.30: Schematic of the Yasutomi Assumption, from Lee (2006).....	51
Figure 3.1: Classification of Two-Phase Flow Patterns (Ghiaasiaan, 2008) .....	56
Figure 3.2: Schematic of Annular Mist Flow in a T-Junction from Sliwicky (1988) ..	57
Figure 3.3: Droplet Bag Breakup, after Rotondi (2001).....	61
Figure 3.4: Droplet Breakup Mechanisms at Higher Weber Number a) Boundary Layer Stripping, b) Catastrophic Breakup, from Liu (1997) .....	61
Figure 3.5: Kelvin-Helmholtz Instabilities, from Hewitt (1970).....	63
Figure 3.6: Droplet Formation from a Surface Film, from Hewitt (1970) .....	63
Figure 3.7: Fuel Injector Spray, from Jakubik (2006) .....	65
Figure 3.8: A Typical Venturi Mist Generator, from Bloch (1987) .....	66
Figure 3.9: Typical Vortex Mist Generator, from Bloch (1987) .....	67
Figure 3.10: Coaxial Nozzle Mist Generator and Particle Sizer, from Smolinski (1996).....	67

Figure 3.11: Standard Apparatus for Measuring Misting Tendency of Oil Mist Lubricants, from ASTM D3705-86(09) (1986).....	69
Figure 3.12: Schematic of Obscurometer and Nephelometer Mist Detectors, after Smith (2005) .....	71
Figure 3.13: Effect of Polyisobutylene Concentration on Droplet Size from a Coaxial Mist Generator, from Gulari (1995).....	73
Figure 3.14: Key Rheological Parameters of Polymer-Containing Liquid.....	75
Figure 3.15: Shear Thinning Behaviour of an SAE 10W50 Oil at Various Temperatures (Harigaya et al., 2006) .....	76
Figure 3.16: Schematic of Phase Angle in Viscoelastic Flow .....	78
Figure 3.17: Fluid Ligaments in a Roll Mill: Non-Linear Viscoelastic Response to Shear, from Fernando (1988).....	80
Figure 3.18: CaBER-Type Extensional Rheometer, from Tuladhar (2008).....	81
Figure 3.19: Polymer Molecular Dynamic Models .....	82
Figure 3.20: Entanglement Molecular Weight for Overlapping Polymer Molecules..	83
Figure 3.21: Defining Polymer Solutions Relative to Critical Concentration, after Schulz (1991).....	85
Figure 3.22: Effect of Critical Concentration on Viscosity of HP-Guar Blends, from Schulz (1991).....	86
Figure 4.1: Venturi Mist Generator .....	93
Figure 4.2: Schematic of Compressed Air System .....	93
Figure 4.3: Schematic of Misting Apparatus .....	94
Figure 4.4: Misting Apparatus Layout.....	95
Figure 4.5: Measured Pressure Data in Venturi Mist Generator .....	95
Figure 4.6: Laser Diffraction Particle Sizer: Malvern Spraytec 2000 (Image from Malvern Instruments (2010)) .....	97
Figure 4.7: Principles of Mie Scattering and Laser Diffraction Particle Sizing. From Simmons (2001).....	98
Figure 4.8: Misting Tendency and Flow Rate Graph for Parametric Testing Incorporating Droplet Size Distributions for Fully Formulated Oil .....	104
Figure 4.9: Characteristic Droplet Sizes: Droplet Size Distribution of PAO 8 at 3ml/min.....	105

Figure 4.10: Mechanisms of Droplet Formation a) Rolling b) Undercutting, after (Hewitt et al., 1970) .....	106
Figure 4.11: Comparison of Mist Flow Rate Measurement Techniques .....	107
Figure 4.12: Misting Tendency and Flow Rate for PAOs of Known Molecular Weight .....	110
Figure 4.13: Misting Tendency versus Molecular Weight for PAOs at Inlet Flow Rate of 3ml/min.....	110
Figure 4.14: Dynamic Viscosity at 20°C versus Molecular Weight for PAOs.....	111
Figure 4.15: Misting Tendency versus Viscosity for PAOs at Inlet Flow Rate of 3ml/min .....	111
Figure 4.16: Droplet Size Distributions for PAOs at Inlet Flow Rate of 3ml/min ....	112
Figure 4.17: Misting Tendency of Different Oil Groups at Inlet Flow Rate of 3ml/min .....	113
Figure 4.18: Carbon Backbone Structure of Refined Hydrocarbons and Polyalphaolefins.....	114
Figure 4.19: Misting Tendency for 5W Group III Base Oil with Commercial Additives at Inlet Flow Rate 3ml/min.....	115
Figure 4.20: Droplet Size Distribution for 5W Group III Base Oil Containing Additives at Inlet Flow Rate of 3ml/min .....	115
Figure 5.1: Typical RI GPC Trace .....	127
Figure 5.2: Typical Light Scattering GPC Trace .....	128
Figure 5.3: Mark-Houwink Plot from GPC for Polymers 1-4.....	128
Figure 5.4: Mark-Houwink Plot from GPC Data for Polymers 5-7 .....	129
Figure 5.5: Schematic of Blends and Comparisons for Polymer Study .....	131
Figure 5.6: Graph of Linear Viscoelastic Region for 8cSt Blend of Polymer 1 .....	134
Figure 5.7: Graph of Crossover for 8cSt Blend of Polymer 1 .....	134
Figure 5.8: Misting Tendency Graph for Polymer 1, Olefin Copolymer .....	141
Figure 5.9: Droplet Size Distributions for Polymer 1 at 3ml/min Oil Inlet Flow Rate .....	142
Figure 5.10: Misting Tendency Graph for Polymer 2, Olefin Copolymer .....	143
Figure 5.11: Droplet Size Distributions for Polymer 2 at 3ml/min Oil Inlet Flow Rate .....	144

Figure 5.12: Misting Tendency Graph for Polymer 3, Low Molecular Weight Olefin Copolymer.....	144
Figure 5.13: Droplet Size Distribution for Polymer 3 at 3ml/min Oil Inlet Flow Rate .....	145
Figure 5.14: Misting Tendency Graph for Polymer 4, Styrene-Butadiene.....	146
Figure 5.15: Droplet Size Distribution for Polymer 4 at 3ml/min Oil Inlet Flow Rate .....	146
Figure 5.16: Misting Tendency Graph for Polymer 5, Isoprene-co-Styrene Star.....	147
Figure 5.17: Droplet Size Distribution for Polymer 5 at 3ml/min Oil Inlet Flow Rate .....	148
Figure 5.18: Misting Tendency Graph for Polymer 6, Micellar-Type Isoprene-co-Styrene Star.....	149
Figure 5.19: Droplet Size Distribution for Polymer 6 at 3ml/min Oil Inlet Flow Rate .....	149
Figure 5.20: Misting Tendency Graph for Polymer 7, Isoprene Star .....	151
Figure 5.21: Droplet Size Distributions for Polymer 7 at 3ml/min Oil Inlet Flow Rate .....	151
Figure 6.1: Ricardo Hydra Engine Setup.....	155
Figure 6.2: Pressure Tapping on Crankcase .....	155
Figure 6.3: Schematic of Engine Misting Apparatus.....	157
Figure 6.4: Intersection of Particle Sizer Beam and Gas Flow.....	159
Figure 6.5: Blow-By Flow Rate for Ricardo Hydra at 50% Throttle .....	160
Figure 6.6: Comparison of Test Recording Time for Obscuration.....	161
Figure 6.7: Simulation Results for Misting Tendency of Engine Test Oils.....	163
Figure 6.8: Droplet Size Distributions for Oils Tested at 4500rpm and 33% Load ..	165
Figure 6.9: Characteristic Regions of Misting Behaviour – Example is SAE 20 + 10% Viscosity Modifier at 4500rpm and 33% Load.....	166
Figure 6.10: Flow Rate of Oil from Piston Assembly under Varying Engine Conditions.....	167
Figure 6.11: Droplet Size Distributions for Base Oils at Various Engine Conditions .....	169

Figure 6.12: Droplet Size Distributions for Oils with Polymer at Various Engine Conditions .....	170
Figure 6.13: Variation of the Diameter-Weighted Droplet Diameter of Mist with Viscosity .....	177
Figure 6.14: Variation of the Diameter-Weighted Droplet Diameter of the Minor Misting Region with Viscosity .....	177
Figure 6.15: Score Plot of Principal Components 1 and 2, by Oil .....	178
Figure 6.16: Score Plot of Principal Components 1 and 2, by Engine Condition .....	178
Figure 6.17: Score Plot of Principal Components 2 and 3, by Oil .....	179
Figure 6.18: Score Plot of Principal Components 2 and 3, by Engine Condition .....	179
Figure 7.1: Sample Locations in the Ricardo Hydra Engine .....	184
Figure 7.2: Top Ring Zone Sampling System .....	184
Figure 7.3: Sample Bottle, after Notay (2009) .....	184
Figure 7.5: Mist Sampling System Inlet .....	186
Figure 7.4: Crankcase Mist Sampling System .....	186
Figure 7.7: Aerosol Sample Bottle .....	187
Figure 7.6: Aerosol Sampling System .....	187
Figure 7.8: Engine Test Procedure and Sample Intervals .....	188
Figure 7.9: Schematic of ATR Element, from Gunzler (2002), $n_1$ and $n_2$ are the refractive indices, $n_1 > n_2$ , $d_p$ is the penetration depth, $\theta$ is the angle of incidence ...	191
Figure 7.10: Schematic of Hydrocarbon Oxidation Leading to Carbonyl Formation, after Emanuel (1997) and Gamble (2002) .....	192
Figure 7.11: FTIR Peak Area Schematic .....	193
Figure 7.12: FTIR Carbonyl Peak Areas for Engine Test Samples .....	198
Figure 7.13: FTIR Trace for Base Oils after 20 Hours, where the Absorbance Axis is scaled to make the Largest Peaks Equal in Magnitude .....	199
Figure 7.14: FTIR Nitration and Unsaturation Peak Areas for Engine Test Samples .....	200
Figure 7.15: GC Fuel Dilution Concentrations for Engine Test Samples .....	202
Figure 7.16: GPC Trace for Fresh Polymer Blends .....	204
Figure 7.17: TRZ Samples of Polymer 1 by GPC .....	204
Figure 7.18: Mist Samples of Polymer 1 by GPC .....	205

Figure 7.19: Sump Samples of Polymer 1 by GPC .....	205
Figure 7.20: RI GPC Trace of Polymer 1 Engine Test Samples .....	206
Figure 7.21: TRZ Samples for Polymer 5 by GPC.....	207
Figure 7.22: Mist Samples for Polymer by GPC .....	207
Figure 7.23: Sump Samples for Polymer 5 by GPC .....	207
Figure 7.24: RI GPC Trace for Polymer 5 Engine Test Samples .....	208
Figure 7.25: Crossover Data for Fresh Polymer 1 Blend.....	209
Figure 7.26: Crossover Data for Used Polymer 1 Blend .....	209
Figure 7.27: Crossover Data for Fresh Polymer 5 Blend.....	210
Figure 7.28: Crossover Data for Used Polymer 5 Blend .....	210
Figure 7.29: Simulator Mist Sampling Apparatus .....	212
Figure 7.30: RI Trace of Polymer 1 Blend .....	214
Figure 7.31: RI Trace of Polymer 5 Blend .....	214
Figure 7.32: RI Trace for Fully Formulated Lubricant.....	214



## List of Tables

Table 2.1: API Base Stock Classification (Hadsburg, 2003).....	35
Table 2.2: SAE J300 Oil Classification (Taylor, 1993).....	35
Table 2.3: Data for Fuel Injector Shear Stability Index Test for VM Polymers (ASTM D6278-02).....	47
Table 4.1: Properties of Engine and Venturi Mist Generator .....	93
Table 4.2: Derived Parameters from Malvern Spraytec, from Malvern Instrument Ltd (2010).....	100
Table 4.3: Oil Formulations for Misting Simulation Stage 1 .....	108
Table 4.4: Variables Used in Principal Components Analysis .....	119
Table 4.5: Outcomes from Principal Components Analysis.....	121
Table 5.1: Properties of Undiluted Polymer Viscosity Modifiers Used in This Study .....	130
Table 5.2: Blend Polymer Concentrations and Viscosities at Blending and Test Temperatures.....	132
Table 5.3: Crossover Results for Polymer Blends .....	137
Table 5.4: Calculated Entanglement Properties for Polymer Blends .....	138
Table 5.5: Derived and Calculated Molecular Coiling Parameters for Polymer Blends .....	139
Table 6.1: Ricardo Hydra Engine Parameters.....	156
Table 6.2: Test Lubricants and Conditions for Engine Misting Tests .....	162
Table 6.3: Variables for Principal Component Analysis .....	172
Table 6.4: Principal Components for Engine Misting Data.....	173
Table 7.1: Engine Test Conditions.....	188
Table 7.2: Lubricant Blends for Engine Tests .....	196
Table 7.3: Entanglement Parameters of Polymer Blends .....	196
Table 7.4: Molecular Parameters of Polymer Blends .....	197
Table 7.5: Viscosity Measurements of Fresh and Used Polymer Blends .....	208
Table 7.6: Crossover Parameters for Fresh and Used Polymer Blends .....	211
Table 7.7: Blend Properties for Mist Separation Study .....	213

## Abbreviations

BDC	=	Bottom dead centre
CaBER	=	Capillary breakup extensional rheometer
EHL	=	Elastohydrodynamic lubrication
FTIR	=	Fourier transform infrared spectrometry
GC	=	Gas chromatography
GPC	=	Gel permeation chromatography
LIF	=	Laser-induced fluorescence
MoDTC	=	Molybdenum dithiocarbamate
OCP	=	Olefin copolymer
PCA	=	Principal component analysis
PE	=	Polyethylene
PI	=	Polyisoprene
PIB	=	Polyisobutylene
PMA	=	Polymethacrylate
PMMA	=	Polymethylmethacrylate
PAO	=	Polyalphaolefin
PP	=	Polypropylene
PS	=	Polystyrene
TDC	=	Top dead centre.
TRZ	=	Top ring zone. Section 1.3.1
VI	=	Viscosity index
VII	=	Viscosity index improver
VM	=	Viscosity modifier
ZDDP	=	Zinc dialkyldithiophosphate

# Chapter 1: Introduction

## 1.1 Introduction

Improvement in efficiency has always been the driver for engineering progress. Tribology, whilst having almost always existed as a pursuit, was formalised as a subject with the Jost Report of 1966. Arising out of discussions into means of improving efficiency by reducing wear in industry, friction and lubrication were recognised fundamentally connected to this process (Stachowiak et al., 2001). In the early 1970s tribology had a greater emphasis on more efficient usage of our natural resources. In the 21<sup>st</sup> century, the concept of improving efficiency has been incorporated into the idea of sustainability, where responsible use of resources and reduction in energy usage are directed towards retaining the long-term stability of the earth's environment. It is considered almost common knowledge that the global climate is affected negatively by the by-products of the industrialised society we now live in. The potential immediacy of rapid and irreversible climate change has intensified the drive for efficiency. Even when there is perceived doubt about human impact on the climate, the traditional motivations of reducing energy usage and efficient use of resources should still drive progress, and particularly tribology, along the same path.

The automotive industry is a sector on which a great deal of pressure is being exerted to become more sustainable. It is widely seen that long-term sustainability lies in alternative fuels. Battery powered cars i.e. fuelled through centrally generated electricity, and hydrogen fuel cells are broadly seen as having the greatest potential. However, the pace of this technological development is slow, particularly in a sector growing so rapidly producing traditional internal combustion engines. In 2008 it was estimated that there were approximately 880 million passenger cars on the roads worldwide (World Bank Open Data Initiative, 2008). Estimates predict that, with

current growth trends, there will be 1.5 billion by 2030 (Kemp, 2007). Current discussions on such issues identify the same critical issues faced nearly twenty years ago (Springer, 1991). Because of the complexity of modern cars, improvements in efficiency are, by nature, multi-disciplinary. However, the most commonly referenced targets are concerned with emissions.

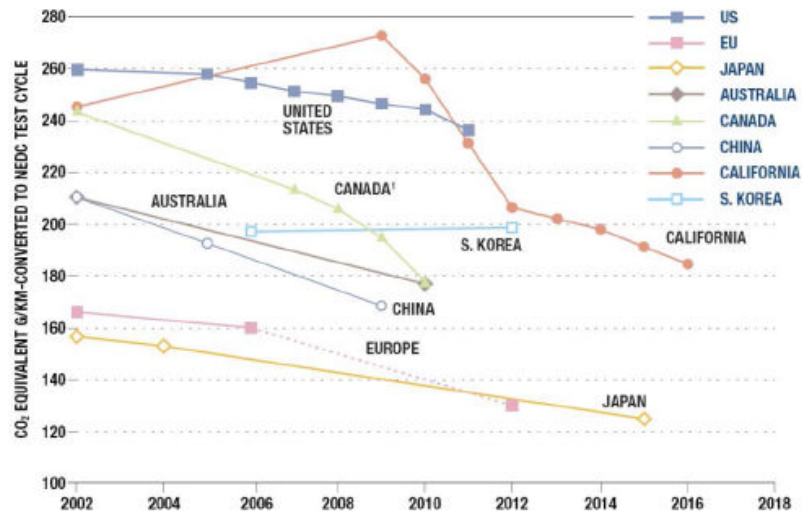
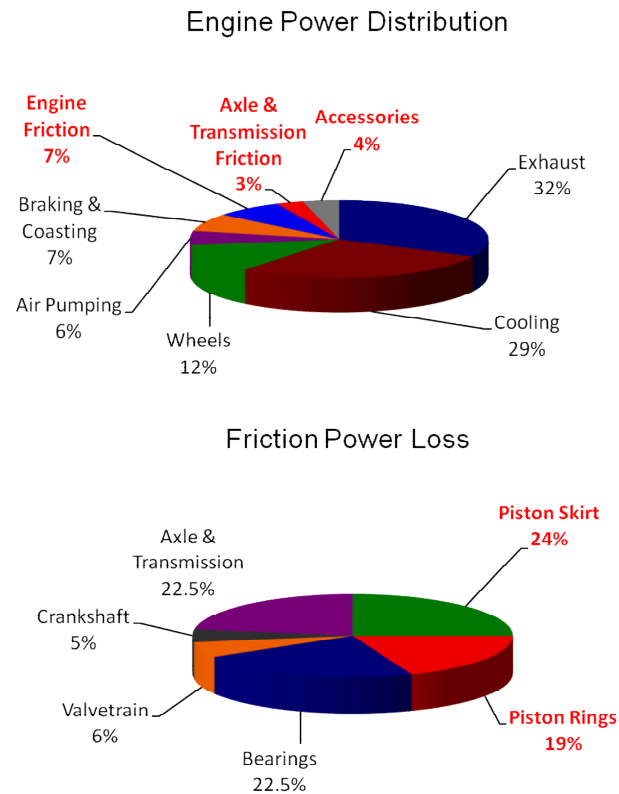


Figure 1.1: The Progression of CO<sub>2</sub> Emission Regulations in Automobiles (Gunsel, 2009)

The limits on potentially harmful chemicals emitted by a running vehicle have been steadily tightened over the years. Figure 1.1 shows the extent to which emissions targets have changed and will change. Products of incomplete combustion, such as nitrogen oxides, NO<sub>x</sub>, are the primary focus of studies in combustion and thermodynamics. Emissions of particulates, metals, and sulphur are a significant issue for tribologists too as these arise from the burning of lubricant oil and its additives. The issue of emissions from complete combustion, such as carbon dioxide, CO<sub>2</sub>, are more complex still. Whilst improvements in combustion allow less fuel to be used, reducing CO<sub>2</sub>, the major gains in these reductions are achieved by reducing the amount of energy demanded by various aspects of the vehicle, rather than improving the efficiency of the energy supply. Improvements in aerodynamics, more efficient auxiliary systems, and weight saving are areas of focussed research to this end. Relatively recent energy analysis of cars show that approximately 10.0% of brake power is lost to friction (Tung et al., 2004), 14% when accessories are included. Older

data by Andersson, quoted by Priest (2000) suggests figures of up to 15%, including accessories. The former analysis is shown in Figure 1.2. Thus, a 10% reduction in overall friction would reduce fuel consumption by 1%, which is significant when aggregated over all cars worldwide.



**Figure 1.2: Engine Power Distribution and Friction Power Loss, after Tung (2004)**

## 1.2 The Piston Assembly

Friction power loss can in turn be subdivided into the various tribological systems of the engine. Mufti (2009), measuring the systems of a 4-valve, single-cylinder engine independently, showed that the distribution of friction power loss between engine systems varies according to engine condition between 33% and 44%, as shown in

Figure 1.3. Tung (2004) reported that 44% of friction power loss (and 5.1% of total power usage) results from the piston assembly, as seen in Figure 1.2. This was further subdivided to show that 43% of piston assembly friction (19% of friction power loss and 2.2% of total energy) is contributed by the piston rings and 57% (25% of power loss and 2.9% of total energy) is contributed by the piston skirt. This emphasises the importance of lubrication in the piston assembly. Besides friction power loss, piston assembly lubrication is a critical factor in other areas. As described previously, many tail-pipe emissions, such as sulphur oxides, particulates and heavy metals, are a result of lubricant being burnt. The piston assembly is the major source of oil that is burned in this way. The piston assembly also produces the aggressive environment for the degradation of lubricant oil. All of these aspects have been studied in detail over the years (Priest et al., 2000; Taylor et al., 2004).

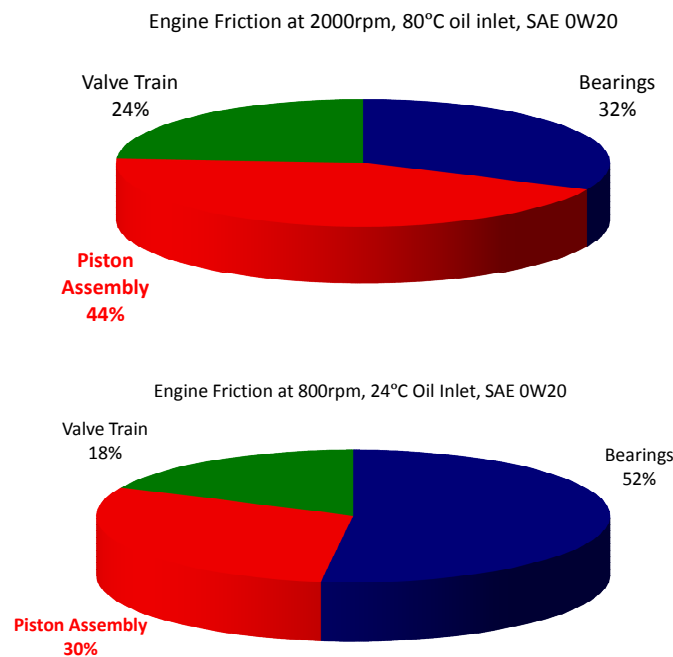


**Figure 1.3: Engine Friction Power Loss Breakdown, after Mufti (2009)**

## 1.3 Piston Assembly Tribology

### 1.3.1 Piston Assembly

The piston assemblies of reciprocating automotive engines have been continually refined over the years, but their general construction is little different from very early designs. A general piston assembly is shown in Figure 1.4.

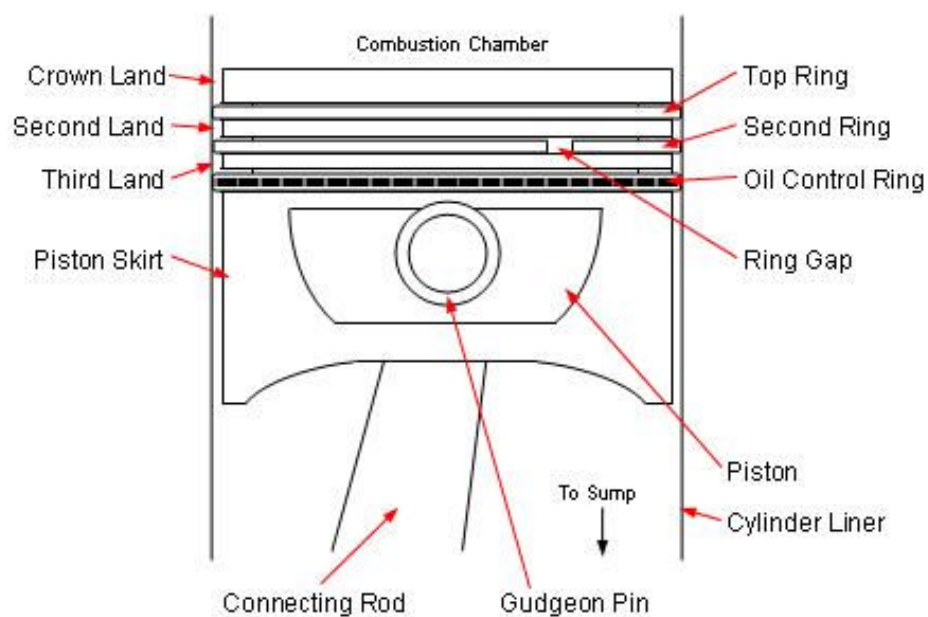


**Figure 1.4: A Typical Automotive Three-Ring Piston Assembly**

#### 1.3.1.1 Piston

The main function of the piston is to apply the force produced by the combustion gas pressure through the gudgeon pin to the con-rod in order to produce torque at the crankshaft, and to do this in as stable a manner as possible, i.e. with as little lateral movement or rotation about the gudgeon pin. However, these demands for tight clearances between piston and liner have to be compromised by the need for

significant clearances to maintain a controllable tribological environment, particularly when thermal expansion and bore distortion are considered. This means that, through this clearance, combustion gas can flow, termed blow-by (Furuhama et al., 1961), interacting with the lubricant, and small lateral and rotational movements of the piston, termed secondary motion, occur (Taylor et al., 2004; Nakamura et al., 2005). In modern gasoline engines, the vertical height of the piston, and thus the tribologically active area of the piston, is significantly shorter than shown in Figure 1.4, in order to reduce inertial mass and power loss. This is not the case for diesel engines as the higher gas pressure would lead to potentially damaging instability and secondary motion.

### **1.3.1.2 Rings**

The piston rings, therefore, have several functions (Taylor, 1993). Firstly, they provide a gas seal in the clearance between the piston and liner, reducing the power loss by reducing blow-by, hence cylinder pressure loss. This, however, is not a perfect seal, as each ring has a gap by which they are stretched and mounted onto the piston. This provides a route, albeit small, for blow-by to occur. Secondly, they provide a route of heat transfer from the piston to the liner and to the cooling circuit. This regulates piston temperature. Thirdly, they provide the stable, controllable tribological environment that is necessary for minimising friction power loss. As designs have improved, the number of rings has decreased. Most automotive engines now have three rings. These are two compression rings and an oil control ring. The compression rings are the most functional in terms of tribology, gas sealing and heat transfer, whereas the oil control ring is designed primarily for passively metering the flow of oil through it. This is reflected in the higher tensions applied to the compression rings, particularly the top ring (Gamble, 2003), on which the greatest demand is placed. The integrated system of piston rings is often termed the ring pack. Fourthly, although very much part connected to the tribological performance, is the control of lubricant supply. A well-designed ring piston assembly should allow sufficient lubricant to reach the upper piston assembly, with any excess to be returned to the sump. The oil control ring has, obviously, the greatest role to play in this. However, all rings are



required to regulate lubricant flow, as oil left above the top ring, in the combustion chamber, is likely to be lost, most likely burnt (McGeehan, 1979). Hence, the piston rings have a large influence on oil consumption. Some studies suggest that 80% of oil consumption is sourced in the piston assembly (Brown et al., 1993), and other, more recent, work has indicated that 90% of oil consumption is from lubricant being transported directly into the combustion chamber, including leakage from the valve train through the valve guides, (Yilmaz 2004)

### **1.3.1.3 Lubricant Supply**

In modern four-stroke automotive engines, the piston rings and the lubricated parts of the piston, the skirt, are not supplied with lubricant directly. Lubricant is introduced from the con-rod by either spray or, in older engines, 'flicked' from the surface of the sump oil by protrusions from the con-rod. The spray is generally produced from holes in the con-rod and bearing shell that align at a relevant point in the cycle. The oil pressure in the bearing forces oil out as a spray. The spray is directed at the liner when the piston is at the top of its stroke, thus lubricating the piston on the downstroke. Any excess is forced back to the crankcase by the oil control ring. The spray is often directed at the underside of the piston too, to aid its cooling (McGeehan, 1979).

## **1.3.2 Lubricant Transport Mechanisms**

Because lubricant is not directly applied to the piston rings, other mechanisms must carry lubricant from the point of supply to the contact. In particular, the top ring zone is seen as crucial due to it experiencing the highest temperatures, highest interaction with combustion products and lowest supply of lubricant. These complex mechanisms are defined by the interactions between the various components of the piston assembly and the gas flows between them. There have been many studies of these mechanisms to further understand and manage the lubrication of the piston assembly. These studies have identified the strong links between lubricant movement, performance, emissions and oil degradation (Gamble et al., 2002; Lee et al., 2006).

Mechanisms such as the scraping of lubricant on the liner by the rings (Yilmaz et al., 2004), shearing of lubricant by the blow-by gas (Gamble et al., 2002) and evaporation (Audette et al., 2000) have been investigated in detail. Others, such as the pumping of oil by axial ring movement (Burnett, 1992; DePetris et al., 1996; Yilmaz et al., 2001), and the inertial movement of oil on the component surfaces (McGeehan, 1979; Thirouard et al., 1998) are known only qualitatively. Detailed models incorporating the best data known show a net flow of oil downwards, inevitably leading to starvation of the upper piston assembly (Gamble, 2003). Therefore, while efforts continue to improve the input data to these models from known mechanisms, the investigation of other mechanisms is seen as necessary. One such mechanism is termed misting (McGeehan, 1979; Burnett, 1992; DePetris et al., 1996).

### **1.3.3 Lubricant Misting**

Misting, in this context, is a loose term describing lubricant droplets entrained in the gas flows through the piston assembly. As well as being thought of as a potentially significant mechanism by which lubricant travels upwards through the piston assembly, its movement through the top ring into the combustion chamber is thought to be a significant mechanism of oil consumption and undesirable emissions. Further hypotheses link misting to lubricant degradation on account of the higher surface area to volume ratio. The aim of this study is, therefore:

- To investigate the nature of misting in the piston assembly. The determination of its source, quantity, stability and end point are of chief importance
- To determine the factors that affect the nature of the mist produced. Lubricant properties engine conditions and flow parameters are the focus of this
- To determine and quantify any link between misting and long-term lubricant performance. The degradation rate of the lubricant is of particular interest in this regard

## 1.4 Outline of the Study

The aims of this study, described above, are met through the following:

- A review of relevant literature (Chapter 2). This covers, principally, the fields of:
  - Piston assembly tribology
  - Lubricant transport through the piston assembly
  - Lubricant formulation
  - Lubricant degradation
- A further review of literature (Chapter 3) describes research that impacts on the study of lubricant misting in the piston assembly. As this area has yet to be investigated thoroughly, this is almost exclusively from other fields. This covers, principally:
  - Two phase gas-liquid flows
  - Hydrocarbon gas-liquid flows
  - Polymeric additives and their effect on rheology
- An experimental method simulating the interaction between oil and gas through the piston ring gaps is developed (Chapter 4). Subsequent investigations using this method are then described. These consider the effect on misting of, firstly, the components of a commercial engine lubricant (Chapter 4) and, secondly, the effect of various polymeric additives at varying concentrations (Chapter 5).
- Measured data describing the nature of mist produced in a test engine is reported, with reference to the effect of engine conditions and lubricant formulation (Chapter 6).
- Further engine tests, quantifying the effect of misting on lubricant degradation, are described (Chapter 7)

## **Chapter 2: Piston Assembly Tribology and Lubricant Chemistry**

### **2.1 Introduction**

The piston assembly is a critical area in reciprocating automotive engines. It contributes greatly to friction power loss in the engine and also to emissions via loss of lubricant into exhaust gases, where it is almost always burned. It is the major region in which lubricant is degraded (Yasutomi et al., 1981), so it has an effect on lubrication performance in other systems. All of these aspects have been studied in detail (Priest et al., 2000; Priest, 2002; Taylor et al., 2004; Wong et al., 2007). The progression and scope of the most relevant of these studies are described here.

### **2.2 Blow-By**

The flow of combustion gases through the piston assembly has major effects on the tribological environment of the piston. It is widely accepted that this gas contains significant amounts of oil (Burnett, 1992; DePetris et al., 1996; Yilmaz et al., 2002; Gamble, 2003; Yilmaz et al., 2004; Usui et al., 2008; Delvigne, 2010). Due to the tortuous path it takes through the piston assembly, and the continual movement of the piston assembly, direct measurement of these gas flows is difficult. Pressure in piston lands has been measured using pressure transducers (Wakuri et al., 1981; Truscott et al., 1983; Thomson, 1996; Kim et al., 1999; Moritani et al., 2003; Cheng et al., 2004; Quillen et al., 2007; Johansson et al., 2010). However, few other direct measurements are possible. The gas flow rate past the piston to the crankcase, termed blow-by, can be inferred by measuring the flow rate of gas from the crankcase when the engine is running. This can be done using various different methods such as orifices (DePetris et al., 1996; Ebner et al., 1998), positive displacement meters (Cheng et al., 2004), vortex shedding meters (Yilmaz et al., 2002; Yilmaz et al., 2004) and low pressure fans (Ebner et al., 1998). However, care must be taken for three reasons. Firstly,

blow-by flow past the piston is driven by the pressure difference between the combustion chamber and the crankcase. With proper venting, the crankcase pressure is only very slightly above atmospheric pressure. Therefore, any slight back-pressure induced by the measurement system will significantly change the flow conditions. This is why Venturi meters are not often used, and orifices should be used with care (Ebner et al., 1998).

Secondly, due to the cyclical changes in crankcase volume and pressure, there will be a corresponding variation in flow rate. For most engines, particularly single cylinder engines, the peak flow rate is much larger than the net flow rate. Single cylinder engines are particularly prone to this due to their small crankcase volume and large change in that volume through a cycle. The displaced air arising from the significant changes in crankcase volume is of significantly higher volume than the net blow-by flow per cycle. Therefore, the flow must be damped for accurate measurements.

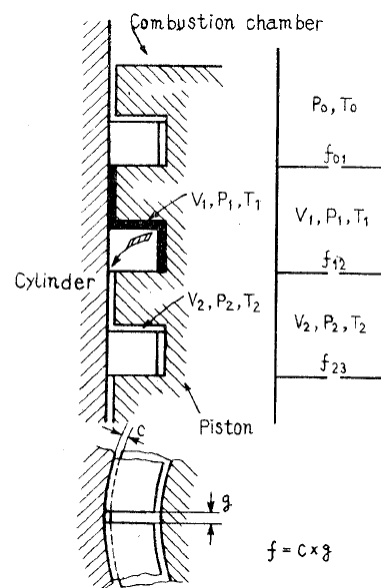


**Figure 2.1: Orifice Model of Piston Assembly Gas Flow from Furuhashi (1961)**

Thirdly, and possibly most importantly, not all the combustion gas that enters the piston assembly reaches the crankcase as blow-by gas (Cheng et al., 2004). Pressure measurements in the piston lands confirm this (Wakuri et al., 1981; Truscott et al., 1983; Thomson, 1996; Kim et al., 1999; Moritani et al., 2003; Cheng et al., 2004).

Most models assume that ring groove pressures are the same as the land to which the ring is open (Furuhama et al., 1961; Ting et al., 1974; Iwakata et al., 1993; Ejakov et al., 1998; Gulwadi, 1998; Tian, 2002; Tian, 2002; Gamble, 2003), Figure 2.1. When gas flow rate is at its peak, the top land has the greatest pressure followed by the second and third respectively. When combustion chamber pressure drops, these pressure differences drive the gas flow from the piston assembly. The greatest pressure difference will be between the second land and the combustion chamber. Therefore, under these conditions, a significant amount of gas will be allowed to flow into the combustion chamber, Figure 2.2. This is termed reverse blow-by (DePetris et al., 1996; Kim et al., 1999; Yilmaz et al., 2004; Tamminen et al., 2005; Johansson et al., 2010).

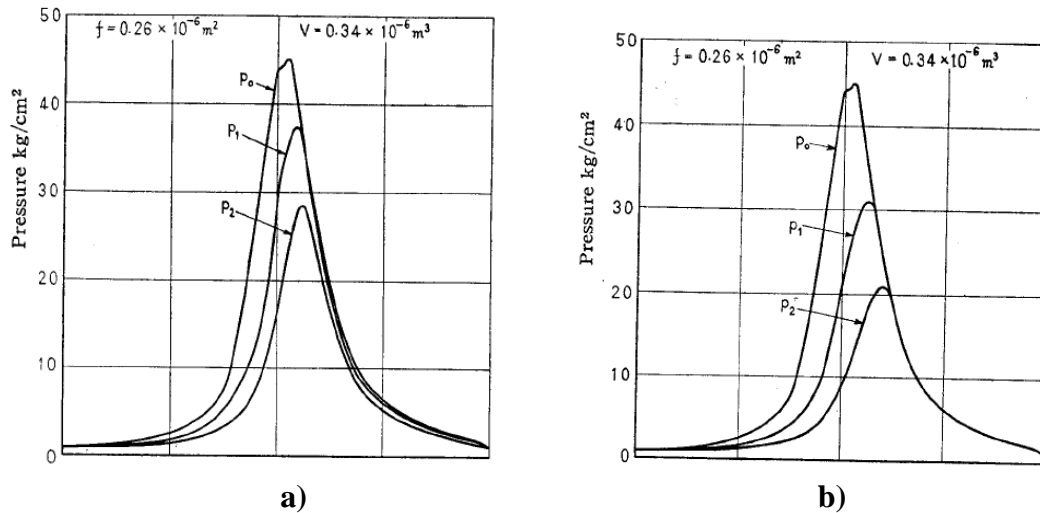


**Figure 2.2: Piston Assembly Gas Flow Properties from Furuham (1961); a) Gas Pressures, b) Gas Flow Rates. 0 = Combustion Chamber, 1 = Below Top Ring, 2 = Below 2nd Ring**

Reverse blow-by can occur in the intake stroke, but is more dominant in the latter stages of the combustion stroke and early in the exhaust stroke (Gamble, 2003; Yilmaz et al., 2004). It is almost impossible to measure as it will form an almost insignificant part of the large volume of gas entering or exiting the combustion chamber at the same time. Modelling has indicated that reverse blow-by is a small proportion of total blow-by (Furuhama et al., 1961; Yilmaz et al., 2004). Experimental investigation of reverse blow-by are limited to secondary indications from measurements of oil products in the exhaust gas (Saito et al., 1989; Bailey et al.,

1990; Winborn et al., 2001; Usui et al., 2008). Therefore blow-by gas cannot define the entire flow environment of the piston assembly. However, as blow-by finds its source in the piston assembly, it can be used as a good indicator of the nature of other flows, such as reverse blow-by, when considered in the context of the whole engine.

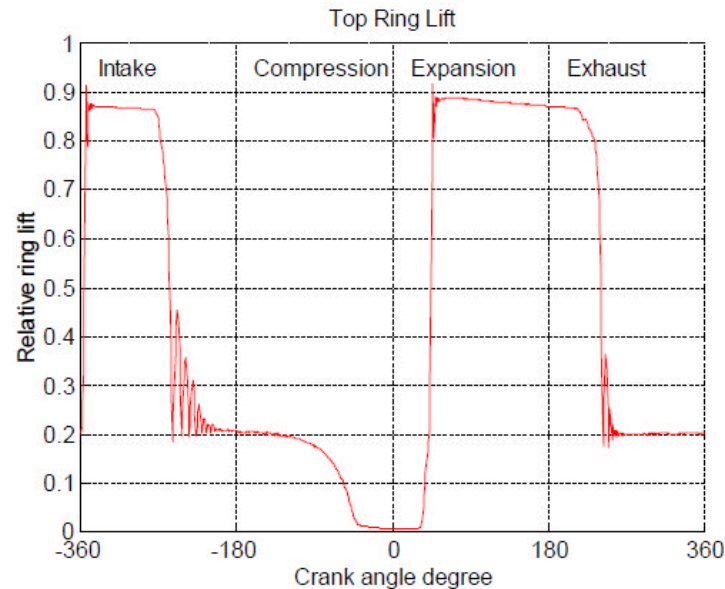


**Figure 2.3: Top Ring Axial Movement from Thirouard (1998)**

Flow of gas into the piston lands is highly dependent on the piston rings. The axial movement of rings governs the major flow path. When a friction force or a significant pressure difference acts on the ring, it is forced onto the side of its groove, forming a strong seal against gas flow. Under these conditions, the only path for blow-by is through the ring gaps. Because of the small orifices and high pressure differences, flow through the ring gaps is choked, with Mach number approaching 1 (Furuhama et al., 1961; Furuhamma et al., 1961; Gamble et al., 2002). However the forces on the ring - friction forces, inertia and pressure differences - may approach equilibrium, most commonly at the dead-centres where sliding speeds are low, and at the end of the intake and exhaust strokes, where gas pressures are relatively low. Under these conditions the ring flutters i.e. oscillates axially, Figure 2.3. This opens up a flow path around the back of the ring, through the groove. In other cases, usually at high loads and when the piston rings twist or tilt, gas can flow between the ring and liner. Here, the gas pressure pushes the ring back into its groove, completely breaking the gas seal

it ordinarily provides: This is termed ring collapse (Tian et al., 1998; Przesmitzki et al., 2007), Figure 2.4. Under both these conditions, abnormally large blow-by flow rates are seen (McGeehan, 1979; Truscott et al., 1983; Keribar et al., 1991; Tian et al., 1998; Taylor et al., 2004; Usui et al., 2008).

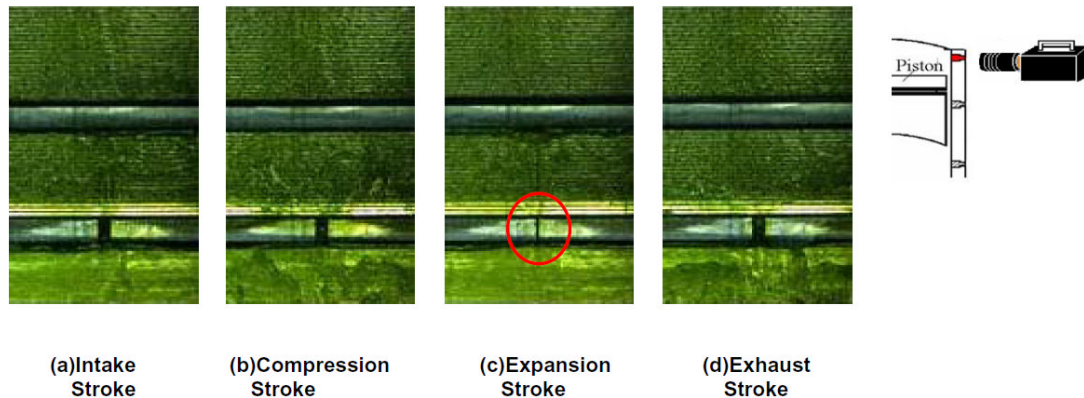


**Figure 2.4: Observation of Ring Collapse from Usui (2008)**

When the piston rings are functioning properly, it has been shown that the radial position of the ring gaps has a significant effect on the flow of gas through and out of the piston assembly (Saito et al., 1989; Nakashima et al., 1995; Min et al., 1998; Thirouard et al., 1998; Gamble, 2003). Investigations have been performed using a variety of techniques such as tracers (Min et al., 1998), two-dimensional laser-induced fluorescence, 2-D LIF (Thirouard et al., 1998) and other forms of direct observation (Saito et al., 1989; Nakashima et al., 1995). Others have pinned the rings in various positions and investigated the resulting blow-by and oil flows (Nakashima et al., 1995; Min et al., 1998; Gamble et al., 2002). When the gaps are aligned vertically, termed in phase, the path through the ring pack is very direct, therefore gas flow rates are extremely high, and the flow rate of gas reaching the crankcase is extremely high. This is shown in Figure 2.5a. Flow circumferentially around the lands is extremely low relative to that through the ring gap as there are low pressure differences driving the flow. This has implications for oil transport as the gas encounters a relatively small area of oil film, reducing gas-driven oil flow. When the gaps are 180° apart, out of phase, the path through the piston is longer and more tortuous. Therefore, the flow rate of gas past the cylinder is lower and the velocity of this flow is lower. This is



shown in Figure 2.5b. Flow through the piston lands is much greater which serves to increase gas-driven oil transport. At intermediate angles, these effects are balanced (Nakashima et al., 1995; Min et al., 1998; Gamble et al., 2002). Thirouard (1998) used phase angles of approximately  $45^\circ$  to optimise both parameters to produce the greatest movement of oil (Thirouard et al., 1998). In terms of gas flow, the absolute position of the ring gaps is not relevant i.e. on the thrust or anti-thrust side of the piston. The most significant parameter is the relative position of the rings, the phase angle (Nakashima et al., 1995; Min et al., 1998).

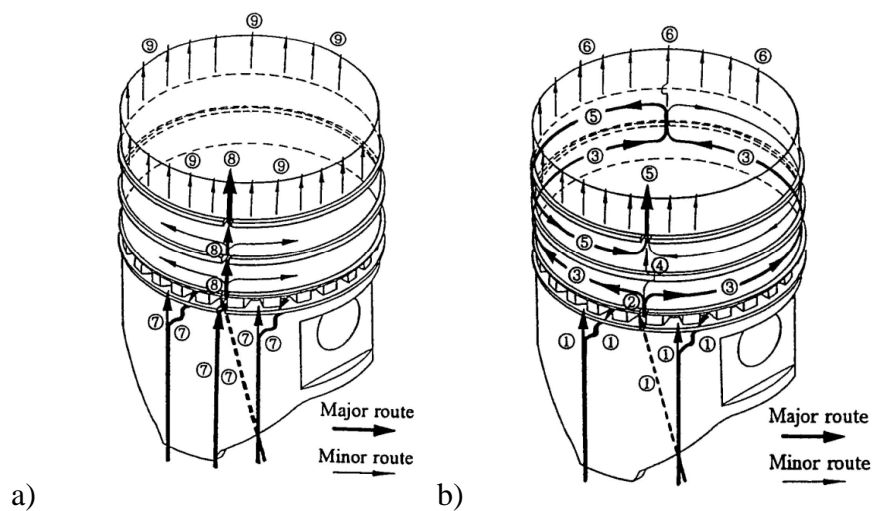


**Figure 2.5: Piston Ring Gap Phase (Nakashima et al., 1995): a) In Phase b) Out of Phase**

Because blow-by originates in the combustion chamber, its chemical make-up is of significant interest to studies in lubricant degradation. Aside from the inevitably high concentrations of nitrogen and oxygen - the main constituent is air - there are also significant quantities of combustion by-products. These include carbon dioxide, carbon monoxide, nitrogen oxides, water vapour, and, more importantly, acids hydroperoxide, radicals and particulates (Gamble, 2003; Moritani et al., 2003; Clark et al., 2006). These attack component surfaces, cause chemical degradation of the lubricant and increase wear (Gamble, 2003; Lee et al., 2006). It is understood that blow-by gas leaving the piston assembly contains significant amounts of oil, in both vapour and droplet form (Burnett, 1992; DePetris et al., 1996; Yilmaz et al., 2002; Yilmaz et al., 2004; Wong et al., 2007; Ma, 2010). In engines where blow-by gases are re-circulated to the inlet manifold to improve combustion and emissions

performance, oil separators are used in the crankcase vent to return this entrained oil to the sump (Yilmaz et al., 2002; 2005; Tissera et al., 2005).

### 2.3 Modelling

Due to the difficulty of accessing the piston assembly experimentally, the use of theoretical models to understand and predict performance has been extensive. These have been validated using experimental data as techniques have developed synergistically.

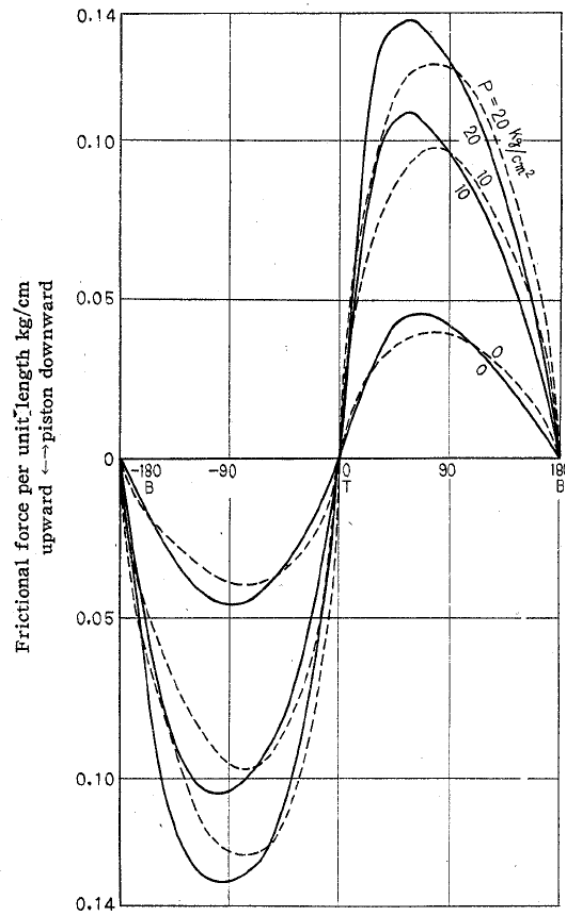
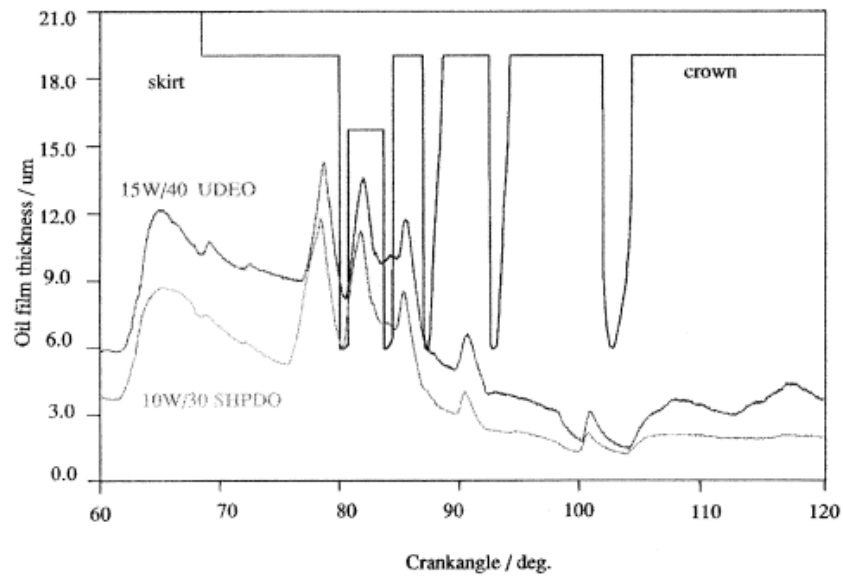


Figure 2.6: Modelled Piston Ring Friction Force from Furuham (1959)

Initial lubrication models of the piston assembly focused on the piston rings, as these are the principal tribological components. These were based on Reynolds' equation of

hydrodynamics, assuming a fully flooded contact and hydrodynamic lubrication throughout the entire stroke and neglecting ring gaps (Ruddy et al., 1981; Taylor, 1993; Gamble, 2003). The contact load was calculated from ring tension and the incorporation of gas pressure data acting on the back of the piston rings. These models showed that film thickness was greatest in the mid-stroke where sliding speeds are highest. The greatest friction power loss was found to be in the mid-stroke, where the high sliding speed produced the greatest viscous losses, Figure 2.6. The spike in gas pressure and contact pressure resulting from combustion produced a large and sudden drop in film thickness and increase in friction in the initial stages of the combustion stroke. Not all oil is entrained through the contact, but some accumulates in front of the ring and is carried to the dead-centre position. The top ring was the most frequently modelled, owing to the great demands placed on it tribologically (Moritani et al., 2003; Lee, 2006).

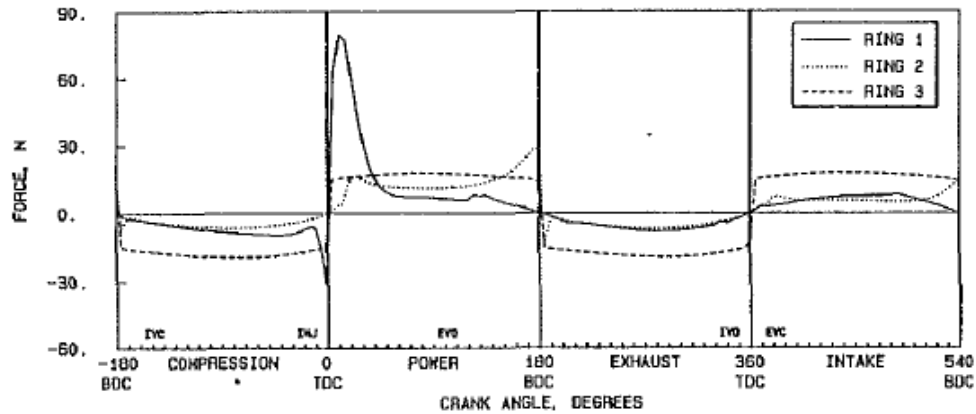
Film thickness models have been validated over the years by various film thickness studies on fired and motored engines. Initially, electrical measurements were made using resistivity and capacitance probes that ran between the ring and liner (Furuhama et al., 1961; Brown et al., 1978; Choi et al., 1993; Sochting et al., 2009). In these, an increase in lubricant film thickness produces an increase in either the resistivity or capacitance of the contact. These showed reasonable agreement between the models and data, but showed much lower film thicknesses than anticipated, particularly at the dead centres where metal-on-metal contact was seen, showing an absence of film. Improved techniques, such as laser-induced fluorescence, LIF, were subsequently developed (Brown et al., 1993; Hoult et al., 1993; Phen et al., 1993; Taylor, 1994; Taylor et al., 2004; Wong et al., 2007). LIF is an optical technique that illuminates the oil with a laser light causing the oil to fluoresce i.e. emit light, of a different wavelength. The intensity of this fluoresced light can be correlated to the thickness of the oil film at this point, Figure 2.7. LIF is advantageous as it can record data for the entire piston assembly as it passes the observation window on the liner surface. Not only does LIF show the film thickness of the film in the contact, but it also shows the thickness of the film in the piston lands and on the edges of the ring. This allows estimates of the quantity of oil that is scraped by the rings.



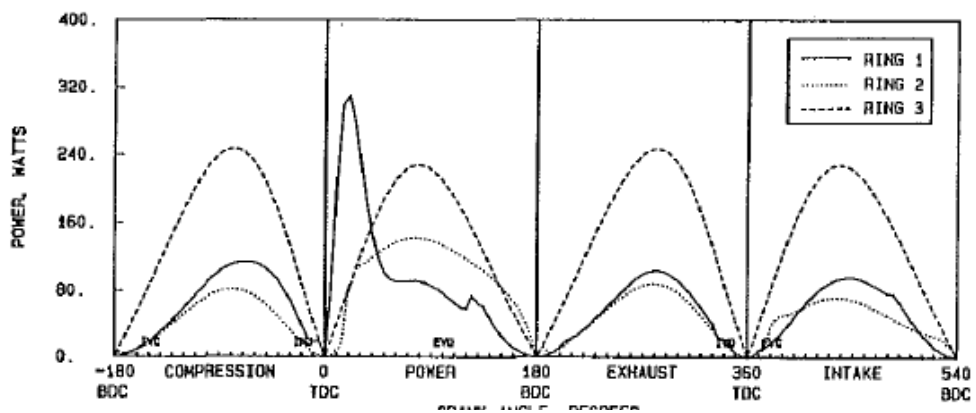
**Figure 2.7: LIF Film Thickness Trace of Piston Assembly, from Taylor (2004)**

Many single-ring models predicted that pressure in the oil film exiting the contact region would be, in some cases, sub-ambient. Therefore, various models for cavitation were included in the existing models (Jeng, 1992; Yang et al., 1995; Ma et al., 1996; Gulwadi, 1998). The formation of bubbles in the oil film has implications for the lubrication of the rings that follow.

Models indicated that, as the piston speed decreases near the dead centre region, the lubricant film thickness would significantly decrease. Thus, elastohydrodynamic, EHL, (Taylor, 1993; Yang et al., 1995; Rycroft et al., 1997; Mishra et al., 2008), boundary (Ruddy et al., 1981; Miltsios et al., 1989; Keribar et al., 1991; Gulwadi, 1998; Ma et al., 2006), and mixed lubrication effects were incorporated in models. Mixed lubrication is generally incorporated into models by following the example of Rohde (1980) and his application of the Greenwood and Tripp mixed friction model to piston rings (Ruddy et al., 1981; Cho et al., 2001; Bolander et al., 2005; Ma et al., 2006; Ligier et al., 2007).



a)



b)

**Figure 2.8: Modelled a) Friction Force and b) Power Loss, Including EHL and Boundary Conditions, from Keribar (1991)**

The incorporation of these sub-models indicate that, as the piston approaches the dead centre, it will pass from hydrodynamic, through EHL, mixed and reach boundary conditions at the dead centre itself. Thus, the piston ring covers most of the Stribeck curve. Due to the metal-to-metal contact between the ring and liner in the dead centre region, the highest friction force and wear is encountered. Despite the high friction forces, the friction power loss in these regions is small, due to the short time spent in this regime and the low sliding speeds, Figure 2.8. However, as long term trends are to reduce lubricant viscosity to reduce friction power loss (Korcek et al., 2000; Priest et al., 2000; Benvenuti et al., 2002), regions of EHL and boundary lubrication in modern engines will increase.

Squeeze film lubrication is included in some models (Rohde et al., 1979; Taylor, 1993). This is the effect of the piston ring being at zero velocity only momentarily, thus not allowing lubricant sufficient time to leave the contact. Lubricant films, therefore, are more substantial at the dead centre regions than models predict, and friction and wear rate lower than predicted.

Most early models assumed a fully flooded contact, where the lubricant completely fills the space between the moving surfaces. Other models considered that this assumption may not be true in many engines, so incorporated lubricant starvation effects (Dowson et al., 1979; Ruddy et al., 1981; Jeng, 1992; Hronza et al., 2007). Such models tend to indicate increased friction due to thinner films and predict higher surface contact between components, Figure 2.9.

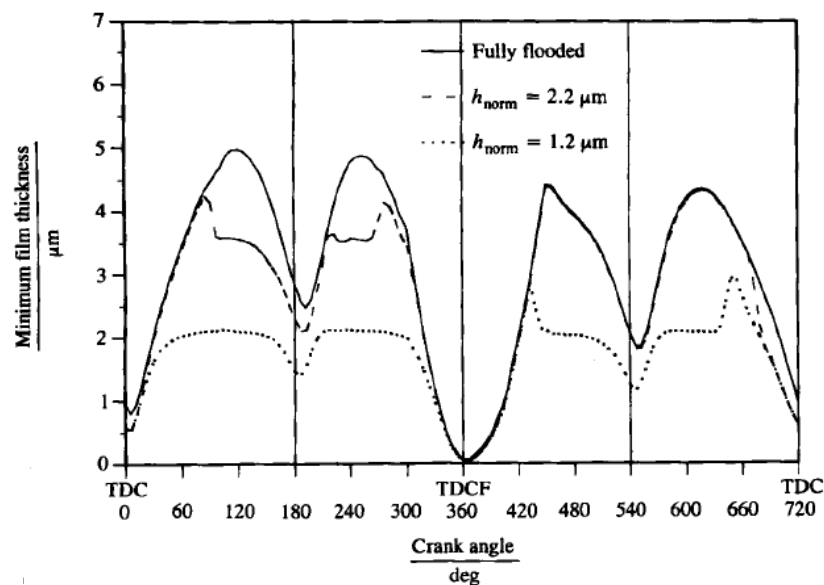


**Figure 2.9: Modelled Piston Ring Film Thickness with Lubricant Starvation, from Ma (1996)**

The various loads placed on the cylinder liner during operation have also been considered in some models (Truscott et al., 1983; Keribar et al., 1991; Ma et al., 1996; Tian, 2002; Ma et al., 2006). Wear resulting from long term use, long term temperature distortion and short term effects resulting from poor manufacture and installation can result in deformation of the liner by up to 45μm (Hennessy et al.,

1995). As well as having an impact on the sealing effectiveness of the piston rings and ring collapse, it has a significant effect on the lubrication conditions. Some models consider this by using generalised profiles based on mathematical geometries (Ma et al., 1996), Figure 2.10, and some use experimental and theoretical data (Tian, 2002).

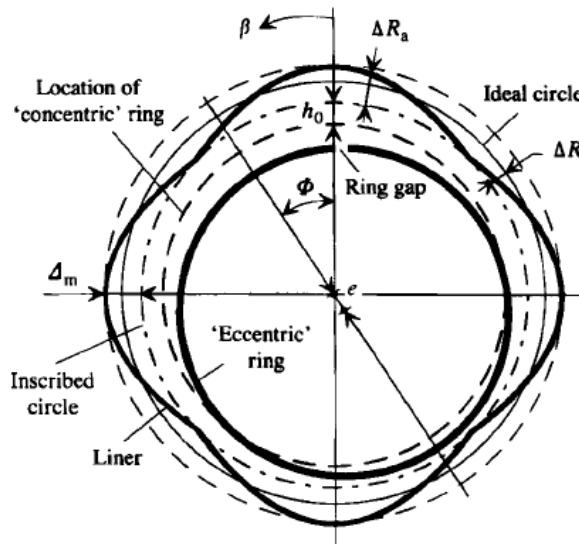


Figure 2.10: Generalised Geometry of Bore Distortion from Ma (1996)

### 2.3.1 Variation with Temperature and Pressure

Most early models used idealised lubricants assuming Newtonian fluids and uniform temperatures. However, it is widely acknowledged that there are significant temperature gradients in the piston assembly. Gas temperatures are highest at the top land, up to 200°C in a modern diesel engine, lowest in the crankcase, 50-60°C likewise, and decrease steadily through the piston between these values (Harigaya et al., 2003; Rakopoulos et al., 2004; Taylor et al., 2004; Wong et al., 2007). Measurements of temperatures on the liner and piston allowed models to incorporate the variation in lubricant viscosity arising from variation in temperature (Harigaya et al., 2003; Harigaya et al., 2006). The relationship between viscosity and temperature is described by the Vogel equation:

$$\eta = ke^{\frac{b}{T+\theta}} \quad [2.1]$$

Where  $\eta$  is dynamic viscosity,  $b$ ,  $k$  and  $\theta$  are constants (Coy, 1998)

With the introduction of EHL conditions to lubrication models, the contact pressures imposed on the lubricant increased greatly (Coy, 1998). Therefore, pressure-viscosity relationships are included in some models to allow for the increase in viscosity with pressure, as described by the Barus equation:

$$\eta = \eta_0 e^{\alpha p} \quad [2.2]$$

Where  $\eta$  is dynamic viscosity,  $\eta_0$  is dynamic viscosity at atmospheric pressure,  $p$  is pressure, and  $\alpha$  is a constant

The Roelands equation can also be used to describe pressure-viscosity behaviour (Kumar et al., 2009):

$$\eta = \eta_0 e^{\left( (\ln \eta_0 + 9.67) \left( -1 + (1 + 5.1 \times 10^{-9} p)^z \right) \right)} \quad [2.3]$$

Where  $z$  is a constant

### 2.3.2 Piston Assembly Models

Models considering all rings simultaneously began initially by imposing the outlet film conditions of the front ring as the inlet conditions of the ring following, and so on for all other rings (Dowson et al., 1979; Rohde et al., 1979). This was then reversed at the dead centre when the sliding direction changed. These models proved successful but, as previously described, would rapidly produce starvation if repeated over many cycles. Therefore, other oil transport mechanisms, such as the axial and radial movement of the piston rings, had to be incorporated into the models (Dowson et al., 1979; Rohde et al., 1979).



As blow-by gas and friction forces on rings can cause rings to twist, the extreme result of this being loss of gas sealing, ring collapse, such effects have been included in lubrication models, Figure 2.11. Whilst twist does not have a large effect on film thickness, particularly on barrel-faced rings, it can have a significant effect on the amount of oil scraped by the ring, particularly on the second ring if a Napier profile is used, Figure 2.12. This is caused by restricting the inlet to the contact, thus scraping a larger volume of oil in front of the ring (Tian, 2002; Tian, 2002; Przesmitzki et al., 2005; Przesmitzki et al., 2007). This effect is greatest during the combustion stroke, when gas pressures, and hence ring twist, is greatest. This results in, by scraping, a net movement of oil down the liner throughout the cycle. This would, theoretically lead to starvation of the contact if this is the only oil transport mechanism but clearly this is not the case.

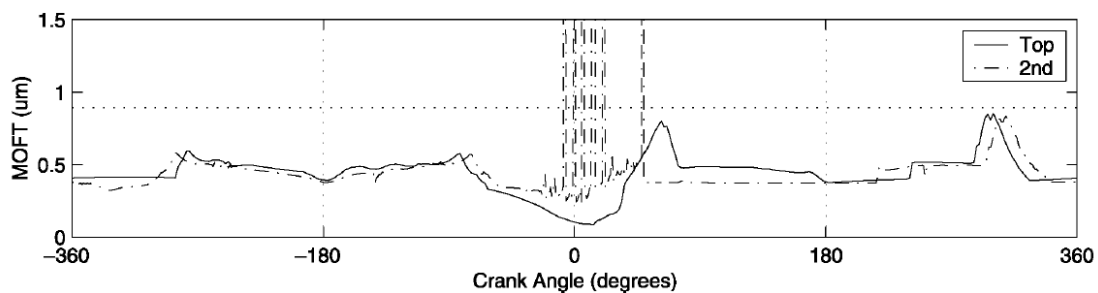


**Figure 2.11: Modified Minimum Oil Film Thickness on the Thrust Side Including Ring Dynamics, from Tian (2002 II)**

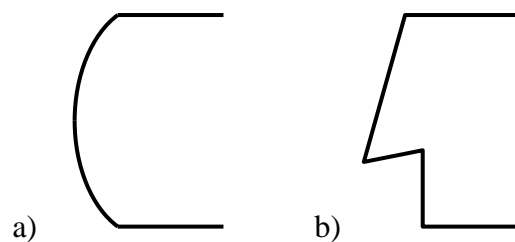


**Figure 2.12: Piston Ring Running Face Profiles a) Barrel-Faced b) Napier**

The incorporation of ring dynamics, particularly the effect of inter-ring gas pressures on ring loading, was considered a necessary improvement to models. This meant that

ring gaps have to be incorporated into lubrication analysis. Blow-by models that separate the lands into smaller elements (Nakashima et al., 1995; Gamble, 2003) have been incorporated into models. These provide two flow paths between ring gaps, clockwise and anti-clockwise, Figure 2.5, as is the case in an engine, allowing consideration of the phase angles of the ring gaps and the effects this has on gas flow and, by extension, lubrication. As well as improving existing lubrication modelling, such models permit the consideration of other oil transport mechanisms. Principal amongst these is the oil moved along the surfaces of the lands and through the ring gaps by the shear induced by the gas flow over it (Gulwadi, 1998; Gamble, 2003). Estimation of this is dependent on the thickness of the oil film on the land. This is usually estimated in models and iterated until solutions produce similar results to experimentation (Gamble, 2003). However, recent observations using 2-D LIF have allowed better estimates of the quantities of oil moved through the lands and the thicknesses of these films (Inagaki et al., 1997; Thirouard et al., 1998; Thirouard et al., 2003; Przesmitzki et al., 2005; Przesmitzki et al., 2007; Wong et al., 2007).

## **2.4 Friction and Power Loss**

Full piston assembly models produced friction and power loss data that was increasingly more comparable with experimental values. The consideration of the many complex factors and interactions that affect the tribological environment further improved these models (Ruddy et al., 1981; Keribar et al., 1991; Jeng, 1992; Jeng, 1992; Gulwadi, 1998; Harigaya et al., 2003; Harigaya et al., 2006; Wannatong et al., 2008; Wakabayashi et al., 2009). They confirmed the behaviour seen previously but with values that were much more accurate. However, friction measurements of the piston assembly, in particular the ring and liner contact, have been a challenge to experimentalists over the years. Two successful techniques have emerged: The floating liner, and the IMEP method. The first is a direct measurement where the cylinder liner is mounted on strain gauges or loads cells and, thus, the axial friction force can be measured (Furuhama et al., 1981; Wakuri et al., 1995; Noorman et al., 2000; Richardson, 2000; Wakabayashi et al., 2007; Wakabayashi et al., 2009). The indicated mean effective pressure, IMEP, method is an indirect method whereby the

friction is calculated by measuring the individual forces on the piston - the gas pressure force on the piston crown, piston assembly inertia and the piston assembly weight- and subtracting these from the total force as measured by strain gauges on the con-rod to leave the friction force (Noorman et al., 2000; Mufti et al., 2005), Figure 2.13.

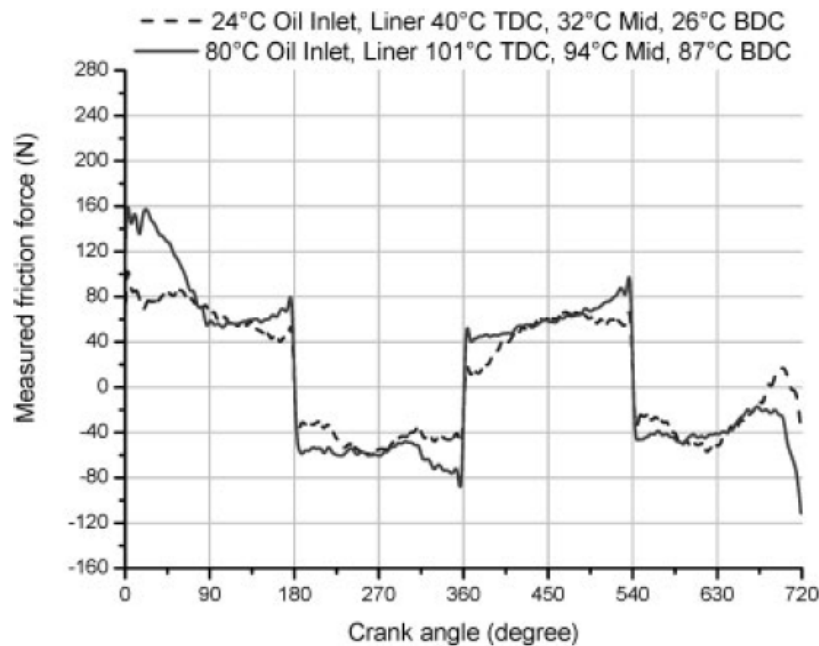


Figure 2.13: Measured Piston Assembly Friction using the IMEP Method, from Mufti (2005)

### 2.4.1 Other Oil Transport Mechanisms

It is clear that scraping is not the only mechanism by which oil is transported through the piston assembly. Several mechanisms have been identified and many have been incorporated into models. The inertia of oil on the surface of the continually accelerating piston surface or of oil given inertia by scraping is included in some models (Gulwadi, 1998; Gamble et al., 2002). This inertia forces oil axially across the piston land (McGeehan, 1979; Burnett, 1992; DePetris et al., 1996; Yilmaz et al., 2004; Ito et al., 2006; Przesmitzki et al., 2007; Kato et al., 2009; McGrogan et al., 2010). At the ring gap regions, this inertia will force the oil through the ring gap onto the next land. In the case of the top ring, this mechanism is a major source of oil consumption (Maekawa et al., 1986; Saito et al., 1989; Nakashima et al., 1995;

Inagaki et al., 1997; Yilmaz et al., 2004; Ito et al., 2006; Todsén et al., 2006; Usui et al., 2008; Delvigne, 2010; Ma, 2010). Models of this generally assume an initial film thickness on the surfaces. Gamble (2002), for instance, assumed  $5\mu\text{m}$  and  $10\mu\text{m}$ . These are educated estimates. More recent work using 2-D LIF has shown that the main inertial movement of the film is from oil scraped in front of the rings, suggesting a larger volume of transport than models predict (Przesmitzki et al., 2007; Wong et al., 2007), Figure 2.14.

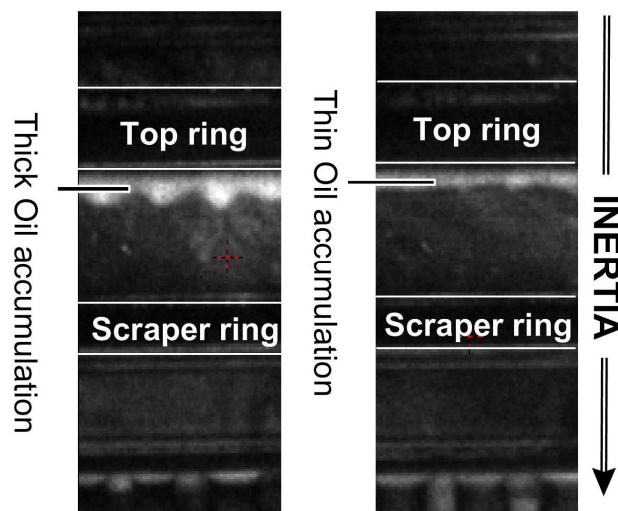


Figure 2.14: Inertial Movement of Oil on Piston, from Thirouard (1998)

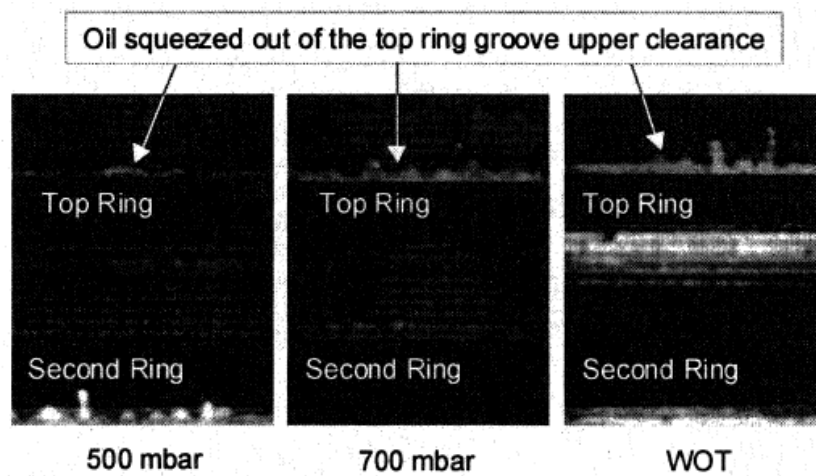
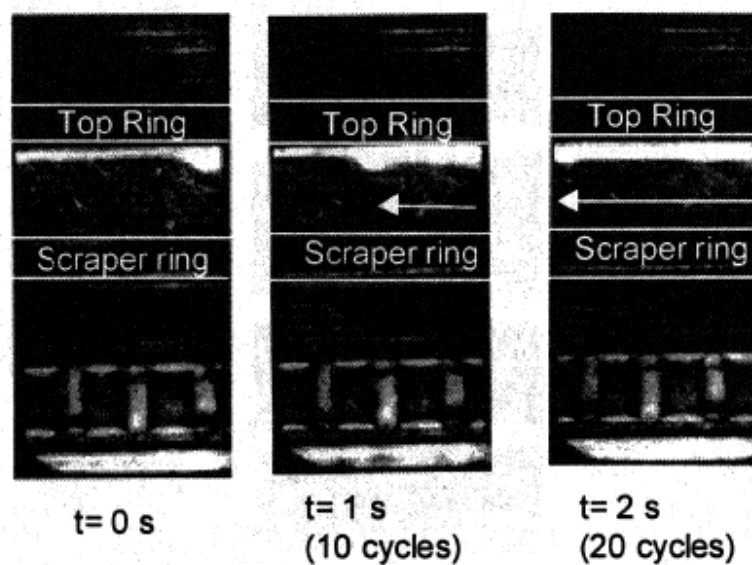


Figure 2.15: Oil Pumping from Ring Groove from Thirouard (2003 II)

As a result of ring axial motion, oil that accumulates in the ring grooves can be ejected from the groove under the pressure produced between the groove surface and the rising ring. Tian (2002) showed how the direction of pumping is dependent on the twist angle of the ring relative to the groove surface. The twist angle dictates the exit path for pumped oil. 2-D LIF imaging has indicated that this mechanism occurs, and works synergistically with inertial mechanisms (Thirouard et al., 1998; Yilmaz et al., 2004; Wong et al., 2007), Figure 2.15. However, no numerical investigation has yet taken this mechanism into account.



**Figure 2.16: Oil Draged Along the Piston Lands by Blow-By Gas, from Thirouard (2003 I)**

Beyond these interactions between oil and components, oil is transported by the blow-by gas. The most clearly observed mechanism is the shear-induced flow of oil along the piston lands, Figure 2.16. Oil transport is, therefore, influenced by the factors that govern blow-by e.g. ring gap relative position (Nakashima et al., 1995), Figure 2.17. Shear induced flow of oil in the direction of gas flow through the ring gaps and lands has been considered in several models (Saito et al., 1989; Keribar et al., 1991; Gulwadi, 1998; Ishihara et al., 1999; Gamble et al., 2002; Usui et al., 2008). Again, this is dependent on accurate data for film thickness, gas flow rate and pressure. In Section 2.2 it is discussed how there is an optimisation between high gas flow (i.e.

high shear) with in-phase gaps, and high shear dissipation into the film with out of phase gaps.

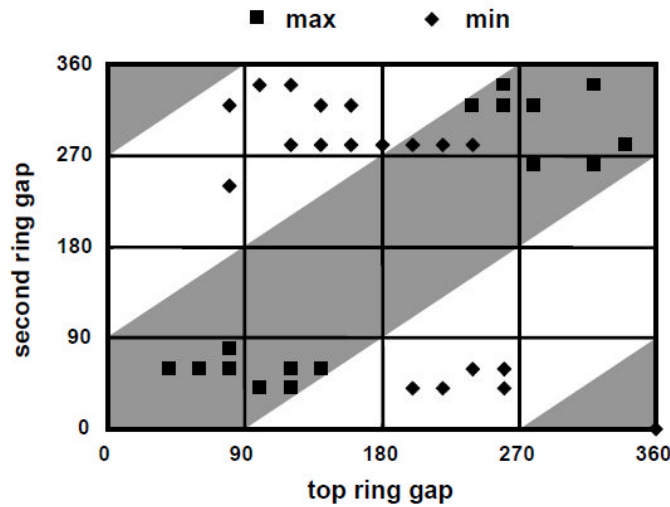


**Figure 2.17: Relationship between Ring Gap Position and Oil Consumption, from Min (1998)**

It has been understood for many years that a significant quantity of oil is entrained in the blow-by gas itself (Truscott et al., 1983; Bailey et al., 1990; Burnett, 1992; DePetris et al., 1996). It has traditionally been taken to be in the form of droplets and vapour. At combustion gas pressures and temperatures, there will clearly be transfer between the two phases. The source of oil vapour in the blow-by gas is understood to be from the high temperature gas and components of the engine causing the evaporation of the more volatile fractions of the oil to evaporate into the gas flow (Burnett, 1992; Guenther et al., 1998; Audette et al., 2000; Yilmaz et al., 2002; Dasch et al., 2008; Tatli et al., 2008). This will change the composition of the oil film on the surface, tending to increase the concentration of higher molecular weight fractions in the film, thickening the oil. The quantity, and thus the flow rate, of evaporated oil in the blow-by is dependent on the temperature of combustion gases and components and the volatility of the oil.

The entrainment of droplets has been termed misting. The source of these droplets has not been known. Some theories suggest they result from the condensation of oil vapour as the blow-by gas cools and expands, particularly as it enters the crankcase. Other theories suggest that the droplets are produced from mechanical action on the oil film surface. Gamble (2003) applied the correlations of Ishii (1989) and Akagawa

(1985) for droplets entraining into a gas flow over a film in a straight duct, Figure 2.18, but concluded that this was not a significant mechanism.

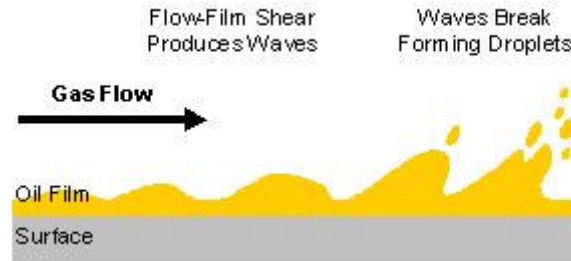


**Figure 2.18: Entrainment of Droplets from a Film on a Surface**

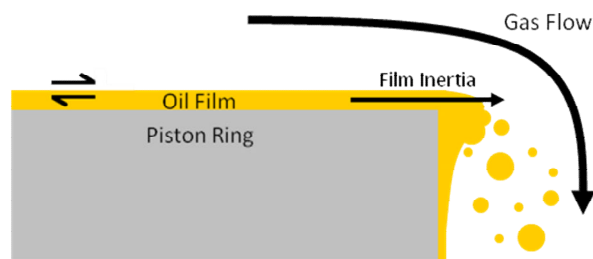


**Figure 2.19: Formation of Droplets at Component Edge**

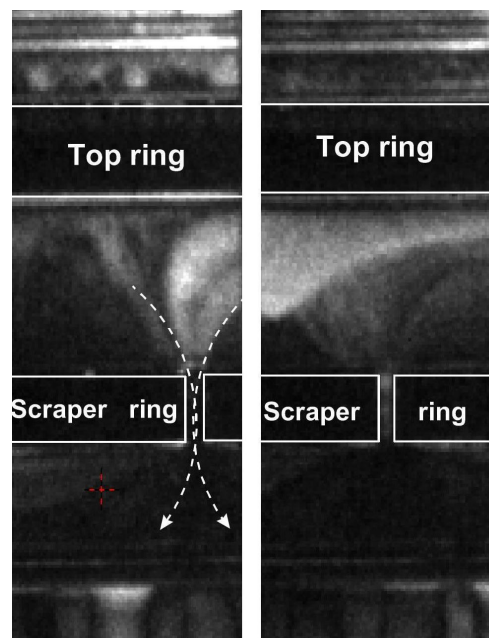


**Figure 2.20: Interaction between Blow-By Gas and Oil at Ring Gap, form Thirouard (1998)**

DePetris (1996), Cho (2004) and Burnett (1992) considered the droplets to be formed from inertial flow of oil reaching the edge of a component. Under these conditions, the inertial energy overcomes the free surface energy (surface tension) and the surface deconstructs, Figure 2.19. The free surface energy tends to the state of lowest potential and therefore acts to keep the oil film on the surface. Others such as Thirouard (1998) and Yilmaz (2004) developed this idea. Thirouard observed, using 2-D LIF, that the flow of oil gas through the ring gaps produces extremely high velocities and shear forces and hypothesised that this mechanism is likely to cause surface destruction and droplet formation at a higher rate than by inertial means (Thirouard et al., 1998), Figure 2.20. Day (2008) suggested that droplets are generated by the flow of gas through the lubrication film between the ring and liner. She suggested that the honed surface finish of the liner contributed to this. However, this theory seems dubious as tests were performed with a static piston, thus eliminating entrained oil through the contact and does not consider blow-by gas pressure that increases the contact pressure between the ring and liner, and the conformity of the surfaces. All of these factors produce strong sealing of the ring and liner contact and strong resistance to the flow of gas through the contact. There is no definite evidence for the source of droplets: Therefore they have not yet been incorporated into any oil transport model. The former three theories are all likely to be realised in the engine environment. However, the dominant mechanism has not been identified experimentally or theoretically (Gamble, 2003; Yilmaz et al., 2004).

There are significant implications for lubrication with the entrainment of oil in the blow-by gas. The flow of reverse blow-by into the combustion chamber is likely to be a significant cause of oil consumption and associated emissions and deposits (Daskivich, 1980; Furuhashi et al., 1981; Saito et al., 1989; Burnett, 1992; Gulwadi, 1998; Min et al., 1998; Tian et al., 1998; Tian, 2002; Tian, 2002; Tatli et al., 2008; Usui et al., 2008). It is also hypothesised that the fractions of oil entrained in the blow-by gas will undergo more rapid chemical and physical degradation due to the greater mixing of reaction products. This theory has yet to be reported as being investigated (Saville et al., 1988; Nattrass et al., 1994; Kinsey et al., 2006; Tatli et al.,



2008). These theories hypothesise that the increased surface area to volume ratio of a droplet compared to the equivalent film on a surface will increase this effect.

Several models have been produced that include all of the quantifiable mechanisms - Scraping, inertial movement, shear-driven flow (Keribar et al., 1991; Gulwadi, 1998; Gamble et al., 2002). These have shown good agreement with experimental observation through a cycle. However, over the length of the whole cycle, these still show a net movement of oil downwards through the piston assembly, (Gamble, 2003). This, as previously discussed, is not sustainable and cannot be the full explanation. Therefore, significant study is being undertaken into quantifying these other mechanisms. Misting is seen as particularly important within this, as this has implications beyond oil transport, in degradation and oil consumption.

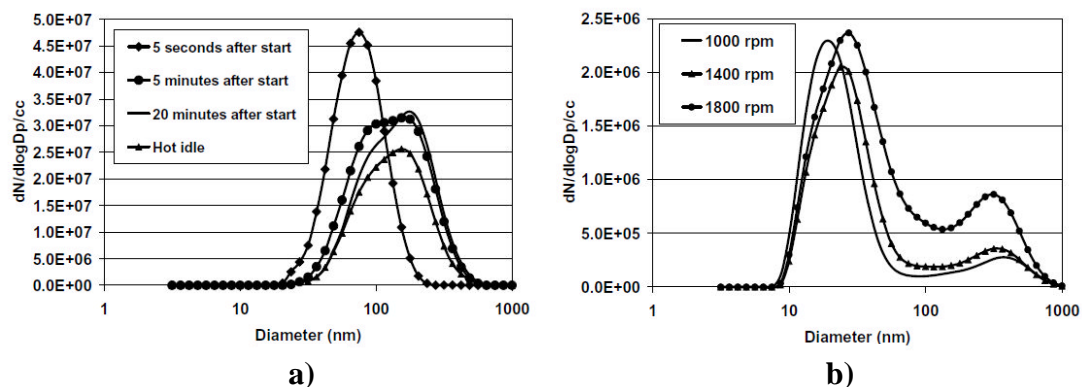


**Figure 2.21: Particulate Emissions from the Crankcase of a Large Diesel Engine, from Tatli (2008); a) DDC 60, b) Mack**

The only studies to date that consider two-phase flow in the gas flows in the engine have been focussed on particulate emissions from the crankcase. Studies by Clark (2006) and Tatli (2008) have extracted gas from the crankcase of heavy duty diesel engines and measured particle sizes. They found that the size distributions were sometimes unimodal i.e. one characteristic size, and sometimes bimodal i.e. having

two distinct characteristic sizes. Unimodal distributions had sizes of between 80-200nm, Figure 2.21a, and bimodal distributions of 20-80nm and 100-700nm, Figure 2.21b. This data was for different engines under different operating conditions. However, both unimodal and bimodal distributions were sometimes seen in the same engine. The study was not able to determine any reason for the changes in distribution (Tatli et al., 2008).

## 2.5 Oil Consumption

It has been reported that 60-90% of an engine's oil consumption is sourced in the piston assembly, (Brown et al., 1993; Yilmaz et al., 2004) respectively. Therefore, an important development in models and experimentally is consideration of the oil reaching the combustion chamber. Initially, models considered the quantity of oil that would be scraped above top dead centre, TDC and how much would be exposed to burning on the liner when the piston is near the bottom of the stroke (Truscott et al., 1983). These, understandably showed that oil consumption would be greatest at higher speed. Increases in load would result in higher oil flow rates into the crankcase due to the larger scraped volumes during the combustion stroke, resulting from the higher gas pressures. Experimental work suggested that an increase in load can produce an increase in oil consumption (Daskivich, 1980). Some models included inertial effects (Gulwadi, 1998; Gamble et al., 2002), and other models that incorporated blow-by models and the associated shear-driven transport, included these mechanisms in theoretical oil consumption calculations (Keribar et al., 1991; Gulwadi, 1998; Gamble, 2003). Whilst these agree on the variation of oil consumption with speed, these considerations introduce a dependence on ring gap position. The model of Gamble (2003) considered out of phase ring gaps to provide the greatest movement of oil. However, whilst there is a clear connection between blow-by and oil consumption, modelling work in this area is limited due to a lack of understanding of how much oil is entrained in the blow-by gas flow (Daskivich, 1980; Furuhashi et al., 1981; Saito et al., 1989; Bailey et al., 1990; Burnett, 1992; Lee et al., 1994; Min et al., 1998; Ishihara et al., 1999; Tatli et al., 2008). This stems from a lack of knowledge about the quantity and source of oil vapour and droplets. These models

provide some prediction of oil consumption but, owing to their clear limitations identified in lubricant supply, they cannot be considered complete until these unquantified mechanisms - evaporation, misting, ring pumping - are incorporated.

## **2.6 Automotive Lubricant Formulation**

Modern automotive lubricants are highly complex fluids. The properties of the base oil are supplemented by the inclusion of other additive chemicals. Whilst the properties of a base oil can be controlled with reasonable precision, additives allow lubricant properties to be extended beyond the confines of base oil properties. Thus, the overall properties of the lubricant can be tailored more specifically to its application.

### **2.6.1 Base Oil**

Automotive lubricant oils generally fall into two categories:

- Mineral oil
- Synthetic oil

### **2.6.2 Mineral Oil**

Mineral oil is produced by the refining of crude oil. Mortier (2010) described the different refining techniques are used to make the oil properties more advantageous. Generally, a greater degree of refinement serves to narrow the distribution of molecular weights within the oil. This allows a finer control of viscosity, volatility etc. Processes like solvent extraction and hydrocracking also include mechanisms to refine the chemistry of the oil too. Saturated hydrocarbons, such as paraffins and naphthenes, are oxidised much less readily than unsaturated hydrocarbons, such as aromatics. Therefore it benefits the long term performance of the lubricant for the oil to contain as many saturated molecules as possible. In solvent extraction, polar i.e. unstable, molecules react with the extracting solvent and are removed. As well as unstable hydrocarbons, compounds containing sulphur, oxygen and nitrogen are

removed by this process. Hydrocracking uses metal catalysts rather than solvent and produces oils with a higher fraction of saturates. As the name suggests, the process involves the breaking of hydrocarbon chains into smaller molecules. This gives a somewhat arbitrary control over molecular weight distribution.

### **2.6.3 Synthetic Oil**

Synthetic oils are produced from oil products, but the extensive processing means they cannot be considered a refined product. The benefit is that their properties can be more precisely controlled than mineral oils. In particular, the molecular weight distribution of a synthetic oil is much smaller than that of an equivalent mineral oil. Many types of synthetics exist: Of particular note are polyalphaolefins, PAOs, which are the most common. These are synthesised from decane ( $C_{10}H_{22}$ ) molecules being joined together. This gives very fine control over molecular weight. PAOs are extremely stable, therefore oxidation rates are low. However, this high stability leads to problems with additive solubility. Therefore, most commercial synthetic lubricants are a combination of PAO and a more polar synthetic, such as an ester, to balance oxidative stability and solubility (Mortier et al., 2010).

### **2.6.4 Base Oil Classification**

Various industry standards control the properties of base oil. The extent of refining is defined using the American Petroleum Institute's API Base Stock Classification. This differentiates oils according to their saturated hydrocarbon and sulphur contents and considers the Viscosity Index, VI, of the oil (Mortier et al., 2010). Groups I-III are normally termed mineral oils whilst Groups IV and V are considered synthetic oils. However, some (generally US) organisations consider Group III to be synthetic. A summary of the API Base Stock Classification is shown in Table 2.1.

The viscosity of a base oil is categorised by the SAE J300 Oil Viscosity Grade system. This groups oils according to their viscosity at particular temperatures. This is shown in Table 2.2. These refer to single grade or monograde lubricants. Due to the

reduction of viscosity with increasing temperature, monograde oils have often sub-optimally low viscosity at high temperatures i.e. in use, and sub-optimally high viscosity at low temperatures i.e. at start-up. This is described by the Vogel equation, Section 2.3.1. Because of this variation, some oils are classified as summer grade, where their specification is defined by the viscosity at higher temperature. Summer grades are given only a number. Likewise, winter grade, a number with a suffix ‘W’, is given to oils produced to give a known viscosity at low temperature.

Group	VI	Saturates	Sulphur	Type
I	80-120	<90%	≥0.03%	
II	80-120	≥90%	<0.03%	
III	>120	≥90%	<0.03%	
IV				PAOs
V				All others

**Table 2.1: API Base Stock Classification (Hadsburg, 2003)**

SAE Viscosity Grade	Low Temperature Dynamic Viscosity (mPa.s)		Kinematic Viscosity at 100°C (mm <sup>2</sup> s <sup>-1</sup> )	
	Cold Cranking Maximum	Pumping Maximum without Yielding	Minimum	Maximum
0W	3250 at -30°C	30000 at -35°C	3.8	-
5W	3500 at -25°C	30000 at -30°C	3.8	-
10W	3500 at -20°C	30000 at -25°C	4.1	-
15W	3500 at -15°C	30000 at -20°C	5.6	-
20W	4500 at -10°C	30000 at -15°C	5.6	-
25W	6000 at -5°C	30000 at -10°C	9.3	-
20	-	-	5.6	<9.3
30	-	-	9.3	<12.5
40	-	-	12.5	<16.3
50	-	-	16.3	<21.9
60	-	-	21.9	<26.1

**Table 2.2: SAE J300 Oil Classification (Taylor, 1993)**

To reduce this effect, viscosity modifier additives, VMs, are added to flatten the Vogel curve. Such oils are termed multigrade as they have significantly different

behaviour at different temperatures compared to monogrades. Multigrade oils are therefore assigned a winter grade for behaviour at low temperatures and a summer grade for behaviour at high temperatures, according to the SAE J300 classification Table 2.2.

The nature of the Vogel curve is described commercially by the Viscosity Index VI. In this, an oil is compared with values for standard references from specific oil fields, Pennsylvania and the Gulf Coast, with equivalent viscosity at 100°C. The subsequent difference in viscosity of the test oil and the references at 40°C is rated on a 0-100 scale (Williams, 2005):

$$VI = 100 \times \left( \frac{L - U}{L - H} \right) \quad [2.4]$$

Where  $U$  is the viscosity of the test oil at 40°C, and  $L$  and  $H$  are the viscosities of Gulf and Pennsylvania oils at 40°C, respectively, that have the same viscosity as the test oil at 100°C

This system was established when Group I monogrades were dominant so the original scale has been exceeded. Values up to 130 are possible with hydrocracking and up to 400 with modern Viscosity Modifiers. The terms Viscosity Modifier, VM, and Viscosity Index Improver, VII, are interchangeable.

### **2.6.5 Tribofilm-Forming Lubricant Additives**

Various chemical additives are used in commercial lubricants to improve performance in the desired application. In an automotive lubricant, the additives are tailored to the demands of the tribological environment - all lubrication regimes, high temperature, high shear rate, high pressure, exposure to reactive chemicals. A large proportion of the additives included in an automotive oil are designed to improve the performance of the surfaces of the contact by forming significant films with beneficial properties, Figure 2.22. These are termed tribofilms, because such films are dependent on the

tribological environment for their formation and, thus, their functionality in protecting this same environment. Anti-wear additives e.g. zinc-dialkyl-dithio-phosphate (ZDDP) friction modifiers e.g. molybdenum-dithio-carbamate (MoDTC), and corrosion inhibitors are additives that function in this way (Korcek et al., 2000; Nicholls et al., 2005; Toplovec-Miklozic et al., 2007; Fan et al., 2008; Mistry et al., 2008; Mortier et al., 2010).

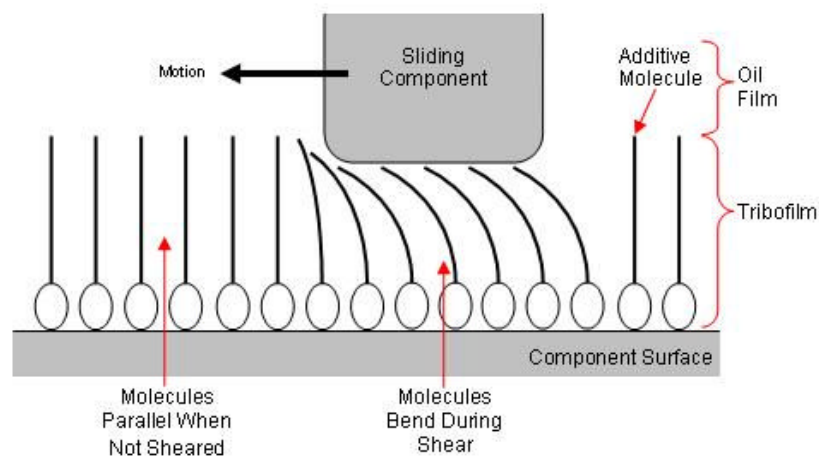


**Figure 2.22: Schematic of a Tribofilm**

### 2.6.6 Surface-Active Lubricant Additives

Surface-active additives perform a variety of functions at the many and varied interfaces encountered by the lubricant. These are polar chemicals that are attracted to interfaces. Many are amphiphilic in order to lend solubility i.e. having oleophobic, oil rejecting, heads and oleophilic, oil attracting, tails (Mortier et al., 2010).

### 2.6.7 Detergent

Detergents are included to neutralise the acids that form from combustion by-products. Oxides dissolve in any water present in the engine to form acids that damage components. Sulphuric acid is formed by the oxidation of sulphur in the fuel

and lubricant, oxy acids from the oxidation of the lubricant, and nitro acids are formed by the oxidation of nitrogen in the air (Mortier et al., 2010).

Detergent molecules are formed from an oleophilic long chain hydrocarbon tail for solubility, connected to a bridging molecule, which connects to a polar metal head on which the acids are neutralised. Bridging molecules vary. Sulphonates are most commonly used. Phenates are also widely used. Both are commonly used together to further tailor performance (Mortier et al., 2010). However, sulphonates have damaging effects on catalytic converters if burned or emitted through the exhaust. Therefore, as emissions regulations tighten, salicylates are becoming more common.

The polar substrate of the detergent, the tail and bridging molecule, can be produced as neutral or overbased. Overbasing makes the substrate alkaline, increasing the total base number, TBN. This allows more acid to be neutralised for a given volume of detergent before it is exhausted. This makes overbased detergents more advantageous (Mortier et al., 2010). Detergents comprise up to 4% by weight of a typical lubricant (Mortier et al., 2010).

### **2.6.8 Dispersant**

Dispersants are designed to manage the larger contaminants in the oil. Particulates and sludge are by-products of combustion and oil oxidation. These can settle on surfaces and form deposits. The purpose of dispersants is to keep these substances in suspension in the oil to prevent this. Dispersant molecules constitute a polar head which is drawn to the surface of the contaminant, and an oleophilic tail (a long chain hydrocarbon) for solubility in oil. Dispersant molecules cover the surface of a contaminant and suspend it in the oil (Taylor, 1993; Mortier et al., 2010). This formation is termed a micelle, Figure 2.23. The most common types of dispersant are succinimides and succinate esters. Polyisobutylene, PIB, is commonly used as a tail (Bair et al., 2003; Mortier et al., 2010). Dispersants comprise 4-8% by weight of a typical lubricant (Mortier et al., 2010).



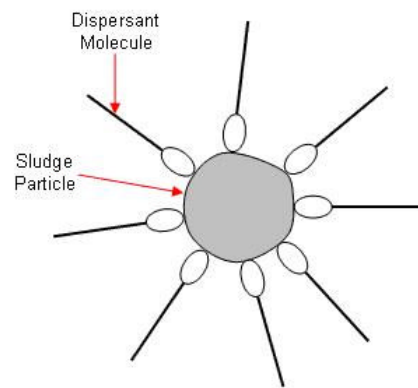


**Figure 2.23: Schematic of a Sludge and Dispersant Micelle**

### 2.6.9 Anti-Foam

The churning and pumping of oil in the piston rings and the blow-by gas flows can produce foams that hinder oil flow, especially through the piston. In order to remove foams, small quantities of silicone fluids e.g. polydimethylsiloxanes, are included in formulations. As these have a lower surface tension than oil,  $\approx 21 \text{ mNm}^{-1}$  compared to  $\approx 30 \text{ mNm}^{-1}$ , they promote the breaking of the thin films between the foam bubbles, causing the foam to collapse (Watkins, 1973; Mortier et al., 2010). Such chemicals have poor solubility in oil, so can only be included in very small quantities. Concentrations of 0.001% (10ppm) by weight are typical for an automotive lubricant (Taylor, 1993).

### 2.7 Viscosity Modifier or Viscosity Index Improvers

The purpose of viscosity modifiers, VMs, is to reduce the variation of viscosity with temperature beyond the feasible parameters of the base oil (Glass et al., 1991; Klaus et al., 1991; George et al., 1993; Sorab et al., 1993; Chen et al., 1994; Williamson et al., 1997; Bair et al., 2007). They are long chain hydrocarbon polymers, but come in various structures and orientations. Depending on the desired performance and polymer type, viscosity modifier can comprise up to 9% by weight of a typical

lubricant (Taylor, 1993). Some are linear chains, such as olefin co-polymers (OCP) and polymethacrylates (PMA), and some are star polymers, such as polyisoprene and styrene-co-isoprene (Taylor, 1993; Mortier et al., 2010). The general mechanism is that at low temperatures, low energies result in the polymers contracting, thus the molecular volume is small and bulk oil properties dominate, Figure 2.24. At higher temperatures, the higher energies in the polymers result in molecules uncoiling. This increases the molecular volume and, nominally, lends the properties of the polymer to a larger proportion of the bulk oil. The extent of this effect is strongly dependent on the type of polymer (Bezot et al., 1993).

This latter simplistic explanation is a generalisation of two mechanisms. The first is that the higher volume, and thus the higher degree of constraint, of the polymer results in an effective increase in the polymer's resistance to shear, i.e. viscosity. The second is that the increased volume of the polymer molecule at higher concentrations can lead to large scale interaction between polymer molecules. This is termed entanglement, and further increases the shear resistance of the fluid, increasing viscosity. The extent of these mechanisms, and thus the viscosity modifier performance, is based on the molecular weight, structure and concentration of these polymers. Typical commercial formulations often blend different viscosity modifiers to more precisely tune viscosity-temperature response (Mortier et al., 2010). However, these blends tend to be variations of molecular weight rather than molecular structure.

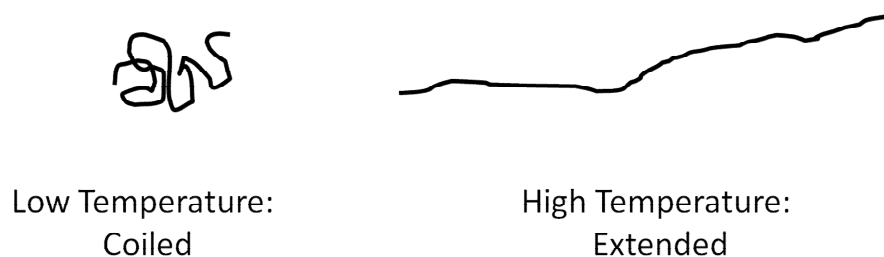


**Figure 2.24: Temperature Response of Linear Viscosity Modifier Molecules**

## 2.7.1 Linear Chain Polymers

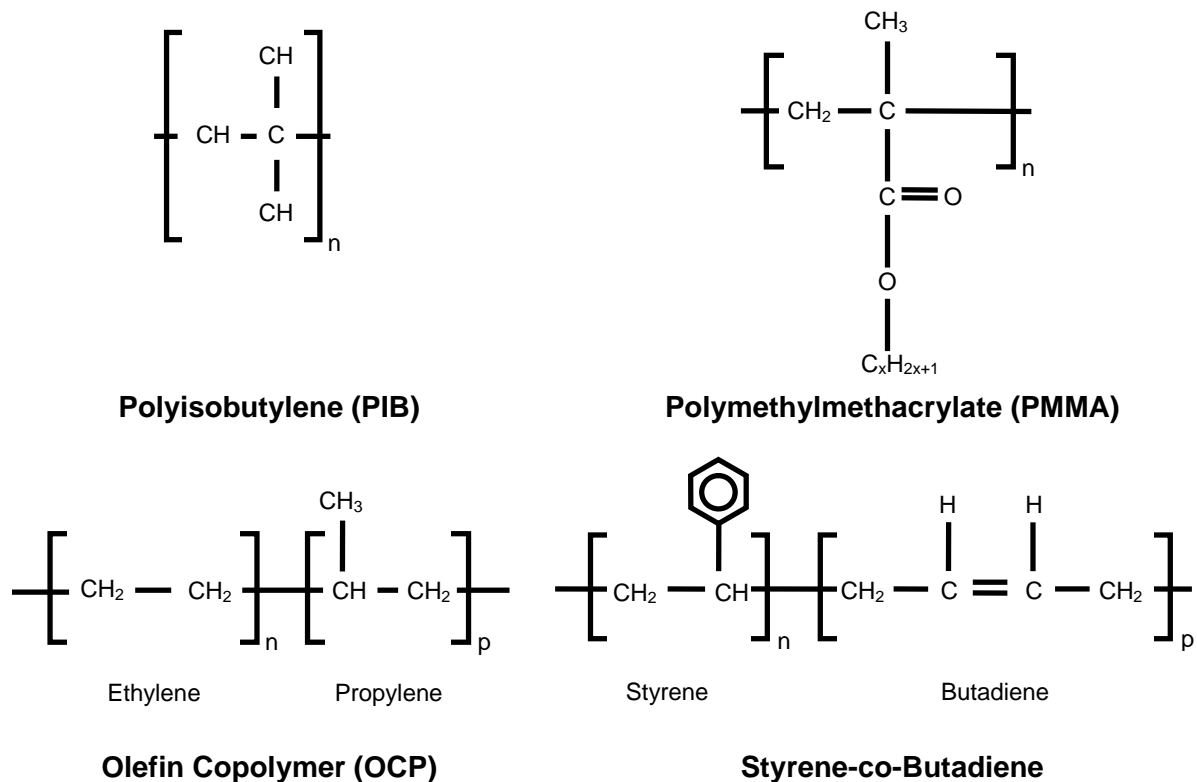
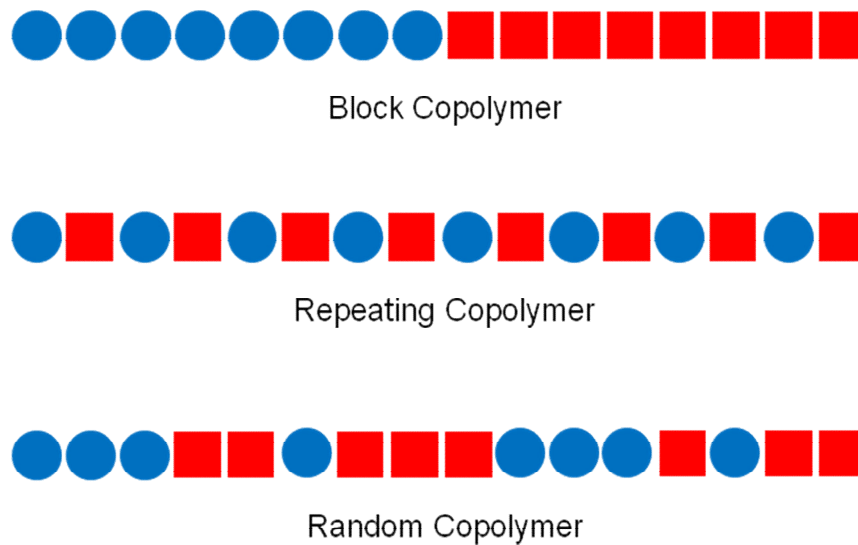


Figure 2.25: Repeating Units in Common Linear Viscosity Modifiers (Taylor, 1993)

Linear polymer chains are the simplest types of viscosity modifier to be used. These were the first to be developed and have been used in lubricants for several decades. Olefin copolymers, OCPs, and polymethacrylates, PMAs, are the most commonly used linear polymers (Peter-Wu et al., 1990; Klaus et al., 1991; Bair et al., 2007; Mortier et al., 2010), Figure 2.25. Copolymers refer to those composed of more than one monomer, Figure 2.26. OCPs are composed from ethylene and propylene in the range of ratio typically 45:55 to 55:45 (Covitch, 2003). PMAs have large side groups of varying size so tend to have a greater thickening effect. Methyl groups are commonly used in these side groups i.e. polymethylmethacrylate, Figure 2.25. Styrene-co-butadiene copolymers are also common viscosity modifiers (Mortier et al., 2010). In terms of the side groups, and thus thickening effect, these are something of an intermediate between OCPs and PMAs. Polyisobutylene is not generally used as a

viscosity modifier in modern lubricants, but is used commonly in dispersants (Bair et al., 2003; Bair et al., 2007; Mortier et al., 2010). Linear polymers are known for relatively high stability under shear. When shear induced cleavage occurs, they tend to break in the centre of the molecule, producing an approximate halving of molecular weight and, thus, a significant effect of their rheological contribution (Flamberg et al., 1994; Bair et al., 2007).



**Figure 2.26: Schematic Ordering of Copolymers**

Some linear viscosity modifiers are considered functionalised (Muller et al., 2006; Bair et al., 2007; Mortier et al., 2010). In these, another chemical group with other properties is attached to the end of the polymer chain. This is most commonly a dispersant group. These molecules can be seen as a normal dispersant molecule with an exceptionally long polymer tail. The term functionalised viscosity modifier merely indicates that the dominant property of the molecule is that of a viscosity modifier. The secondary properties, as well as those of a typical dispersant, Section 2.6.8, can allow the molecules to bond to a surface, forming a film: These show promising properties in reducing friction during boundary lubrication (Muller et al., 2006).

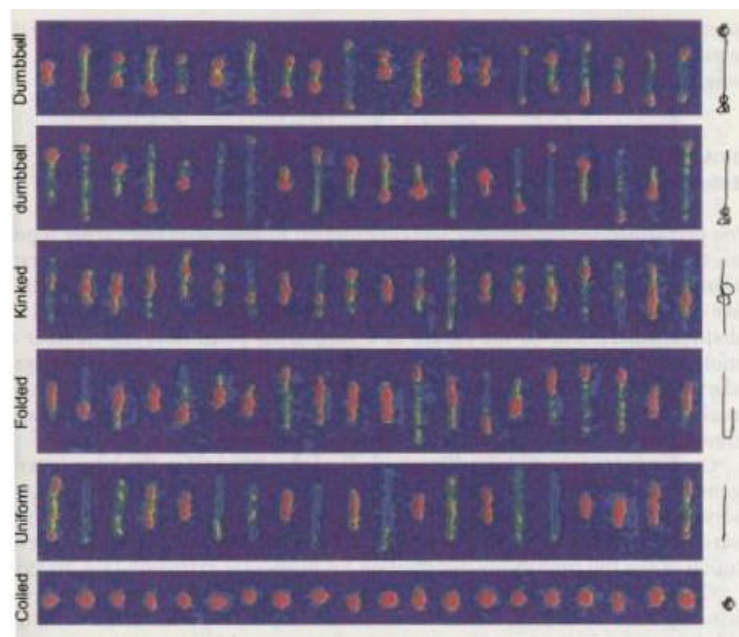


**Figure 2.27: Extension Mechanisms of DNA, Representative of Long Chain Polymer Viscosity Modifiers (Nguyen et al., 1999)**

There have been several studies investigating the dynamics of linear polymers with increasing temperature and with applied shear stress. Optical studies of polymer molecules in elongational flow i.e. under applied shear, have shown these mechanisms (Nguyen et al., 1999; Graessley, 2008). Polymers have clearly defined coiled properties when under low shear, which are broadly linearly elastic. Beyond this limit, the molecule responds non-linearly (Graessley, 2008). Extension increases exponentially with accumulated strain, a function of the shear stress and the residence time under shear. Once the molecule is completely extended, the limiting value of extension is reached (Graessley, 2008). Different modes of extension or uncoiling were observed. These are shown in Figure 2.27. This shows that it is rare for extension to be uniform. There is a tendency that, under uniaxial stress for linear molecules to align with the axis of stress (Schulz et al., 1991; Nguyen et al., 1999; Graessley, 2008). The energy required to align and stretch the molecules in this direction means oils containing such polymers respond extremely non-linearly under shear.

## 2.7.2 Star Polymers

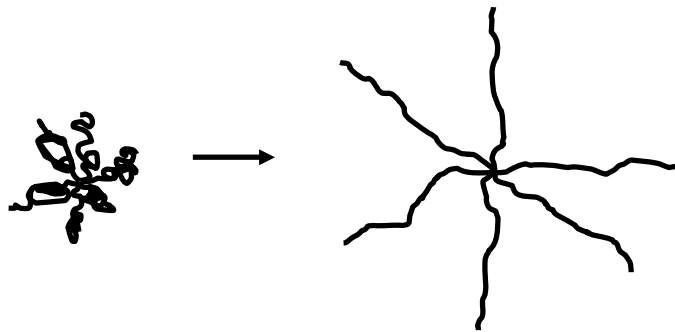


Figure 2.28: Extension of Star Polymers

Star polymers are a more recent development than linear polymers (George et al., 1993). They are considered more effective as viscosity modifiers as, when extended, their effective molecular volume is much greater than for linear polymers (Klaus et al., 1991; Bezot et al., 1993; Fetters et al., 1993; Bair et al., 2003; Stanciu, 2009). This enables more entanglements and interactions per molecule, enabling greater thickening at higher temperatures (Graessley, 2008). They are comprised of a complete polymer chains with several branched arms. Arms are grafted together chemically to form a star, Figure 2.28. Their advantage is that they are relatively simple. However, the large effective volume means they are more prone to degradation by chain scission, the breaking of carbon chain producing two or more smaller molecules, than linear polymers. Because the branched construction restricts the tendency of chains to align with shear, the response to shear is much less non-linear than for linear polymers. Such polymers can be homopolymers comprising only one monomer (repeating molecule) such as polyisoprene, polystyrenes (Bair et al., 2007; Mortier et al., 2010). Others are heteropolymers, more commonly referred to as co-polymers, which set different monomers in the same chain to optimise properties and manufacture (Bezot et al., 1993). Commonly used co-polymers are poly(isoprene-co-propylene) and poly(ethylene-co-propylene) (Mortier et al., 2010). The commonly used Infineum SV range of viscosity modifiers are hydrogenated poly(isoprene-co-styrene) (Stanciu, 2009). Some star polymers are not permanent structures, but bond with a micellar structure like dispersants, Section 2.6.8. These are resistant to long-term viscosity loss, as molecular breakup is not permanent. However, their

rheological effects at high shear are obviously compromised, rendering them analogous to many small linear polymers when the micellar structure is broken up.

### 2.7.3 Polymer Degradation

Polymer viscosity modifiers degrade in the piston assembly environment. As they are chemically very stable, the dominant degradation mechanism is physical. Chain scission is the most common mechanisms, whereby excessive stress and strain causes the central polymer chain to break. The scission of polymer chains reduces their molecular weight, which affects their function as viscosity modifiers (Taylor, 1993; Stanciu, 2009). Larger molecules tend to cleave more readily as they are generally subject to greater shear and bending stress due to greater interaction with other molecules. This places a practical limit on the molecular weight and, particularly, the chain length of viscosity modifier polymers. This is why star polymers are widely used, as they have a large effective molecular volume whilst not exceeding the practical limit of length. However, they are more prone to scission than linear polymers of equivalent function.

The industry standard test for assessing the shear stability of viscosity polymers is the fuel injector shear stability test, FISST, described in ASTM D5275-03 and D6278-07 (ASTM, 2003; ASTM, 2007), Figure 2.29. In this test, a Group II base oil is produced using viscosity modifier to SAE 10W40. 100cm<sup>3</sup> of the oil is cycled 20 times through a diesel fuel injector at 20.7 MPa (ASTM, 2007). This subjects the fluid to extremely high shear stress and strain, causing major chain scission. The loss of viscosity, given as a percentage of the viscosity increase the viscosity modifier gave to the base oil, is termed the shear stability index, SSI. Bair (2007) reports manufacturer's data and George (1993) investigates experimentally several standard VM polymers of comparable behaviour but unspecified molecular weight or concentration. This is shown in Table 2.3. It can be seen that, in general, linear polymers such as PMA, PIB and OCP have improved resistance to degradation when compared to star polymers, therefore retain their performance for a greater time. Other standard tests use sonic oscillators, rather than fuel injectors, to impart shear to the fluid, ASTM D2603-

01(07) (2010). The results of this test do not correlate well with those from the FISST rig for engine oils. However, this method has been found to be useful for hydraulic and transmission fluids.

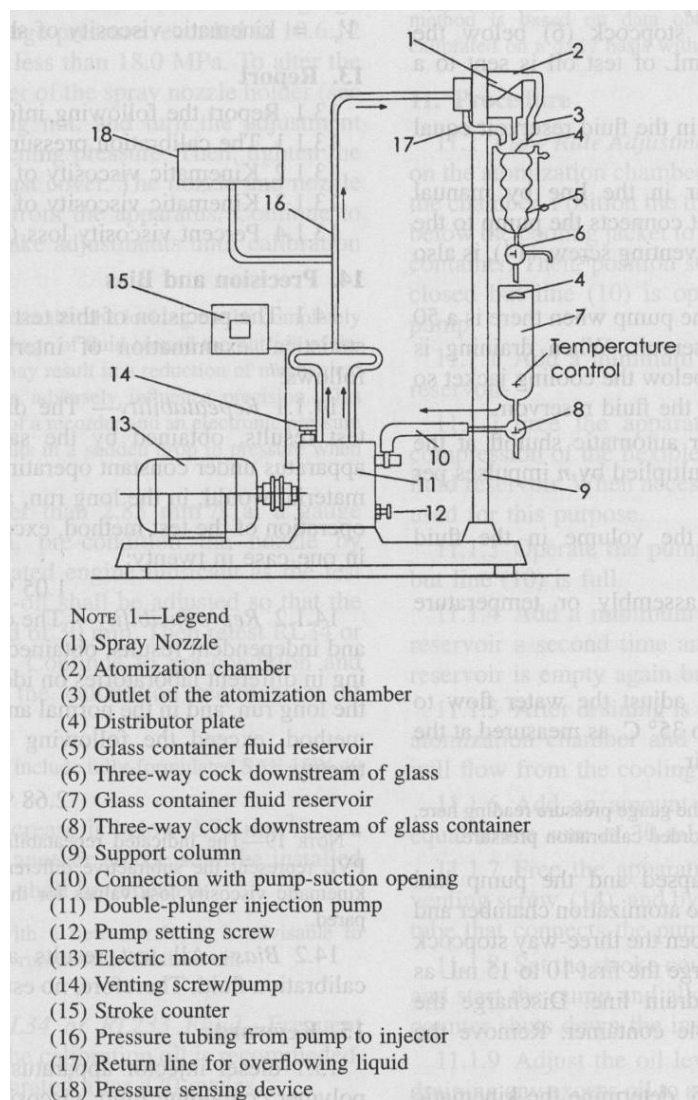


**Figure 2.29: FISST Rig for Measuring Shear Stability of Polymeric Fluids, ASTM 6278-07 (2010)**



Polymer Type	Shear Stability Index (%)
For an SAE 5W30 oil (George et al., 1993)	
OCP	9-19
Dispersant styrene ester copolymers	21
Styrene hydrogenated isoprene copolymers	19
Radical hydrogenated isoprene	4
Styrene hydrogenated butadiene copolymers	6-12
PMA	16
For an SAE 10W40 oil (Bair et al., 2007)	
(Non-dispersant) styrene 1	60
(Non dispersant) OCP 1	45-40
PIB 1	50
Unidentified star polymer	25
(Non-dispersant) styrene 2	15
(Non-dispersant) OCP 2	15
PIB 2	5
Dispersant PMA	0

**Table 2.3: Data for Fuel Injector Shear Stability Index Test for VM Polymers (ASTM D6278-02)**

## 2.8 Lubricant Degradation

The harsh environment in the piston assembly places extreme demands on the lubricant. Inevitably, the lubricant will lose its initial properties as a result of use and exposure to this environment. The mechanisms of degradation are numerous and complex (Zuidema, 1945; Taylor, 1993).

### 2.8.1 Thermal Degradation

As described by Lansdown (1994), at any temperature, lubricant oil degrades thermally, however slowly and insignificantly it may appear. Any increase in temperature will increase the reaction rate. Free alkyl radicals can be formed by any

chain breaking that may occur. This will form two alkyl radicals in the following reaction. R signifies an alkyl group and a dot signifies a radical, where the number of electrons is odd.



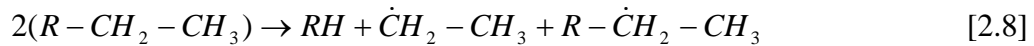
These will go on to react with further hydrocarbon molecules. The removal of hydrogen from other hydrocarbons produces more alkyl radicals by the following reactions.



or



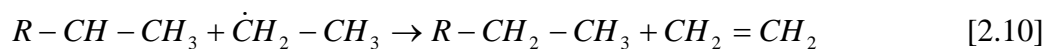
The following summarised reactions form a stable molecule and two alkyl radicals:



These radicals will continue to attack hydrocarbon molecules and the reaction chain will continue. The chain can be stopped by either the combination of radicals into a stable molecule,



or by reaction into stable molecules:



Lansdown (1994) describes how this reaction can typically progress through several hundred steps before termination.

## 2.8.2 Evaporation Loss

As previously described, the more volatile fractions of the lubricant evaporate more readily into the blow-by gas (Cecil, 1973; McGeehan, 1979; Ellermann et al., 1981; Guenther et al., 1998; Audette et al., 2000). This has the effect of skewing the molecular weight distribution of the base oil to be larger, thus increasing the viscosity of the oil (Cecil, 1973). With the current trend of base oils reducing in viscosity, this mechanism will continue to be significant. However, as refining techniques improve i.e. the commercialisation of Group III oils, and synthetic oils become more common, molecular weight distributions will become narrower. The volatility of the lubricant is an important indicator of this behaviour.

## 2.8.3 Additive Depletion

Additives are included to enhance the properties of a lubricant. The loss of additives and additive function will, therefore, reduce the performance of the lubricant. Additives such as ZDDP and MoDTC are consumed steadily with use, i.e. they form a tribofilm which is worn away and replenished from the bulk oil (Mortier et al., 2010). When all the additive has been used consumed, the tribofilm cannot be replenished, and performance will decrease. This principle applies to detergents and dispersants too. ZDDP also has antioxidant properties, which can also be depleted with time. Viscosity modifier polymers, as discussed in Section 2.7.3, are degraded by chain scission and become ineffective (Flamberg et al., 1994).

## 2.8.4 Low Temperature Oxidation

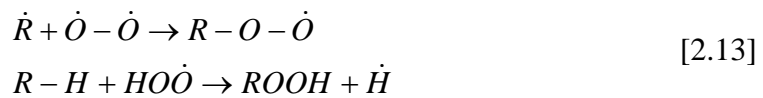
The main mechanism of base oil degradation is chemical, by way of oxidation. Oxidation has two distinct regimes (Lansdown, 1994). The first is termed low temperature oxidation,  $<120^{\circ}\text{C}$ , is slow and happens to the oil at every point in the oil system. The reaction occurring in three stages: Initiation, propagation and termination. Initiation most commonly begins with alkyl hydroperoxide (ROOH) which decomposes, leaving radical molecules:



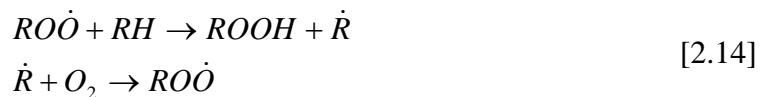
Oxygen may also react directly with a hydrocarbon to produce an alkyl radical:



When the radical is formed, it can react with an oxygen molecule to form an alkyl peroxy radical. The hydroperoxy radical from the second initiation can attack a hydrocarbon to produce alkyl hydroperoxide:



A simple mechanism of propagation involves the alkyl hydroperoxide producing more initiation reactions. The alkyl radical reacts with oxygen and a chain reaction becomes self propagating:



Lansdown (1994) again reports that over one hundred steps are typical before termination. Termination, as with thermal degradation, relies on radicals combining to form a stable molecule:



## 2.8.5 High Temperature Oxidation

Above 120°C, the oxidation reactions are significantly different than below this threshold. This behaviour is considered high temperature oxidation (Lansdown, 1994). In high temperature oxidation, two phases of oxidation occur. The first contains initiation and propagation steps similar to the low temperature reactions. The cleaving of hydroperoxides is the most significant stage as this produces a large quantity of hydroxyl radicals. Carboxylic acids form which produce esters and ethers. Some termination reactions occur as at low temperatures. However, the higher temperatures cause peroxy radicals to react in a non-terminating manner, forming alkoxy radicals. In the second stage, various polymerisation and polycondensation reactions take place, producing insoluble high molecular weight (approximately 2000) intermediates. These reactions can be catalysed by iron and can be slowed by lead. These chemicals then form sludge and varnish. The condensation of these chemicals causes the viscosity of the oil to increase, thus having profound effects on lubrication performance.

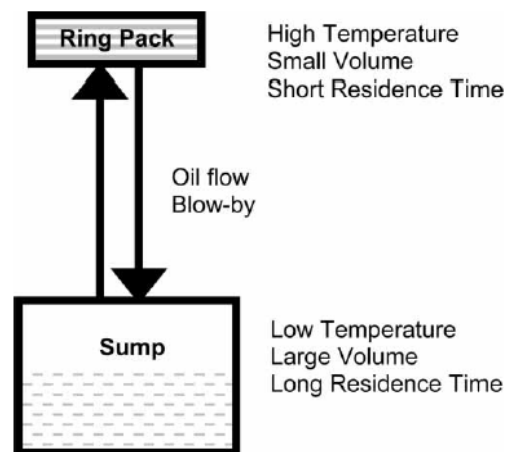


Figure 2.30: Schematic of the Yasutomi Assumption, from Lee (2006)

The significant difference between the high and low temperature reaction is manifested in the engine as a marked difference between oxidation in the sump and in the piston assembly. This is due to both systems being in different reaction regimes. The far higher reaction rate of the high temperature reactions accounts for the far

greater oxidation rate in the piston assembly. Yasutomi (1981) simplified this situation by describing degradation occurring exclusively in the small volume of the piston assembly, Figure 2.30. This has been observed in several experiments where lubricant is extracted from the piston assembly of a running engine using a tube routed loose through the crankcase or through a linkage (Moritani et al., 2003). This lubricant is heavily degraded and has high concentrations of common indicators of degradation, carbonyl groups.

### **2.8.6 Anti-Oxidant**

The oxidation rate of a lubricant drastically affects its life span by slowing or stopping the reactions, as described in Sections 2.8.4 and 2.8.5, at various stages. The two major types are radical scavengers and hydroperoxide decomposers. These work synergistically, so both are generally included in commercial formulations (Mortier et al., 2010).

Radical scavengers work simply by reacting preferentially with radical molecules so they do not react with oil molecules. This greatly reduces the oxidation rate by reducing the quantity of radicals to be reacted. The most common types of radical scavengers are sterically hindered phenols and aromatic amines (Lansdown, 1994; Mortier et al., 2010).

In the oxidation chain reaction, hydroperoxide is formed as a precursor to radicals (which are formed by the break-up of hydroperoxide). When hydroperoxide decomposers are present, they encourage hydroperoxide to decompose into non-radical molecules. This reduces the oxidation rate by reducing the production of radicals. The most commonly used hydroperoxide decomposers are organosulphur and organophosphorous compounds. As an organic sulphur and phosphorous compound, ZDDP makes a good hydroperoxide decomposer (Cecil, 1973; Masuko et al., 2007).

### **2.8.7 Nitration**

The presence of nitrogen oxides in blow-by gases reacts with the lubricant oil. These reactions are less well understood than those of oxidation. The presence of water can also lead to the formation of nitric acid in the lubricant, which can attack both the oil and the component surfaces (Gallopoulos, 1970; Powell et al., 1992; Moritani et al., 2003).

### **2.8.8 Fuel Dilution**

Unburned fuel can impact the oil film on the liner, particularly on the inlet stroke. This can serve to dilute the lubricant oil, reducing its effective viscosity and properties as a lubricant. The extent of this is partially dependent on the design of the engine. However, it is more dependent on the use of the engine. Winborn (2001) found that dilution levels on long motorway trips can be as low as 2% by weight but can be as high as 15-20% in short cold trips. Partially oxidised fuel can contribute to the chemical degradation of the lubricant. The thinning effect of fuel dilution opposes the thickening effect of chemical degradation. The balance of these processes is extremely specific to different engine designs. During repeated short cycles, one engine may cause oil to thicken and another to thin. However, over a long cycle, the higher operating temperatures will cause the fuel to evaporate and the degradation of the lubricant will be the dominant effect seen (Winborn et al., 2001). It is understood that the emulsifying properties of some biofuels can cause water to contaminate the lubricant too (De-Silva et al., 2010).

### **2.8.9 Particulates and Sludge**

Incomplete combustion or burning of lubricant can form soot, sludge or other carbon deposits (Zuidema, 1945; Covitch, 1988; Powell et al., 1992; Schwartz et al., 1994; McGeehan et al., 1999; Kinsey et al., 2006; Van-De-Voort et al., 2006; Diaby et al., 2009). These can be held in suspension in the oil, particularly with effective dispersants. These can, if they become extreme, increase wear rates, restrict oil flow

through the piston assembly and block oil filters. Carbon deposits such as varnishes and soot on surfaces (Zuidema, 1945; Powell et al., 1992; Schwartz et al., 1994; Kinsey et al., 2006) can increase wear of tribological surfaces (Burnett, 1992), restrict ring motion (Burnett, 1992), block injectors (Houser et al., 1992), restrict valve function (Caress, 1992; Houser et al., 1992), and interfere with blow-by gas flow. These effects are almost always but not exclusively negatively (Burnett, 1992) .

## 2.9 Summary

- Modern lubricants are complex fluids with large physical, chemical and tribological stress placed on them. The many additives they contain are designed to optimise performance and defend against degradation.
- The piston assembly environment, in particular, is a harsh environment for a lubricant. This is where the most lubricant degradation occurs.
- To understand the environment with a view to optimising performance, many studies have investigated the flow of oil through this system.
- Many different mechanisms of oil transport have been identified.
- As modelling and experimentation have developed, results have become more accurate and the implications of oil transport mechanisms for emissions, oil consumption and oil degradation have been better understood.
- Detailed models still predict starvation of lubrication in the piston assembly after relatively few cycles. This is clearly not the case and other mechanisms must be at work.
- Therefore, research is directed at the mechanisms that have not yet been quantified adequately. These are ring pumping, evaporation and misting.
- Of these, misting appears to have the greatest implications for oil consumption, emissions and oil degradation. It is also, to date, the mechanism that has been studied the least.



## **Chapter 3: Review of Relevant Studies on Two Phase Flow and Hydrocarbon Misting**

### **3.1 Introduction**

As described in Chapter 2, the nature of the mist in the piston assembly and crankcase of a fired engine is not yet known. Therefore, in this chapter, relevant literature from fields other than engine tribology is discussed, setting lubricant misting in the piston assembly in its context within the field of two phase flows, particularly those of hydrocarbons.

### **3.2 Two Phase Flow**

Two phase flow refers to a flow in which materials in separate states move together. For misting, this is a flow of liquid in gas. Whether the gas and liquid are chemically identical or different affects the boundary between the phases, and the heat and mass transfer between phases.

#### **3.2.1 Classification**

The nature of a two phase flow is governed by the relative proportions of each phase and the Reynolds number. Many studies have sought to separate the various natures into regimes. These studies are often rather arbitrary and biased towards the subtleties of particular applications. However, several common flow structures are agreed upon (Hewitt et al., 1970; Ghiaasiaan, 2008), Figure 3.1. They refer to closed systems under steady-state conditions, so cannot be used to directly model the environment in the piston assembly. However, fundamental studies on the interactions between phases prove useful. Annular mist flow appears to best visually represent the flow

through the piston ring pack. Through the piston lands, the blow-by gas carries droplets through a channel covered with a lubricant film on all surfaces.

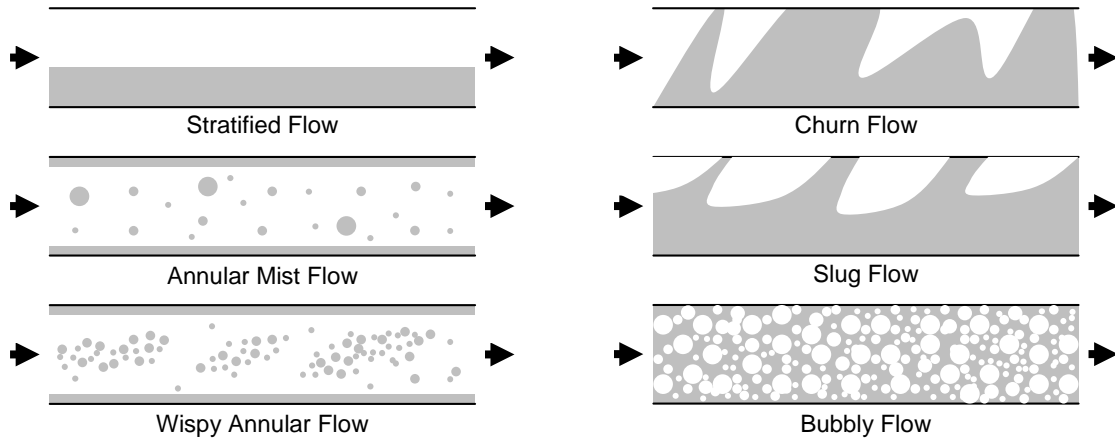


Figure 3.1: Classification of Two-Phase Flow Patterns (Ghiaasiaan, 2008)

### 3.3 Annular Mist Flow

Annular mist flow refers to a central core of droplets entrained in gas flowing over surfaces coated relatively uniformly in liquid. It is presumed that the liquid in the droplets and the film are of the same material and droplets are sourced from the film (Hewitt et al., 1970).

#### 3.3.1 Film Behaviour

The flow of gas over the film causes surface disturbance by shear and the eventual destruction of the surface, producing droplets. The entrainment of droplets from the film has been described by the mathematical correlations, firstly by Akagawa (1985):

$$\dot{v}_e = 4.88 \times 10^{-8} \left( \frac{B' \Delta h}{\lambda} \right) (u_{g0})^{4.5} \rho_1 \quad [3.1]$$

Where  $\dot{v}_e$  is the entrainment volume flow rate of liquid,  $B'$  is the disturbance wave length,  $\Delta h$  is the disturbance wave height,  $\lambda$  is the distance between disturbance wave peaks,  $u_{g0}$  is the superficial gas velocity and  $\rho_l$  is the liquid density. The correlation of Ishii (1989) is also used:

$$\dot{v}_e = (j_g^*)^2 (Re_f)^n \quad [3.2]$$

Where  $n$  is typically 1,  $Re_f$  is the Reynolds number of the fluid flow, and  $j_g^*$  is the dimensionless gas flux, defined as:

$$j_g^* = j_g \left[ \frac{\sigma g \Delta \rho}{\rho_g^2} \left( \frac{\rho_g}{\Delta \rho} \right)^{2/3} \right]^{-0.25} \quad [3.3]$$

Where, in turn,  $j_g$  is the total gas mass flux,  $\rho_g$  is the gas density,  $\Delta \rho$  is the difference in density between the liquid and gas, and  $\sigma$  is the interfacial tension between the liquid and gas.

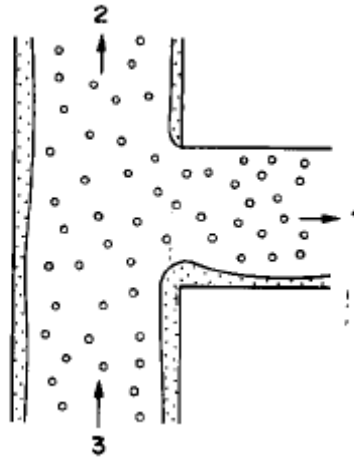


Figure 3.2: Schematic of Annular Mist Flow in a T-Junction from Sliwicky (1988)

Gamble (2003) applied these mechanisms to the flow of gas through the lands of the piston. They were not found to produce oil droplets in significant quantities. It is therefore hypothesised that droplets are broken from the surface at the piston ring

gaps. No studies have directly investigated this phenomenon. Sliwicky (1988), when considering annular mist flow past a branch in a straight pipe, highlighted the extremely large stresses placed on the film at the component edge, Figure 3.2. However, his model did not allow the surface to be broken and droplets to be produced.

### 3.3.2 Droplet Behaviour

Droplets can be deposited on the film surface. The rate of deposition is governed by the size of droplet and the Reynolds number of the flow around it (Crowe et al., 1998). An increase in droplet size produces an increase in the deposition rate. Akagawa (1985) also describes deposition as a function of total droplet flow rate:

$$\dot{v}_d = \dot{v}_e - \frac{1}{B} \frac{dG_E}{dz} \quad [3.4]$$

where  $\dot{v}_d$  is the deposition volumetric flow rate,  $\frac{dG_E}{dz}$  is the change in total droplet flow rate with downstream distance, and  $B$  is the channel width.

Various studies described how different ranges of droplet size exhibit greatly different properties (Holness, 1995; Lawes et al., 2006; Seinfeld et al., 2006). The simplest explanation describes three groups, aerosols, mists and sprays. Aerosol refers to droplets less than 10 $\mu$ m in diameter (Lawes et al., 2006). As they are extremely small, having low mass, the motion of aerosols are governed principally by diffusion. Due to their low inertia, aerosols are not readily deposited and therefore have an extremely high residence time in a gas flow. Aerosols are seen as ideal for combustion due to their high surface area to volume ratio. This ratio is typically described by the Sauter Mean Diameter, SMD (Crowe et al., 1998):

$$SMD = d[3,2] = \frac{d_v^3}{d_s^2} \quad [3.5]$$

Where  $d_v$  is the mean volume diameter:

$$d_v = \sqrt[3]{\frac{6V_p}{\pi}} \quad [3.6]$$

and  $d_s$  is the mean surface diameter:

$$d_s = \sqrt{\frac{A_p}{\pi}} \quad [3.7]$$

Where, in turn,  $V_p$  is the particle volume and  $A_p$  is the particle area. These latter parameters can be taken as the means of a distribution in order to calculate a mean SMD.

The high value of SMD in aerosol sized droplets gives a higher propensity for mass transfer i.e. evaporation and condensation, and chemical reaction than for larger droplets. Therefore, under cooling, there may be a significant increase in the volume of aerosol droplets due to high condensation flow rates into existing droplets (Davis et al., 2002; Ghiaasiaan, 2008).

Mists are commonly defined as droplets with diameters from 10-50 $\mu\text{m}$  (Lawes et al., 2006), although some industries prefer to lower this range to 1 $\mu\text{m}$ , encompassing most aerosols (Holness, 1995). Mists refer to droplets whose behaviour is greatly dependent on the conditions of the gas flow they are entrained within. i.e. the dynamic and kinematic forces acting on a droplet - gravity, inertia, drag, pressure - are of a similar magnitude. This makes mist droplets reliant on gas flows for their suspension, as diffusion forces are insignificant. Therefore a significant increase in the deposition rate can be instigated by a reduction in flow velocity, change in flow path, or an increase in droplet size. Generally, mist droplets change more greatly through destruction or coalescing than through evaporation or condensation, due to their large diameter but low SMD.

Sprays commonly refer to droplets with diameters greater than  $50\mu\text{m}$  (Edwards, 1995; Lawes et al., 2006). Such droplets contain much more kinetic energy and inertia than the gas flow around them can impart. Therefore, the behaviour of sprays is governed by droplet motion, particularly the degree of interaction between droplets i.e. coalescing or destruction. Sprays do not tend to stay entrained in their gas flow.

It is anticipated that lubricant droplets in each of these regimes are present in a typical engine. Aerosols are likely to form through the condensation of vapour in the cooling blow-by flow past the piston (Dasch et al., 2008), and through the destruction of larger droplets (Liu et al., 1997). Mists are thought to form in the piston assembly, particularly through the ring gaps, through the complex interaction of gas flow, oil film, and changing flow paths on complex components (Thirouard et al., 1998; Gamble, 2003; Thirouard et al., 2003; Yilmaz et al., 2004). Sprays are formed through throw-off, the inertial ejecting of droplets from components, particularly from the crankshaft and con-rod, but also from the piston (Burnett, 1992; DePetris et al., 1996).

### **3.3.3 Droplet Coalescence and Destruction**

In many systems, for example, a fuel injector, transfer between these flow regimes can be critical to its performance. Therefore, many studies have investigated these transitions (Crowe et al., 1998). Coalescence is the more difficult process to describe beyond the qualitative increase in droplet size. Much of the work on this subject is empirical and application-based as it is generally seen as a process by which deposition is achieved, therefore final droplet size is slightly meaningless. Whilst coalescence occurs naturally in two-phase flows, unless particles are charged, it can be increased in several ways. An increase in particle concentration i.e. droplets per unit volume, an increase in Reynolds number or a decrease in flow area are the most common ways to achieve this (Davies, 1973; Fischer, 1995; Crowe et al., 1998).

Droplet destruction has been much more thoroughly researched. Three regimes describe the behaviour of droplets (Arcoumanis et al., 1994; Liu et al., 1997), defined by the dimensionless parameter, the Weber number (McKinley, 2005):

$$We = \frac{\rho_G U^2 d}{\sigma} \quad [3.8]$$

Where  $\rho_G$  is the gas density,  $U$  is the relative velocity of the gas and droplet,  $d$  is the droplet diameter and  $\sigma$  is the interfacial tension between the gas and droplet liquid. This is the ratio of the inertial forces to the surfaces tension i.e. the forces pulling the droplet apart and those holding it together.

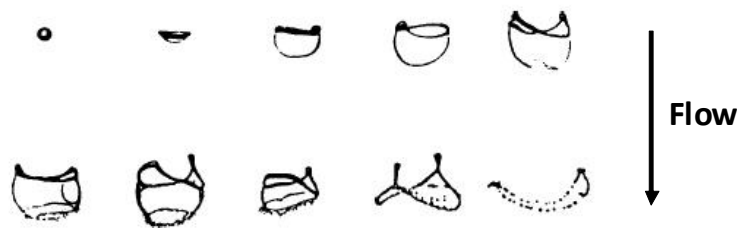


Figure 3.3: Droplet Bag Breakup, after Rotondi (2001)

At lower values of  $We$ , droplets remain intact. At Weber numbers between 12 and 80, droplets flatten under dynamic pressure and the droplet centre is broken, forming filaments of fluid, Figure 3.3. This mechanism is termed bag breakup due to the shape of the deformed droplet under these conditions.

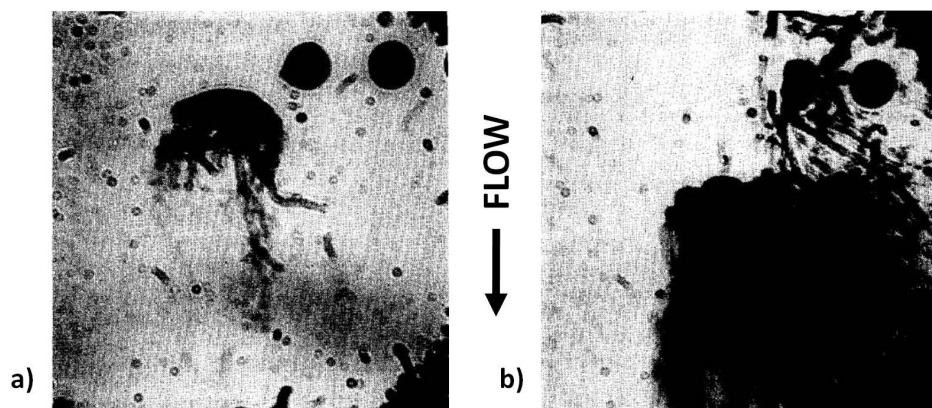


Figure 3.4: Droplet Breakup Mechanisms at Higher Weber Number a) Boundary Layer Stripping, b) Catastrophic Breakup, from Liu (1997)

For Weber numbers between 80 and 300, pressure drag causes large deformation around the periphery of the droplets, pulling filaments and droplets from the edges. This mechanism is termed boundary layer stripping, Figure 3.4a. For Weber numbers greater than 300, the huge difference in kinetic energy between the droplet and gas flow produces and almost instantaneous atomisation of the droplet, Figure 3.4b. This is termed catastrophic destruction and produces droplets much finer than the other mechanisms, generally mists, often aerosols. This latter behaviour is typical of the behaviour seen in high pressure sprays and jet breakup processes, such as fuel injectors (Yule et al., 1995).

### **3.3.4 Droplet Formation**

As described in Chapter 2, the sources of lubricant droplets in the piston assembly are potentially numerous. The condensation of oil vapour, the disturbance of an oil film by a gas flow, and the inertial breaking of the surface at component edges, with the oil film inertia resulting from either component acceleration or shear from a gas flow, are all considered to be sources of droplets in the piston assembly of a fired engine

### **3.3.5 Droplet Formation from a Surface Film**

A gas flowing over a surface film will produce a complex interface between the two phases. Where temperature differences exist, evaporation and convection will produce mass transport from the film. Shear between the film and gas flow will cause local changes in velocity. In a typical annular mist flow, Hewitt (1970) describes how this can give rise to a boundary layer, or critical layer, in the gas flow near the interface where the velocity may reverse. Shear instabilities in the interface, termed Kelvin-Helmholtz Instabilities, resembling waves, can also result, Figure 3.5. The critical layer forms initially on the downstream side of the wave peak, producing eddies that cause the wave to 'crest'. At higher viscosities, the critical layer will cover the waves more uniformly. Under extreme conditions, the critical layer may produce its own boundary layer, cresting the wave on the upstream peak, Figure 3.6. These interactions introduce shear stress to the film surface, which can cause droplets to be



removed from the surface (Hewitt et al., 1970; Trabold et al., 2000; Holowach et al., 2002; Nepomnyashchy et al., 2002; Ghiaasiaan, 2008).

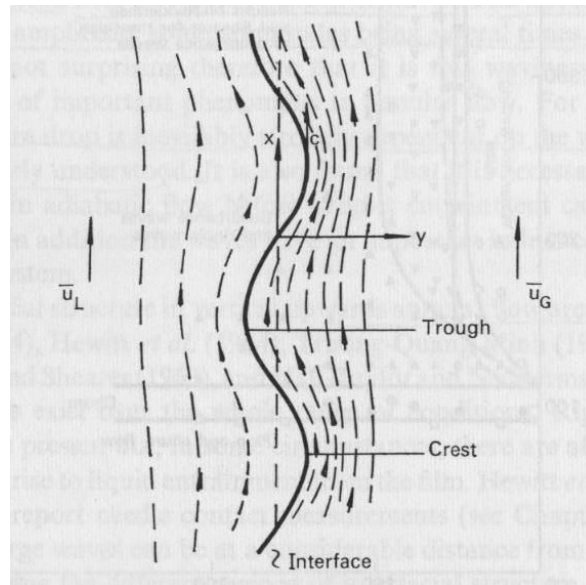


**Figure 3.5: Kelvin-Helmholtz Instabilities, from Hewitt (1970)**

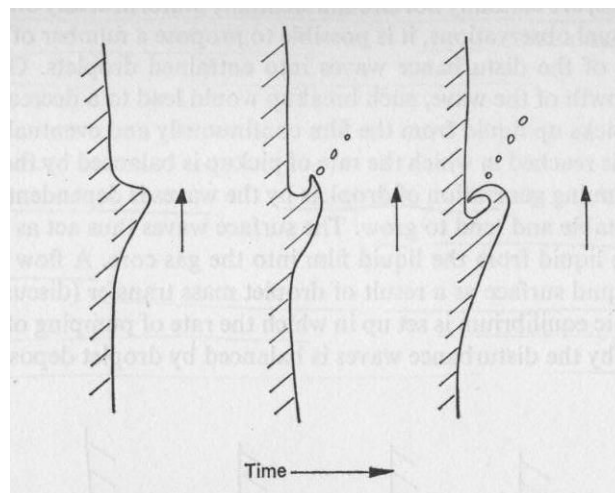


**Figure 3.6: Droplet Formation from a Surface Film, from Hewitt (1970)**

The process of removing droplets from the peaks of these waves has been described by the empirical correlations of Ishii (1989) and Akagawa (1985). Details of these are

given in Section 3.3.1. Gamble (2003) applied these correlations to the piston assembly. This suggested that droplets would be entrained at a maximum rate of between  $1.21 \times 10^{-26} \text{ m}^3 \text{ s}^{-1}$  (Ishii) and  $2.37 \times 10^{-70} \text{ m}^3 \text{ s}^{-1}$  (Akagawa) in the lands, a rate deemed insignificant. Maximum entrainment rates of  $5.34 \times 10^{-13} \text{ m}^3 \text{ s}^{-1}$  (Ishii) and  $6.47 \times 10^{-58} \text{ m}^3 \text{ s}^{-1}$  (Akagawa) were found for the top ring gap. Ishii's rate in the ring gaps was considered to be a more viable source of droplets, but still extremely low. Whilst this is likely to occur in the piston assembly, it is insignificant relative to other oil transport mechanisms.

### 3.3.6 Droplet Formation by Inertia

Studies into idealised annular mist flows, very often those investigating coolant flows in nuclear reactors where ducts are complex, identified the extreme conditions encountered by the film on reaching the sharp edge of a branch (Sliwicky et al., 1988; Teclemariam et al., 2003). Under these conditions, the surface tension of the film tends to retain the integrity of the film as it turns the corner, and the inertia of the film tends to remove the film from the surface. These studies observed that the inertia under these conditions may well overcome the surface tension, causing this film to at least partially leave the surface, forming filaments and droplets. However, no models exist to incorporate this behaviour (Sliwicky et al., 1988).

In the piston assembly, the concept of throw-off refers to this effect as films moving across component surfaces to their edges (Burnett, 1992; DePetris et al., 1996). Traditional definitions of throw-off describe the inertia as resulting from component acceleration. Such inertial effects have been observed on the piston surface using 2-D LIF (Inagaki et al., 1997; Thirouard et al., 1998; Wong et al., 2007). It is thought, however, that the inertia imparted to oil films on the piston lands by blow-by gas flows will far exceed that caused by component acceleration. This latter mechanism is likely to form droplets at the piston ring gap. These mechanisms are discussed in greater detail in Chapter 2.

### 3.4 Industrial Droplet Formation

Various applications of two phase flow require the controlled production of droplets. Several simple types of device, loosely termed mist generators, are used. Several of these are described.

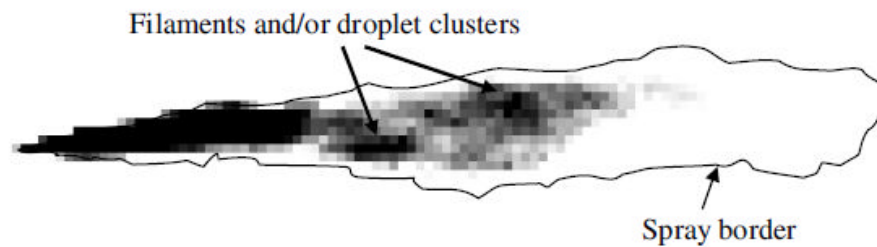


**Figure 3.7: Fuel Injector Spray, from Jakubik (2006)**

Fuel injectors are designed to atomise fuel in order to produce droplets with as large a value of SMD as possible, as a larger SMD increases combustion rates (Lefebvre, 1989; Willauer et al., 2007), Figure 3.7. Droplets with conventional diameters of less than  $25\mu\text{m}$  are considered good (Lawes et al., 2006). This allows the rapid production of vapour from the droplets, essential for combustion, and allows more complete combustion as small droplets can be completely oxidised far more rapidly. This is achieved by pressurising the fuel, over 10MPa in modern fuel injectors, and releasing it through one or several nozzles (ASTM, 2007). This produces a central jet of fuel that destructs into droplets as it encounters the surrounding gas. The central jet is surrounded by a cloud of droplets, fine droplets and vapour (Lawes et al., 2006). Fuel injectors have useful applications in quickly producing droplets and delivering large shear stresses to liquids (Obokata et al., 1995; Rottenkolber et al., 1999; ASTM, 2007; Hung et al., 2008). However, the mechanism by which the droplets are produced, a rapid expansion of a highly pressurised liquid through the surrounding gas, is not representative of any known mechanism of lubricant misting in the piston assembly.

Venturi mist generators are one of several common means of droplet production used in oil mist lubrication systems (ASTM, 1986; Bloch, 1987; Khonsari et al., 2005). A typical venturi mist generator is shown in Figure 3.8. A high velocity air flow passes

through a contraction into which oil is fed, which is atomised under the large shear stresses, and carried downstream. Baffles are often incorporated to give finer control over the droplet size (Khonsari et al., 2005). Venturis are convenient as the contraction increases gas velocity, thus shear stress on the oil, and the resulting drop in static pressure in the contraction often removes the need for a pump. This mechanism of droplet formation, disturbance of a film at a sharp edge by large shear forces exerted by a gas flow, could be adapted to represent the flow of oil and gas through the piston ring gaps, albeit with certain limitations such as the steady state operation.

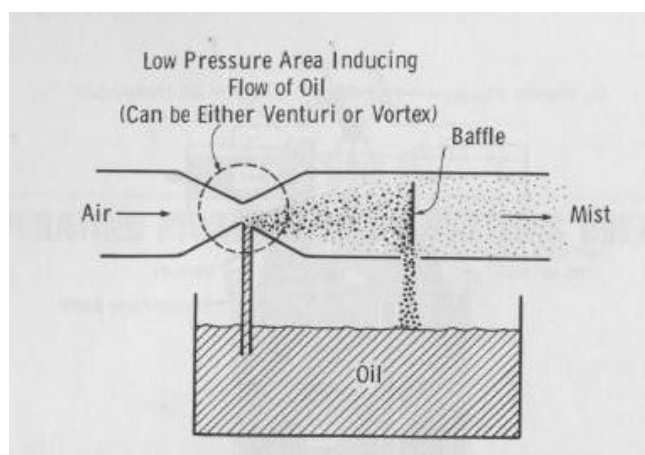


**Figure 3.8: A Typical Venturi Mist Generator, from Bloch (1987)**

Another common device in oil mist lubrication systems is the vortex mist generator (Bloch, 1987; Khonsari et al., 2005), Figure 3.9. This is extremely similar in principal to the venturi generator, however greater turbulence is produced by giving significant swirl to the air on entry to the contraction. Thus, the contraction is at a much greater angle than a conventional venturi. The turbulence generated produces a greater drop in static pressure and greater local gas velocities than in a venturi. However, the swirling flow at the outlet is much more difficult to control and keep droplets in suspension. Observations, discussed and shown in Sections 2.2-2.3 and 2.4.1, have suggested that the flow through the piston assembly does not produce large amounts of swirl and turbulence, making a venturi a closer representation of this flow than a vortex.

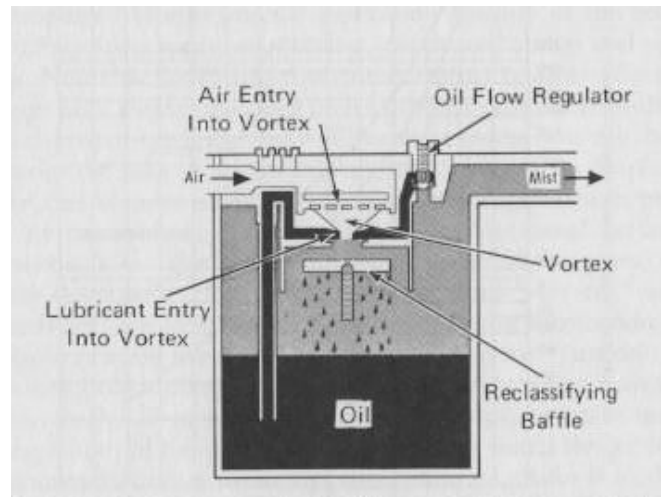


**Figure 3.9: Typical Vortex Mist Generator, from Bloch (1987)**

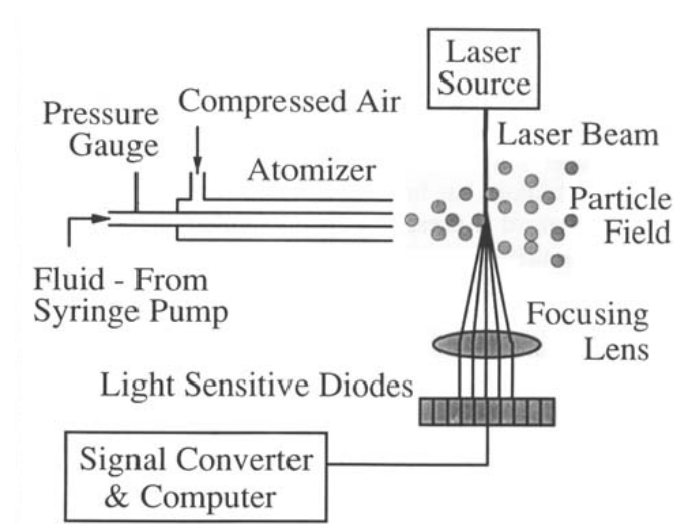


**Figure 3.10: Coaxial Nozzle Mist Generator and Particle Sizer, from Smolinski (1996)**

Various types of nozzle are used to produce droplets of mist (Arcoumanis et al., 1994; Shrimpton et al., 1995; Yule et al., 1995; Smolinski et al., 1996; Kim et al., 2003; Szydlo, 2007). Some discharge into static gas, while others discharge into moving gas. Some discharge only liquid, whilst others discharge both liquid and gas. For example, Marano (1995) and Smolinski (1996) investigated the mists produced in

metalworking oils using a co-flowing nozzle where oil was injected into the centre of an air flow, Figure 3.10. The difference in kinetic energy between the liquid and gas in a nozzle dictates the degree of relative dependency of droplet formation on the nozzle geometry or downstream droplet interaction. Thus nozzles can be designed precisely to their application, with reference to dimensionless parameters such as the Reynolds and Weber numbers (McKinley, 2005)

For other applications, mists can be produced by allowing droplets to fall into a high velocity gas flow at a controlled rate (Arcoumanis et al., 1994; Liu et al., 1997). This type of device relies on droplet destruction mechanisms to produce the desired droplet size distribution. In order for droplet destruction to occur and droplets to fall individually, the oil to gas ratios are required to be very low. Such devices are of little use in approximating the generation of mist in the piston assembly. However, they have value in investigating droplet breakup.

### **3.5 Hydrocarbon Mists**

Whilst hydrocarbon mists are not readily understood in automotive engines, they are more widely studied in other fields. Some of these are described here.

#### **3.5.1 Oil Mist Lubrication**

Oil mist lubrication is used on some large sites in heavy industry to centrally supply lubricant to critical components (Texaco Inc, 1968; Shell International, 1995; Paschall et al., 2003; Khonsari et al., 2005; Alemite LCC, 2011). A fine mist, generally  $<5\mu\text{m}$  diameter, of oil is generated and carried through various ducts to the components they lubricate, whereupon the mist is passed through fittings to coalesce the droplets into one resembling a spray, allowing it to be more directly applied to the component. Venturi and vortex mist generators are common devices for producing the mist. Standard test methods for determining the misting tendency of the lubricants for these systems use a venturi mist generator, ASTM D 3705-86(09) (1986), and calculate the misting tendency by measuring the accumulations of oil at particular points in a

standard system to determine the quantity of mist produced, (Szydlo, 2007), Figure 3.11.

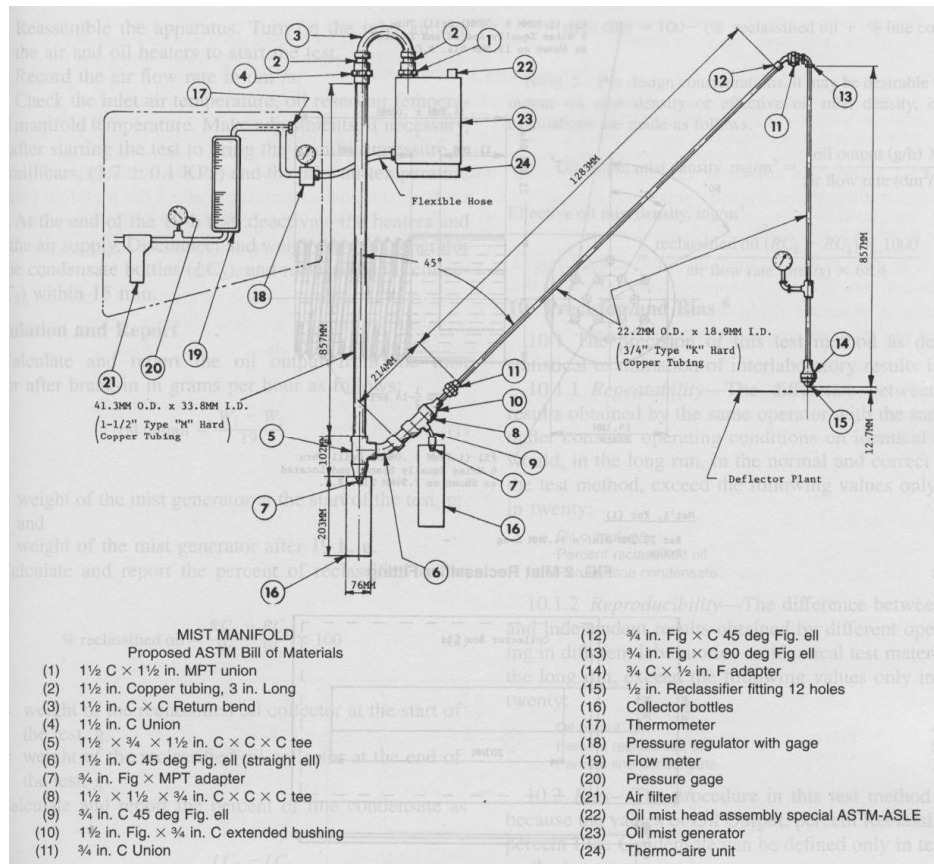


**Figure 3.11: Standard Apparatus for Measuring Misting Tendency of Oil Mist Lubricants, from ASTM D3705-86(09) (1986)**

Oil mist lubrication systems are designed to be in continuous operation with little supervision. Performance is monitored by measuring the temperature of lubricated components (which is also an indicator of more general failure) and the quality of the mist. The latter is measured very empirically by light obscuring detectors (Bloch, 1987). Such detectors work by passing the mist between a light source of known intensity and a detector. This records measurements of transmittance  $T$ :

$$T = \frac{\text{Measured Light Intensity in Use}}{\text{Measured Light Intensity in Clean Air}} \times 100 \quad [3.8]$$

Obscuration is often used as an alternative measurement where:

$$\text{Obscuration} = \text{Obs} = 100 - T \quad [3.9]$$

As light is scattered and absorbed by the mist droplets, the transmittance of the system is related to both the droplet size and the oil to gas ratio. Thus, assuming one of these parameters is largely constant, usually the droplet size, the mist quality is related to the known transmittance of an ideal mist, and safe operating boundaries are placed on the measured value (Bloch, 1987).

### 3.5.2 Marine Crankcase Mists

In large marine diesel engines, lubricant mists are of particular concern (Holness, 1995; Schaller et al., 2001). Oil mists, particularly in blow-by gases where fuel vapour may be present, are potentially extremely explosive, especially if pressures increase. In the crankcases of such engines, it can be extremely dangerous if mist accumulates and is allowed to pressurise, even slightly. Crankcase explosions are sufficiently common and dangerous to warrant the installation of safety systems. Such mists are formed from the condensation of evaporated lubricant as it enters the crankcase. The temperature gradient through the piston assembly and crankcase of marine diesel engine is much greater than in an automotive engine. Therefore, condensation of vapour is the dominant source of droplets by a considerable distance. The lower operating temperatures of such engines mean that evaporation of lubricant is not likely to occur under normal operation. However, during in the initial stages of failure, local component temperatures can rise significantly. Therefore, crankcase mist is seen as a sign of failure and safety systems are used jointly as cost-saving diagnostic tools (Smith, 2001).

Mist is detected using similar tools to those in the oil mist lubrication industry. Two common designs are used, obscuroimeters and nephelometers. Both systems pass the crankcase gas between a light source and a detector. As described previously, the scattering and absorbance of light by any mist present will decrease the transmittance.



In an obscurometer, the transmittance or obscuration is bounded by particular safe limits that trigger warnings or shutdown, Figure 3.12. In a nephelometer, the primary measurement is by a detector placed, generally, at  $60^\circ$  to the light source i.e. measuring light that has been scattered  $120^\circ$ , Figure 3.12. In this case, a positive measurement of light indicates the presence of mist, and safe limits are set on this value. In a nephelometer, the obscurometer system is used merely as a calibration for optical contamination. Nephelometer users say that their system is better because there is a set zero value, a linear response to mist concentration and means to correct for optical contamination (Holness, 1995; Smith et al., 2005). Obscurometer users say their system is better because it is simpler, correction for optical contamination and zero values is possible and that the signal response does not peak, thus eliminating the possibility that at higher concentrations, low values may be indicated (Schaller et al., 2001). Both systems are extremely empirical but sufficiently accurate for their applications.

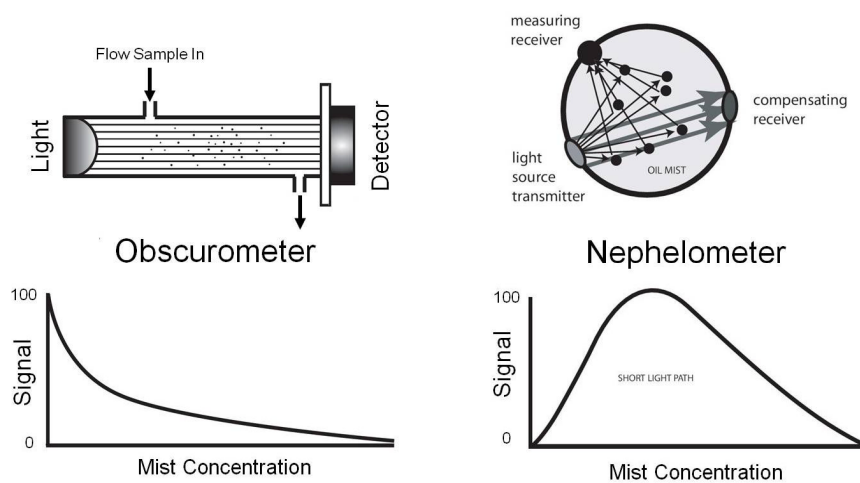


**Figure 3.12: Schematic of Obscurometer and Nephelometer Mist Detectors, after Smith (2005)**

### 3.5.3 Metalworking Fluids

In metalworking, the combination of rapidly moving components, high local temperatures and large temperature gradients means that droplets readily form. Of

particular concern are the mist and aerosol fractions of these droplets, due to their explosive potential and their effect on health if inhaled. The latter issue is dealt with in this country by the Health and Safety Executive, HSE, and in the US by the Occupational Safety and Health Administration, OSHA. HSE hazard determination guidelines (1997) dictate that machine works are required to keep airborne oil droplet volume concentrations to  $5\text{mg m}^{-3}$  if an environment is to be worked in for up to 8 hours, although current trends aim for  $0.5\text{mg m}^{-3}$  (OSHA, 2008). Concentrations are determined, according to requirements, by filtering ambient air at a known 2 litres per minute for 8 hours, and weighing the accumulated oil at the end of the shift. The detector can be placed on the shoulder of a machine operator. This method is described as being limited to those working with oils with a kinematic viscosity greater than  $18\text{mm}^2\text{s}^{-1}$  at  $40^\circ\text{C}$ , due to potential volatile losses during the test period, and deal only with liquid concentrations, neglecting vapour as this cannot be collected using this method. This highlights the challenges of sampling aerosols and mists, where vapour and liquid phases are not always clear, and composition can be altered significantly with small differences in temperature. However, it should be noted that metalworking oils have significantly lower viscosity than engine oils: Typically, these are  $10\text{-}20\text{mm}^2\text{s}^{-1}$  at  $40^\circ\text{C}$ , compared to  $36\text{mm}^2\text{s}^{-1}$  at  $40^\circ\text{C}$  for a 5W Group III engine oil (Hadsburg, 2003; Dasch et al., 2008), and thus have a significantly greater volatility, 20-55% compared to 5.2% respectively by the NOACK method (ASTM, 2005).

Other organisations have applied this, and similar, legislation and investigated preventative measures to reduce the concentration of oil droplets in the air. Large companies with large machine shops, such as Ford and GM, have done significant work on mist suppressants (Gulari et al., 1995; Marano et al., 1995; Dasch et al., 2008). These generally consider that effective suppression of mist comes from an increase in deposition rate of the droplets generated. This is most effectively achieved by increasing the droplet size of the mist. Research by Dasch (2008) has shown that this can be achieved in several ways. This research isolated formation of droplets by vapour condensation, with droplet diameters  $0.1\text{-}1\mu\text{m}$ , and those formed centrifugally i.e. throw-off, with droplet diameters in the range  $1\text{-}10\mu\text{m}$ , for metalworking oils.

Different oil groups (I-II) showed a decrease in misting with increasing refining i.e. narrower distribution of molecular weights. This decrease resulted from the vapour condensation component of the mist, indicating that the increased concentration of lower molecular weight fractions in Group I oils resulted in greater volatility, as indicated by NOACK. A 27% increase in viscosity resulted in a 20% reduction in vapour sourced mist. More significantly, the addition of 180ppm PIB to the base oil reduces throw-off by 45%. This has potentially significant implications for engine lubricants, where polymers such as polyisobutylene are used in dispersants and detergents, and long chain polymers used as viscosity modifiers can often make up 8% by weight of the lubricant (Mortier et al., 2010).

### 3.6 The Effect of Polymers on Misting

As described previously, PIB has been used successfully as a mist suppressant in metalworking applications. This application resulted from earlier work including PIB in aircraft fuels to prevent potentially explosive mists forming in crashes (David, 2008). In metalworking, Marano (1995), Gulari (1995), Smolinski (1996) and Ergungor (2006) linked polymer concentration, PIB in all but the latter case who used polyethylene-oxide-based surfactants, with a change in rheology, particularly the resistance to extension, the extensional viscosity, which contributes to larger droplets being produced, Figure 3.13.

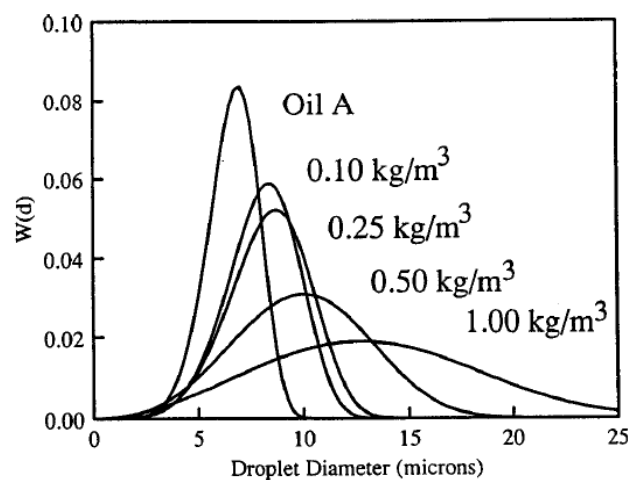


Figure 3.13: Effect of Polyisobutylene Concentration on Droplet Size from a Coaxial Mist Generator, from Gulari (1995)

Larger droplets are deposited more quickly, thus suppressing the mist. Relatively small concentrations of PIB are required to have a large effect on reducing the throw-off misting in metalworking fluids. Concentrations of 20-100ppm were found to produce 70-90% reduction in mist production. Dasch (2008) produced similar results and hypothesised the mechanism by which larger droplets are formed. It is suggested that the increased resistance to extensional deformation leads to the production of larger oil filaments from the surface film when disturbed, particularly at component edges. Larger droplets are formed when these larger filaments break apart. This research also suggests this effect reduces the quantity of liquid removed from the surface, suppressing mist production as well as increasing droplet deposition.

### 3.7 Polymer Rheology

Considering the significant role of polymeric additives in engine lubricant formulation and their effect on misting potential highlighted in the previously described studies, it is clear that the effects of polymers on rheology are of great importance to this study.

It is understood that lubricant base oil is generally Newtonian under most shear conditions. However, the inclusion of polymers produces a thinning effect at higher shear rates, generally beginning above  $10^6 \text{s}^{-1}$ , Figure 3.14. Several equations can be used to represent this behaviour. Kumar (2009) gives a comparison between several common models. Four notable models are listed below:

The sinh-law, or Ree-Eyring model:

$$\dot{\gamma} = \frac{\tau_0}{\eta} \sinh\left(\frac{\tau_0}{\tau}\right) \quad [3.10]$$

Where  $\dot{\gamma}$  is the shear rate,  $\tau$  is the shear stress,  $\eta$  is the low shear dynamic viscosity and  $\tau_0$  is the shear stress at the Newtonian limit, see Figure 3.14

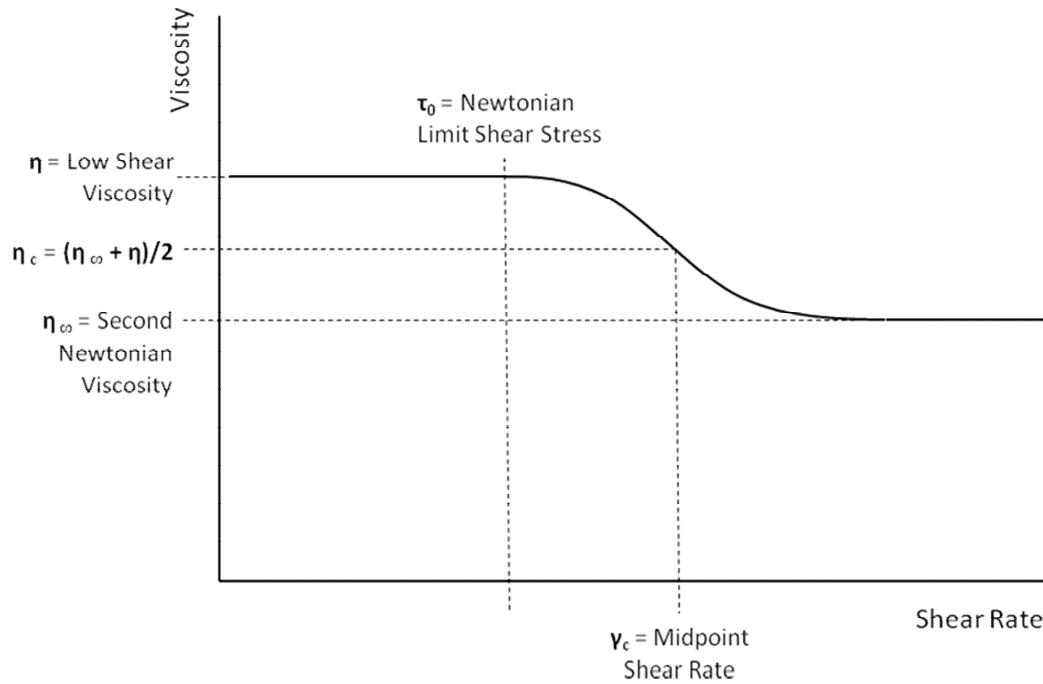


**Figure 3.14: Key Rheological Parameters of Polymer-Containing Liquid**

The power-law model of Carreau:

$$\eta = \frac{\tau}{\dot{\gamma}} = \eta_\infty + (\eta - \eta_\infty) \left[ 1 + \left( \frac{\dot{\gamma} \eta}{G_{cr}} \right)^2 \right]^{\frac{(n-1)}{2}} \quad [3.11]$$

Where  $\eta_\infty$  is the second Newtonian viscosity,  $G_{cr}$  is the shear modulus at the longest relaxation time

The Cross equation considers an initial Newtonian region up to a critical shear rate where thinning begins (Cross, 1965). When viscosity tends to the Newtonian viscosity of the base oil, a second Newtonian region is started:

$$\eta(\gamma) = \eta_\infty + \frac{\eta - \eta_\infty}{1 + \left( \frac{\gamma}{\gamma_c} \right)} \quad [3.12]$$

Where  $\eta_0$  = low shear viscosity at a constant temperature,

$\eta_\infty$  = limiting high shear viscosity,

$\gamma$  = shear rate,

$\gamma_c$  = shear rate at midpoint between  $\eta$  and  $\eta_\infty$ ,

It is noted that the Cross equation reports that the relaxation time for the fluid under the given conditions is given by:

$$\lambda = 1/\gamma_c \quad [3.13]$$

The Rabinowitsch Model, as described by Charles (2010), is similar to the Cross model, though relating viscosity to shear stress rather than shear rate:

$$\eta(\tau) = \eta_\infty + \frac{\eta - \eta_\infty}{1 + \left(\frac{\tau}{\tau_0}\right)^2} \quad [3.14]$$

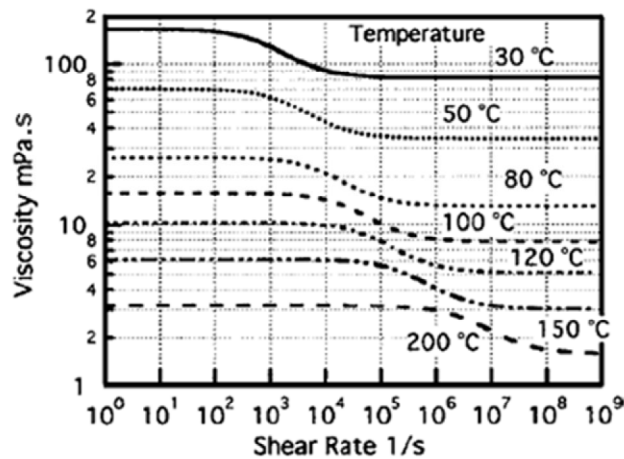


Figure 3.15: Shear Thinning Behaviour of an SAE 10W50 Oil at Various Temperatures (Harigaya et al., 2006)

Shear thinning is described in terms of molecular dynamics as the region when the rate of alignment and disentanglement of polymers exceeds the rate at which molecules entangle and interact (Schulz et al., 1991). The models described apply only for constant temperatures (Graessley, 2008). A variation in temperature results in a change in this relationship. A decrease in temperature results in the onset of thinning at a lower shear rate. Likewise, an increase in temperature will increase the onset of shear thinning to a higher shear rate. This can be attributed, molecularly, to the increasing effective molecular volume of the polymer with temperature i.e. as its length extends. This increases the interaction and interaction rate between molecules, thus requiring a larger shear rate to accelerate alignment and disentanglement rates beyond the limiting value of molecular interaction. This effect is shown in Figure 3.15.

### 3.7.1 Viscoelasticity

As described, the dynamics and interactions in long chain polymers produce an extremely non-linear shear response to shear in lubricant oils. This is partly due to the viscoelastic properties of polymer-containing fluids. Viscoelasticity can be defined as the nature of a material's fluidity or solidity when sheared. This is most simply defined by measuring the material's response to a sinusoidal shear stress of frequency  $\omega$ . The stress and strain functions are represented by the following relationships, as described by Riande (2000):

$$\sigma(t) = \sigma_0 \sin(\omega t + \delta) \quad [3.15]$$

$$\varepsilon(t) = \varepsilon_0 \sin(\omega t) \quad [3.16]$$

Where  $\sigma_0$  is the maximum amplitude of the shear stress and  $\varepsilon_0$  is the maximum amplitude of the strain.

The relationship between the input stress and response strain is shown in Figure 3.16. The nature of the fluidity/solidity is defined by the phase angle,  $\delta$ . If a material is

completely solid, the input energy is stored elastically and released as the stress is released, thus the input and response will be in phase,  $\delta = 0^\circ$ . If a material is completely fluid, the input energy is dissipated by the viscosity, and cannot be recovered. In this case, the input and response are out of phase,  $\delta = 90^\circ$ . In reality, no material is fully fluid or fluid solid, thus having a phase angle somewhere between these values. At  $\delta = 45^\circ$ , the material behaves in an equally solid and fluid manner. This latter condition is referred as the crossover point and is seen as the threshold between a material's behaviour being dominantly fluid or solid (Riande et al., 2000).

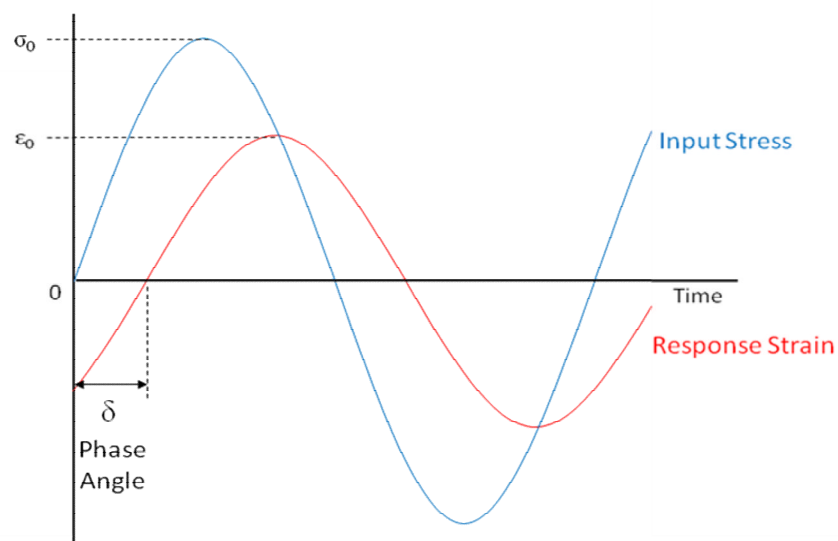


**Figure 3.16: Schematic of Phase Angle in Viscoelastic Flow**

Similarly to solid mechanics, the ratio of the stress and strain is termed the complex modulus  $G^*$ , which quantifies the resistance of the material to shear. It is termed complex because the stress and strain vary sinusoidally, thus  $G^*$  also varies with time. This can be represented as a complex viscosity,  $\eta^*$ , by the following relationship (Riande et al., 2000):

$$\eta^* = \frac{G^*}{i\omega} \quad [3.17]$$



The complex modulus can be considered as having two components, an elastic or storage modulus,  $G'$ , and a viscous or loss modulus,  $G''$ , defined using the complex notation as:

$$G^*(\omega) = G'(\omega) + iG''(\omega) \quad [3.18]$$

These are defined by the angular frequency and the phase angle:

$$G'(\omega) = \frac{\sigma_0}{\varepsilon_0} \cos \delta \quad [3.19]$$

$$G''(\omega) = \frac{\sigma_0}{\varepsilon_0} \sin \delta \quad [3.20]$$

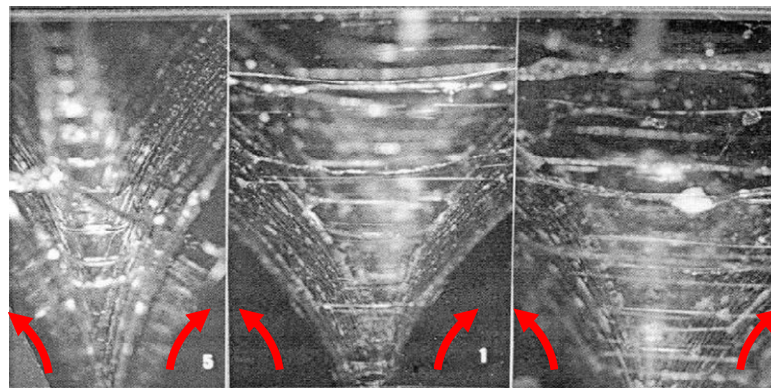
Hence,  $G'$  is zero when  $\delta = 90^\circ$  and  $G''$  is zero when  $\delta = 0^\circ$ , the elastic modulus is the in-phase component, and the viscous modulus the out-of-phase component. It also follows that:

$$\tan \delta = \frac{G''(\omega)}{G'(\omega)} \quad [3.21]$$

These relationships are limited in their application to linear viscoelasticity. This is defined in terms of the ratio between the imposed stress,  $\sigma(t)$ , and maximum strain,  $\gamma_0$ , is independent of variation in the maximum strain i.e. linear (Graessley, 2008):

$$\frac{\sigma(t)}{\gamma_0} = \text{independent of } \gamma_0 \quad [3.22]$$

At higher values of strain,  $\gamma_0$ , the linearity of this relationship breaks down due to the large amount of energy being stored in the material. Under these conditions, the material will become very resistant to shear, thus will become extremely solid and viscous flow will be suppressed until the shear stress is relaxed.



**Divergent Surfaces on Rotating Cylinders**

**Figure 3.17: Fluid Ligaments in a Roll Mill: Non-Linear Viscoelastic Response to Shear, from Fernando (1988)**

In a sinusoidal system, the shear stress, and thus the highly elastic response, is relaxed when the shear rate,  $\dot{\gamma}$ , is reduced. Therefore, many rheometers define the limit of viscoelasticity as the shear rate at which the viscous modulus,  $G''$ , reduces to 95% of the value under linear viscoelastic conditions (Graessley, 2008). It is these non-linear elastic responses that cause large strains to accumulate under stress, for example in Figure 3.17, showing a roll mill exerting an extensional stress on a polymeric fluid.

Like most polymeric fluids, lubricant oils containing viscosity modifiers behave as fluids at lower shear rates, but exhibit solid tendencies at higher shear rates (Schulz et al., 1991; Graessley, 2008). This is the mechanism by which it is thought that polymers can reduce the tendency of a fluid to form droplets. The high shear rates experienced in many misting processes impart a great deal of energy to the fluid that can be dissipated as kinetic energy when droplets are formed. However, the inclusion of polymers will allow more of this energy to be stored elastically in the polymer molecules under these conditions.

As highlighted by the studies described in Sections 3.5.3 and 0, the extensional viscosity,  $\eta_e$ , of a fluid is of particular note. This is resistance of a fluid to being extended i.e. stretched in one axis (Fernando et al., 1988; Al-Hadithi et al., 1992;

Tirtaatmadja et al., 1993; Ferguson et al., 1997; Della-Valle et al., 2000; Tuladhar et al., 2008). This parameter requires a steady rate of strain, which is extremely difficult to achieve due to fluid filaments thinning with extension (Tirtaatmadja et al., 1993; Tuladhar et al., 2008). Therefore it is not uncommon for this parameter to be estimated from shear viscosity (Al-Hadithi et al., 1992; Ferguson et al., 1997). The Trouton ratio describes the ratio of extensional viscosity to the shear viscosity. For a Newtonian fluid this is 3 (Nguyen et al., 1999):

$$\frac{\eta_e}{\eta} = 3 \quad [3.23]$$

i.e.

$$\eta_e = 3\eta \quad [3.24]$$

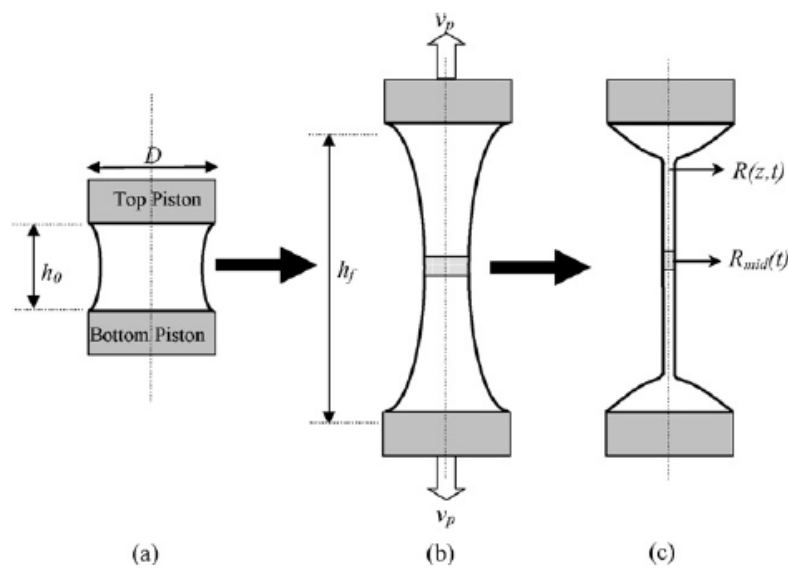
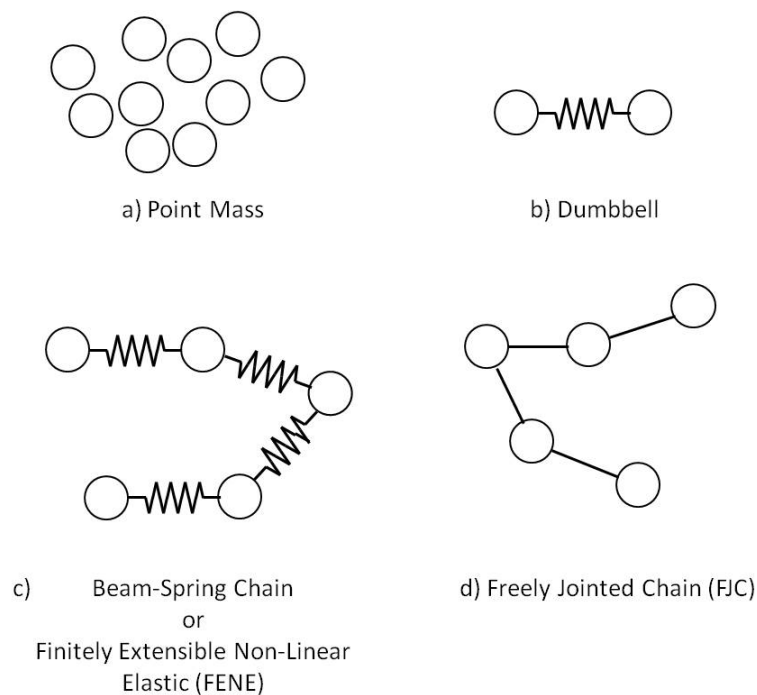


Figure 3.18: CaBER-Type Extensional Rheometer, from Tuladhar (2008)

The most common test for extensional viscosity is the capillary breakup extensional rheometer (CaBER) test (Nguyen et al., 1999). This constitutes two parallel plates that move apart, stretching the fluid between them. The stress and strain are recorded until the fluid filament breaks.

### 3.7.2 Molecular Dynamics of Polymers

As previously described, the means by which long chain polymers improve the temperature-viscosity response of oil is by extension of arms with increasing energy caused by higher temperatures. This extension and stretching causes interaction with other polymer molecules when polymer is present at suitable concentrations. The response of molecules to shear by extension, stretching and alignment affects the shear response of the fluid. This behaviour has been modelled, with reference to experimental data, in various ways. Some studies consider these molecules as acting at a point at their centre of mass (Schulz et al., 1991; Nguyen et al., 1999; Jain et al., 2009), Figure 3.19a. Whilst this can approximate the behaviour of chemicals of different molecular weight in solution, the model cannot consider the dynamics of the chain and interactions between molecules.



**Figure 3.19: Polymer Molecular Dynamic Models**

More complex models such as the dumbbell approximate the molecule as two masses connected by a spring, Figure 3.19b. This permits extension, but only in one axis

(Schulz et al., 1991; Jain et al., 2009). Increased computing power enabled this model to be extended into ‘beam-spring chain’ models, Figure 3.19c, which facilitates different rates of extension within a molecule (Jain et al., 2009). These models include bending and torsion terms, to allow movement in all axes. Limits to the extension were applied to keep solutions realistic and nonlinear extension was incorporated. These models are termed finitely extensible nonlinear elastic, FENE, models, Figure 3.19c (Hunt et al., 2009; Kabanemi et al., 2009). Similar models with fixed bond length are called freely jointed chain, FJC, models, Figure 3.19d (Hunt et al., 2009). Interaction between molecules is included by considering energy flow (Karyappa et al., 2008). More complex analyses combine FENE molecules with energy analysis (Hunt et al., 2009).

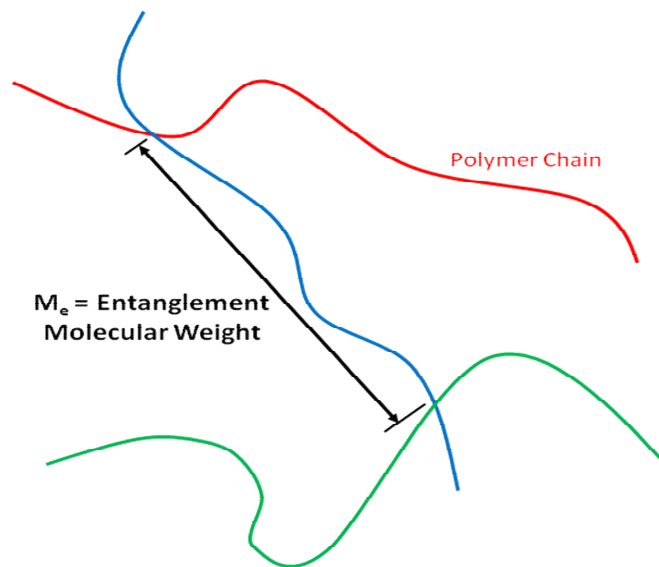


**Figure 3.20: Entanglement Molecular Weight for Overlapping Polymer Molecules**

Entanglement has been investigated and has shown that viscoelastic behaviour can be attributed to molecular alignment and entanglement (Graessley et al., 1981; Fetters et al., 1993; Gell et al., 1997). The degree of interaction is related to the number of other molecules that a single molecule overlaps with, or is entangled with. The most useful parameter to define this is the entanglement density, literally the number of entanglements per molecule, given by the ratio:

$$E = \frac{M}{M_e} \quad [3.25]$$

Where  $M$  is the molecular weight of the polymer molecule, and  $M_e$  is the entanglement molecular weight. This latter parameter is the average distance between overlaps on a polymer molecule, Figure 3.20. This can be calculated empirically for an undiluted polymeric liquid, as has been reported by (Ferry, 1980; Schulz et al., 1991).

Graessley (2008) describes that the entanglement density is affected by the concentration of polymer when it is diluted. This is described by the following relationships:

$$M_e(\phi) = M_e \phi^{-1.3} \quad [3.26]$$

$$E(\phi) = E \phi^{1.3} = \frac{M \phi^{1.3}}{M_e} \quad [3.27]$$

Where  $\phi$  is the concentration of the polymer by volume

This relationship applies for linear polymers only. For star polymers, or other highly branched molecules, the nature of entanglement has been more accurately described by the entanglement density of an arm or branch, rather than for the whole molecule (Gell et al., 1997; Graessley, 2008). This requires knowledge of the number of arms in the molecule, which is often difficult information to find. Thus:

$$E_a(\phi) = E_a \phi^{1.3} = \frac{M_a \phi^{1.3}}{M_e} \quad [3.28]$$

Where  $M_a$  is the molecular weight of an arm of the molecule

However, it is understood that not all solutions are entangled. Below certain polymer concentrations, the entanglement density reaches a value that indicates that molecules

will rarely interact. Thus, each polymeric fluid will have a critical concentration,  $c^*$ , below which the fluid is termed dilute, and above which it is termed entangled. At the critical concentration, the fluid is termed semi-dilute (Schulz et al., 1991), Figure 3.21. This parameter is dependent on the polymer molecular weight and molecular structure, and its effective volume in the solution. Thus, the critical concentration is also dependent on temperature, pressure and the solubility-related properties of the polymer and diluent. Graessley (2008) first defines the concentration of the polymer within its own effective molecular volume:

$$c_{molecule} = \frac{3M}{4\pi N_a R_g^3} \quad [3.29]$$

Where  $N_a$  is Avogadro's number, and  $R_g$  is the radius of gyration of the molecule i.e. the radius of the sphere equivalent to the effective volume of the molecule.

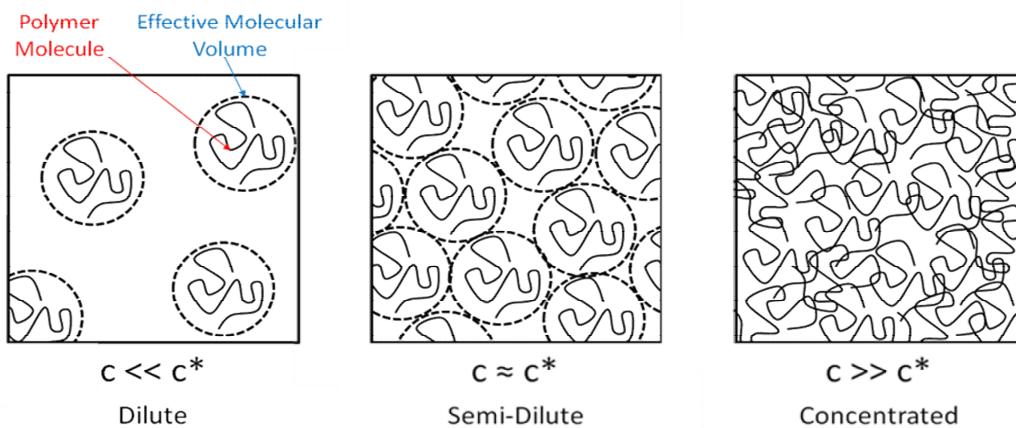


**Figure 3.21: Defining Polymer Solutions Relative to Critical Concentration, after Schulz (1991)**

It is then suggested that the critical concentration is reached when the concentration of polymer in the dilute solution is equivalent to the concentration in the effective volume of the polymer themselves i.e. the solution is made up entirely of polymer

molecules' effective volumes whilst, theoretically, overlap isn't necessary (Schulz et al., 1991):

$$c^* = c_{molecule} \quad [3.30]$$

This is a well defined theory, and the difference in viscosity and rheology either side of this threshold is seen in many studies, Figure 3.22. However, in practice, it is difficult to be used predicatively, as  $R_g$  is extremely difficult to measure and is sensitive to temperature, pressure and shear (Schulz et al., 1991).

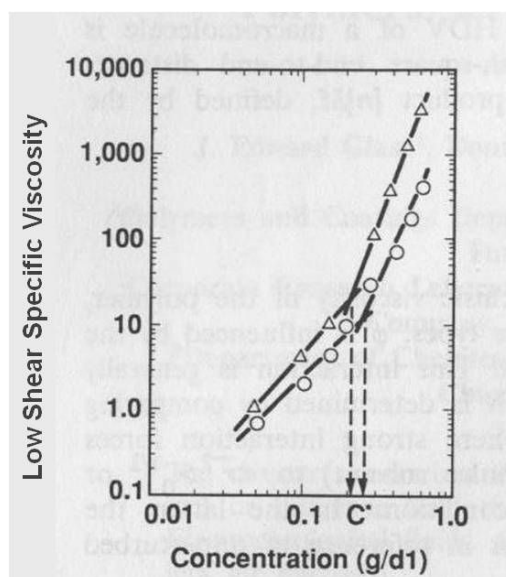


**Figure 3.22: Effect of Critical Concentration on Viscosity of HP-Guar Blends, from Schulz (1991)**

The relationship between viscosity and polymer molecular weight for entangled solutions of linear polymers i.e. at polymer concentrations above  $c^*$ , is described by Graessley (2008). The viscosity is defined by the product of two terms: One defined by the frictional properties between interacting molecules,  $\zeta$ , and the other a structural term,  $F_s$ . The former is dependent on temperature and polymer species, the latter is dependent on chain length:

$$\eta = \zeta F_s \quad [3.31]$$



A characteristic molecular weight,  $M_c$ , is observed which represents a boundary between two regions of molecular weight dependency of viscosity, such that:

$$F_s(M) = \rho M \quad M < M_c \quad [3.32]$$

$$F_s(M) = \rho M \left( \frac{M}{M_c} \right)^{2.4} \quad M > M_c \quad [3.33]$$

More simply:

$$\eta \propto M \quad M < M_c \quad [3.34]$$

$$\eta \propto M^{3.4} \quad M > M_c \quad [3.35]$$

This value of  $M_c$  is dependent on species, but is not sensitive to temperature and polymer concentration.

### 3.8 Summary

- There are many qualitative descriptions of different types of two phase flow. Current theories and observations suggest that misting in the piston assembly is best described as an annular mist flow.
- The application of existing models of phase interaction to the piston assembly does not indicate that these mechanisms are significant sources of droplets. However, studies on annular mist flow in junctions suggest that droplets are ripped from the surfaces at component edges in significant quantities.
- The study of mists in other disciplines has shown a clear difference in the source and behaviour of aerosols, mists and sprays.
- Misting has been shown to be greatly suppressed by the inclusion of small quantities of large molecular weight polymers. This is attributed to the

viscoelastic properties such polymers give a fluid. This indicates a potential influence of viscosity modifier on lubricant misting in the piston assembly.

- The viscoelastic behaviour of a lubricant is highly dependent on the molecular dynamics of the polymers, particularly their alignment with stress and entanglement. The nature of these interactions is a function of polymer chemistry, molecular weight and concentration.

## **Chapter 4: Simulation of Misting in the Piston Ring Gap and Considering the Components of a Commercial Lubricant**

### **4.1 Introduction**

In light of previous discussion in Chapters 2 and 3, in this chapter the development of apparatus designed to simulate lubricant misting in the piston assembly is described. This apparatus was then used to test the hypothesis that it is base oil properties and viscosity modifying polymers that have the greatest effect on the misting properties of a lubricant oil.

### **4.2 Mist Generator**

It was decided that producing representative conditions in an existing design of mist generator would be the best approach to simulate misting conditions at the piston ring gap. Based on the research discussed in Chapter 3, the venturi mist generators commonly used in oil mist lubrication systems were seen to best represent the desired misting mechanism. Such generators rely on a high velocity gas flow encountering oil moving at low velocity, resulting in considerable interfacial shear. A raised oil feed pipe produces an edge over which this shear can rip droplets from the surface. The venturi effect, though very gently tapered rather than the orifice geometry of the ring gap, produces a contraction and expansion of the flow, such as in a ring gap, where velocity and, thus, shear gradients are experienced. The linear flow path of the venturi is not representative of the 90° change in flow direction experienced by gas exiting the ring gap region. However, as such geometry would greatly increase droplet deposition rates, and the investigation is concerned with analysing as complete a mist as possible, it was felt that this compromise was justified.

The flows through the ring gaps are extremely complex and vary greatly both in magnitude and direction throughout a typical engine cycle. It was decided that the most extreme conditions would be simulated and run at steady state. In the interest of consistency with later engine tests, the data produced by Gamble (2003) whilst modelling the piston assembly of the Ricardo Hydra test engine was used. The most extreme condition, peak gas flow rate through the top ring gap, is found 20-25° crank angle after firing top dead centre, TDC (Gamble, 2003). The relevant conditions are shown in the second column of Table 4.1. As this simulation considers only physical effects, it was decided that air would be used as the gas as it has, naturally, almost identical physical properties to blow-by gas (Keenan et al., 1983). It was considered impractical to reproduce the extremely high absolute pressure of the gas flow. Therefore, other parameters would be used to replicate the flow environment.

The parameters reported in Table 4.1 were calculated in several stages. Firstly, the compressibility of the flow through the top piston ring gap was defined, in order that the correct models were applied in the rest of the calculations. Secondly, the flow parameters in the engine were defined using the most appropriate models. Thirdly, the dimensions of a venturi producing these flow parameters were calculated.

Gamble (2003), modelling the engine at 2500rpm and full load, reports the peak flow rate of gas through the top ring gap as  $1.01 \times 10^{-3} \text{ kgs}^{-1}$ . At the maximum top ring gas pressure, 3.94MPa gauge, the apparent density of air can be calculated from the Ideal gas law (Massey et al., 1998):

$$\rho = \frac{P}{RT} \quad [4.1]$$

Where  $\rho$  is the density,  $p$  is the absolute pressure,  $T$  is the temperature in Kelvin, 573K, and  $R$  is the gas constant for air,  $287 \text{ Jkg}^{-1}\text{K}^{-1}$ . Thus the apparent density of air under these conditions is  $23.96 \text{ kgm}^{-3}$ . Therefore, the apparent volumetric peak flow rate through the top ring is  $1.24 \times 10^{-3} \text{ m}^3\text{s}^{-1}$ . Due the secondary motion of the piston, the area of the piston ring gap varies between  $1.70\text{-}2.35 \times 10^{-7} \text{ m}^2$ . This indicates an apparent maximum peak velocity through the ring gap of  $248 \text{ ms}^{-1}$ . According to Ideal

gas laws, the local speed of sound can be calculated as  $480 \text{ ms}^{-1}$  using the following equation:

$$a = \sqrt{\gamma RT} \quad [4.2]$$

Where  $a$  is the speed of sound, and  $\gamma$  is the ratio of specific heats,  $C_p/C_v$  which is 1.4 for air (Massey et al., 1998). A Mach number ( $v/a$ ) of greater than 0.30 is considered the threshold above which flow should be considered compressible, where  $v$  is the local gas velocity. Thus, as the apparent Mach number of the flow is 0.52, the flow should be considered compressible, the Ideal gas law does not apply.

In order to calculate the flow parameters of the engine, compressible flow relationships should be used. In order to calculate the choking conditions for the top ring, the flow was considered using the equations for a frictionless contraction, described by Massey (1998), similar to the orifice model used by Furuhashi (1961, 1979) and others (Munro, 1981; Miyachika et al., 1984; Keribar et al., 1991; Tian, 2002; Gamble, 2003; Tamminen et al., 2005; Wannatong et al., 2008; Johansson et al., 2010). Thus, the relation between the critical pressure,  $p_c$ , i.e. the pressure in the top ring gap when the flow is choked, and the stagnation pressure,  $p_o$ , i.e. the pressure if no flow occurred, is given as:

$$\frac{p_c}{p_o} = 0.528 \quad [4.3]$$

Taking the stagnation pressure as the maximum pressure above the top ring, 3.94 MPa, the critical pressure is 2.08 MPa. The critical density  $\rho_c$  is defined in terms of the stagnation density  $\rho_o$  by the following relationship:

$$\rho_c = \left( \frac{p_c}{p_o} \right)^{\frac{\gamma+1}{2}} \rho_o \quad [4.4]$$

The stagnation density is taken as the previously calculated value of  $23.96 \text{ kgm}^{-3}$ , as the lack of flow permits the Ideal gas law to be applied. Thus, the critical density is  $15.18 \text{ kgm}^{-3}$ .

The critical mass flow rate, the maximum flow rate possible through the ring gap,  $\dot{m}_{\text{max}}$ , is then given by the following:

$$\dot{m}_{\text{max}} = A \left( p_o \rho_o \gamma \left( \frac{2}{\gamma + 1} \right)^{\left( \frac{\gamma + 1}{\gamma - 1} \right)} \right)^{1/2} \quad [4.5]$$

The ring gap area,  $A$ , is  $1.7 \times 10^{-7} \text{ m}^2$ , as given by Gamble (2003). Thus, the critical flow rate is calculated to be  $1.13 \times 10^{-3} \text{ kgs}^{-1}$ . From this the critical velocity through the ring gap,  $u_c$ , can be calculated using the relationship:

$$u_c = \frac{\dot{m}_{\text{max}}}{\rho_c A} \quad [4.6]$$

This was calculated to be  $438 \text{ ms}^{-1}$ . It can be seen that, with particular reference to the critical mass flow rate and modelled flow rate, the flow calculated from the data of Gamble (2003) indicates that the flow in the top ring is almost choked. The Mach number is calculated as 0.91.

Therefore, the design for the venturi mist generator assumed a fully choked flow. In a venturi, a choked flow is defined by a Mach number of 1 (Ward-Smith, 1971). Thus, Equations 4.2-4.6 for the critical conditions are applied with the stagnation conditions defined by the laboratory environment. This analysis produced a venturi mist generator with the geometry shown in Figure 4.1 and the flow conditions described in the third column of Table 4.1. It can be seen that, other than pressure, this design is a good simulation of the piston ring gap environment.

Parameter	Piston Ring Gap after Gamble (2003)	Venturi Mist Generator
Peak mass flow rate ( $10^{-3} \text{ m}^3 \text{ s}^{-1}$ )	1.01	1.54
Peak gas velocity ( $\text{ms}^{-1}$ )	438	300
Mach number	0.91	1
Expansion ratio	3.42 - 13.23	11.67
Throat gauge pressure ( $\times 10^6 \text{ Pa}$ )	3.94	0.053

**Table 4.1: Properties of Engine and Venturi Mist Generator**

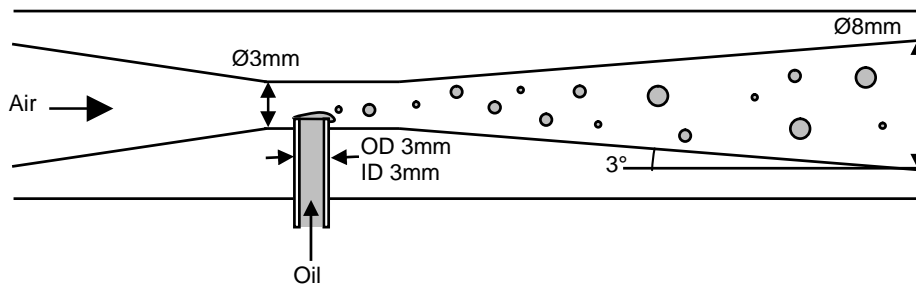


**Figure 4.1: Venturi Mist Generator**

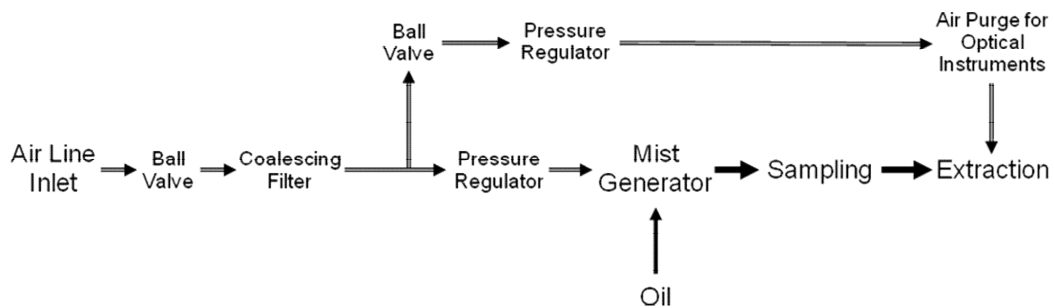


**Figure 4.2: Schematic of Compressed Air System**

A mist generator of this geometry was manufactured from glass-filled polyethylene by selective laser-sintering. The inner surfaces of the venturi were smoothed with fine sandpaper to remove the rough surface that laser sintering naturally produces. A laboratory compressed air line was attached to the inlet using high pressure fittings.

The air supply produces a maximum gauge pressure of 0.7 MPa and a maximum flow rate of  $0.05 \text{ m}^3\text{s}^{-1}$ . A standard ball valve and a Norgren R74 pressure regulator were used to control these parameters. The compressed air was passed through a Norgren F74-4GD-QPO  $0.01\mu\text{m}$  coalescing filter to remove any oil or water contamination from the flow. This system is shown schematically in Figure 4.2. The apparatus was installed in a room with a controlled ambient temperature of  $20^\circ\text{C}$  and relative humidity of 33%.

The mist generator outlet was an 8mm PTFE-lined pipe. The pipe was lined with PTFE in order that the oil would not ‘wet’ the pipe and be retained on the walls. As PTFE is oleophobic, oil impacting the pipe will not ‘wet out’, but will flow out under the action of gas flow. This pipe discharged into a painted wooden box that served as an enclosure for the sampling systems. This was necessary to prevent the oil mist becoming a fire hazard or being inhaled by operators. The box was attached by flexible ducting to the local exhaust ventilation system. This extracted the air at a rate of approximately  $1.5 \times 10^{-2} \text{ m}^3\text{s}^{-1}$ . The apparatus is shown schematically in Figure 4.3 and photographically Figure 4.4.

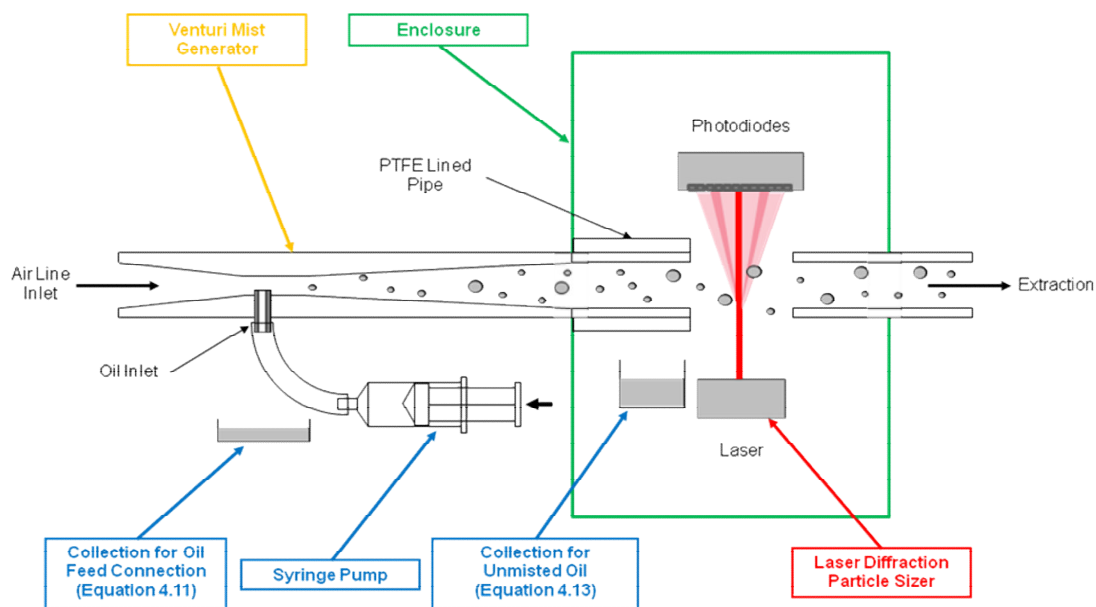


**Figure 4.3: Schematic of Misting Apparatus**



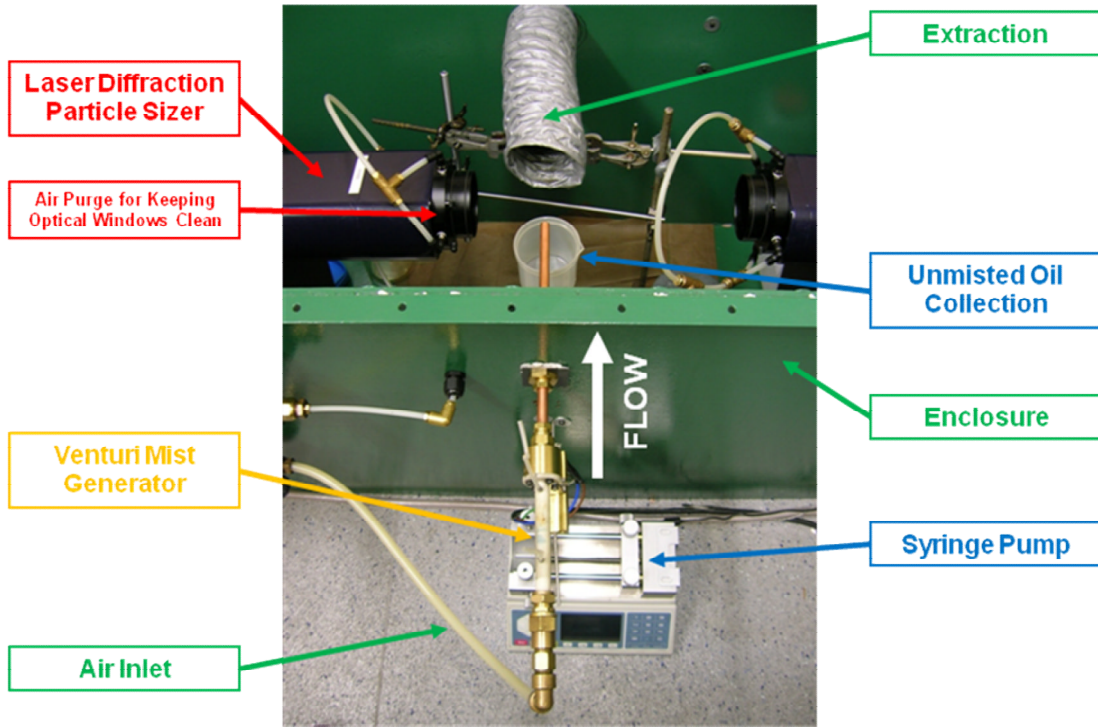


Figure 4.4: Misting Apparatus Layout

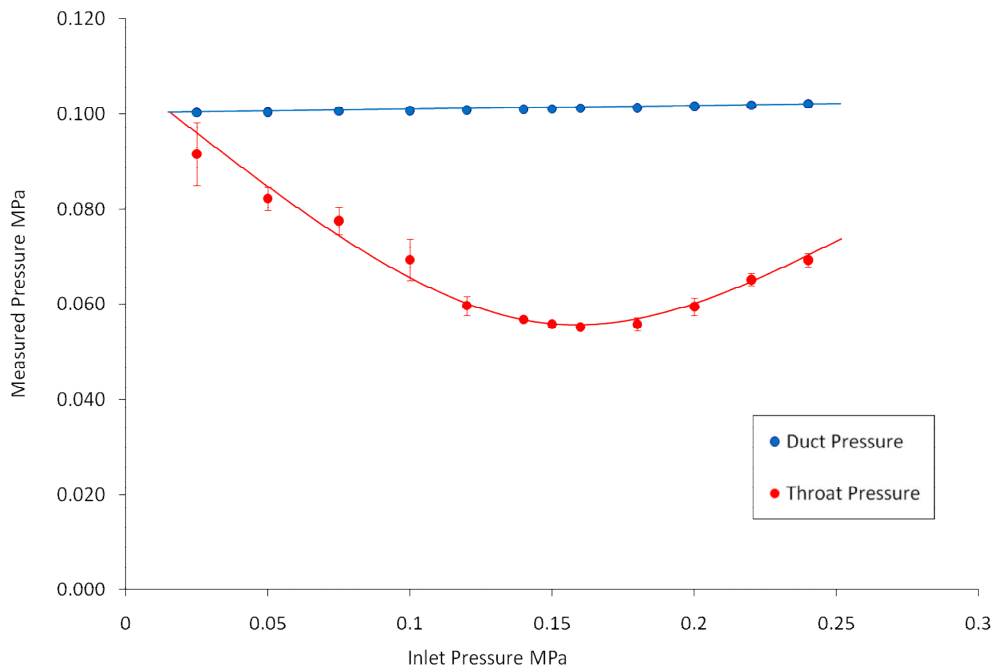


Figure 4.5: Measured Pressure Data in Venturi Mist Generator

The venturi was commissioned with a no oil flow and with pressures recorded at the throat and in the outlet duct after expansion. This showed that the static gauge pressure at the throat was a minimum of 0.055 MPa at an inlet pressure of 1.5 MPa, as shown in Figure 4.5. This indicates that the flow is choked at this inlet pressure i.e. the Mach number in the venturi throat is 1 and the flow rate is a maximum. This correlates with the theoretical result using Equation 4.3, shown in Table 4.1, thus the theoretical flow rate can be assumed. The real throat area was calculated by taking a monochrome image through the venturi and calculating the area from known dimensions. The final parameters for the venturi are shown in Table 4.1.

### **4.3 Measurement**

There are several ways to describe and define a mist flow of this kind. Lawes (2006) describes three parameters:

- Mean droplet size
- Droplet size distribution
- Liquid to volume ratio

Whilst the mean droplet size is derived from the droplet size distribution, thus not required to define the mist, it is an important comparator between mists, particularly when predicting behaviour of the droplets. Care is required however, as such flows may have more than one characteristic droplet size. Another parameter commonly used is the droplet concentration. This is defined as the number of droplets per unit volume. This is not considered relevant to this study as it can be derived from the parameters listed above. As the flow can be defined fully by the latter two parameters, measurements of these were made.

#### **4.3.1 Droplet Size Distribution**

Several techniques for measuring droplet size distribution were considered. White light-based techniques, such as CCD cameras, are simple but limited in their resolution to larger droplet sizes (Fry et al., 1995). Laser Doppler Particle Sizing, as

described by Rizzo (1975) and Jakubik (2006), is an extremely accurate technique. However, it can only measure a small volume and, thus, is limited to highly homogeneous flows containing small droplets (Hung et al., 2008). Such apparatus is extremely sensitive and takes extensive calibration (Hung et al., 2008).



**Figure 4.6: Laser Diffraction Particle Sizer: Malvern Spraytec 2000 (Image from Malvern Instruments (2010))**

Light scattering techniques, such as laser diffraction particle sizers, are more general methods (Nasr et al., 2002; Triballier et al., 2003). Due to their large beams, they are able to measure large flows, thus are less sensitive to local variation in flow. They are able to measure a large range of droplet sizes, though at a lower degree of accuracy than laser Doppler techniques (Nasr et al., 2002). Light scattering apparatus is much more heavily commercialised than other techniques, thus is more user-friendly, robust and easier to calibrate than more precise techniques (Nasr et al., 2002; Triballier et al., 2003).

Therefore, the droplet size distribution of the mists generated was measured by a laser diffraction particle sizer, a Malvern Spraytec 2000, Figure 4.6. This equipment was set up to measure droplets in the range of 0.1-1000 $\mu\text{m}$  in 1 second averaged time steps. This equipment measured the droplet size distributions based on classical light scattering principals. These are dependent on the field wavelength, the ratio of the particle frontal area, assumed to be spherical, and the wavelength of the light (Barth, 1984; Chu, 1991):

$$\zeta = \frac{2\pi r}{\lambda} \quad [4.7]$$

Where  $r$  is the particle radius and  $\lambda$  is the light wavelength

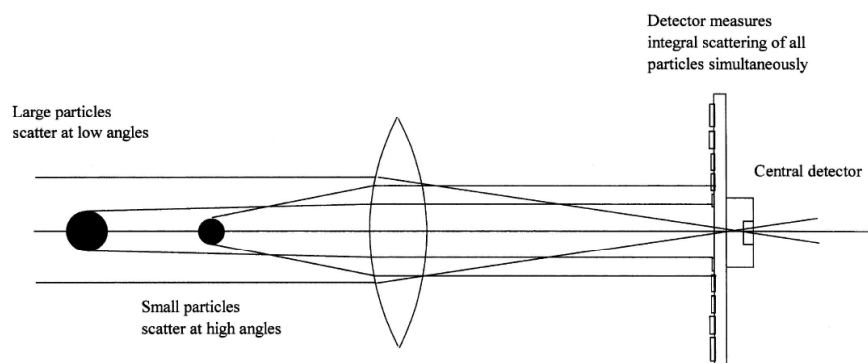


**Figure 4.7: Principles of Mie Scattering and Laser Diffraction Particle Sizing. From Simmons (2001)**

A reduction in droplet diameter relative to the wavelength increases the angle of scatter, Figure 4.7, (Simmons et al., 2001). Where  $\zeta \approx 1$ , at the lower range of the diffraction particle sizer, Mie scattering equations are used. This is ‘a series expression in terms of spherical harmonics’ (Cadle, 1965), which can be expressed in a simplified form:

$$s = \frac{\lambda^2}{2\pi} \sum_{v=1}^{\infty} \left( \frac{a_v^2 + p_v^2}{2v+1} \right) \quad [4.8]$$

Where  $s$  is the total scattering by one spherical particle per unit intensity,  $a_v$  and  $p_v$  are functions of  $\zeta$  and  $\beta$  where  $\beta = \zeta m$ , where  $m$  is the relative refractive index of the particle material. This can also be expressed as a scattering per unit cross sectional area,  $K$ , known as the scattering coefficient.

$$K = \frac{2}{\zeta^2} \sum_{v=1}^{\infty} \left( \frac{a_v^2 + p_v^2}{2v+1} \right) \quad [4.9]$$

When  $\zeta \gg 1$ , at the upper range of the equipment, Fraunhofer diffraction equations are used (Barth, 1984; Chu, 1991; Malvern Instruments Ltd, 2008):

$$I = I_0 \left[ \frac{2J_1(x)}{x} \right]^2 \quad [4.10]$$

Where  $I$  is the intensity of the light detected at a particular radius,  $I_0$  is the intensity at the centre of the pattern,  $J_1$  is the first-order Bessel function, and:

$$x = \frac{2\pi rR}{\lambda F} \quad [4.11]$$

Where  $R$  is the radial distance from the centre in the detection plane, and  $F$  is the focal length of the lens (Barth, 1984).

These relationships hold for elastic scattering i.e. scattering does not alter the wavelength of the light. In this apparatus, mist is passed between a laser source producing a 10mm diameter beam of known light wavelength (632.8nm) and a series of concentric detectors of known distance from the centre of the beam. Thus, the proportion of light being scattered by a particular angle (i.e. the intensity received at a particular detector as a fraction of the total) is correlated to the droplet size

distribution. Various algorithms are applied to allow accurate measurement of higher concentration flows where light may be scattered by more than one droplet. These allow flows with high liquid to gas ratios to be analysed (Barth, 1984; Chu, 1991; Malvern Instruments Ltd, 2008). It is understood that not all light is scattered, some is refracted and some is absorbed. A known refractive index of the fluid analysed means that refraction can be compensated for. Laser diffraction particle sizing is standardised by ISO 13320:2009 (Malvern Instruments Ltd, 2008).

The measured distributions are averaged over the total length of the test and several derived parameters are averaged in the same procedure. The most important derived parameters collected are shown in Table 4.2.

Parameter		Description
Trans	Transmittance	Intensity of laser at measured detector with mist present, as a percentage of when no mist present
d(10%)	10% drop diameter	Droplet diameter where 10% of droplets are smaller
d(50%)	50% drop diameter	Median droplet diameter
d(90%)	90% drop diameter	Droplet diameter where 90% of droplets are smaller
%V<10 $\mu$ m		% of volume flowing in droplets smaller than 10 $\mu$ m
Mean d(v)	Volume-weighted mean diameter	The diameter of the droplet with the mean volume of the droplets in the distribution
Mean d(a)	Area-weighted mean diameter	The diameter of the droplet with the mean surface area of the droplets in the distribution
Obs	Obscuration	Percentage reduction in measured laser intensity when mist is present. The inverse of Transmittance
C <sub>v</sub>	Concentration	The Oil : Air ratio of the mist in %
Span		A measure of the range of the droplet sizes. Defined by: $(d(10\%)-d(90\%))/d(50\%)$

**Table 4.2: Derived Parameters from Malvern Spraytec, from Malvern Instrument Ltd (2010)**

The oil to air ratio of the flow can be derived from measurements taken on this apparatus. The difference between the light intensity measured at the central detector when mist is present and when no mist is present can be defined as the obscuration or the transmittance where:

$$\text{Transmittance (\%)} = \frac{\text{Intensity}_{\text{With Droplets}}}{\text{Intensity}_{\text{Without Droplets}}} \times 100 \quad [4.12]$$

$$\text{Obscuration (\%)} = \frac{\text{Intensity}_{\text{Without Droplets}} - \text{Intensity}_{\text{With Droplets}}}{\text{Intensity}_{\text{Without Droplets}}} \times 100 = 100 - \text{Transmittance (\%)} \quad [4.13]$$

These can be related to the tendency of the droplets in the particular distribution to scatter light and thus the volume of droplets per unit total volume passing the detector can be calculated by the Beer-Lambert Law:

$$\text{Oil : Air (\%)} = C_v (\%) = \frac{-0.2 \ln(T)}{3b \sum \frac{Q_i v_i}{d_i}} \quad [4.14]$$

Where  $C_v$  is the percentage concentration of oil in air,  $T$  is the % transmittance,  $b$  is the path length through the mist (mm),  $Q_i$  is the efficiency of scattering (by absorption and Mie theory) for a droplet of diameter  $d_i$ ( $\mu\text{m}$ ).  $v_i$  is the proportion of droplets with diameter  $d_i$  (Barth, 1984; Chu, 1991; Malvern Instruments Ltd, 2008). Knowing the total flow rate past the detector, the total oil flow rate can be calculated.

The particle sizer was placed in the enclosure, downstream of the mist generator, as shown in Figure 4.4. The centreline of the laser beam normally intersected the centreline of the flow from the mist generator outlet. Whilst the pipe diameter is smaller than that of the laser beam, the expansion of the flow as it discharges into the enclosure means that the particle sizer will measure only part of the mist flow. However, observation has shown that only a small proportion of the flow does not pass through the beam.

### 4.3.2 Oil to Air Ratio and Other Flow Rate Data

The flow rate of oil and gas through the system can be measured more directly by measuring the input and output flows. The gas flow rate through the system, as

described in Section 4.2, is constant during these tests ( $1.54 \times 10^{-3} \text{ m}^3 \text{ s}^{-1}$ ). The oil feed into the system is metered by a syringe pump, a Chemyx Nexus 6000, through a 50mm long silicone tube into the venturi mist generator. This produces a maximum linear force of 2000N, equating to a maximum pressure of 82.83kPa in the nominally 50ml syringes used in these tests. The pressure losses in the supply system are considerably less than the maximum pressure produced in the pump, approximately 3kPa. Therefore, the gauge input flow rate is theoretically extremely accurate. However, as syringes deform under pressure, the syringe and the supply tube were weighed before and after each test to determine the total quantity of oil fed into the system. The oil injected into the system was kept at room temperature, 20°C. When the supply tube was attached to and detached from the venturi oil feed, some oil was able to leak: This was caught in a tray, shown in Figure 4.3. The tray was also weighed before and after each test. Thus, the total oil passing through the mist generator during a test is:

$$\textit{Total Oil Past Detector} = \textit{Oil Out From Syringe} - \textit{Oil Catch} \quad [4.15]$$

It was observed in initial testing that some of the oil exiting the mist generator was flowing along the pipe walls and dripping out. This means that not all of the oil entering the system reaches the detector as a mist. There are three explanations for this: Firstly, that some of the oil is not misted and flows down the pipe walls. Secondly, some of the droplets are sufficiently large to be deposited on the wall before reaching the end of the pipe. Thirdly, and most probably, both mechanisms occur to some degree. The exact contribution of each mechanism is not known. In order to calculate the quantity of oil reaching the detector as a mist, the oil dripping from the pipe i.e. the un-misted or deposited oil, was collected throughout the test and weighed at the end: A beaker was placed under the outlet of the mist generator to collect this oil, Figure 4.3. The pipe carrying the flow between the mist generator and particle sizer was lined with PTFE to prevent wetting and allow all oil on the walls to reach the collector. Thus, the mass flow rate of oil reaching the detector as a mist is:



$$\dot{m} = \frac{\text{Total Oil Misted}}{\text{Test Duration}} \quad [4.16]$$

Where,

$$\text{Total Oil Misted} = \text{Oil Out From Syringe} - \text{Oil Catch} - \text{Unmisted Oil} \quad [4.17]$$

#### 4.4 Parametric Testing

Initial tests were concerned with defining an appropriate range of oil flow rates (i.e. oil to air ratios) for the study. These tests showed that a two minute duration of oil flow, once the air flow had stabilised, was a suitable compromise between lengthening the test to reduce error magnitude and reducing the test duration to allow higher input flow rates as limited by the syringe oil volume. Data for a Group III 5W base oil and a Group III fully formulated 5W30 lubricant is shown in Figure 4.8. In this, the oil leaving the system as mist as a percentage of the oil entering the system represents the tendency of the oil to form mist, the misting tendency. This parameter is defined as:

$$\% \text{ Droplets} = \% \text{ Mist} = \frac{\text{Total Oil Out as Mist (from Equation 4.17)}}{\text{Total Oil In (from Weighing Syringe)}} \times 100 \quad [4.18]$$

It can be seen that the tendency of an oil to mist is strongly affected by the flow rate of oil into the mist generator. The relationship is approximately linear between 5 and 15ml/min, above which the rate of increase drops. Below 5ml/min, the misting behaviour is more constant, with an increase then observed below 2 ml/min.

Analysis of the droplet size distributions for these tests indicates several characteristic droplet sizes are formed. Figure 4.8 shows that, as oil flow rate increases, the flow rate of droplets with diameters between 135 and 1000 $\mu\text{m}$  increases progressively. This is termed the spray region. The distributions also show two other characteristic

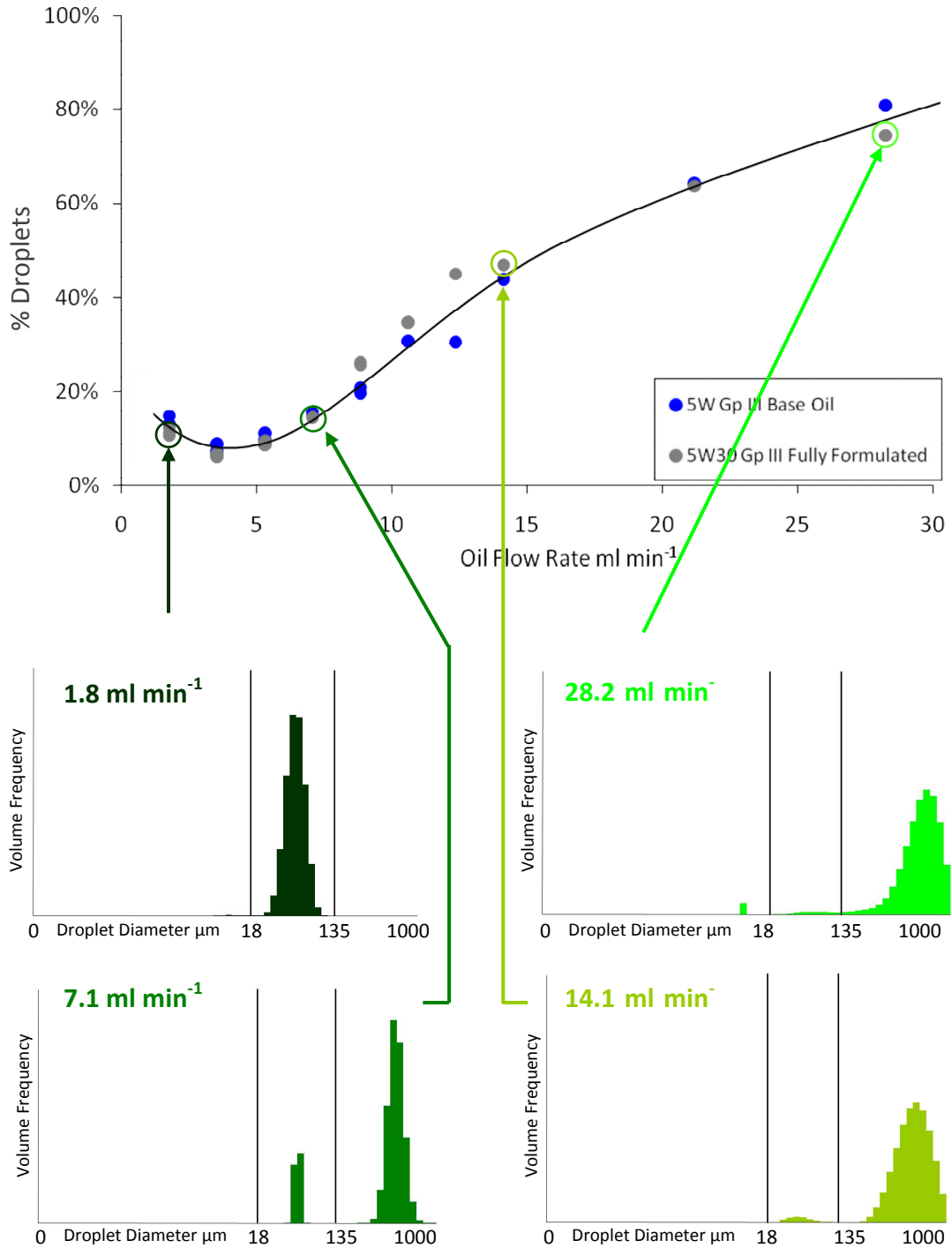


**Figure 4.8: Misting Tendency and Flow Rate Graph for Parametric Testing Incorporating Droplet Size Distributions for Fully Formulated Oil**

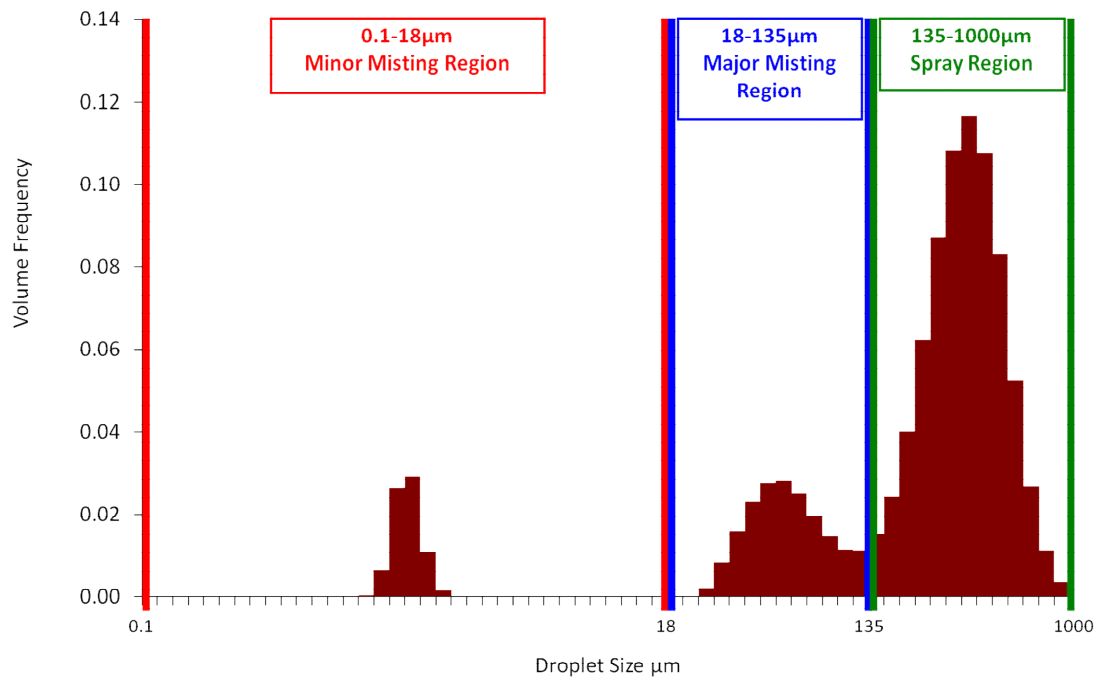


**Figure 4.9: Characteristic Droplet Sizes: Droplet Size Distribution of PAO 8 at 3ml/min**

regions, though others exist in other oils, termed the minor and major misting regions, with droplet sizes in the range 0.1-18 $\mu\text{m}$  and 18-135 $\mu\text{m}$  respectively, as shown in Figure 4.9, using data for a Group IV PAO as an example. The major misting region is so called because it occurred with almost every oil, whereas the minor misting region was not present in many oils: The distinction is not based on droplet size per se.

There was little variation in the flow rate of droplets in the major and minor misting regions with increasing oil flow rate. Thus, the linear variation in misting tendency with oil flow rate can be attributed to a variation in the tendency to produce droplets in the spray region. Therefore, conditions above the onset of the linear increase in misting tendency above 5ml/min, seen in Figure 4.8, will be termed the spray regime. The onset of the spray regime is defined as the flow rate above which the linear increase in misting tendency is significant i.e. where the next point along the x-axis has non-overlapping error bars. It is thought that the difference in misting seen in the spray regime is due to the onset of a different mechanism of misting. It is

hypothesised that in this region the quantity of oil accumulating at the inlet feed is sufficient for the interaction between oil and gas flow to change. This can be explained in terms of the difference between ‘rolling’ and ‘undercutting’ described by Hewitt (1970), shown in Figure 4.10. Alternatively, this behaviour could be thought of as an increase in the curvature of the interface with increased flow rate, whereby the misting mechanisms will tend to shift from those of a film to those of a droplet (see Section 3.1.2.2). Which of these explanations is more viable was not investigated.

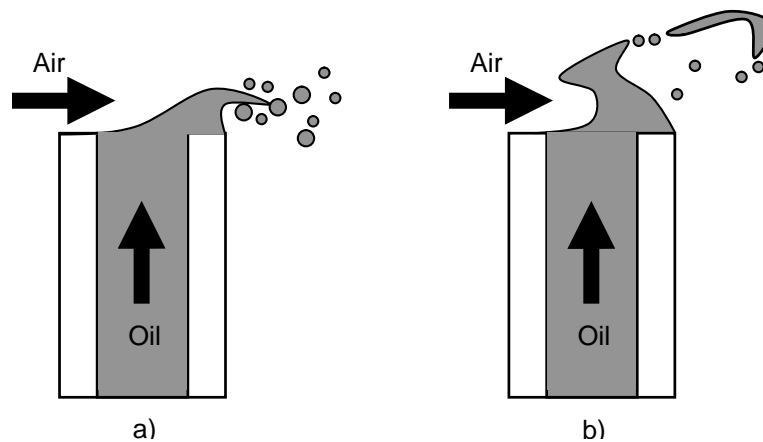


**Figure 4.10: Mechanisms of Droplet Formation a) Rolling b) Undercutting, after (Hewitt et al., 1970)**

Droplets in the spray region are not considered to be of great relevance to misting in the piston assembly as the ring gap size of an engine is not significantly greater than these droplets; for example 0.603mm for the top ring of the Ricardo Hydra used in the study. This, and the tortuous flow path, would mean that such droplets would not be transported a significant distance through the piston. Therefore, droplets with diameters below 135 $\mu$ m will form the main focus of the analysis. However, as droplets greater than 135 $\mu$ m are formed in the misting regime also, they cannot be neglected completely. Therefore, it was decided to test with oil flow rates in the range 3-9 ml/min. This allowed measurement of the misting regime and the transition into the spray regime. Flow rates below 3 ml/min are more difficult to produce in a repeatable manner, so were not tested. The range of measurements was extended where relevant i.e. where the onset of the spray regime occurred above 9ml/min.

There are two methods for this system by which the flow rate of oil as a mist can be calculated. Firstly, the oil entering and exiting the system can be weighed to find the parameters in Equation 4.18. Secondly, by applying the Beer-Lambert Law to the obscuration data measured by the particle sizer, Equation 4.14, and with the known flow rate of air past the detector, the flow rate of oil can be calculated. Figure 4.11 shows a comparison between the two methods for the data from the preliminary tests.

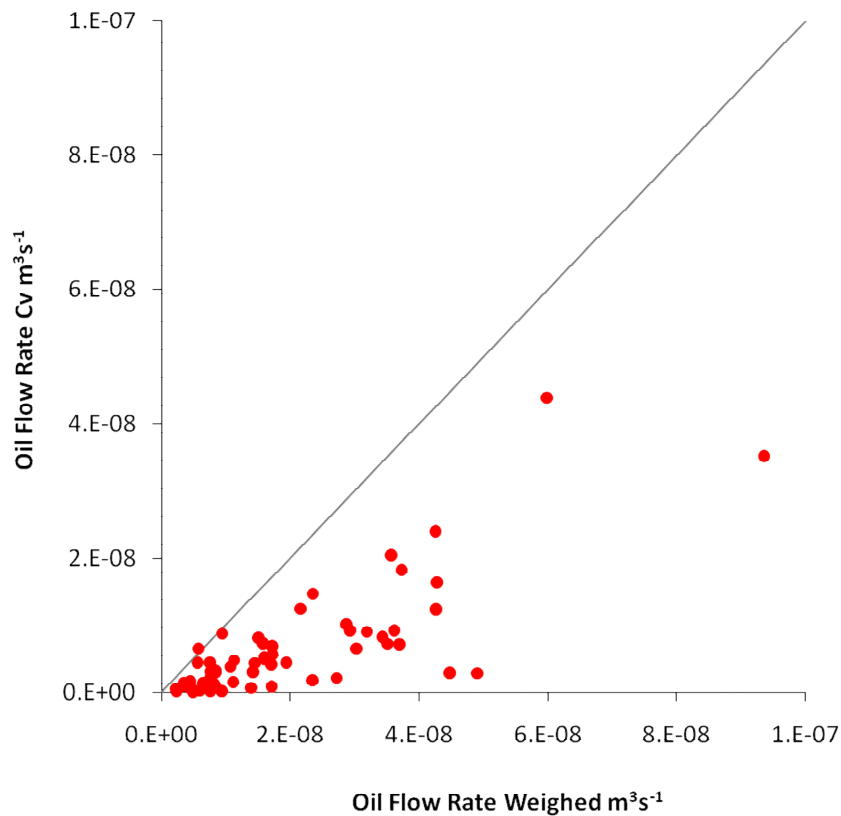


**Figure 4.11: Comparison of Mist Flow Rate Measurement Techniques**

The former, weighing method produces higher values for flow rate than the optical method. This difference is attributed to the fact that not all droplets pass through the detector beam, thus reducing the accuracy of the optical method. Therefore, as the weighing method is more accurate, this was used to define flow rate measurements for this system.

## 4.5 Test Matrix

The aim of this investigation was to assess the critical parameters in a lubricant that affect this type of misting, and their relative importance in a typical engine lubricant.

Base Oil			Viscosity @20°C, Pa.s	Additive		Reference
API Group	SAE Grade	Ave. Mol. Wt.		Type	Chemistry	
III	5W	-	97.93	-	-	Gp III
III	5W30	-	115.36	Fully Formulated		FF
III	5W30	-	130.15	Viscosity Modifier	Poly(isoprene-co- styrene) Star	VM
III	5W	-	94.91	Detergent	Sulphonate Phenate	SP
III	5W	-	94.42	Detergent	Calcium Salicylate	CS
III	5W	-	116.88	Dispersant	Not Known	Disp
III	5W	-	91.50	Anti-foam	Silicone	AF
I	5W	-	72.10	-	-	Gp I
II	5W	-	65.89	-	-	Gp II
IV	5W	620	80.94	-	-	Gp IV
IV	-	285	7.97	-	-	PAO 2
IV	-	436	32.16	-	-	PAO 4
IV	-	530	62.02	-	-	PAO 6
IV	-	600	97.99	-	-	PAO 8

Table 4.3: Oil Formulations for Misting Simulation Stage 1

Firstly, a typical commercial automotive lubricant was considered in its component parts. A 5W Group III base oil and a fully formulated 5W30 Group III were chosen as reference lubricants and the additives that may have a significant effect on the rheology (viscosity modifier) or surface properties (anti-foam, detergent, dispersant) were systematically added to the reference base oil. These additives were included at the concentrations found in a commercial lubricant, which were not disclosed by the industrial sponsor. The known properties of the tested oils are shown in Table 4.3.

Secondly, the base oil properties were considered. A base oil from each of the first four groups in the API classification with similar viscosities were chosen to compare the effect of molecular weight distribution (i.e. with reference to the narrowing of the distributions with greater refining). These are shown in Table 4.3.

Thirdly, the viscosity and molecular weight of base oil were considered by the use of four Group IV polyalphaolefins with different molecular weights. These are also shown in Table 4.3.

Viscosity was measured using an Anton Paar Stabinger 3000 viscometer, which is used in ASTM D2770 and ISO2909 to determine an accurate viscosity index. This device functions by inductively rotating a cylinder in a tight-clearance cavity, in which the lubricant is sheared. The inputted inductive energy allows the cylinder to rotate, and, as the total energy in the system is constant, an increase in viscous loss is manifested as a reduction in rotational speed.

## 4.6 Results

In order to statistically determine the significance of the results, 95% confidence intervals were applied to each measured variable presented. The 95% confidence interval is calculated from a set of 4 repeated batches of tests for the 5W Group III base oil reference. These are rendered as error bars on all graphs.

Figure 4.12 shows the variation of misting with flow rate for different PAO base oils. The tendency to mist is given as percentage mist. This parameter is defined in Equation 4.18. It can be seen that there are significant differences in behaviour between the oils tested. At low flow rates, where conditions are predominantly in the misting regime, there is a significant increase in misting tendency with a decrease in the viscosity and molecular weight of the oil. This is shown more clearly in Figure 4.12 and Figure 4.13 where the variation of misting potential at an input flow rate of 3ml/min is plotted against dynamic viscosity at 20°C and molecular weight respectively.

The variation with molecular weight appears to be linear in the range studied. Figure 4.14 shows that for these chemically similar PAOs  $\eta \propto M^{3.3}$ , where  $\eta$  is the dynamic viscosity at 20°C in Pa.s and  $M$  is the average molecular weight of the PAO. Thus, as could be imagined by an approximate superposition of these trends, the variation of

misting tendency with dynamic viscosity can be described closely with a third order polynomial, Figure 4.15.

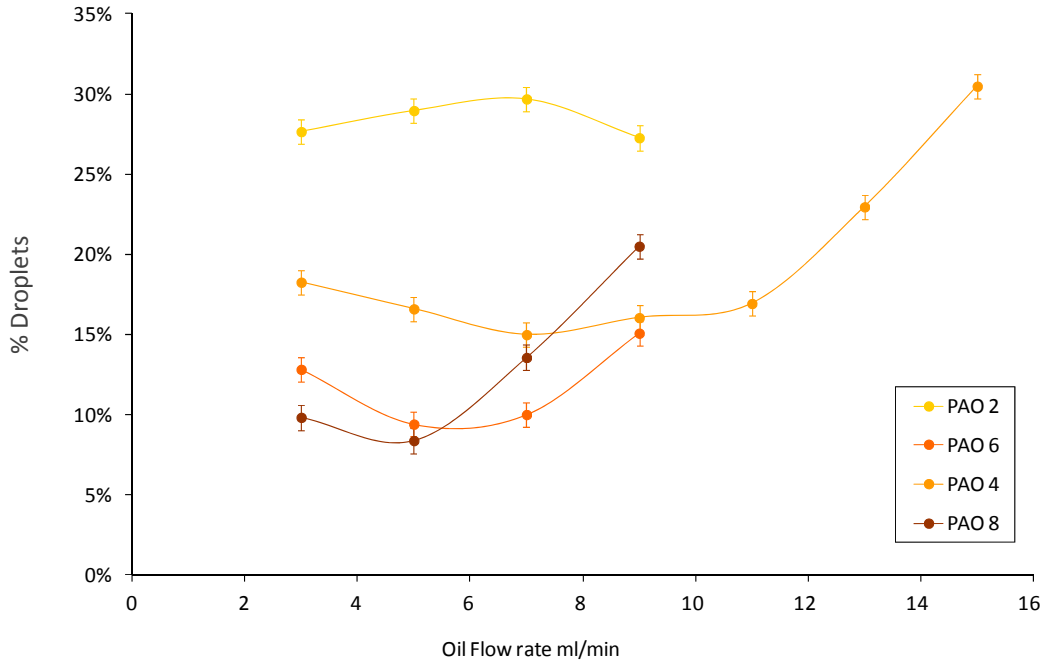


Figure 4.12: Misting Tendency and Flow Rate for PAOs of Known Molecular Weight

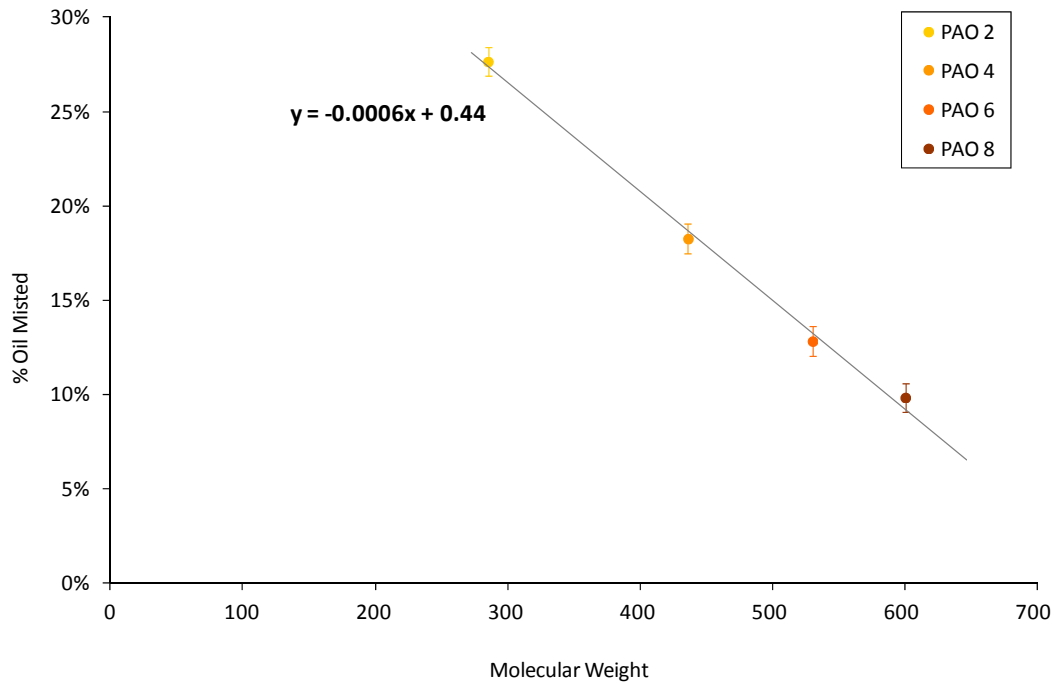


Figure 4.13: Misting Tendency versus Molecular Weight for PAOs at Inlet Flow Rate of 3ml/min



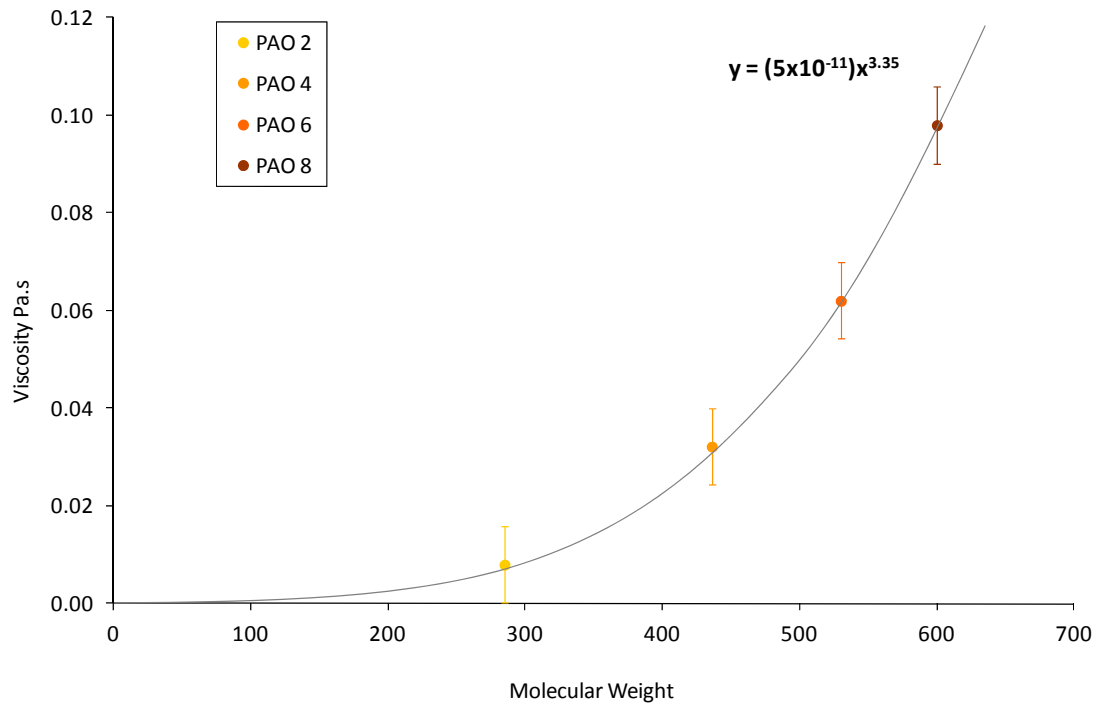


Figure 4.14: Dynamic Viscosity at 20°C versus Molecular Weight for PAOs

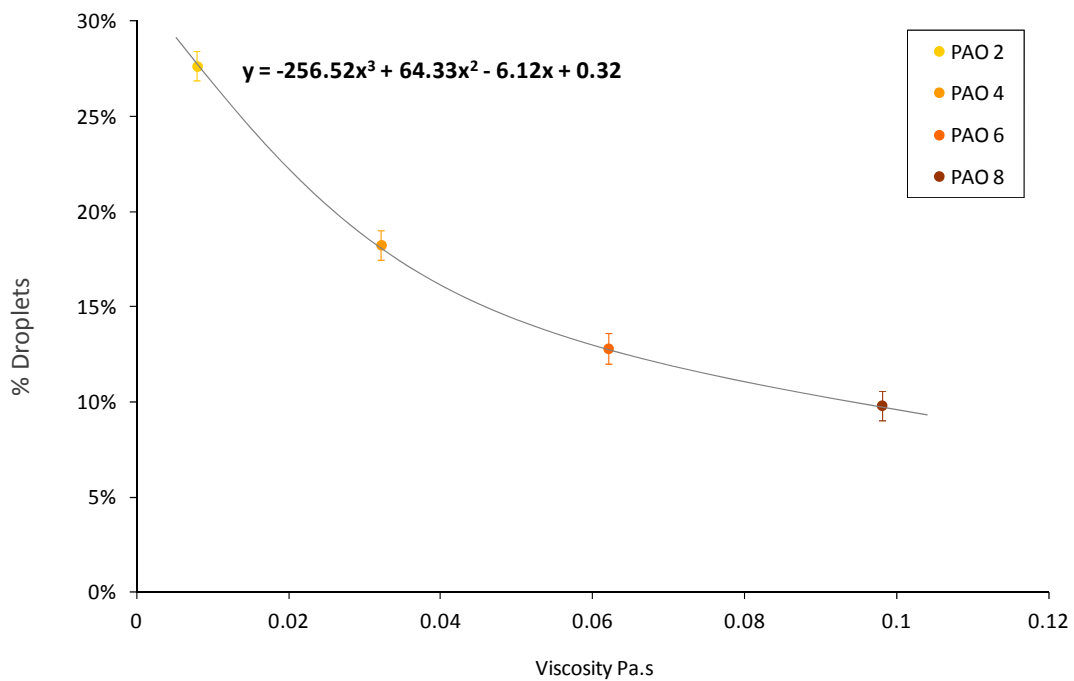
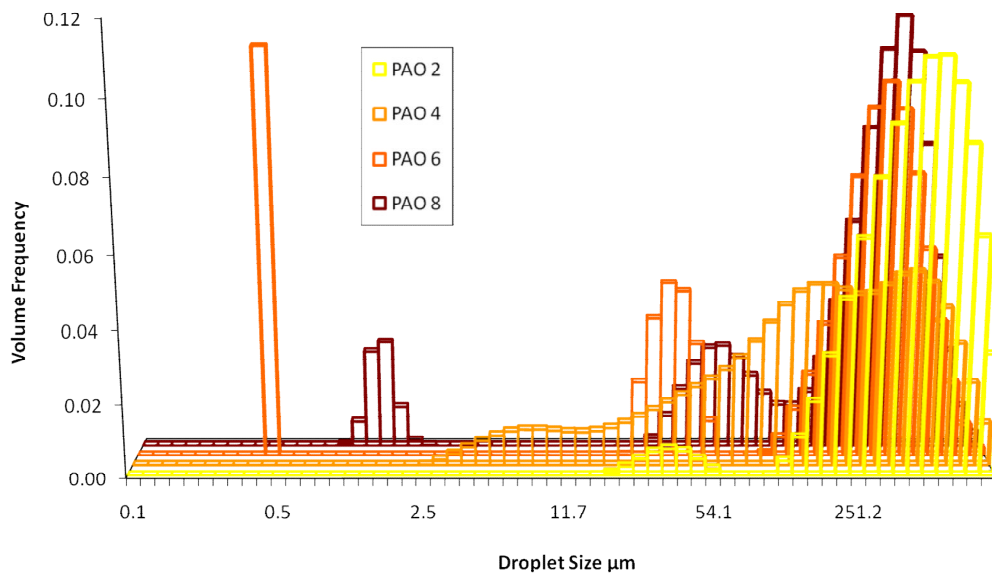


Figure 4.15: Misting Tendency versus Viscosity for PAOs at Inlet Flow Rate of 3ml/min

At higher inlet flow rates, as seen in Figure 4.12, there are differences in the onset of the spray regime. Oils with a lower viscosity enter the spray regime at higher inlet flow rates. The range of flow rates for PAO 4 is extended to show this, though for PAO 2 it was not possible. This appears to reinforce the concept that the spray regime is dependent on the accumulation of oil at the inlet, Section 4.4. An increase in resistance to shear, i.e. viscosity, should result in a greater accumulation of oil at the inlet for an equivalent inlet flow rate. This is manifested in the onset of the spray region for PAO 8 being at approximately 5 ml/min and at approximately 11 ml/min for PAO 4.



**Figure 4.16: Droplet Size Distributions for PAOs at Inlet Flow Rate of 3ml/min**

Figure 4.16 shows the droplet size distributions for these oils at 3 ml/min. It can be seen that the volume in the spray region (135-1000 $\mu\text{m}$ ) is relatively large but it should be noted that the number of droplets in this region is very small. The minor misting region (0.1-18 $\mu\text{m}$ ) is intermittent in its presence, suggesting that it may be a secondary mechanism (e.g. droplet destruction). In the major misting region (18-135 $\mu\text{m}$ ), there is an increase in the characteristic droplet size with viscosity. This neglects the result for PAO 4 where the characteristic size is larger and appears to merge with the spray region. The increased droplet size will result in a higher

deposition rate from the mist, resulting in a reduced mist flow rate. It is thought too that increased viscosity will decrease the production of droplets (i.e. the entrainment rate). These results reflect these relationships and confirm the findings of previous work, such as Dasch (2008).

It is thought, as molecular weight has an effect on misting, that the molecular weight distribution will also have an effect. Such variation is seen most commonly in lubricant oils in terms of the API group. The distribution of molecular weights around the mean decreases from Group I to Group IV. This variation is a result of the degree of refining undergone by each oil. Thus, there will be chemical differences between oils of different groups. Figure 4.17 shows the tendency to mist of a lubricant from each API Group, each with a similar dynamic viscosity at 20°C (Table 4.3), tested at an inlet flow rate of 3 ml/min. A fully formulated reference oil is also shown. The tendency to mist appears to decrease for Groups I-III, the refined mineral oils. However, as can be seen with the error bars, this variation is not statistically significant. The Group IV PAO mists much more readily than the others. This suggests that there is some other mechanism beyond just viscosity and molecular weight.

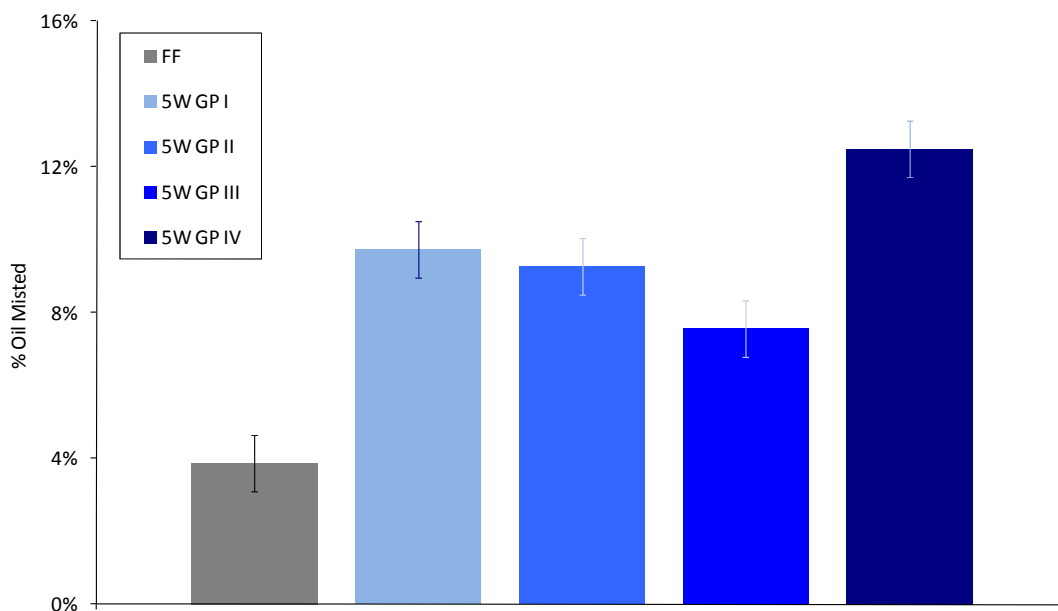


**Figure 4.17: Misting Tendency of Different Oil Groups at Inlet Flow Rate of 3ml/min**

The surface tensions of all these oils were measured on a White Electrical Instruments surface tension balance with a 4cm platinum ring, and were found to be the same,  $0.031 \text{ Nm}^{-1}$ . Thus, surface tension effects cannot be the cause. It is thought that the differences in molecular structure between refined and synthetic hydrocarbons may be the cause. Refined hydrocarbons are generally linear with some minor branching, whereas synthetic hydrocarbons, such as PAO, can be highly non-linear (Mang et al., 2001), Figure 4.18. Thus, differences in molecular dynamics, such as chain bending and stretching, and molecular interactions, such as entanglement, may be the cause of this phenomenon. However, it should be noted that these differences are significantly smaller in magnitude than those arising between base oils with different molecular weight, Figure 4.14, and a base oil and its fully formulated equivalent, Figure 4.17.

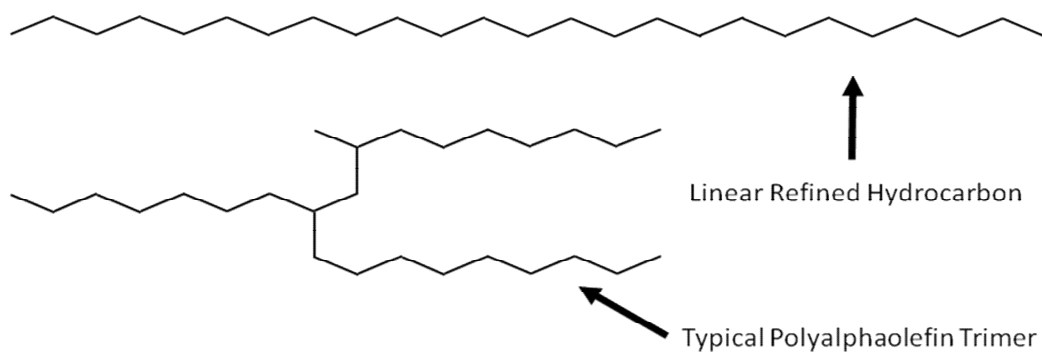


**Figure 4.18: Carbon Backbone Structure of Refined Hydrocarbons and Polyalphaolefins**

Figure 4.19 shows the misting potential of the 5W Group III base oil containing various additives, tested at an inlet flow rate of 3 ml/min. It is clear that there is a significant difference in misting tendency between the base oil and its fully formulated equivalent. The dispersant and sulphonate-phenate detergent do not change the misting tendency of the base oil in a statistically significant way. Small but significant increases in misting potential are seen with anti-foam and the salicylate detergent. These suggest that surface tension has an effect on the tendency of an oil to mist.

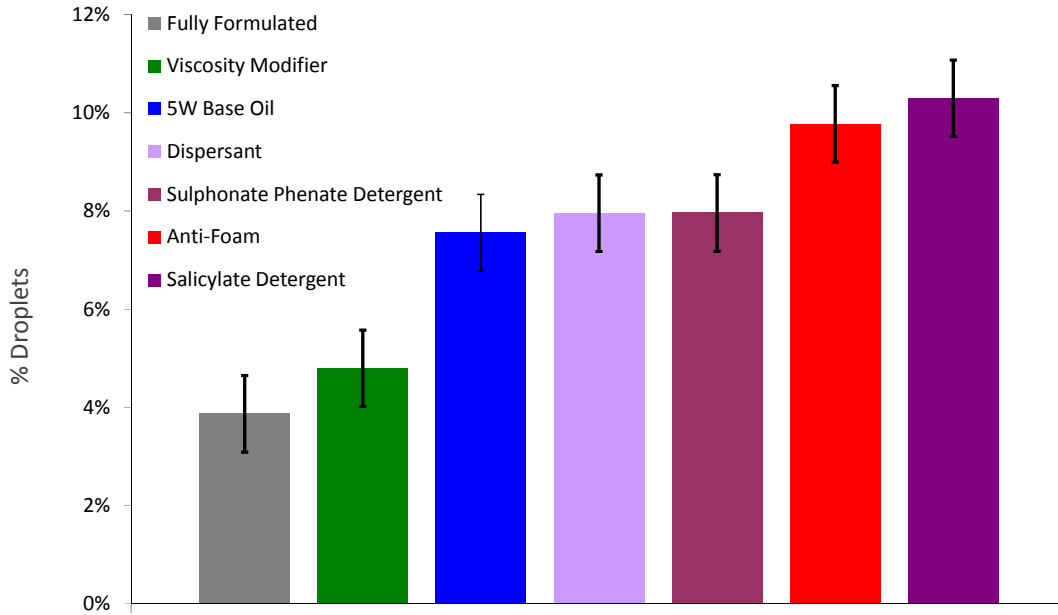


**Figure 4.19: Misting Tendency for 5W Group III Base Oil with Commercial Additives at Inlet Flow Rate 3ml/min**

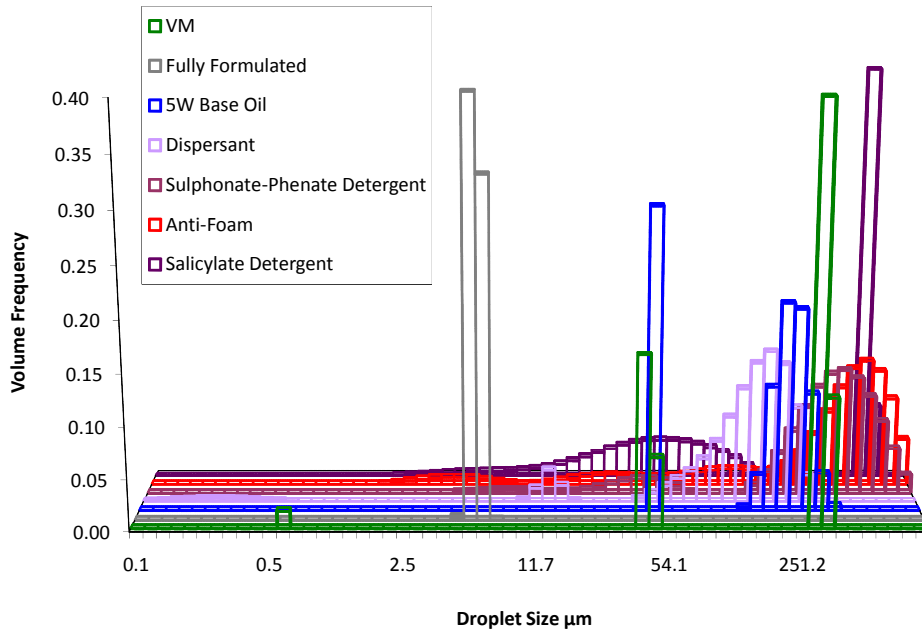


**Figure 4.20: Droplet Size Distribution for 5W Group III Base Oil Containing Additives at Inlet Flow Rate of 3ml/min**

The droplet size distributions for these tests, Figure 4.20, show that surface-active additives tend to widen the distribution of droplet sizes, particularly in the major misting region, and particularly in those oils that produce a significant increase in misting tendency. This suggests that these chemicals affect the entrainment process, and perhaps cause local variation in the misting tendency within the oil. The large decrease in misting tendency in a fully formulated oil, when compared to its original base oil, appears to be produced by the viscosity modifier, as the misting tendency of the oil containing viscosity modifier and the fully formulated lubricant are most closely matched.

The viscosity modifier, as discussed in Section 2.2.4 and Section 3.1.6, alters the temperature-viscosity response of the oil, but also has an effect on the viscoelastic properties of the oil i.e. whether the oil behaves more like a fluid or a solid under shear, or somewhere intermediate. Polymer-containing liquids tend to increase solid behaviour under shear, causing the material to stiffen. Energy is stored elastically in the polymer molecules and less is dissipated through viscous loss. It is thought that it is the viscoelastic response of the polymer-containing oil that causes the reduction in misting tendency. The droplet size distribution for the polymer-containing oil shows a narrowing of the droplet size distribution relative to its base oil. However, there appears to be little change in the average size of the droplets, as might be predicted from other studies e.g. Dasch (2008). This, therefore, suggests that the major effect of the polymer is to suppress the entrainment of droplets. It is thought that this is a result of the viscoelastic response of polymer-containing oils. In such polymeric systems, shear energy is dissipated through molecular dynamics (e.g. stretching, elongation) and molecular interactions (e.g. entanglement) of the large molecules, thus increasing resistance to bulk deformation. It should be noted that the reduction in misting tendency from the base oil reference by the inclusion of polymers (2.8-3.7%) is greater than the increase by the inclusion of salicylate detergent (a 2.7% increase).

## 4.7 Statistical Analysis

### 4.7.1 Principal Component Analysis

In order to better evaluate the significance of the results, and to determine the dominant trends in the data, statistical analysis was performed. Of the various multivariate tools available, principal component analysis (PCA) was chosen. Such analysis is suitable for this study as it is able to quickly identify significant and insignificant trends. The technique was developed in the 1930s but was limited by the scope of hand calculated to small numbers of variables until computers became more accessible (Manly, 1994). As described by Manly (1994), this technique correlates each variable against each other variable and uses Eigen analysis to identify which groups of variables correlate most strongly with each other. This analysis treats variables independently, i.e. does not consider interactions between variables like a Taguchi analysis, and does not distinguish between input and output variables. However, unlike other analyses, it does not require a specific test matrix, so complex and varied datasets can be analysed; though this clearly places the burden of wise experimental design on the operator. Datasets are best described if highly correlating and non-correlating variables are included, so that the significance of identified relationships can be qualified (Manly, 1994).

This technique was used as a linear analysis in this study, so preventing accurate analysis of highly non-linear variables. The data for  $p$  variables in  $n$  cases is taken. In this study,  $n$  refers to the number of tests performed ( $n=109$ ) and 43 variables are studied ( $p=43$ ). The analysed variables are shown in

Table 4.4. A matrix is produced of the covariance of each combination of variables, defined as:

$$c_{jk} = \sum_{i=1}^n (x_{ij} - \bar{x}_j)(x_{ik} - \bar{x}_k) / (n-1) \quad [4.19]$$

Where  $j$  and  $k$  refer to the two variables,  $i$  refers to the number of the case (between 1 and  $n$ ),  $\bar{x}$  is the mean of the variable.

The covariance values are transposed into distributions with a mean of zero and a variance of 1. This new value is termed the correlation coefficient, and the resulting matrix the correlation matrix. The correlation coefficient is defined as:

$$r_{jk} = c_{jk} / (\sqrt{c_{jj}} \times \sqrt{c_{kk}}) \quad [4.20]$$

Where  $c_{jj}$  and  $c_{kk}$  are the variances of the variables  $j$  and  $k$ .

Principal component analysis hypothesises that the variation in the dataset can be expressed as a series of linear equations, the principal components, containing each variable weighted by a coefficient:

$$\begin{aligned} \text{Component 1} &= a_{11}X_1 + a_{12}X_2 + \dots + a_{1p}X_p \\ \text{Component 2} &= a_{21}X_1 + a_{22}X_2 + \dots + a_{2p}X_p \\ &\dots \\ \text{Component } p &= a_{p1}X_1 + a_{p2}X_2 + \dots + a_{pp}X_p \end{aligned} \quad [4.21]$$

The first principal component represents the combination of coefficients that produce the greatest variance when the data is input, but only when the coefficients meet the condition that:

$$a_{11}^2 + a_{12}^2 + \dots + a_{1p}^2 = 1 \quad [4.22]$$

In turn, the second principal component is the combination that produces the second greatest variation of whilst exhibiting no correlation with component 1 and fulfilling the same condition:

$$a_{21}^2 + a_{22}^2 + \dots + a_{2p}^2 = 1 \quad [4.23]$$



Variable		Description
1	Input Flow Rate	Nominal flow rate from syringe pump
2	Test Start	Time between starting equipment and oil reaching venturi
3	$\eta$ @20°C	Oil dynamic viscosity at test temperature
4	$\nu$ @20°C	Oil kinematic viscosity at test temperature
5	$\rho$ @20°C	Oil density at test temperature
6	Weight Catch	Weight of oil caught until pump reaches steady state
7	Total Out Syringe	Weight of oil leaving syringe during test
8	Total Into Venturi	Weight of oil entering venturi during test
9	Total Unmisted	Weight of oil collected from pipe end during test
10	Total Misted	Calculated weight of oil flowing as mist during test
11	% Misted	Misted oil as a percentage by weight of input into venturi
12	Transmittance	Optical transmittance measured by particle sizer
13	10% Drop d	Diameter below where 10% of droplets are smaller
14	50% Drop d	Median droplet diameter
15	90% Drop d	Diameter below which 90% of droplets are smaller
16	%V<10 $\mu$ m	% of droplets with a diameter less than 10 $\mu$ m
17	Mean d(a)	Mean droplet diameter weighted by surface area
18	Mean d(v)	Mean droplet diameter weighted by volume
19	Oil : Air Ratio	Oil : Air ratio of flow as measured by particle sizer
20	Span	A measure of the range of the droplet sizes. See Table 4.2
21	Obscuration	Optical obscuration
22	$\dot{v}$ (weighed)	Mist flow rate calculated from weighted data
23	$\dot{v}$ (Cv)	Mist flow rate calculated from optical data
24	$\dot{v}$ % <18 $\mu$ m	% of volume flowing as a mist with droplets smaller than 18 $\mu$ m
25	$\dot{v}$ % 18-135 $\mu$ m	% of volume flowing as a mist with droplets between 18-135 $\mu$ m
26	$\dot{v}$ % >135 $\mu$ m	% of volume flowing as a mist with droplets larger than 135 $\mu$ m
27	$\dot{v}$ <18 $\mu$ m	Volume flow rate of mist as droplets smaller than 18 $\mu$ m
28	$\dot{v}$ 18-135 $\mu$ m	Volume flow rate of mist as droplets between 18-135 $\mu$ m
29	$\dot{v}$ >135 $\mu$ m	Volume flow rate of mist as droplets larger than 135 $\mu$ m
30	$\dot{v}$ <135 $\mu$ m	Volume flow rate of mist as droplets smaller than 135 $\mu$ m i.e. mist region
31	Drops/s <135 $\mu$ m	Droplet flow rate for mist regions
32	$\dot{a}$ <135 $\mu$ m	Diameter flow rate for mist regions
33	$\dot{a}$ <135 $\mu$ m	Area flow rate for mist regions
34	$\dot{v}$ <135 $\mu$ m	Volume flow rate for mist regions (should be identical to 30)
35	Mean a <135 $\mu$ m	Mean droplet surface area for misting regions
36	Mean v <135 $\mu$ m	Mean droplet volume for misting regions
37	Mean d(d) <135 $\mu$ m	Mean droplet diameter for misting regions
38	Mean d(a) <135 $\mu$ m	Mean area-weighted droplet diameter for misting regions
39	Mean d(v) <135 $\mu$ m	Mean volume-weighted droplet diameter for misting regions
40	Mean d(smd) <135 $\mu$ m	Sauter Mean Diameter for misting regions
41	Small Drop d	Characteristic droplet diameter for droplets with diameters <18 $\mu$ m
42	Medium Drop d	Characteristic droplet diameter for droplets with diameters 18-135 $\mu$ m
43	Large Drop d	Characteristic droplet diameter for droplets with diameters >135 $\mu$ m

**Table 4.4: Variables Used in Principal Components Analysis**

These equations are produced by Eigen analysis of the correlation matrix. The variance of each component is the Eigen value of the particular equation. When given as a percentage of the sum total of all the Eigen values, the individual Eigen value indicates the contribution of its component to the total variation in the dataset. These equations indicate correlation, not causation. Therefore, any relationships must be interpreted from the outcomes (Manly, 1994).

### 4.7.2 Outcomes

A principal component analysis was performed on the data for the variables shown in Table 4.4 using Minitab, a piece of statistical analysis software. This yielded four significant components: Table 4.5 shows each of these components and the significant variables within each that cause their variation, as indicated by their '*a*' coefficients, the weightings that indicate their contribution to the variance of the component.

The first principal component, describing 38.4% of the data variation, indicates a strong correlation between the flow rate of oil into the system (including the 'total...' parameters as the test duration is fixed – i.e. they could be considered as a flow rate in units per two minutes) and the percentage leaving the system as mist (also represented as the 'Oil : Air Ratio' and 'total misted'). This is confirmation of the relationship shown in Figure 4.8. As discussed previously, this is caused by an increase in droplet flow rate in the spray region. This, in turn, is reflected in the component by the increase of flow rate of droplets in this region ( $>135\mu\text{m}$ ) and area weighted droplet size with misting tendency.

The second principal component explains 22.4% of the data variation. In this, the strongest correlations are between obscuration, transmittance and the area flow rate of droplets in the misting regimes ( $<135\mu\text{m}$ ). Obscuration is closely related to transmittance, so this should not be a surprise. This component appears to reflect the variation in optical conditions. Obscuration and transmittance are affected, firstly, by the absorption of light, indicated by parameters such as '% misted' and the various flow rates of droplets which increase the area of absorbent droplets in the light path.

Secondly, as the obscuration (and thus transmittance) are affected by light being scattered past the detectors. According to Mie theory (Section 4.3.1), scattering increases with droplet diameter. Therefore, strong inverse relationships between droplet size parameters and obscuration exist. The particular strength of the correlation with area flow rate is due to changes in this parameter affecting both absorption and scattering.

Component 1		Component 2		Component 3		Component 4	
Eigenvalue Proportion: 38.4%		Eigenvalue Proportion: 22.4%		Eigenvalue Proportion: 18.7%		Eigenvalue Proportion: 7.8%	
a	Variable	a	Variable	a	Variable	a	Variable
0.213	Input flow rate	0.165	Total misted	0.239	$\dot{v}$ % 18-135 $\mu$ m	-0.309	$\eta$ @20°C
0.215	Total out syringe	0.154	% Misted	0.267	$\dot{v}$ 18-135 $\mu$ m	-0.306	$v$ @20°C
0.215	Total into venturi	-0.294	Transmittance	0.250	$\dot{v}$ <135 $\mu$ m	-0.354	$\rho$ @20°C
0.214	Total unmisted	-0.178	10% Drop d	0.250	$\dot{v}$ <135 $\mu$ m	-0.315	Weight catch
0.204	Total misted	-0.210	50% Drop d	0.237	Mean a <135 $\mu$ m	0.335	Span
0.203	% Misted	-0.180	90% Drop d	0.218	Mean v <135 $\mu$ m	0.273	Drops/s <135 $\mu$ m
0.225	Mean d(a)	-0.197	Mean d (v)	0.262	Mean d(d) <135 $\mu$ m	0.218	$\dot{d}$ <135 $\mu$ m
0.218	Oil : Air Ratio	0.286	Obscuration	0.259	Mean d(a) <135 $\mu$ m	-0.196	Small Drop d
0.222	$\dot{v}$ >135 $\mu$ m	0.166	$\dot{v}$ (weighed)	0.255	Mean d(v) <135 $\mu$ m		
		0.259	$\dot{v}$ <18 $\mu$ m	0.232	Mean d(smd) <135 $\mu$ m		
		0.168	$\dot{v}$ <135 $\mu$ m	0.237	Medium Drop d		
		0.162	$\dot{d}$ <135 $\mu$ m				
		0.302	$\dot{a}$ <135 $\mu$ m				
		0.168	$\dot{v}$ <135 $\mu$ m				
		-0.218	Large Drop d				

**Table 4.5: Outcomes from Principal Components Analysis**

The third principal component explains 18.7% of the data variation. This component is related entirely to the behaviour of droplets in the misting regions (<135 $\mu$ m). The flow rate of oil as mist (<135 $\mu$ m) is correlated most strongly with the flow rate and

percentage flow rate in the major misting region (18-135 $\mu\text{m}$ ). The equivalent properties for the minor misting region (<18 $\mu\text{m}$ ) do not have any such correlation. This suggests that misting behaviour is dominated by the major misting region. Whilst this is not surprising, this is an important conclusion. Common sense indicates that the observed correlation between droplet sizes, areas, volumes and flow rates are also to be expected.

The fourth principal component explains 7.8% of the data variation. This is the final significant component, as those remaining describe less than 5% of the total variance each. This component indicates a correlation between oil properties and the droplet distributions that are produced. An increase in the viscosity and density of the oil increases the size of droplets in the minor misting region (<18 $\mu\text{m}$ ). As misting is shear-driven, it is thought that the viscosity has a greater effect on the misting than density. The span, a representation of the range of droplet sizes in the distribution, reduces with an increase in viscosity. The droplet flow rate (number per second) and the diameter flow rate in the misting region both decrease with viscosity, suggesting that an increase in viscosity tends to decrease the amount of mist produced. However, this is not correlated with any flow rate parameters. This, and the effect of the span, suggests that an increase in viscosity narrows the droplet size distribution, indicating an increased resistance to droplet breakup, a process that yields droplets in the minor misting region.

From this statistical analysis, we can deduce that the transition between the mist and spray regimes causes the greatest variation in the dataset. Therefore, it is critical to keep test conditions either totally within the misting regime or up to the transition to maximise the insight on misting. The misting behaviour is dominated by the droplets in the major misting region. The viscosity of the oil appears to affect the tendency of droplets to break up.

The most significant trends observed were, firstly, the increase in misting tendency produced by increasing input flow rate when in the spray regime. Secondly, while lesser in magnitude but more important for mists in the piston assembly, an increase

in mist-sized droplets with overall droplet flow rates is seen. Thirdly, perhaps unsurprisingly, the flow rate of mist-sized droplets is dependent on the size parameters of the droplets in this range. Fourthly, an increase in the lubricant viscosity resulted in a decrease in the mist produced, specifically the droplet count per second. This latter trend implies the observation that increasing viscosity tends to produce larger droplets by forming and breaking liquid ligaments. It should be noted that the effects of additives and oil groups are not included in this analysis as they are a discontinuous variable i.e. they are logical categories rather than continuous variables, and, thus, cannot be incorporated into this analysis. The effects arising from additives are of greater magnitude and significance than those observed in components 3 and 4. Thus, whilst general flow parameters that control the mechanism of droplet formation are most significant, the oil composition, particularly the additives it contains, is the most significant variable that can be controlled in the engine environment. In terms of the oil composition, the viscosity of the base oil and the presence of viscosity modifying polymers have the greatest effect on the misting tendency of the oil. The trends observed with variation of viscosity are well defined and in agreement with other work. The significant reduction in misting tendency seen with the inclusion of viscosity modifier is the most significant effect of any additive in a commercial lubricant. Therefore, as there are many varieties of viscosity modifier and many ways in which it can be blended into a lubricant, it is felt that this parameter deserves more detailed study.

## **4.8 Summary**

This investigation has produced the following outcomes:

- A mist generator replicating flow conditions through the top ring gap of an engine has been used to investigate the effect of different oil properties on misting.
- The variation of misting tendency with the inlet oil flow rate is defined by two regimes of distinct behaviour, termed misting and spray.

- The tendency to mist varies linearly with molecular weight and with a third order polynomial for viscosity.
- The change in molecular weight distribution seen in different API Groups does not produce significant variation in the tendency to mist. However, Group IV oils (PAOs) mist significantly more than refined mineral oils.
- The effect of some surface-active additives (dispersants and sulphonate-phenate detergents) do not have a significant effect on misting tendency. Anti-foams and salicylate detergents, however, produce a significant increase in misting.
- The most significant additive in defining the misting behaviour of a commercial lubricant is the viscosity modifier. This suggests that the viscoelastic properties of the lubricant have a major effect on the tendency to produce droplets. This agrees with the conclusions of other research into misted oils in other applications.
- Statistical analysis of the results produced shows that the most significant influence on misting tendency are the general flow parameters that influence whether the droplet formation mechanism is based on rolling or undercutting, as described by component 1.
- However, the most significant variable that can be controlled in the engine environment is oil composition, particularly polymer content.

## **Chapter 5: Simulation of Misting in the Piston Ring Gap and Considering the Effects of Viscosity Modifying Polymers**

### **5.1 Introduction**

The outcomes of Chapter 4 show that the viscosity modifier in a typical commercial lubricant has a greater effect on the misting properties of the lubricant than any other additive. The ability of viscosity modifier to reduce misting tendency is attributed to the viscoelastic properties long chain polymers produce. This chapter reports more detailed investigation of this effect using the same techniques. The effect of polymer molecular structure and concentration is considered.

### **5.2 Method**

The same mist generation and measurement apparatus was used as in Chapter 4, the venturi mist generator upstream of a laser diffraction particle sizer, no modifications were made. For detailed characterisation of the polymer blends, measurements of molecular weight and rheological analyses were undertaken.

### **5.3 Polymer Molecular Weight Characterisation**

Various polymers were chosen for this investigation, with different molecular weights and molecular structures. The molecular weight distributions of polymers used in this study were measured using gel permeation chromatography, GPC. This technique is often referred to as size exclusion chromatography, SEC (Mori et al., 1999). It involves a polymer in solution passing through a column of porous particles, termed the packing material, which differentiates the mixture by molecular weight. The pore sizes of the column are manufactured to a close tolerance and are of comparable size to a polymer molecule, so that some molecules are small enough to diffuse into the

pores, and others are too large to do so. Thus, the column can be considered to comprise several different volumes, related by the following equation:

$$V_t = V_0 + V_i \quad [5.1]$$

Where  $V_i$  is the pore volume of the packing material,  $V_0$  is the void volume between the packing material i.e. where material can freely flow and  $V_t$  is the sum of these volumes, which is termed the total mobile phase volume (Mori et al., 1999).

Thus, as the polymer solution flows through the column, the smaller polymer molecules will diffuse into the pore volume, causing a change in polymer concentration between  $V_i$  and  $V_0$ . Thus, the behaviour of polymer in solution can be described by the retention volume,  $V_R$ , which is the volume of sample that has passed through the column at a particular time:

$$V_R = V_0 + \frac{c_i}{c_0} V_i \quad [5.2]$$

Where  $c_i$  is the polymer concentration in the pore volume, and  $c_0$  is the polymer concentration in the void volume (Mori et al., 1999). Because they cannot diffuse into the gel pores, larger polymers leave the column early in the test i.e. when  $V_R$  is low and test time is small. Smaller polymers will leave the column later i.e. when  $V_R$  is high and test time is large.

The polymer molecules leaving the column can be detected in several ways. In this study, refractive index and light scattering detectors were used. Refractive index, RI, detectors measure the change in refractive index of the sample at a particular time where:

$$n = n_o + (n' - n_o)c \quad [5.3]$$

Where  $n$  is the measured refractive index,  $n_o$  is the refractive index of the solvent,  $n'$  is the refractive index of the polymer and  $c$  is the concentration by weight of the



polymer (Mori et al., 1999). Thus, the concentration of particular polymer species can be measured. An RI trace of the analysis on polymers 5-7 is shown in Figure 5.1 as an example: The polymer peaks are seen at 10.2, 10.4 and 11.2 minutes.

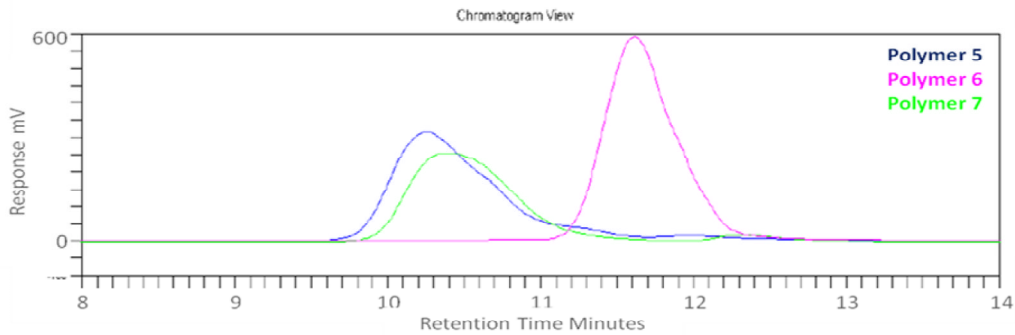


**Figure 5.1: Typical RI GPC Trace**

Light scattering, LS, detectors operate similarly to the laser diffraction particle sizer discussed in Section 4.3.1. Light is shone through the sample and the relationship defined by the Rayleigh ratio is calculated, the ratio of measured light intensity between the solution present and the solvent on its own:

$$R_{\theta} = \frac{I_{\theta} r^2}{I_o V} \quad [5.4]$$

Where  $R_{\theta}$  is the Rayleigh ratio,  $I_{\theta}$  is the measured intensity of the measured light at a scattering angle  $\theta$ ,  $I_o$  is the equivalent intensity when the solvent alone is measured,  $r$  is the light path length, i.e. the distance between source and detector, and  $V$  is the scattering volume of the sample (Mori et al., 1999). Scattering angle decreases with increasing molecular weight, so placing detectors at multiple angles is necessary for this type of detector. A light scattering trace of the analysis on polymers 5-7 is shown in Figure 5.2 as an example, where the light intensity measurement is recorded as a voltage from the detector.

It should be noted that the time to pass through the column is more closely related to the polymer effective molecular volume than the molecular weight. Thus, the test time needs to be correlated with molecular weight for each polymer species. Thus, light scattering measurements are taken at various known polymer concentrations and scattering angles. When extrapolated to zero concentration and zero scattering angle, the weight average molecular weight can be determined. This process is also aided by the use of standard reference polymers that are used in the test solvent. In this case, an almost monodisperse linear polymethylmethacrylate ( $M_n = 103600$ ).

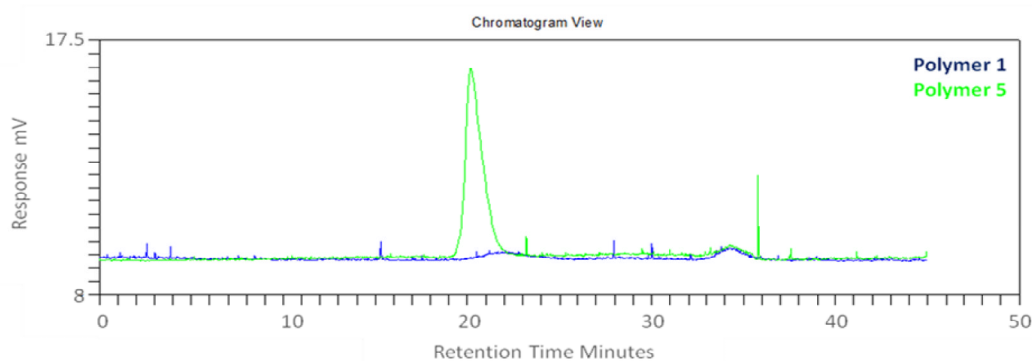


Figure 5.2: Typical Light Scattering GPC Trace

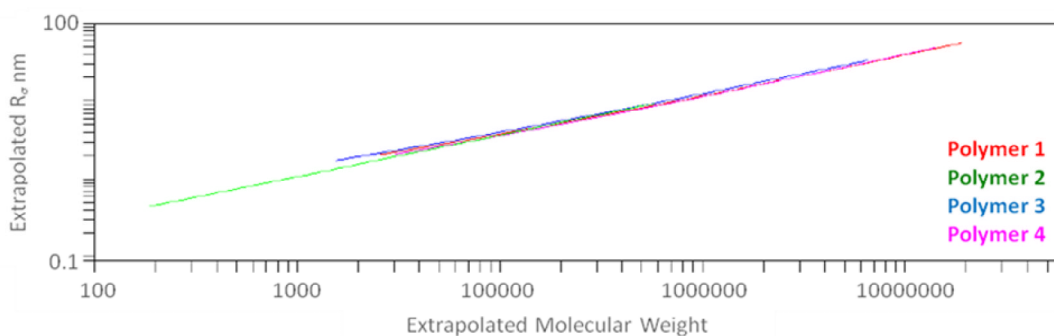
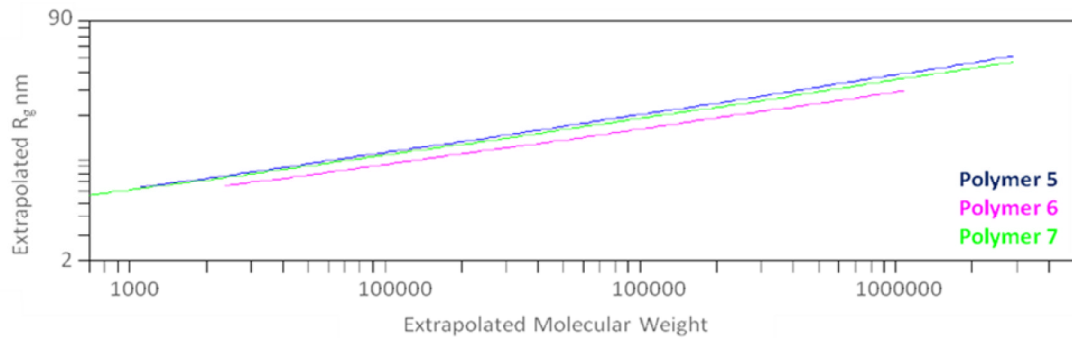


Figure 5.3: Mark-Houwink Plot from GPC for Polymers 1-4



**Figure 5.4: Mark-Houwink Plot from GPC Data for Polymers 5-7**

When RI and LS measurements are combined, the effective molecular volume of the polymer can be estimated. The relation of concentration and molecular weight for specific polymer species, i.e. at the same test time, can be used to correlate the molecular radius of gyration,  $R_G$ , which is the root mean square distance of the nominal elements of a polymer chain to the centre of mass:

$$\left(R_G^2\right)^{1/2} = \left(\frac{\sum_i m_i R_i^2}{\sum_i m_i}\right)^{1/2} \quad [5.5]$$

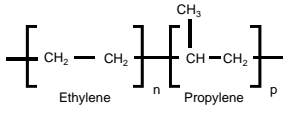
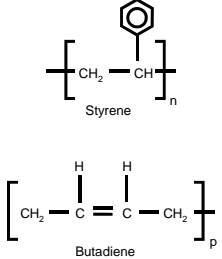
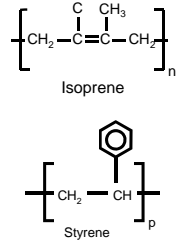
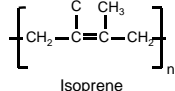
Where  $m_i$  is the mass of each element and  $R_i$  is its distance to the centre of mass (Mori et al., 1999). This correlation is shown on a Mark-Houwink plot. The plots for the analysis on the tested polymers are shown in Figure 5.3 or Figure 5.4.

GPC analysis was performed by technicians at BP Technology Centre, Pangbourne, UK. The analytical report of these measurements is attached as Appendix 1. The molecular weight values of the polymers tested are shown in Table 5.1.

## 5.4 Oil Matrix

Seven types of polymer viscosity modifier were considered. These were based on two generic molecular structures: Linear chains and stars. The linear chain polymers were three olefin copolymers of varying molecular weight, and a styrene-butadiene random

copolymer. The three star polymers were styrene-co-isoprene with varying molecular weight and styrene content.

Type	Linear			Star			
	Olefin Copolymer			Styrene-Butadiene	Isoprene-co-Styrene		Isoprene
							
<b>Reference</b>	<b>1</b>	<b>2</b>	<b>3</b>	<b>4</b>	<b>5</b>	<b>6</b>	<b>7</b>
Ratio of Monomers (estimated from manufacturers data)	E = 50% P = 50%	E = 20% P = 80%	E = 50% P = 50%	S = 50% B = 50%	I = 80% S = 20%	I = 50% S = 50%	I=100%
Number Average Molecular Weight $M_n$ (from GPC)	51945	42359	2997	75412	146499	65039	80003
Average Monomer Molecular Weight $M_o$ (from Graessley (2008))	34.3	28	34.3	65.5	75	86	68
Chain Molecules per Monomer $j$ (from Graessley (2008))	2	2	2	4	3.6	3	4
Entanglement Molecular Weight $M_{e,max}$ (From Ferry (1980))	1660	1250	1660	3000	8572	12145	4706
Number of Arms (Estimated from Rhodes (1999))	-	-	-	-	10	10	10
Arm Molecular Weight $M_o$ (Calculated)	-	-	-	-	14650	6503	8000
Chain Length (Calculated)	3028	3025	175	4605	7031 (1 arm)	2289 (1 arm)	4706 (1 arm)

**Table 5.1: Properties of Undiluted Polymer Viscosity Modifiers Used in This Study**

The lowest molecular weight star polymer was a micelle-type star, also known as an associated polymer, whereby the arms join at the centre by weak attraction forces rather than being fixed. Under high shear, therefore, the molecule may break down into its individual arms, but will tend to reform when stress is relaxed (Mortier et al., 2010). In order to make the lubricant blends representative of commercial lubricants, commercially available viscosity modifiers were used. The polymers and their molecular structures are shown in Table 5.1.

As these were commercial compounds, many of their properties were not disclosed. Therefore several assumptions were made regarding these blends:

- The ratio of monomers were defined as: 50:50 for a block copolymer or a random copolymer; 80:20 for when the content of one species is described as ‘high’, i.e. polymer 2 has ‘high propylene content’
- The number of arms on a star polymer molecule was assumed to be 10. Patents for these compounds describe the manufacturers desired range as 6-13 (Rhodes, 1999) and other literature as 10-16 (Schulz et al., 1991)
- Average values were used for calculations, i.e. all molecules of a particular polymer were assumed to be identical in size and composition. The arms of star polymers were, likewise, assumed to be the same length and composition.

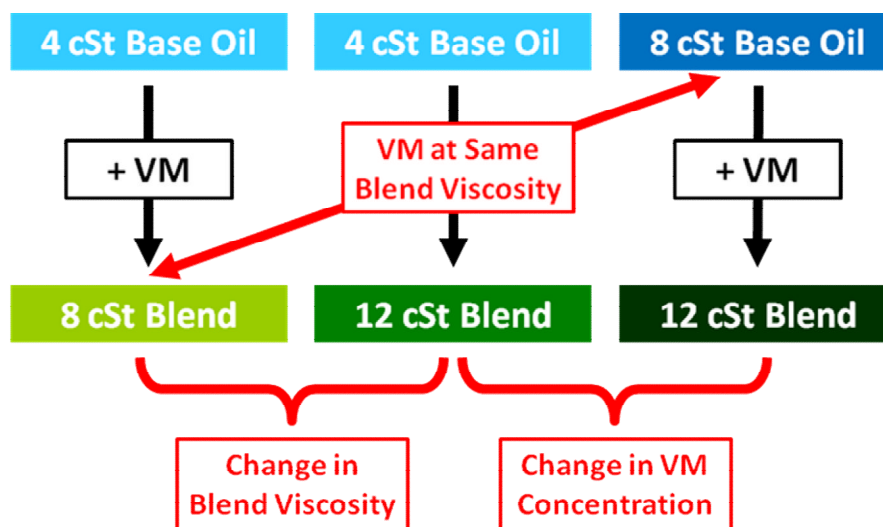


Figure 5.5: Schematic of Blends and Comparisons for Polymer Study

The polymers were blended into two Group III base oils, with kinematic viscosities at 100°C (KV100) of 4.4 cSt and 8.1 cSt respectively. In order to remove any variation in base oil properties arising from unknown diluents, polymers were blended from solid rather than using pre-diluted viscosity modifiers. Three blends were made from each polymer: two based on the 4cSt base oil, containing sufficient polymer to

produce a nominal blend KV100 of 8cSt and 12cSt respectively, and a blend based on the 8cSt base oil to produce a nominal KV100 of 12cSt. Thus, comparisons could be made of the effect of polymer concentration and blend viscosity, Figure 5.5. Blend viscosities were measured using an Anton Paar Viscometer, as described in Section 4.5.

Polymer	Type	Polymer Concentration (wt)	Kinematic Viscosity at 100°C (cSt or mm <sup>2</sup> s <sup>-1</sup> )	Dynamic Viscosity at 20°C (mPa.s)
1	Olefin Copolymer	1.00%	8.4	77.0
		1.90%	13.0	129.0
		0.70%	12.1	161.3
2	Olefin Copolymer	1.16%	8.4	85.7
		1.90%	12.7	141.4
		0.80%	11.9	183.3
3	Olefin Copolymer	6.20%	7.7	81.9
		10.90%	12.2	148.4
		4.80%	12.4	194.2
4	Styrene-Butadiene	0.83%	8.4	86.6
		1.25%	11.8	129.0
		0.62%	12.9	194.5
5	Styrene-co-Isoprene	0.70%	7.7	70.8
		1.30%	12.1	127.1
		0.52%	12.3	187.2
6	Styrene-co-Isoprene Micellar-type	1.46%	8.5	78.4
		1.78%	11.9	115.4
		0.90%	11.9	167.4
7	Isoprene	1.00%	8.2	80.8
		1.78%	13.0	139.0
		0.80%	13.3	200.0
	4 cSt Base Oil		4.4	43.2
	8 cSt Base Oil		8.1	107.4

**Table 5.2: Blend Polymer Concentrations and Viscosities at Blending and Test Temperatures**

It should be noted that the misting tests and other analyses were performed at 20°C but the blends were formulated to have similar viscosities at 100 °C. Viscosity modifiers uncoil with increasing temperature, increasing their effective molecular volume, thus thickening the oil. However, it has been observed that imposed shear stress on a polymer also causes it to extend (Nguyen et al., 1999), increasing its thickening effect above its low shear contribution at the same temperature and, thus, the viscosity of the blend.

Therefore, finding a characteristic temperature and shear rate at which to match properties of polymer-containing fluids is not simple. Thus, the difference between the blending and testing temperatures should not be considered to be of major importance. The base oils were also tested to give a further reference. The blends, concentrations and relevant data are shown in Table 5.2.

## 5.5 Rheological Testing

Theory suggests that the reason for polymeric additives suppressing droplet formation is due to extensional properties arising from greater viscoelasticity in polymer-containing fluids (Gulari et al., 1995; Marano et al., 1995). Therefore the viscoelastic properties of the various blends were measured. These were taken using a Malvern Kinexus rheometer with a 60mm diameter parallel plate arrangement.

Firstly, the extent of the linear viscoelastic region was defined, using the method described in Section 3.7.1. In this, the fluid is sheared at a constant frequency but with increasing amplitude until the viscous modulus decreases to 95% of the steady value. The stress and strain at this point are considered the limit of stress and strain that can be allowed before the response of the material becomes extremely non-linear and unpredictable. The oscillation frequency for this was chosen to be 43Hz, as this represents the frequency of gas flow through the piston ring gaps under typical conditions, i.e. 2500rpm. It should be noted that, as this simulation rig ran under steady state conditions, there was no characteristic frequency, thus the chosen value is merely nominal. A typical graph of this test is shown in Figure 5.6.

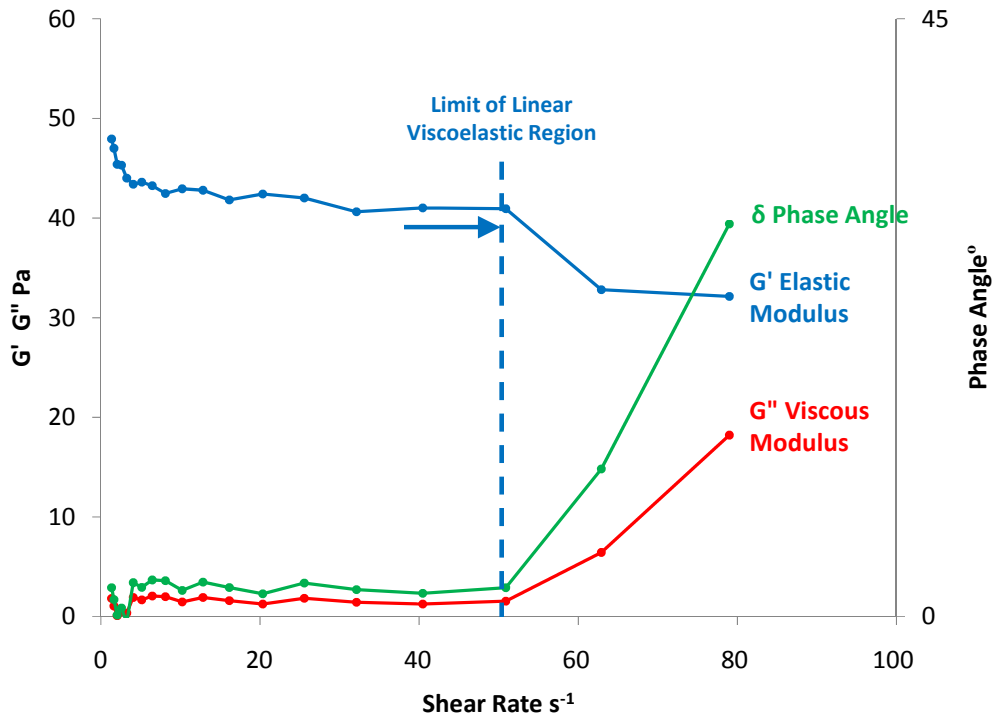


Figure 5.6: Graph of Linear Viscoelastic Region for 8cSt Blend of Polymer 1

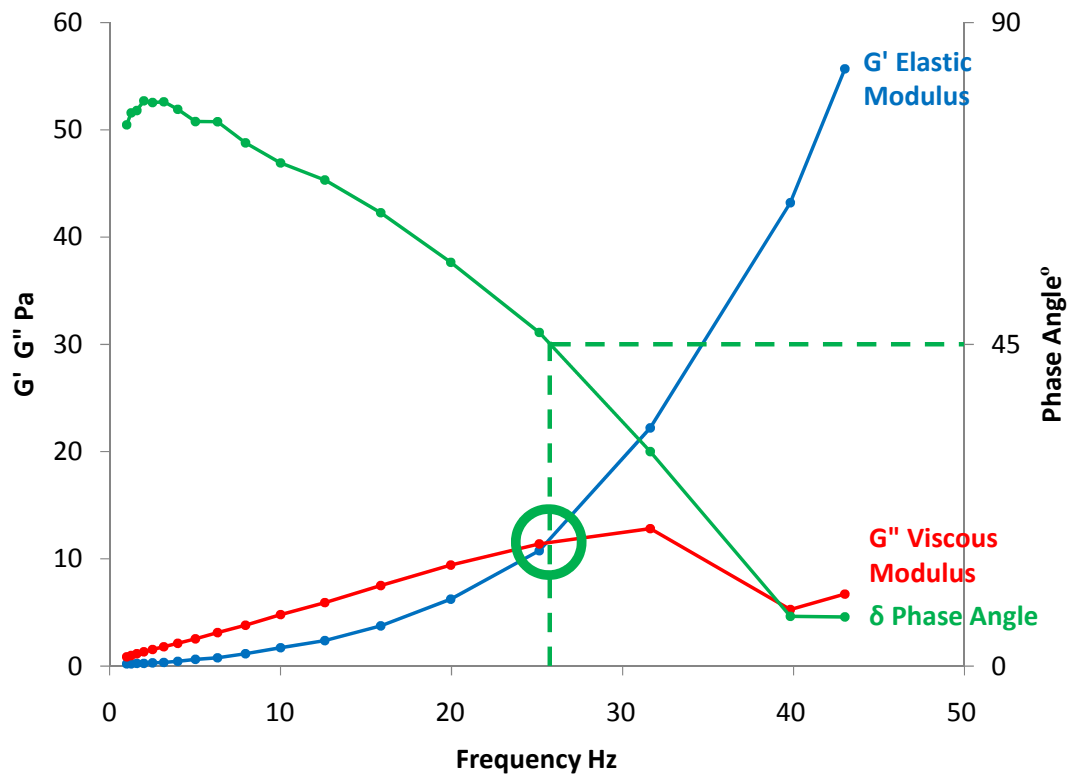


Figure 5.7: Graph of Crossover for 8cSt Blend of Polymer 1



Secondly, knowing the limits of the linear viscoelastic region, enabling appropriate conditions to be defined within it, the conditions of the crossover point could be found. This test involves a fixed maximum shear strain and an increasing oscillation frequency, thereby increasing the shear rate. Thus, the shear rate and stress at which the blend behaviour begins to be more characteristically solid than fluid is measured i.e. when the phase angle is  $45^\circ$ . A maximum shear strain of 5% was chosen as this was significantly within the linear viscoelastic region for all the blends tested. The shear stress, strain, complex modulus and complex viscosity at the crossover point were recorded. A typical curve for this test is shown in Figure 5.7.

The viscoelasticity of polymer blends can be attributed to the extension of polymer molecules under shear, and, at higher concentrations, the entanglement of the molecules. The latter of these conditions produces the greatest viscoelastic response. Therefore, these blends were characterised in terms of their entanglement using the parameters described in Section 3.7.2. Knowing the entanglement molecular weight of the neat polymer species,  $M_e$ , from literature and the volumetric concentration of the polymer, the entanglement molecular weight of the blend,  $M_{e\ Blend}$ , was calculated. From this, knowing the molecular weight of the polymer in the blend, the entanglement density,  $E_{Blend}$ , was calculated. Values of  $M_e$  were obtained from Ferry (1980) and values of polymer density, required to calculate polymer concentrations by volume, were obtained from Graessley (2008) and Stanciu (2009) for linear and star polymers respectively. Where density values were not available for a copolymer, the density was calculated from that of its monomers.

Taking the derived value for polymer radius of gyration,  $R_g$ , from the Mark-Houwink plots for these polymers, Figures 5.3 and 5.4, several other parameters were calculated. The values for  $R_g$  on the Mark-Houwink plot were taken at  $40^\circ\text{C}$  and using tetrahydrofuran, THF, as a solvent. However, it is assumed that these values of  $R_g$  will be comparable to those at  $20^\circ\text{C}$  and in mineral oil as, firstly, shear stress will cause  $R_g$  to increase and, secondly, both mineral oil and THF are good solvents for these polymers. The hydrodynamic volume of a molecule was calculated using the following relationship, described by Graessley (2008):

$$HDV = \frac{4\pi R_G^3}{3} \quad [5.6]$$

The self-concentration of a molecule, the concentration of the polymer molecule within its effective volume, i.e. an indication of coiling, was calculated using method of Graessley (2008):

$$c_{molecule} = \frac{3M}{4\pi N_a R_g^3} \quad [5.7]$$

Where  $N_a$  is Avogadro's number,  $6.022 \times 10^{23}$  and  $M$  is the molecular weight of the polymer.

The packing length, an indicator of how well extended a molecule is also described, following the approach of Graessley (2008):

$$l_p = \frac{M}{\rho N_a R_G^2} \quad [5.8]$$

The latter two relationships are well defined for linear polymers, but not necessarily for star polymers.

## 5.6 Results

### 5.6.1 Rheological Analysis

Table 5.3 shows the measured crossover parameters from the rheometer. Several blends show higher values of stress and strain at crossover than others. These conditions were far in excess of values predicted by the test input conditions. These apparent anomalies suggest that some non-linear viscoelastic effects are being seen in these blends. There is no explanation for this behaviour. The blends exhibiting this

behaviour are higher molecular weight polymers at higher concentrations. Two polymers do not exhibit this behaviour in any of their blends, the lowest molecular weight OCP and the micellar-type star polymer. This indicates that the viscoelastic contribution of these polymers was small. The main outcome of these measurements is that all these blends are viscoelastic, even at low shear stresses, <100MPa.

Polymer	Type	Polymer Concentration (wt)	Stress at Crossover (Pa)	Strain at Crossover (%)
1	Olefin Copolymer	1.00%	0.64	4.10
		1.90%	11.16	37.13
		0.70%	1.44	3.64
2	Olefin Copolymer	1.16%	0.45	2.45
		1.90%	10.55	41.94
		0.80%	0.98	2.80
3	Olefin Copolymer	6.20%	0.69	3.64
		10.90%	0.40	0.96
		4.80%	0.99	2.81
4	Styrene-Butadiene	0.83%	0.80	3.63
		1.25%	11.20	37.75
		0.62%	1.22	2.81
5	Styrene-co-Isoprene	0.70%	0.65	4.09
		1.30%	8.96	37.51
		0.52%	1.02	2.81
6	Styrene-co-Isoprene Micellar-type	1.46%	0.62	3.66
		1.78%	1.06	3.63
		0.90%	1.15	3.63
7	Isoprene	1.00%	6.97	37.80
		1.78%	9.48	37.53
		0.80%	1.31	3.64

**Table 5.3: Crossover Results for Polymer Blends**

Polymer	Type	$M_e$	$M_e$ Blend	$E$ Blend	Semi-Dilute Blend
1	Olefin Copolymer	1660	606852	0.086	
		1660	263664	0.197	←
		1660	947926	0.055	
2	Olefin Copolymer	1250	367534	0.115	←
		1250	193681	0.219	←
		1250	585245	0.072	
3	Olefin Copolymer	1660	56883	0.053	
		1660	27431	0.109	←
		1660	77930	0.038	
4	Styrene-Butadiene	3000	1763473	0.043	
		3000	1034977	0.073	
		3000	2532847	0.030	
5	Styrene-co-Isoprene	8572	1293534	0.011	
		8572	587630	0.025	
		8572	1862237	0.008	
6	Styrene-co-Isoprene Micellar-type	12145	718941	0.009	
		12145	560275	0.012	
		12145	1306393	0.005	
7	Isoprene	6190	592157	0.014	
		6190	285558	0.028	
		6190	773930	0.010	

**Table 5.4: Calculated Entanglement Properties for Polymer Blends**

Table 5.4 shows the calculated entanglement molecular weights and entanglement densities for the various blends. An entanglement density greater than 0.1 is considered a semi-dilute solution, i.e. displaying some molecular interaction but not yet fully entangled. Semi-dilute blends should, theoretically, have a greater viscoelastic response than other polymer blends, and, theoretically, should reduce

misting tendency further. Blends exhibiting this behaviour are highlighted. These blends are exclusively OCPs, including low molecular weight polymer number 3. Star polymers and the styrene butadiene are not well entangled. That the 12cSt from 4cSt base oil blend from polymer 3 (indicated by arrow) is significantly entangled indicates that entanglement and viscoelasticity can be, to some degree, independent.

Polymer	Type	$R_G$ nm	$HDV$ $m^3 \times 10^{-24}$	$C_{molecule}$ $\times 10^{-5}$	$l_p$ pm
1	Olefin Copolymer	8.2	2.3	4.8	1.65
2	Olefin Copolymer	8.1	2.2	4.1	1.41
3	Olefin Copolymer	1.9	0.03	22.3	1.77
4	Styrene- Butadiene	9.9	4.1	3.3	1.37
5	Styrene-co- Isoprene	11.2	5.9	15.2	7.13
6	Styrene-co- Isoprene Micellar-type	10.8	5.3	7.5	3.40
7	Isoprene	10.4	4.7	10.4	4.52

**Table 5.5: Derived and Calculated Molecular Coiling Parameters for Polymer Blends**

The derivation of the coiling parameters from  $R_G$  values gives some insight into the viscoelastic mechanisms of these molecules, Table 5.5. As may be expected, the star polymers have a larger radius of gyration and, thus, a larger hydrodynamic volume.

The high self concentrations of the stars indicate that their structures are relatively dense. The micellar star has the lowest self concentration i.e. the most loosely packed molecule. For the linear polymers, the radii of gyration are large for the long chains, 1, 2 and 4, but very low for polymer 3, the short chain polymer. There is a corresponding variation in the hydrodynamic volumes. Generally, the hydrodynamic volumes are smaller than the star molecules and the self concentration values are significantly lower than the fixed stars, indicating that they are much more loosely packed. This is clearly a result of the structural differences between linear polymers and stars. Polymer 3 has an extremely small hydrodynamic volume, reflecting its small size. It also has the largest packing length, indicating it is relatively well stretched. Polymers 1, 2 show increasing packing length with molecular weight, indicating that a longer chain OCP will be less well coiled. Polymer 4, despite having higher molecular weight and chain length than polymers 1 and 2, has a lower packing length, suggesting that it is better coiled under these conditions. Polymer 4 also has a significantly greater hydrodynamic volume than polymers 1 and 2, and a lower self concentration, indicating that, though it is more coiled, is more loosely coiled. It is hypothesised that, because of the larger side groups on polymer 4, arising particularly from the styrene groups, that the chain is less flexible than the OCP chain.

Thus, it is hypothesised that polymers 1 and 2 will produce a high viscoelastic response, as their chains are relatively well coiled i.e. with a lot of potential for extension. Thus, as shown in Table 5.4, they have the potential for molecular interaction as they have a higher degree of entanglement than other blends. It is thought that polymer 4 will have similar viscoelastic behaviour to polymers 1 and 2. However, as the chain is less extended but having a much looser coil, the apparently less flexible chain may reduce the viscoelastic response when compared to polymers 1 and 2. As polymer 4 solutions are not well entangled, viscoelastic contribution will be from the stretching of molecules only. Polymer 3 has an extremely low hydrodynamic volume, as might be expected from a small chain. Although the blends for polymer 3 are, theoretically, relatively well entangled, their viscoelastic response is likely to be small as their molecules are naturally more extended than others, a feature of small molecules. This means that shear stress cannot produce significant amounts of

extension in the molecule and that any molecular interaction will be easily escaped as molecules can be pulled away from each other under shear.

The fixed star polymers, 5 and 7, are likely to show significant viscoelastic behaviour. They are large and open molecular structures that interact with a large quantity of base oil. However, these solutions are not well entangled and the central fixed point in the structure restricts arm dynamics. The viscoelastic contribution of these blends will come from molecular bending and stretching. Polymer 6, the micellar star polymer, will, theoretically, behave similarly to polymers 5 and 7 as its properties are similar. However, the micellar structure is known to come apart under shear. Thus, the behaviour of these blends cannot be well predicted.

### 5.6.2 Misting Tendency

Graphs showing the variation of misting and spraying tendency with inlet oil flow rate, and the corresponding droplet size distributions, as measured from the venturi mist generator at 3 ml/min inlet flow rate as per Section 4.2-4.4, are shown in Figure 5.8 to Figure 5.21. 3 ml/min values are shown as these are considered to contain the greatest proportion of misted droplets rather than sprayed droplets, see Section 4.4.

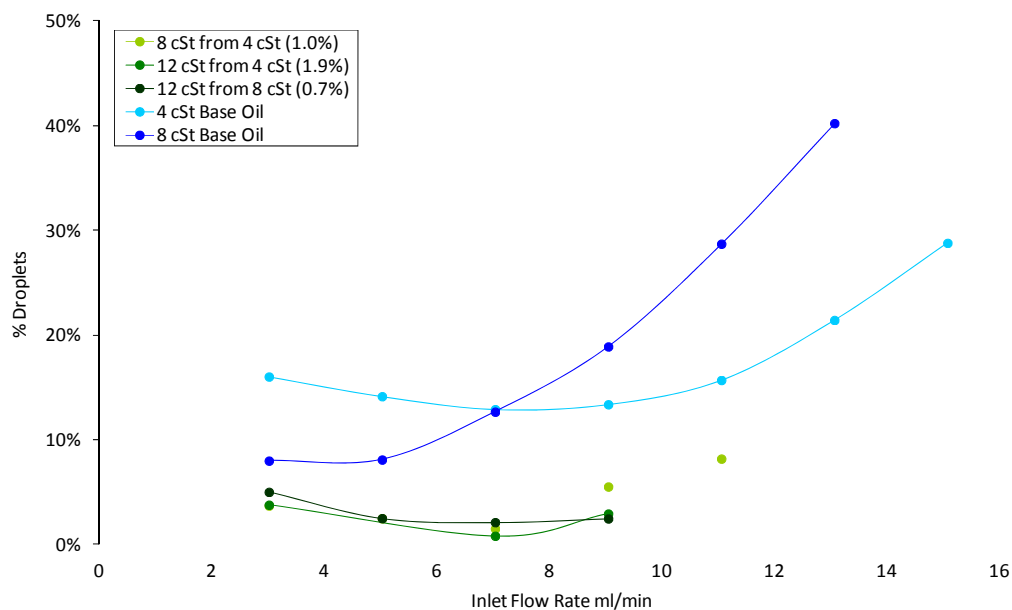
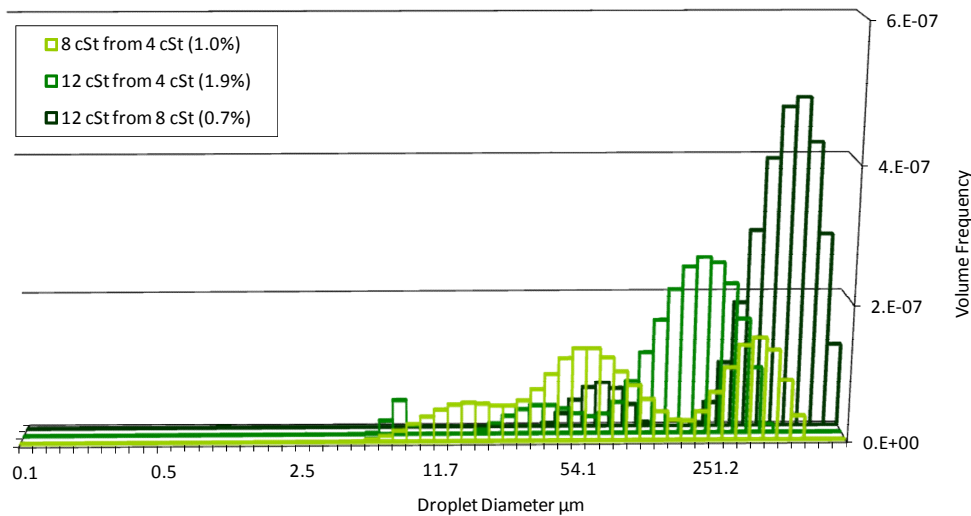


Figure 5.8: Misting Tendency Graph for Polymer 1, Olefin Copolymer



**Figure 5.9: Droplet Size Distributions for Polymer 1 at 3ml/min Oil Inlet Flow Rate**

Polymer 1 is a high molecular weight olefin copolymer. The 12cSt blend from 4cSt base oil is both significantly entangled and viscoelastic. It can be seen in Figure 5.8 that the mist tendency, even at high inlet flow rates, is extremely low. It is thought that the longer chain length of the polymers in this blend produce a greater viscoelastic response to the shear experienced in the misting process, thus suppressing the formation of droplets from the surface. This phenomenon appears to be exaggerated by a higher degree of entanglement. The droplet size distribution, Figure 5.9, indicates that an increase in blend viscosity increases the proportion of spray to mist. This polymer appears to have excellent mist reduction properties.

Polymer 2 is a high molecular weight olefin copolymer. Though it has a similar molecular weight to polymer 1, it has a slightly lower hydrodynamic volume and is a looser coil, indicating a less flexible molecule. Comparing the 8cSt polymer blend and 8cSt base oil in Figure 5.10, it can be seen that the presence of the polymer reduces the tendency to form mist i.e. at lower oil inlet flow rates. It can be seen that the onset of the spray region begins at a lower flow rate when polymer is present. This implies a greater resistance to shear and, hence, greater accumulation on the oil feed, leading to the undercutting spray formation described in Section 4.4. This implies that the difference in spraying behaviour in these blends is not a function of blend viscosity,



but is related to blend viscoelasticity. When comparing the 12cSt blends, with a significant difference in polymer content, it is seen that the misting tendency is similar at low oil flow rates. At higher flow rates, the 12cSt blends follow a similar pattern, though the spray onset occurs at a lower flow rate when polymer content is higher. The similarity in mist and spray formation of polymer containing blends suggests that the presence of polymer has a greater effect than the blend viscosity. The droplet size distributions, Figure 5.11, show that, even at low oil flow rates, a large proportion of large spray-sized droplets are formed. The size of mist-sized droplets increases with polymer concentration, and there are no aerosol-sized droplets present. This implies that droplets are formed by a ligament breakup-type mechanism than droplets being ripped from the surface, suggesting significant viscoelasticity in the blends, see Section 3.6. This indicates that, although the degree of entanglement of these blends is marginally higher than those for polymer 1, the tendency to suppress mist formation is not as great. It is thought that, perhaps, the greater number of side groups on the molecule, relative to polymer 1, will reduce molecular flexibility and hinder the rate of molecule stretching under shear, due to greater interaction with the base oil, thus limiting the magnitude of elastic deformation possible in the timescale of the misting process. Thus the extensional effects required to prevent the formation of droplets from ligaments may be reduced, see Section 3.7.1.

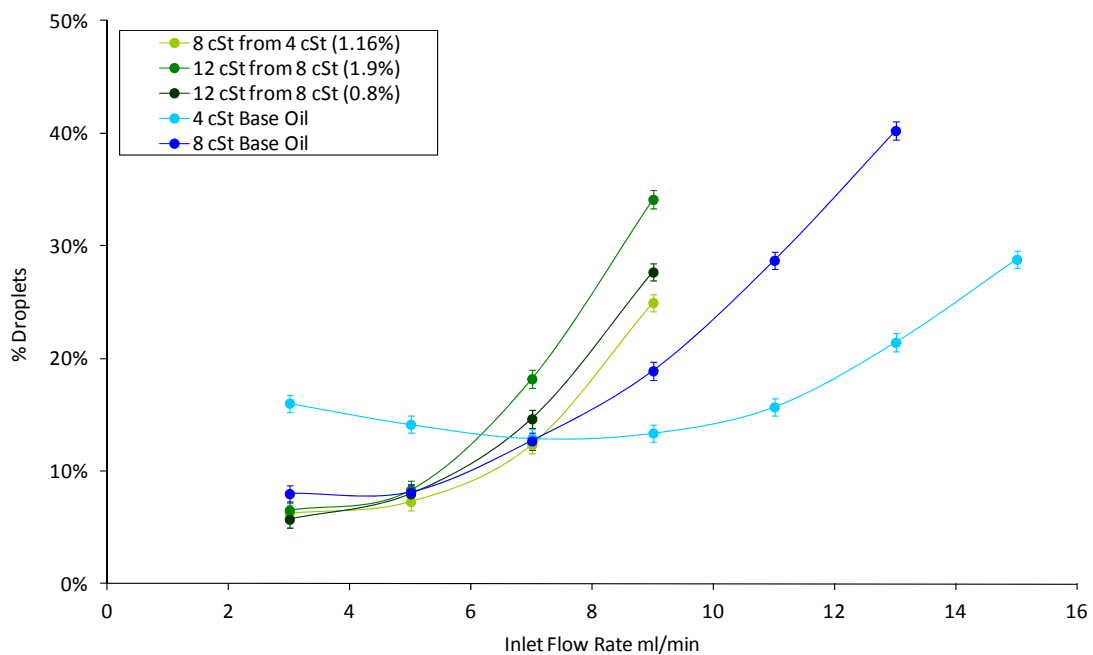


**Figure 5.10: Misting Tendency Graph for Polymer 2, Olefin Copolymer**

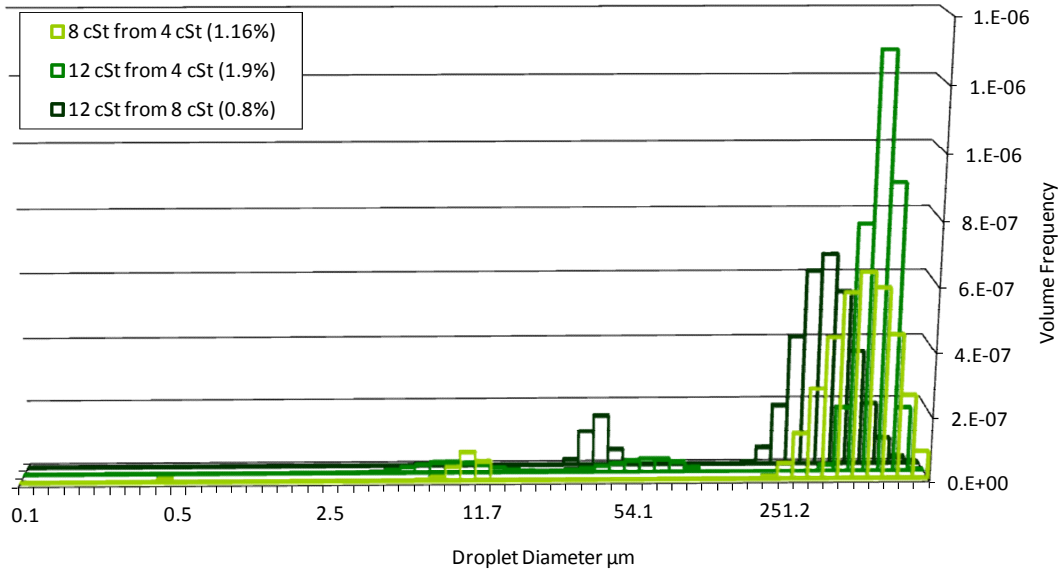


Figure 5.11: Droplet Size Distributions for Polymer 2 at 3ml/min Oil Inlet Flow Rate

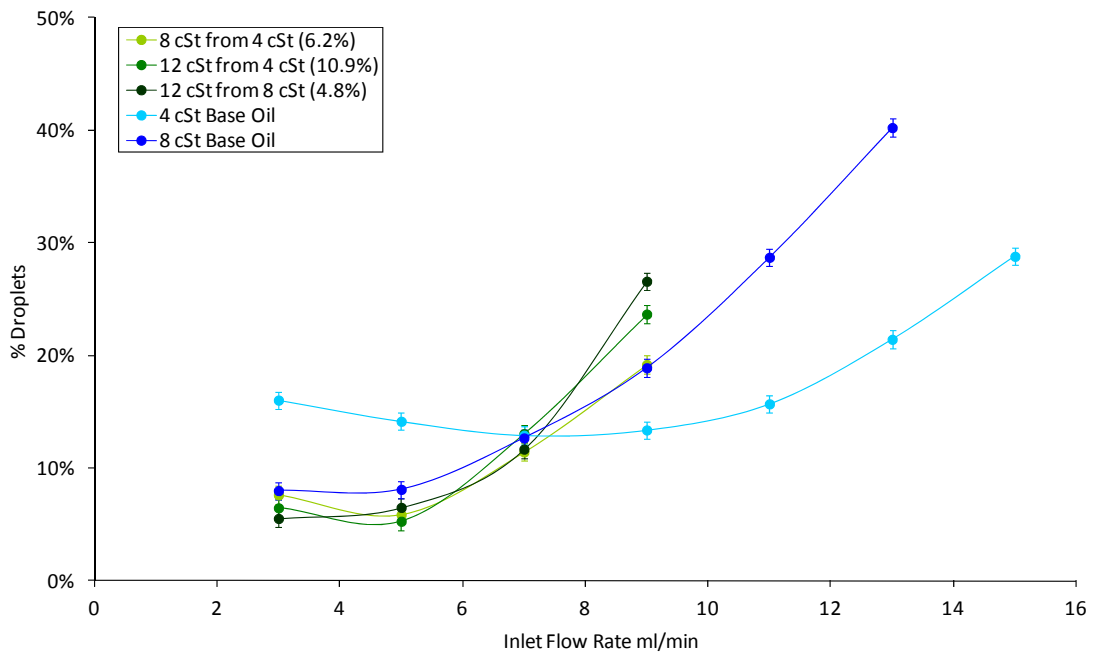
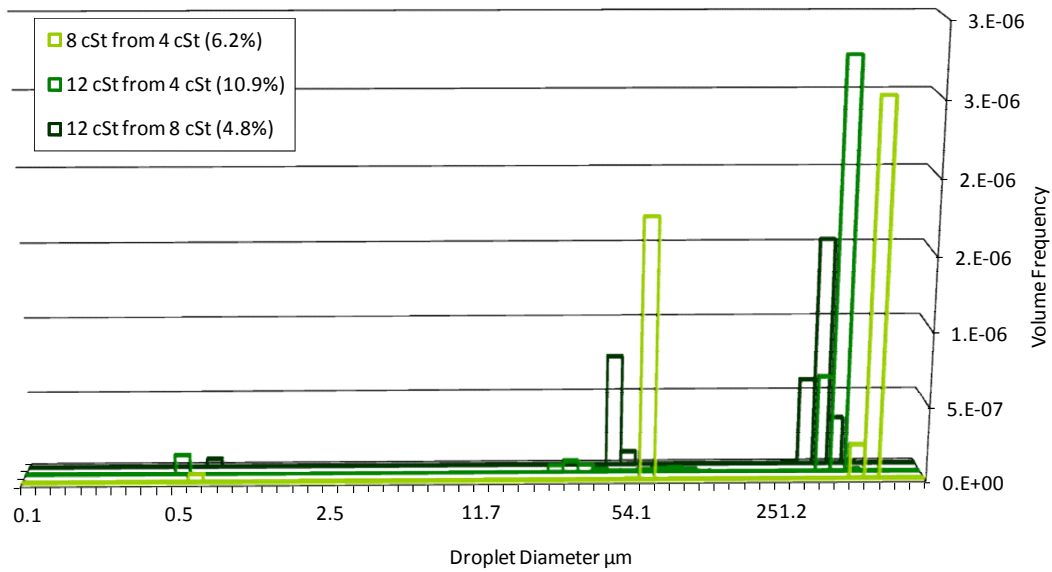


Figure 5.12: Misting Tendency Graph for Polymer 3, Low Molecular Weight Olefin Copolymer



**Figure 5.13: Droplet Size Distribution for Polymer 3 at 3ml/min Oil Inlet Flow Rate**

Polymer 3 is a low molecular weight olefin copolymer. Whilst the degree of entanglement of these blends is relatively high, it is thought that the viscoelastic contribution is relatively low. Comparing the misting tendency of the 8cSt blends in Figure 5.12, one containing polymer and one without, it can be seen that there is some reduction in the tendency to form mist i.e. at low oil flow rates. This reduction is smaller than other blends seen so far. At higher oil flow rates, when spray formation prevails, both 8cSt blends show identical behaviour, implying that blend viscosity has more of an influence over spray formation than polymer content. Comparing the 12cSt blends, the mist and spray formation behaviour is not significantly different. This, again, implies that blend viscosity is more significant than polymer content in defining droplet formation. The droplet size distributions, Figure 5.13, show that the polymer content and blend viscosity does not produce significantly different mist-sized droplets. Fine aerosol droplets of approximately  $0.5\mu\text{m}$  were formed by all blends. This suggests that the mist suppression tendencies of the blend were relatively poor, and that the viscoelastic response of the blend is not sufficient to prevent the formation of small aerosol-sized droplets. Though the entanglement of these blends was relatively high, the short chain length molecules can relatively easily slide past each other during shear, aligning themselves in the shear axis and being removed

from entangling interactions. Thus, although the blends are apparently entangled, they are not in practice. Also, the chains are shown to be naturally relatively well extended, thus less energy can be stored elastically through molecule stretching. This explains the relatively weak viscoelastic response of these blends and their poor mist reducing tendencies.

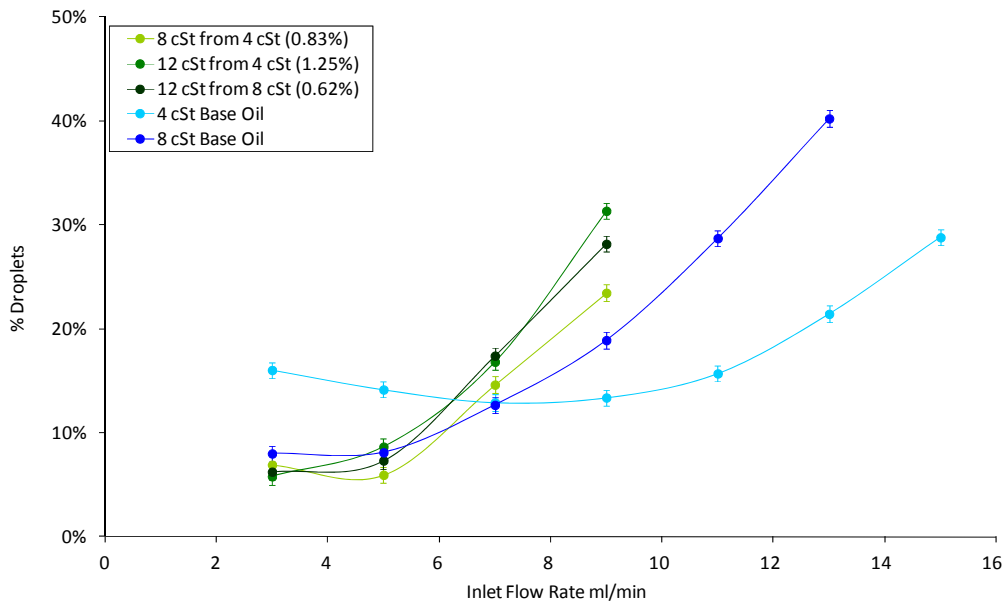


Figure 5.14: Misting Tendency Graph for Polymer 4, Styrene-Butadiene

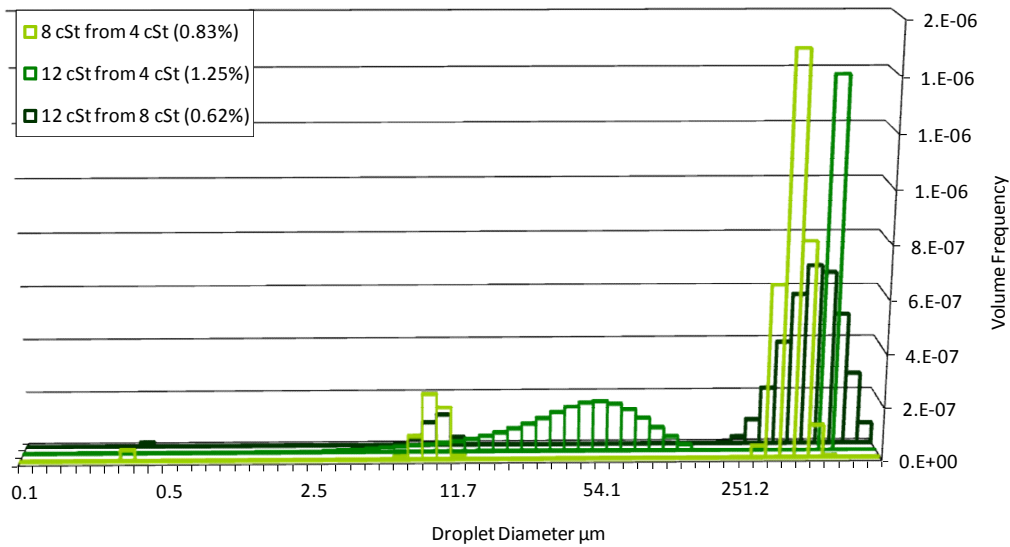
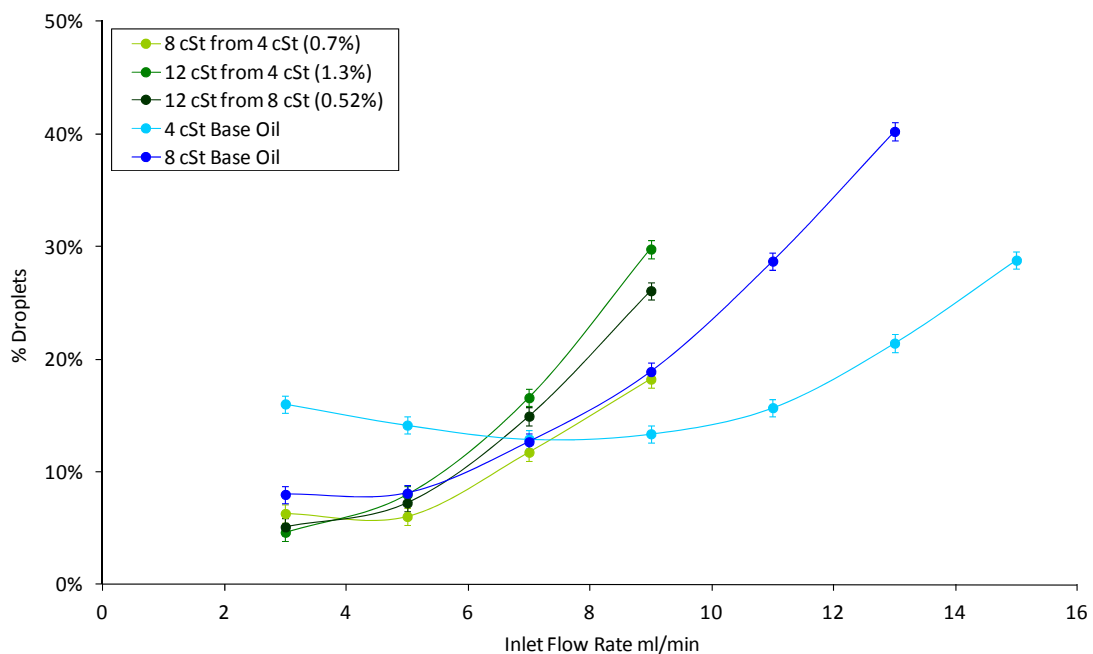
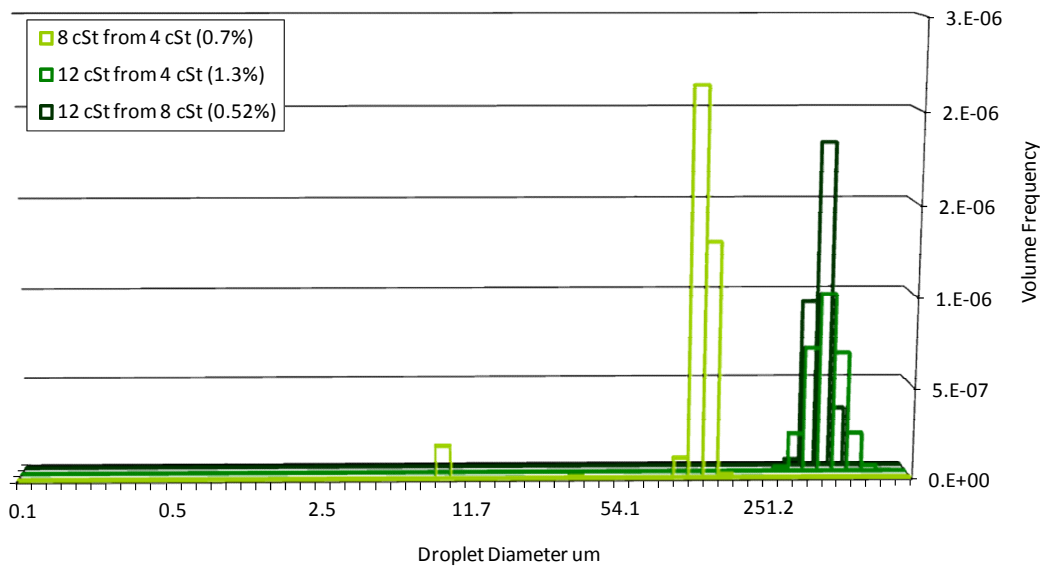


Figure 5.15: Droplet Size Distribution for Polymer 4 at 3ml/min Oil Inlet Flow Rate

Polymer 4 is a high molecular weight styrene-butadiene of higher molecular weight and greater chain length than polymers 1 and 2. However, the degree of entanglement is relatively low, due to the large side groups increasing the spacing of molecules. The side groups also increase the thickening effect of the molecule, thus reducing the volumetric concentration required to produce a certain blend viscosity. The misting and spraying tendency graph, Figure 5.14, shows similar behaviour to polymer 2. The significant differences are that the 12cSt blends show very similar behaviour, and the curves in the spray region, i.e. at higher oil flow rates, follow the 8cSt base oil more closely. The misting tendency at lower oil flow rates, i.e. misting by the ring gap-like misting mechanism, is reduced by a similar degree to the equivalent polymer 2 blends. Droplet size distributions, Figure 5.15, indicate a stronger dependency of mist-sized droplet diameter on polymer concentration. Overall, like polymer 2 which is also a long chain linear polymer with larger side groups, this indicates that the polymer contributes significant viscoelasticity to the blend. However, the apparently greater influence of blend viscosity on behaviour, particularly in the spray region, indicates a lower degree of entanglement and viscoelasticity. This could be attributed to the large side groups on the molecule reducing the flexibility of the chain.



**Figure 5.16: Misting Tendency Graph for Polymer 5, Isoprene-co-Styrene Star**



**Figure 5.17: Droplet Size Distribution for Polymer 5 at 3ml/min Oil Inlet Flow Rate**

Polymer 5 is a high molecular weight isoprene-co-styrene star polymer. These blends show a significant viscoelastic contribution, but a low degree of entanglement, reflected by the correlation of entanglement with arm molecular weight rather than total molecular weight. The droplet forming tendency is significantly different in behaviour to the high molecular weight linear polymers, Figure 5.16. The behaviour seen in these graphs has greater similarity with the lower molecular weight linear polymer, polymer 3. It should be noted that the tendency to reduce mist is greater than the polymer 3, more comparable to polymer 2, a higher molecular weight linear polymer. This reflects the greater viscoelasticity of these blends. The similarity in spray behaviour between the 8cSt blend and 8cSt base oil indicate that blend viscosity defines the spray behaviour. The reduced tendency to form mist when polymer is present indicates a viscoelastic contribution from the polymer. The low degree of entanglement indicates that this arises from stretching and deforming the molecule rather than interaction between molecules. The behaviour of the 12cSt blends is very similar, even with different base oil and polymer concentration, implying a dependency of blend viscosity rather than polymer concentration. The droplet size distributions, Figure 5.17, under conditions that indicate mist-sized droplets should be expected, show that extremely high proportions of spray-sized droplets are formed.

The size of these droplets is apparently highly dependent on blend viscosity. The dependence on blend viscosity confirms the low entanglement of these blends and appears to confirm that entanglement is correlated more strongly with arm molecular weight for star polymers.

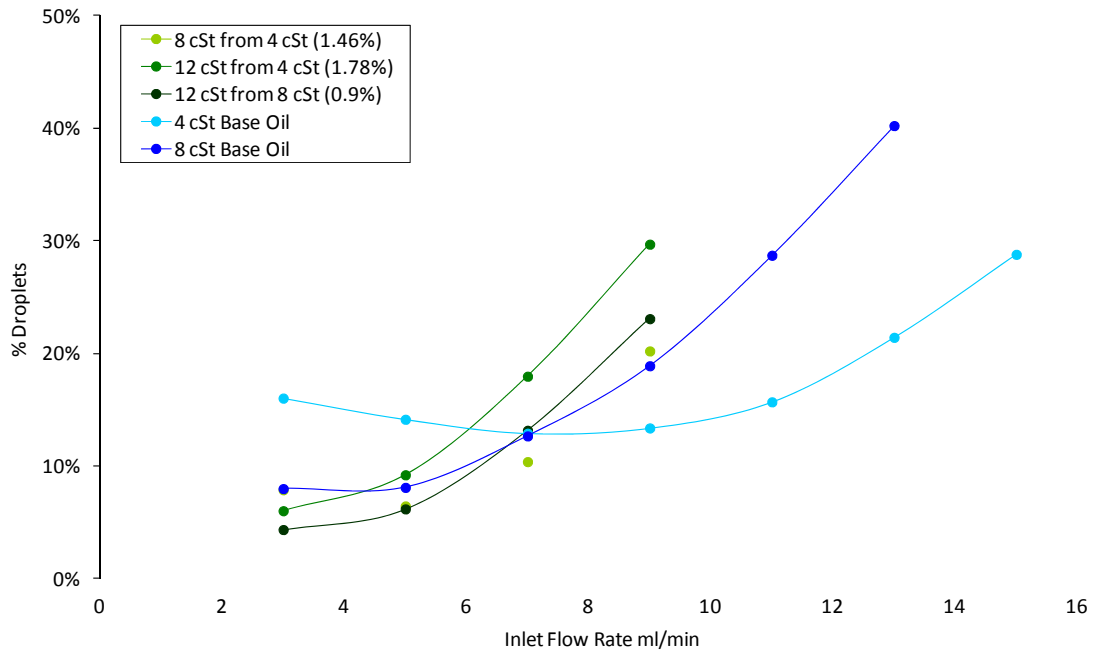


Figure 5.18: Misting Tendency Graph for Polymer 6, Micellar-Type Isoprene-co-Styrene Star

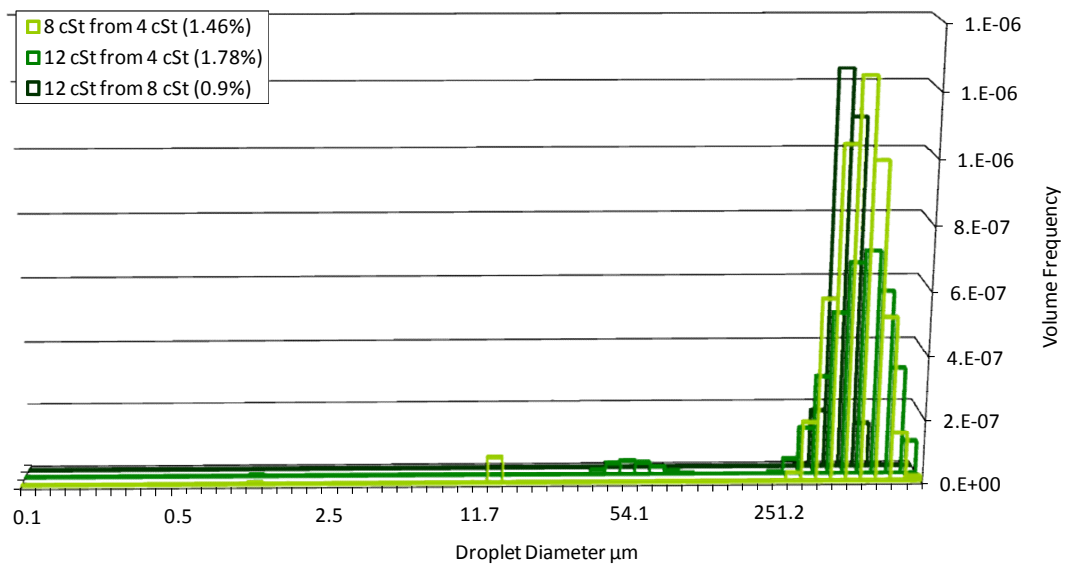


Figure 5.19: Droplet Size Distribution for Polymer 6 at 3ml/min Oil Inlet Flow Rate

Polymer 6 is a micellar-type isoprene-co-styrene star polymer. The droplet forming tendency of these blends is shown in Figure 5.18. Comparison between the 8cSt blend and 8cSt base oil indicate some similar behaviour at flow rates where spray is expected. At lower flow rates, where misting is expected, there is a small reduction in misting tendency, though not significantly at 3ml/min. Comparing the 12cSt polymer blends, the behaviour appears to follow a similar pattern, with a spray onset at similar flow rate. The magnitude of the spraying tendency, however, is significantly lower with higher polymer concentration. Generally, the polymer blends follow a similar pattern to the 8cSt base oil at higher oil flow rates, implying some dependency on blend viscosity and independence of polymer concentration. At lower flow rates, where the misting process dominates, misting tendency increases with a decrease in blend viscosity at low temperature, see Table 5.2. This implies that there is dependency on viscosity, and that there is very little shear-induced stretching of the molecules. This suggests that the micellar star structure separates into its arms, i.e. short linear polymers, under shear. This is reflected in the low viscoelastic contribution of the molecules, even though their total molecular weight is high. The droplet size distributions indicate the formation of aerosol-sized droplets from these blends, Figure 5.19. This behaviour is seen in polymer 3, a low molecular weight linear polymer, indicating low entanglement, low viscoelastic contribution and poor suppression of droplet formation. Thus, the behaviour of polymer 6 reflects that of low molecular weight linear polymers.

Polymer 7 is an isoprene star with molecular weight intermediate to the other star polymers. It shows significant viscoelastic properties, but low entanglement, similar to polymer 5. Droplet forming behaviour is, likewise, similar to polymer 5. However, the reduction in misting tendency is significantly greater, Figure 5.20. This may be attributed to the significantly smaller arms and smaller side groups on the molecule relative to polymer 5, which is a larger molecule and contains 50% styrene. The increase in molecule flexibility arising from this could allow a more rapid stretching of the molecule under transient shear, increasing the extensional deformation possible during the droplet formation process, reducing the quantity of droplets that can be produced. The droplet size distributions, Figure 5.21 show that a higher proportion of



spray-sized droplets and a lower proportion of mist-sized droplets are produced when polymer concentration is higher. Thus, there is some degree of dependency on viscosity and on polymer concentration, implying that there may be some interaction between polymer molecules.

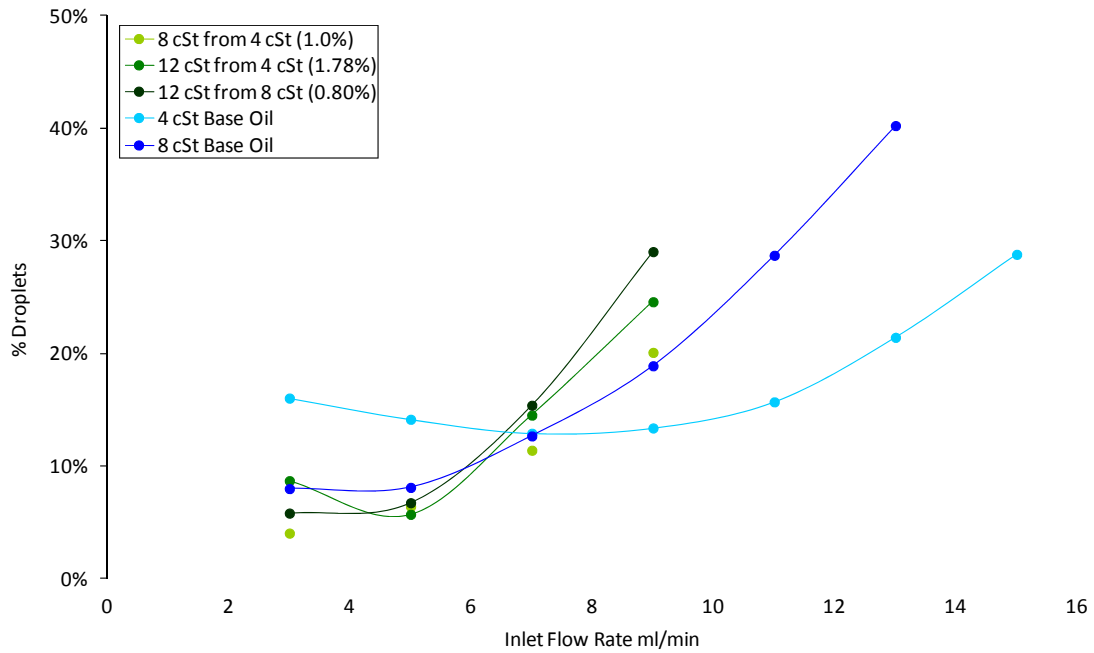


Figure 5.20: Misting Tendency Graph for Polymer 7, Isoprene Star

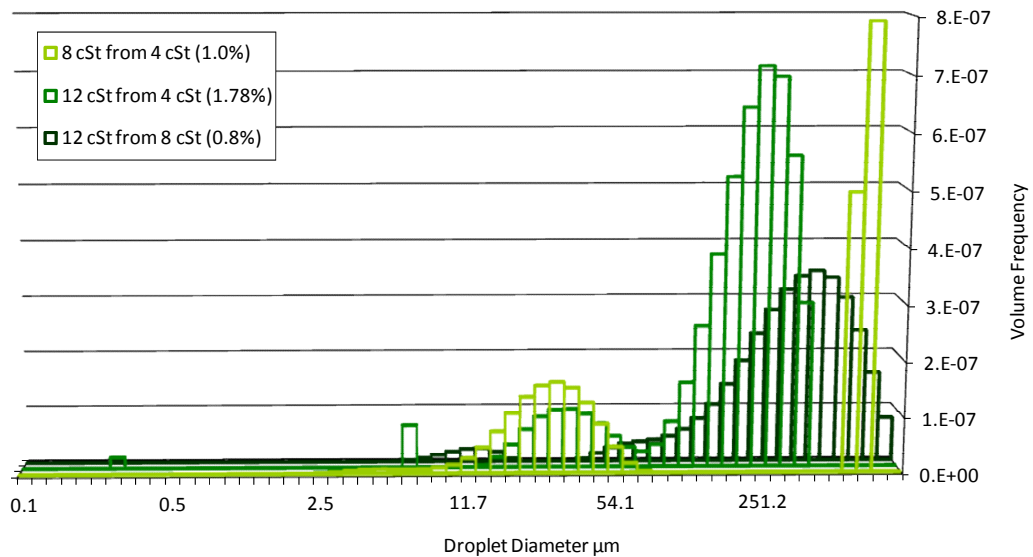


Figure 5.21: Droplet Size Distributions for Polymer 7 at 3ml/min Oil Inlet Flow Rate

In these results, it can be seen that significant differences exist in the droplet formation behaviour of different polymer architectures. Linear polymers show a wide variety of properties arising from a wide range of viscoelastic properties and entanglement. An increase in the viscoelasticity of a blend by the simple presence of polymer molecules reduces the tendency to produce mist. This is only the case when the polymers exceed a certain molecular weight where the stretching of the molecule requires sufficient energy to contribute to the viscoelasticity of the blend. Also, smaller molecules appear to be naturally more extended, reducing the energy that can be stored by their further extension under shear. The mechanism of suppressing droplet formation is related to the extensional viscoelastic properties of the blend, rather than the shear viscoelasticity (Fernando et al., 2000). This means that molecules with large side groups that cause higher shear viscoelasticity, may not exhibit the expected reduction in misting as the extensional viscoelasticity of the blend may be hindered by large side groups on the molecule reducing its flexibility. The viscoelastic properties of the blend can be significantly enhanced if the blend is semi-dilute i.e. there is significant molecular interaction. The molecular entanglement seen in some blends absorbs larger quantities of energy elastically, thus leading to more extreme reduction in misting tendency. This phenomenon, too, is dependent on the polymer molecular weight being above a certain value. For low molecular weight linear polymers, theoretically high degrees of entanglement can be practically ignored as molecules are easily separated under shear and any interaction quickly removed.

Fixed star polymers display a narrower range of droplet formation tendency and blend properties. However, this may be a result of the smaller range of molecular weights that were tested. Star polymer blends show that the presence of polymer significantly reduces the misting tendency, but that the spraying tendency is largely independent of polymer concentration and more dependent on blend viscosity. This implies that star polymers contribute significantly to the viscoelasticity of the blend, but that the degree of entanglement is low and the viscoelastic contribution is from stretching of the molecule rather than molecular interaction. The behaviour of fixed stars confirms that the entanglement of star polymers is best described in terms of arm molecular weight than total molecular weight. For micellar-type star polymers, it was seen that

the droplet forming and viscoelastic behaviour represents that of a low molecular linear polymer. This indicates that the micellar structure comes apart into individual arms under relatively low shear stresses, and blends containing these polymers should be blended to reflect this.

It can also be seen from Table 5.3 and Table 5.4 that the variation in entanglement and viscoelastic properties in blends of the same polymer does not result in changes of similar magnitude in droplet forming tendency. There is greater variation in the apparent viscoelastic mechanisms seen between different polymers than between different blends of the same polymer, despite significant differences in these predictive properties. It should be considered that the calculations for entanglement do not take account of temperature or shear and that an increase in either of these parameters will increase the effective volume of the polymer in the blend, thus increasing the interaction between molecules i.e. the average  $M_e$  will remain constant, but the effective  $M$  of the polymer will increase, see Equation 3.25. This is because this theory is based on the entanglement of the neat polymer where molecular interaction is almost completely independent of temperature, pressure and shear. This assumes an amorphous continuum, which is not necessarily valid when polymers in solutions are known to coil at low temperature. This suggests that the viscoelastic mechanism seen during the misting process may be independent of entanglement and, to some extent, independent of the viscoelastic crossover parameters. It is predicted that the shear stresses encountered will be significantly greater than those at the viscoelastic crossover, and those at the linear viscoelastic limit. Thus, it is thought that the viscoelastic mechanism that causes the suppression of droplets is a non-linear mechanism seen at higher shear stresses and strains. It is thought, therefore, that extensional viscoelastic properties might well define this behaviour. Studying the extensional behaviour of these blends is likely to exaggerate differences between polymer architectures: Star polymers are less well extended than linear polymers as the arms hinder each others alignment with the shear axis.

## 5.7 Summary

- The effect of polymer viscosity modifiers on the misting tendency of lubricants was considered in detail. It was confirmed that the presence of polymers in a blend generally reduces the droplet forming tendency significantly. Polymers of low molecular weight do not have such a great effect.
- Linear and star polymers of varying molecular weights and compositions were blended into comparable blends. These blends were characterised in terms of their viscosity, viscoelasticity and their molecular interaction.
- The droplet forming tendency of polymer-containing blends was affected by their viscoelasticity, molecular orientation, and their molecular entanglement.
- Blends hypothesised to show higher viscoelastic response have a lower tendency to form mist and spray. This mechanism is attributed to the stretching of polymer molecules under shear.
- Blends with significant polymer entanglement show even greater tendencies to reduce mist and spray formation. Only linear polymers were seen to show this tendency under the tested conditions.
- Shear viscoelasticity does not appear to fully predict the droplet forming tendency of blends. Where viscoelastic response is increased by the presence of large side groups on molecules, the droplet forming tendency does not reduce proportionally. It is suggested that extensional viscoelastic properties will better predict droplet formation behaviour.
- Linear polymers exhibit a large variety of droplet forming behaviour. This is due to the greater variation in viscoelasticity and entanglement that can be achieved with commercially available polymers. Short chain linear polymers below a certain molecular weight do not contribute significantly to viscoelasticity or mist and spray reduction.
- Star polymers are generally poorly entangled in these blends but contribute significantly to the viscoelasticity of the blend.
- Micellar-type star polymers readily come apart under shear, meaning their behaviour is more like those of a short chain linear polymer.

## Chapter 6: Measurement of the Lubricant Mist Formed in a Fired Engine

### 6.1 Introduction

As previous simulation work has shown, the nature of misting is dependent on the formulation of the lubricant, particularly on the base oil viscosity and the polymers included as viscosity modifiers. This chapter describes investigations into the nature of mist in a running engine. Of particular interest was the effect of engine conditions on the nature of the mist. The simulation rig, although tuned to the flow conditions of the piston ring gap, was necessarily run under steady state conditions, so was unable to predict this behaviour.

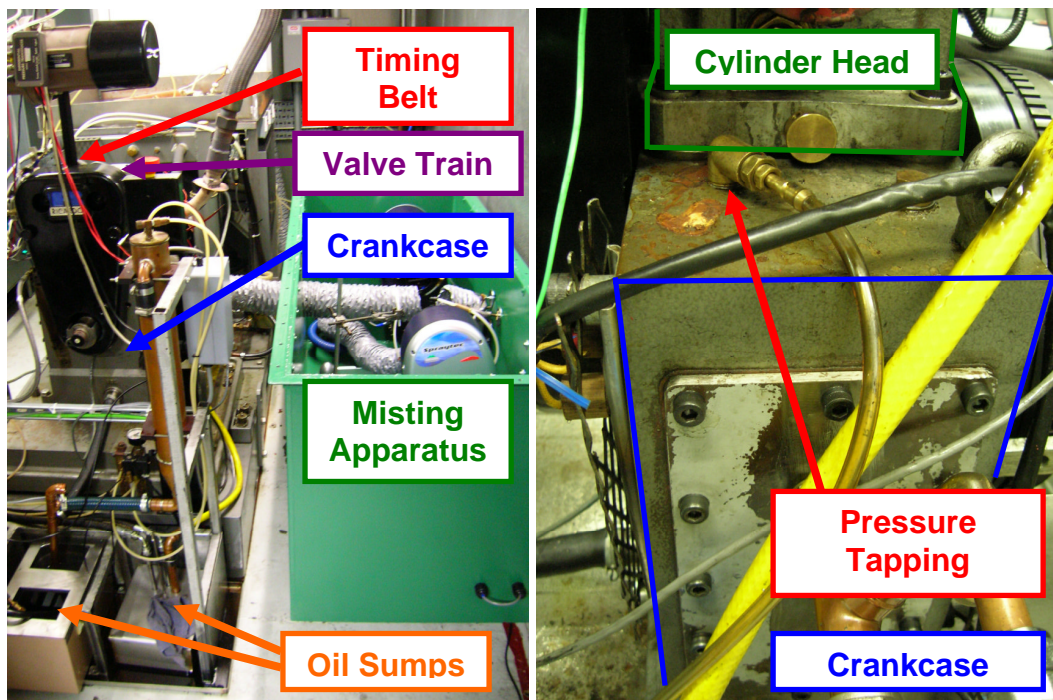



Figure 6.1: Ricardo Hydra Engine Setup

Figure 6.2: Pressure Tapping on Crankcase

## 6.2 Method

### 6.2.1 Engine

Ricardo Hydra Test Engine			
Maximum speed		6000 rpm	
Maximum torque (Load)		36 Nm	
Cylinder bore		86 mm	
Piston stroke length		86 mm	
Connecting rod length		143.5 mm	
Gudgeon pin offset from piston centre line		1 mm	
Nominal piston-cylinder clearance			
Crown land		3.46 mm	
Second land		3.22 mm	
Third land		3.00 mm	
Piston Rings	Profile	Fitted Gap	Tangential Tension
Top ring		0.603 mm	28 N
Second ring		0.577 mm	25 N
Oil control ring – Upper rail		0.812 mm	17 N
Oil control ring – Spring		-	-
Oil control ring – Lower rail		0.784 mm	18 N

**Table 6.1: Ricardo Hydra Engine Parameters**

The engine used was a Ricardo Hydra four-stroke single cylinder, gasoline research engine. This is based on a four-cylinder, 2.0 litre General Motors engine from 1988. A schematic of the engine is shown in Figure 6.1. It is a normally aspirated, with indirect fuel injection and four valves. The stroke and bore are both 86mm. It is mounted on a dynamometer so that it can be either motored or fired and all ancillary devices are run independently. The oil supply to the valve train and the crankcase are separate: The valve train is run on a fully formulated commercial oil to maximise durability as it is not the main focus of testing. The crankcase lubricant, that which lubricates the piston and main bearings, can be readily varied as the oil sumps are external to the engine and the crankcase is, at least nominally, dry. Thermocouples monitor coolant, exhaust gas, crankcase and cylinder head temperatures. These measurements and components are monitored and controlled through a centralised

control system. Crankcase gas pressure is measured using a Digatron Instrumentation handheld manometer, which can record gauge pressures up to 2000 mbar, attached by a hose to a 6mm diameter hole in the top of the crankcase, Figure 6.2. The temporal resolution of this apparatus and the damping produced by the length of sampling tube were not sufficient to produce a steady average pressure. Thus, the maximum and minimum values of pressure were recorded. The relevant engine parameters are shown in Table 6.1.

### 6.2.2 Mist Extraction and Measurement

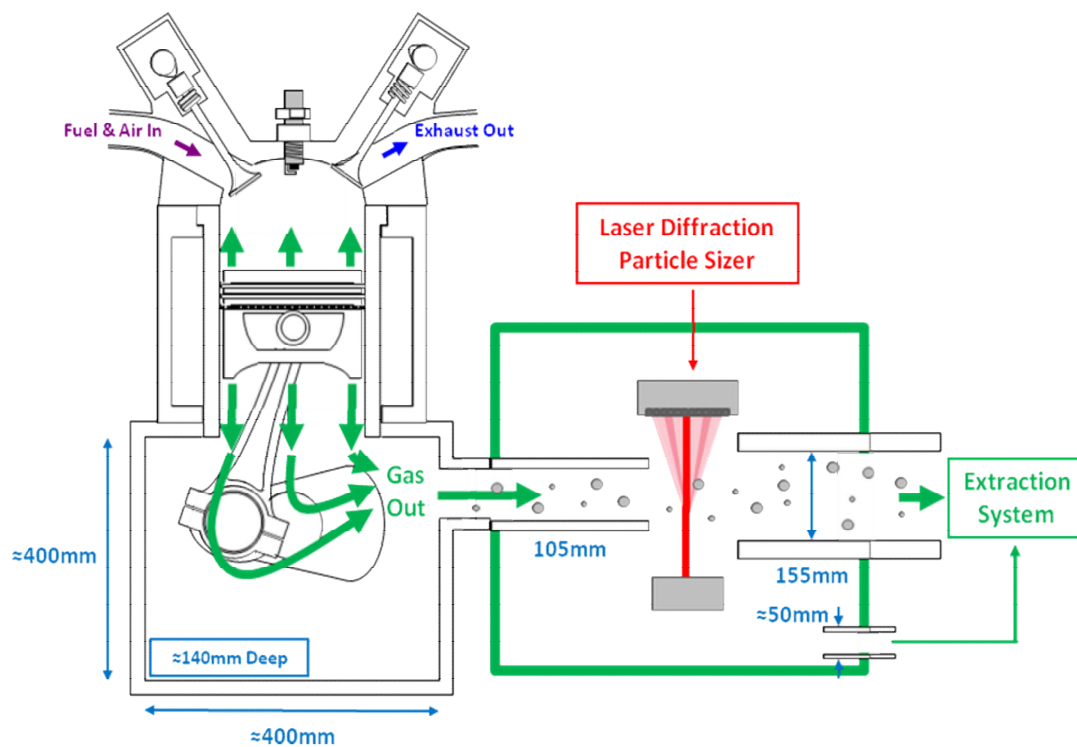


**Figure 6.3: Schematic of Engine Misting Apparatus**

The experimental setup is shown schematically in Figure 6.3. As in situ measurement of the mist in the piston assembly is beyond any technique currently available, it was decided that the droplets readily present in the crankcase of the engine would be studied. The droplets in the crankcase are understood to be from four sources:

- Mist formed in the piston assembly and carried to the crankcase in the blow-by gas
- Oil evaporated in the piston assembly and carried to the crankcase in the blow-by gas. The temperature of this flow significantly decreases, particularly with expansion into the crankcase and condensation will therefore take place and fine aerosol droplets are likely to form, 0.1-1 $\mu$ m diameter
- The excess oil from the crankshaft bearings inertially ‘thrown off’ the rapidly spinning components.
- The liner in this engine is lubricated by a spray from the con-rod. As the piston approaches TDC, a hole in the bearing casing aligns with a hole in the con-rod and oil, under the hydrodynamics pressure imposed by the bearing, is sprayed onto the liner. Whilst the extraction system may bring some of these droplets through the particle sizer, it is thought that, due to the finely directed nature of the spray onto the liner, this should not be a significant effect

Measurement of the mist was made using the same laser diffraction particle sizer as in the simulation rig, the Malvern Spraytec. It was enclosed in a similar way to the simulation rig, in order to control the flow of mist safely. In addition to the combustion risks of mist discussed in the simulation work, the elevated temperatures and the presence of oil and fuel vapours made the need for enclosure much more important. The extraction system for removing gas from the crankcase went through several iterations before settling on the final system shown in Figure 6.1 and Figure 6.3. A 4” diameter ( $\approx$ 105mm) flexible duct allowed the flow to leave the crankcase and pass through the particle sizer. This diameter was chosen as it was sufficiently large to prevent the deposition of droplets from the flow. For a single cylinder engine such as this, the crankcase volume changes significantly during a cycle. Therefore, it was found that, with smaller pipes, the highly pulsatile flow that results would cause a zero gas velocity at various stages of the cycle. At low or zero velocity, the gas flow is unable to keep larger droplets entrained, causing droplet deposition to occur. The measure of flow damping provided by the larger diameter pipe greatly reduces this phenomenon. As the particle sizer has a 10mm diameter laser beam, and the flow at the point of analysis was approximately 105mm diameter, the axial centre of the beam



was shone through the axial centre of the mist flow, in order to capture the greatest quantity of mist data, Figure 6.4, i.e. where the flow has the greatest thickness and where, due to the highest gas velocity being produced in the centre of the flow, the highest entrainment potential exists. For the purposes of analysis, the data collected was presumed to be representative of the whole flow.

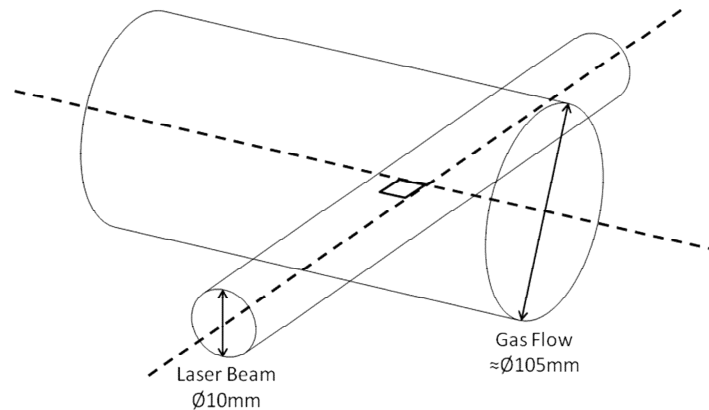


**Figure 6.4: Intersection of Particle Sizer Beam and Gas Flow**

The extraction system was designed to draw the gas from the crankcase. A 6" diameter ( $\approx 155\text{mm}$ ) flexible duct channelled the flow from the particle sizer to the room extraction system. This duct contained an extraction fan in series to supplement the extraction rate. This was a Vent-Axia ACM-150, which, operating independently, produces a flow rate of 767 l/min. The extraction rate of air in the flow path past the detector was measured at 500 l/min using a LCA 6000 VT 100mm vane anemometer that covered the whole extraction outlet. In this, the average velocity was measured and converted into a flow rate. This was smaller than the total flow rate as there was also a second flow path from the corner of the enclosure for more general extraction, Figure 6.3. Measurements of the blow-by gas flow rates were taken under normal conditions i.e. with no mist extraction and a normal crankcase using an AVL 442 orifice blow-by meter. This data is shown in Figure 6.5. It can be seen that, typically, the blow-by flow rate varied between 11.8 l/min at 1500rpm and 33% load, and 16.8 l/min at 2500rpm and 75% load, both with 50% throttle. Thus, clearly, the 500 l/min of gas passing the particle sizer was not entirely crankcase gas: A large proportion of

it would be drawn from the surrounding test cell. Therefore, the gas flow as a whole cannot be considered representative of the crankcase gas flow only. However, as all oil and droplets in the flow are from the crankcase gas, the nature of the oil droplets measured can be considered representative of the crankcase gas.

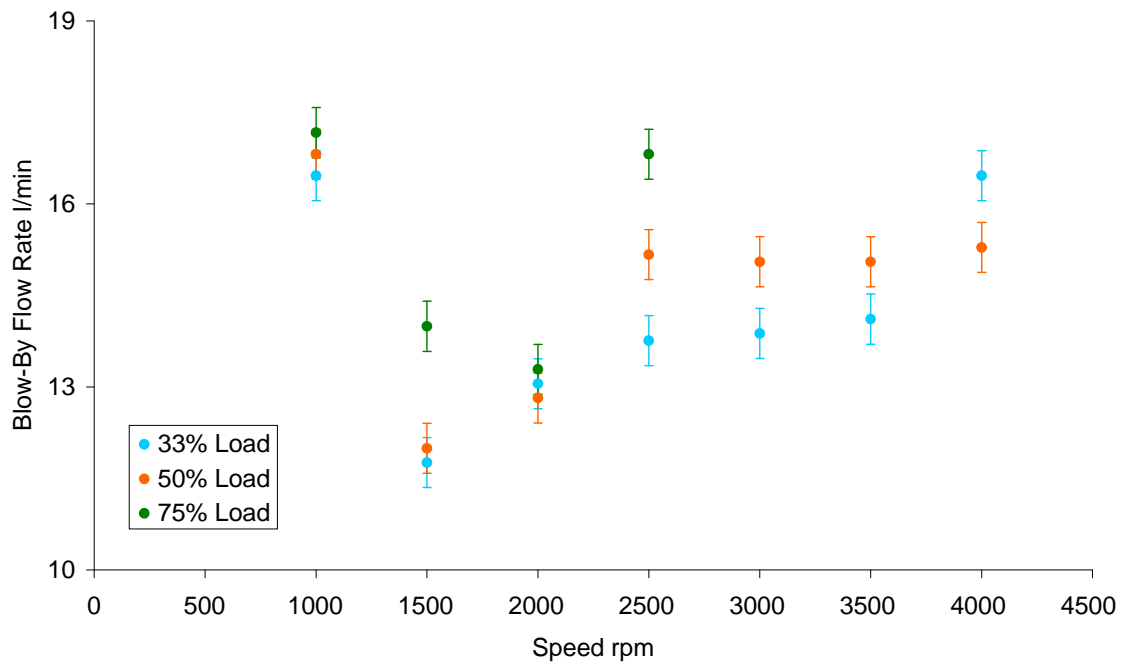


**Figure 6.5: Blow-By Flow Rate for Ricardo Hydra at 50% Throttle**

### 6.2.3 Procedure

As could be expected with large-scale extraction of gas from the crankcase, the oil consumption of the engine was considerably higher than normal. Therefore, the greatest challenge of this method was to control oil consumption so that the engine performance was not altered. The temperature of critical components was taken to be the indicator of lubricant starvation. Therefore, the temperature of the coolant, cylinder head and crankcase were recorded. These showed no significant deviation from conditions without extraction, suggesting that lubricant supply to the piston assembly was not affected.

Before a batch of tests, the engine was flushed with the test lubricant with a normal crankcase side plate i.e. no extraction of gas. A fresh 3 litre sump of the test lubricant was attached, the oil filter changed and the engine was motored for 30 minutes at 1500rpm and 50% throttle, whereupon the sump was changed for a fresh 3 litre sump and the engine motored for a further 30 minutes under the same conditions.

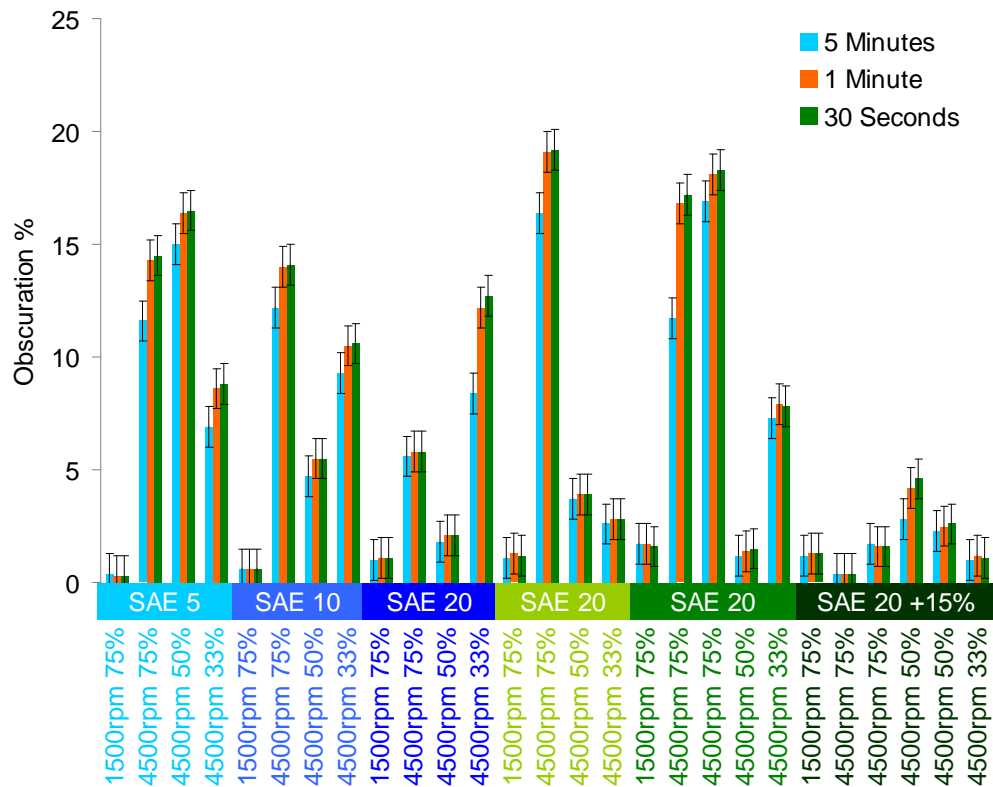


**Figure 6.6: Comparison of Test Recording Time for Obscuration**

For each test condition, the engine was run until it reached a stable operating temperature with a standard side plate. The engine was then stopped, 5 minutes were given for mist to be extracted from the test cell and the side plate including the extraction system was attached. The engine was run until the stable operating temperature for the condition was reached and the data recorded for the subsequent 30 seconds. Initially, readings were taken for the subsequent 5 minutes after thermal stabilisation, but showed no significant transience in the nature of the mist, as seen in Figure 6.6. In fact, it was noticeable that the size distribution and flow rate of the droplets tended to be stable within 2-3 minutes of the engine reaching a constant

speed. Therefore, a shorter recording time of 30 seconds was used. The engine was stopped, allowed to cool and the procedure begun again for a different set of conditions. When a different lubricant was to be tested, the flushing procedure described above was used.

### 6.3 Test Matrix

The primary concern of this investigation is the effect of engine conditions and lubricant properties on the mist produced. The engine conditions used are shown in Table 6.2.

Base Oil			SAE 5	SAE 10	SAE 20	SAE 20	SAE 20	SAE 20
Additives						5% VM	10% VM	15% VM
			1% Detergent + 1% Dispersant					
$\eta$ @40°C mPa.s			18.0	23.2	31.8	50.6	77.8	120.8
Speed	Load	Throttle						
1500	75%	50%						
3200	75%	50%			repeated			repeated
4500	75%	50%					repeated	repeated
4500	50%	50%						repeated
4500	33%	50%						

**Table 6.2: Test Lubricants and Conditions for Engine Misting Tests**

It was intended to measure data at 2500rpm. However, preliminary tests found a resonance peak for the extraction apparatus at this speed, which caused large quantities of oil to be thrown up from the surfaces of the ducting. Therefore, 3200rpm was chosen as an alternative, away from the main resonant peak. Arising from the conclusions of Chapter 4, the lubricants tested have varying viscosity and viscosity modifier (VM) concentration. These are shown in Table 6.2. Due to the age and design of the engine, the components were optimised for an SAE 20 lubricant. Thus, the reference lubricant was a Group III SAE 20 lubricant. When compared to the reference lubricant for the simulation work, an SAE 5W, the average molecular weight of the engine lubricant is significantly higher.

The viscosity modifier was an Infineum SV261, a diluted styrene-co-isoprene star. This type of viscosity modifier is pre-blended with another base oil for easier formulation. Therefore, the concentrations of 5, 10 and 15% by weight are the concentrations of the final product, not the polymer. The composition of the diluent base oil is not known. Also, to preserve the engine components, detergent and dispersant were added to each formulation. Also, as the ratio of polymer to diluents was not known, no calculations for the degree of polymer entanglement were possible. A treat rate of 1% by weight of a succinimide dispersant and 1% by weight of an overbased calcium sulphonate detergent was used. A repeat set of data was taken for the tests indicated in Table 6.2.

## 6.4 Simulation

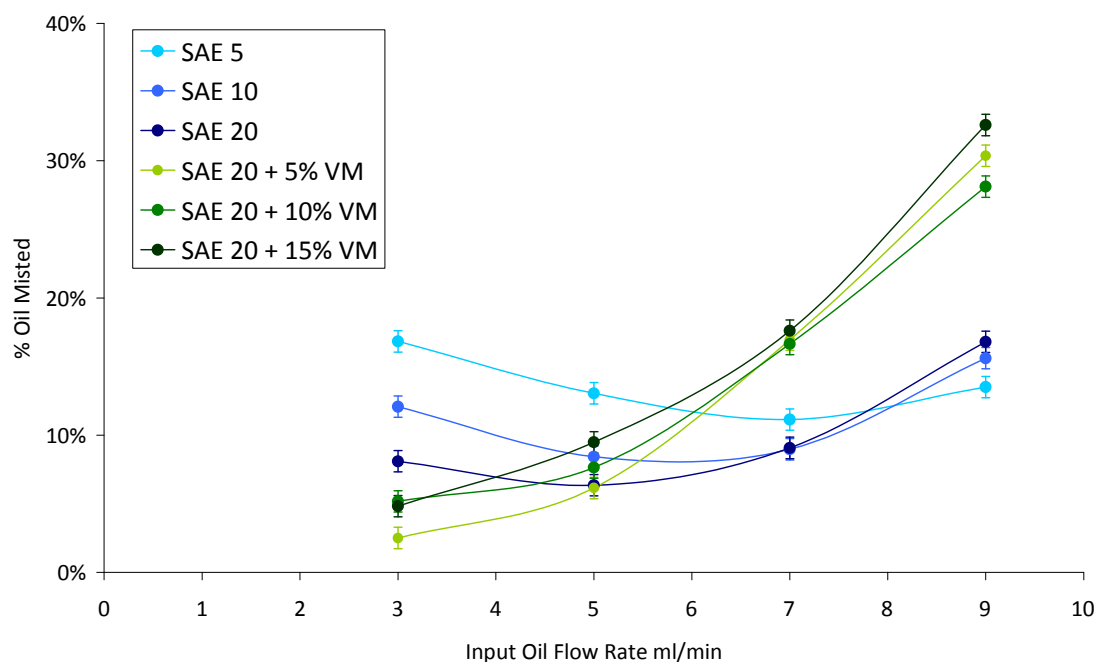


**Figure 6.7: Simulation Results for Misting Tendency of Engine Test Oils**

The oils used in these engine tests were first tested in the simulation rig used in Chapters 4 and 5. The variation of misting tendency with input flow rate is shown in Figure 6.7. As predicted in the results of Chapters 4 and 5, an increase in the base oil

viscosity produces a decrease in the tendency of the oil to produce mist and decreases the flow rate at which spray is produced, as defined in Section 4.4, i.e. indicating a greater resistance to shear. It can clearly be seen that the presence of viscosity modifier reduces the tendency to mist significantly. However, it can be seen that variation in the concentration of viscosity modifier does not greatly affect the misting tendency of the oil, despite having a significant effect on the viscosity of the blend, Figure 6.7. This suggests that, under these conditions, the presence of viscosity modifier produces changes in the mist tendency of the oil, but this effect is independent of concentration in the range tested, 5-15%. This suggests that the degree of entanglement of the polymer molecules is not large as the behaviour shows more variation with base oil than with viscosity modifier content, despite its presence having a significant effect. All this confirms, therefore, that the misting behaviour of these formulations is similar to that indicated by the simulator work.

## 6.5 Results

Figure 6.8 shows the droplet size distributions for the three base oils used in the engine, at 4500rpm and 33% load. There are three characteristic droplet sizes in each distribution, as in the simulation rig. Several observations can be made: Firstly, aerosol sized droplets, with diameters typically 0.1-1 $\mu$ m, are rarely seen on measured distributions, though droplets with diameters of 5-15 $\mu$ m are seen on many traces. Observation when clear windows are fitted to the engine indicates that small droplets are abundant in the crankcase under normal conditions. Droplets with diameter 0.1-1 $\mu$ m are characteristic of vapour condensation. Either this mechanism is not produced in the engine, or occurs to the extent that droplets with diameters 5-15 $\mu$ m are produced by condensation. This, though seemingly an extreme increase in droplet volume, may occur as water, fuel and oil may all form condensate under these conditions. The extraction may also cause these small droplets to coalesce or be deposited

Secondly, the distributions appear to correlate well with the known sources of droplets. The droplets with diameters between 250-1000 $\mu$ m indicate throw-off and

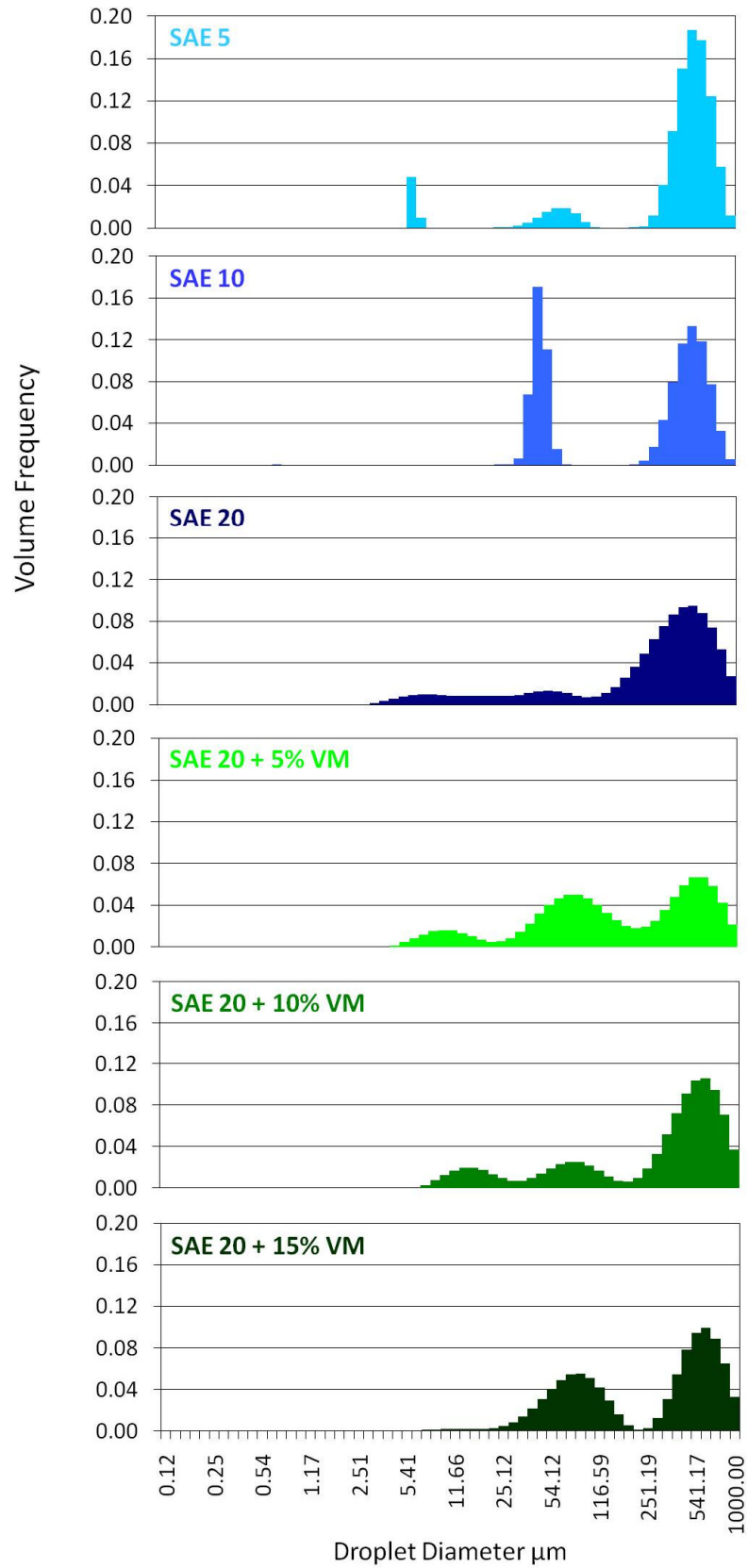


**Figure 6.8: Droplet Size Distributions for Oils Tested at 4500rpm and 33% Load**

stray spray from the con-rod, whilst those with diameters less than 250 $\mu\text{m}$  indicate mist, which is thought to be formed in the piston assembly. As with the results from the simulation rig, there are two distinct regions of mists. These are seen to be between 0.1-30 $\mu\text{m}$  diameter, with characteristic sizes generally 5-15 $\mu\text{m}$ , and 30-250 $\mu\text{m}$  diameter, with characteristic sizes generally 50-120 $\mu\text{m}$ . Owing to the typically greater volume frequency and more consistent presence in distributions, these ranges are termed the Minor and Major Misting Regions respectively, Figure 6.9.

Thirdly, whilst the distributions are similar to those in the simulation rig, the characteristic droplet sizes in each region are noticeably greater. This is either a result of the differences in the misting environment they are formed in, by condensation causing droplets growth, or by the higher molecular weight of the oils relative to those in the simulation rig, where, as indicated by Dasch (2008), higher molecular weight oils base oil tends to form larger droplets.

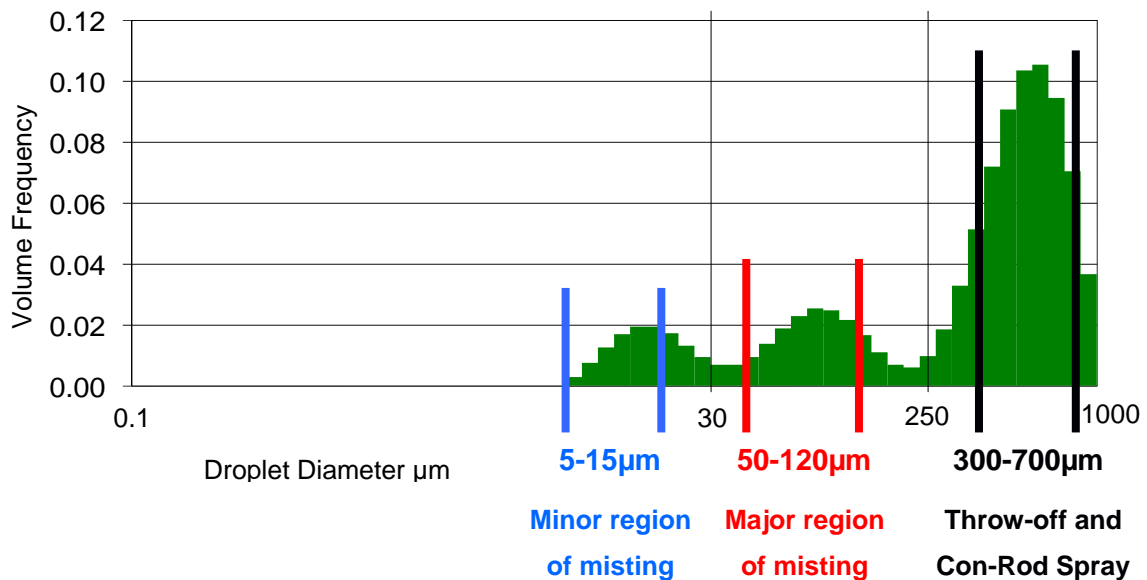


**Figure 6.9: Characteristic Regions of Misting Behaviour – Example is SAE 20 + 10% Viscosity Modifier at 4500rpm and 33% Load**



Considering that the focus of the investigation is on mist from the piston assembly, the flow rate of oil is computed in terms of the flow rate contained in droplets smaller than  $250\mu\text{m}$ . This is computed by taking the oil to air ratio, or  $C_v$ , measured by the particle sizer, and multiplying this by the total flow rate past the detector and the proportion of the volume flowing in droplets smaller than  $250\mu\text{m}$ , calculated from the droplet size distribution:

$$\text{Oil Flow Rate from Piston Assembly} = \text{Oil : Air Ratio} \times \text{Total Flow Rate} \times (\text{Flow} < 250\mu\text{m}) \quad [6.1]$$

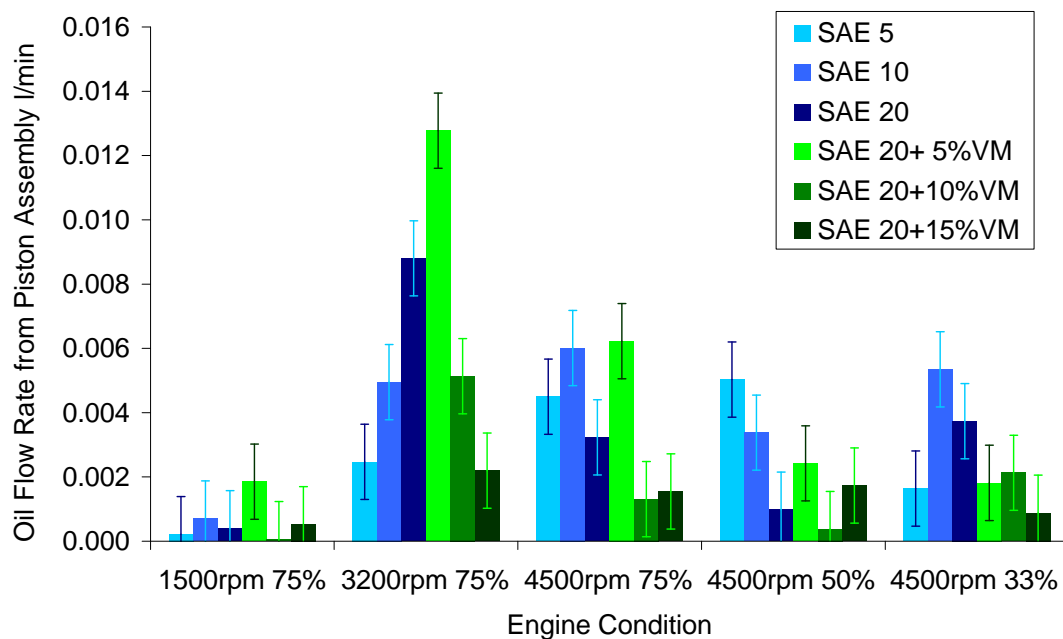


**Figure 6.10: Flow Rate of Oil from Piston Assembly under Varying Engine Conditions**

Figure 6.10 shows the oil flow rate from the piston assembly for each oil tested under each condition. It is noticeable that the flow rate values are larger than is possible. To explain, consider the reference SAE 20 lubricant at 4500rpm and 33% load: Here the flow rate from the piston assembly is 0.0037 l/min and the total oil flow rate is 0.013 l/min. The test duration with the extraction system was typically 30-35 minutes, therefore, for this test, if the data were realistic, 0.46 litres of oil would be lost per

test, which was not the case. Throughout the tests, oil would be deposited on the screens of the particle sizer. The large extraction flow rate drawing in ambient air, and compressed air purges across the screens reduced this, but not completely. The accumulation of oil on the screen increases the degree of light scattering and absorbance. As the oil to air ratio is calculated using the Beer-Lambert Law, which is based on transmittance and scattering values, as seen in Equation 4.4, oil coating the screens will yield artificially high oil to air ratios. This appears to be the phenomenon at work here.

This renders the magnitude of flow rate data as unusable, as the effects of mist and screen contamination cannot be decoupled. However, relative values are still of some use. It can be seen that the flow rate at 3200rpm is significantly higher than for all other conditions. This is thought to be due to the resonance peak seen at 2500rpm. Although testing at 3200rpm rather than 2500rpm greatly reduced the visible vibration, it still seems to occur to some extent at 3200rpm. This vibration produces more droplets that impact the screen, hence the even higher flow rate values. In an attempt to reduce this effect, the obscuration at the end of the test, when no oil was flowing, was recorded i.e. when all obscuration is caused by droplets on the screen, termed End Obscuration. This was then subtracted from the original obscuration readings to give a value, theoretically, of obscuration resulting only from the mist, given by the following equation:

$$\text{Obscuration} = \text{Obscuration from Mist} + \text{End Obscuration} \quad [6.2]$$

However, for data recorded at 4500rpm, in order that the End Obscuration reading could be taken, the engine decelerated through the resonant speed of 2500rpm during stopping. Thus, more oil was disturbed and the screens were covered with more droplets, making the End Obscuration values less accurate. Thus, End Obscuration was retained as a variable for statistical purposes only.

Figure 6.11 shows the droplet size distributions for base oils under each engine condition. It can be seen that under all conditions, a higher viscosity base oil produced

larger mist droplets. It can also be seen, most prominently at 4500rpm, that a higher viscosity base oil produces wider distributions around a characteristic droplet size. This may be an effect of a wider molecular weight distribution in the base oil. Droplet size distributions are narrower for tests at 1500rpm. This may be a result of their being fewer droplets i.e. a lower flow rate of oil. However, as discussed previously, the flow rate data cannot illuminate this observation.

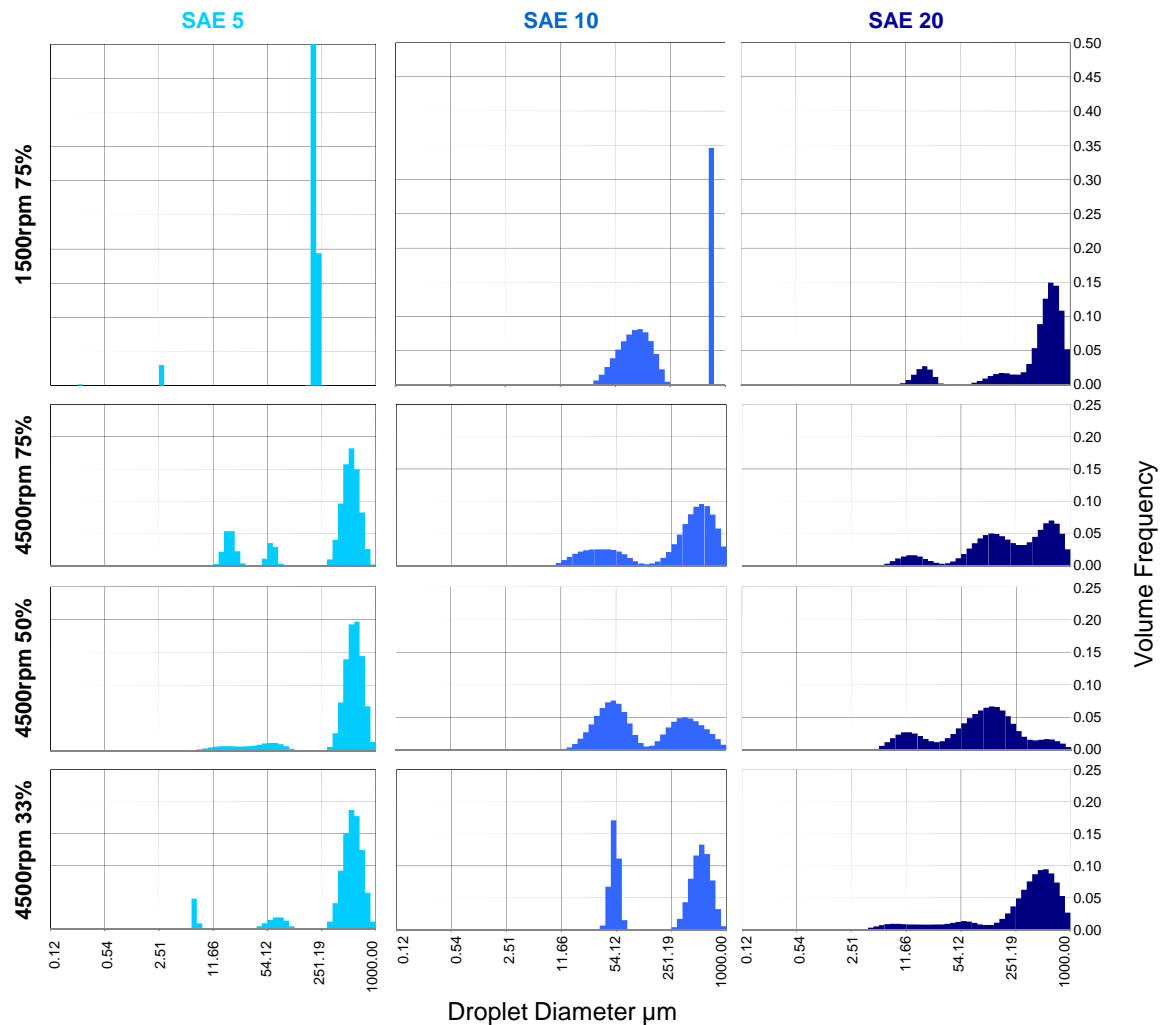


**Figure 6.11: Droplet Size Distributions for Base Oils at Various Engine Conditions**

Figure 6.12 shows the droplet size distributions for lubricants with varying concentrations of viscosity modifier. As can be seen, under all conditions, an increase

in viscosity modifier produced an increase in the proportion of throw-off in the mist measured i.e. the flow rate of mist decreases relative to the flow rate of throw-off. This suggests that either the flow rate of throw off is increasing or the flow rate of mist is decreasing. Whilst measured flow rate data cannot indicate which situation this is, the flow rate of throw-off is likely to vary less than for mist, particularly when tests taken at the same engine speed are compared. Therefore, it is hypothesised that increasing concentration of viscosity modifier reduces the flow rate of mist. It can also be seen that the inclusion of viscosity modifier reduces the amount of droplets in the minor misting region. This effect is likely to be due to the viscoelasticity produced by the viscosity modifier reducing the formation of mist and, possibly, preventing the breakup of droplets in the gas flow.

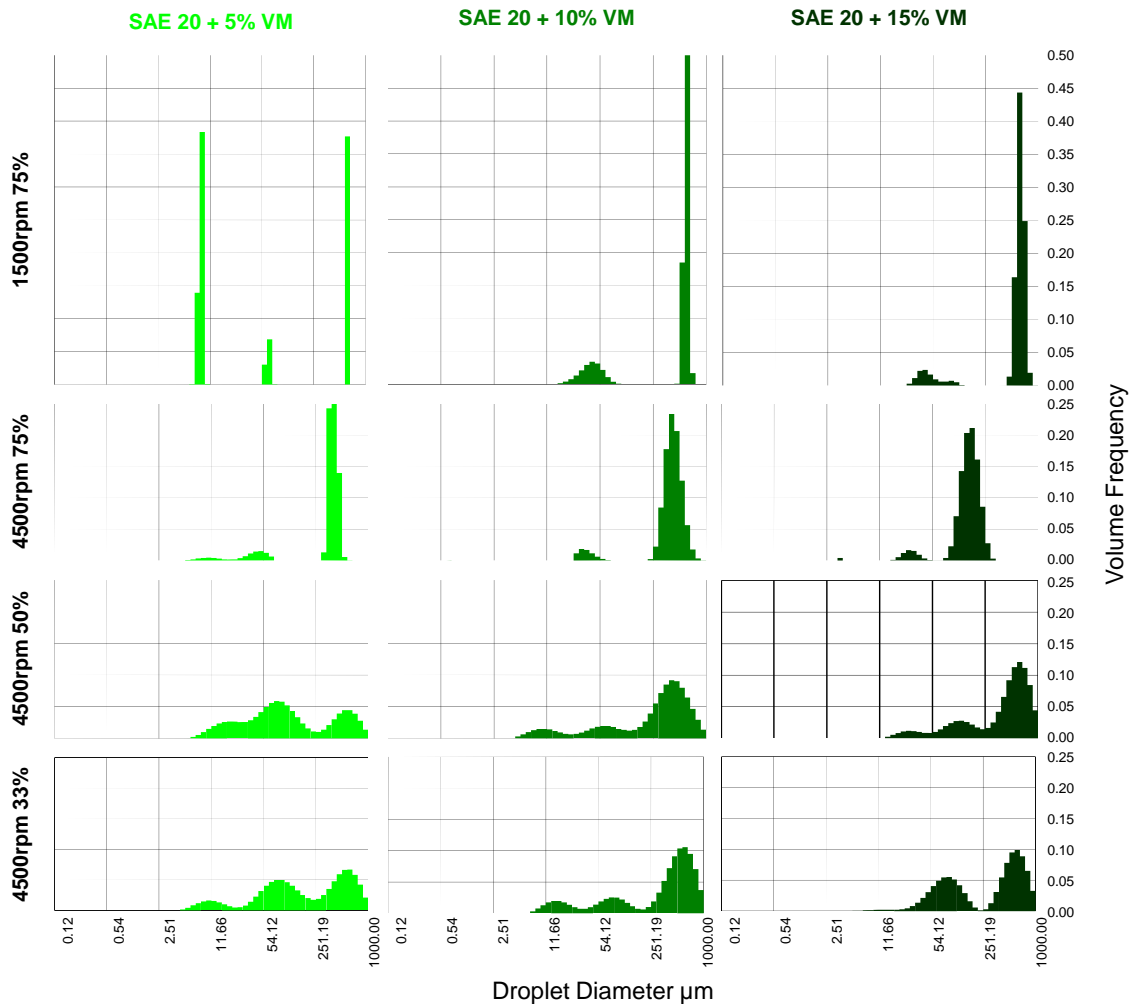


**Figure 6.12: Droplet Size Distributions for Oils with Polymer at Various Engine Conditions**

The characteristic droplet sizes are also affected by viscosity modifier. Using the example of the tests at 4500rpm and 33% load, the presence of viscosity modifier increased the characteristic droplet size in the major misting region uniformly; From 54 $\mu\text{m}$  without viscosity modifier to 75-80 $\mu\text{m}$  with viscosity modifier. In the minor misting region, for these conditions, the characteristic droplet size increases with concentration of viscosity modifier: From 7.5 $\mu\text{m}$  in base oil, 10 $\mu\text{m}$  with 5% viscosity modifier and 15 $\mu\text{m}$  with 10% and 15% viscosity modifier. This trend, however, is less clearly seen under other conditions.

## 6.6 Statistical Analysis

In order to better understand the data arising from these experiments. A principal component analysis was performed, as with the simulation rig data. The variables included in the analysis are shown in Table 6.3. As principal component analysis is a linear analysis only, highly non-linear variables were not included. Also, data for 3200rpm was not included, on the basis that any flow rate data artificially makes these variables highly non-linear. The results from the analysis, the principal components and the coefficients of the dominant variables within them, are shown in Table 6.4. Variables were considered dominant if their coefficients were greater than  $\pm 0.15$ .

The first principal component, which accounts for 37.7% of the variation in the data, appears to link oil flow rate, engine speed and temperature. An increase in speed is seen to affect several parameters:

- Several parameters correlated in this component are related to the normal functioning of the engine. An increase in speed necessitates a backward increase in the ignition timing and produces an increase in the temperatures of the crankcase oil, cylinder head oil, the exhaust gas, the coolant inlet and outlet. The difference in temperature between the coolant inlet and outlet is reduced, as typically occurs at higher operating temperatures.
- When the engine runs at a higher temperature, the time to reach thermal equilibrium increases. Thus, the time at which the test data is recorded increases with speed.

	Variable	Description
1	VM Content	Concentration of viscosity modifier (%)
2	Speed	Engine Speed (rpm)
3	Load	Engine Load (%)
4	Test Start	Time for engine to reach thermal equilibrium (minutes)
5	Fuel	Injector duration (ms)
6	Timing	Ignition timing (degrees backwards)
7	Torque	Engine Torque (Nm)
8	Crankcase Pressure High	Upper reading of crankcase gas pressure (mbar)
9	Crankcase Pressure Low	Lower reading of crankcase gas pressure (mbar)
10	T Exhaust	Exhaust temperature (°C)
11	T Coolant In	Temperature of coolant at inlet (°C)
12	T Coolant Out	Temperature of coolant at outlet (°C)
13	T Cylinder Head Oil	Temperature of oil in cylinder head (°C)
14	T Crankcase Oil	Temperature of crankcase oil (°C)
15	dT Coolant	Difference in temperature between coolant inlet and outlet (°C)
16	dT Crankcase-Head	Difference in temperature between cylinder head and crankcase oil (°C)
17	Obscuration	Optical obscuration (%)
18	End Obscuration	Optical obscuration at end of test (%)
19	Obscuration Difference	Difference between optical obscuration during and at end of test (%)
20	End Obscuration /min	End obscuration per minute of test (% /min)
21	Oil : Air Ratio	Oil : Air ratio calculated from obscuration, 'Cv' in optical software (%vol)
22	Mist Flow /min	Oil flow rate as mist, calculated optically (l/min)
23	Mist Flow /cycle	Oil flow rate as mist, calculated optically (l/cycle)
24	$\eta$ @40°C	Dynamic viscosity of test lubricant at 40°C (mPa.s)
25	$\eta$ @100°C	Dynamic viscosity of test lubricant at 100°C (mPa.s)
26	$\nu$ @40°C	Kinematic viscosity of test lubricant at 40°C (mm <sup>2</sup> s <sup>-1</sup> )
27	$\nu$ @100°C	Kinematic viscosity of test lubricant at 100°C (mm <sup>2</sup> s <sup>-1</sup> )
28	$\rho$ @40°C	Density of test lubricant at 40°C (g/cm <sup>3</sup> )
29	$\rho$ @100°C	Density of test lubricant at 100°C (g/cm <sup>3</sup> )
30	Oil : Air Ratio <250µm	Oil : Air ratio considering only oil in droplets smaller than 250µm (%vol)
31	Flow Rate <250µm /min	Oil flow rate of mist from piston assembly (l/min)
32	Flow Rate <250µm /cycle	Oil flow rate of mist from piston assembly (l/cycle)
33	% Flow Rate <250µm	Proportion of flow rate of oil as droplets smaller than 250µm (%)
34	% Flow Rate <30µm	Proportion of flow rate of oil as droplets smaller than 30µm (%)
35	% Flow Rate 30-250µm	Proportion of flow rate of oil as droplets 30-250µm (%)
36	% Flow Rate >250µm	Proportion of flow rate of oil as droplets larger than 250µm (%)
37	Mean d (d) <250µm	Diameter-weighted mean droplet diameter of piston assembly mist (µm)
38	Mean d (A) <250µm	Area-weighted mean droplet diameter of piston assembly mist (µm)
39	Mean d (V) <250µm	Volume-weighted mean droplet diameter of piston assembly mist (µm)
40	Mean d (smd) <250µm	Sauter mean droplet diameter of piston assembly mist (µm)
41	Mean d (d) <30µm	Diameter-weighted mean droplet diameter in minor misting region (µm)
42	Mean d (A) <30µm	Area-weighted mean droplet diameter in minor misting region (µm)
43	Mean d (V) <30µm	Volume-weighted mean droplet diameter in minor misting region (µm)
44	Mean d (smd) <30µm	Sauter mean droplet diameter in minor misting region (µm)
45	Mean d (d) 30-250µm	Diameter-weighted mean droplet diameter in major misting region (µm)
46	Mean d (A) 30-250µm	Area-weighted mean droplet diameter in major misting region (µm)
47	Mean d (V) 30-250µm	Volume-weighted mean droplet diameter in major misting region (µm)
48	Mean d (smd) 30-250µm	Sauter mean droplet diameter in major misting region (µm)
49	Mean d (d) >250µm	Diameter-weighted mean droplet diameter in spray/throw off (µm)
50	Mean d (A) >250µm	Area-weighted mean droplet diameter in spray/throw off (µm)
51	Mean d (V) >250µm	Volume-weighted mean droplet diameter in spray/throw off (µm)
52	Mean d (smd) >250µm	Sauter mean droplet diameter in spray/throw off (µm)

**Table 6.3: Variables for Principal Component Analysis**

Principal Component 1		Principal Component 2		Principal Component 3	
37.7% of Variation		22.6% of Variation		17.0% of Variation	
-0.18	Speed	-0.19	VM Concentration	0.21	VM Concentration
-0.18	Test Start	-0.15	T Coolant In	-0.19	dT Crankcase-Head
-0.18	Timing	-0.16	T Coolant Out	0.20	$\eta$ @40°C
-0.15	Cylinder Pressure High	-0.15	T Crankcase Oil	0.20	$\eta$ @100°C
0.17	Cylinder Pressure Low	0.15	Obscuration Difference	0.20	$v$ @40°C
-0.15	T Exhaust	-0.20	$\eta$ @40°C	0.20	$v$ @100°C
-0.18	T Coolant In	-0.19	$\eta$ @100°C	0.22	$\rho$ @40°C
-0.18	T Coolant Out	-0.20	$v$ @40°C	0.21	$\rho$ @100°C
-0.19	T Cylinder Head Oil	-0.19	$v$ @100°C	-0.20	Flow Rate <250 $\mu$ m
-0.16	T Crankcase Oil	-0.17	$\rho$ @40°C	-0.18	% Flow Rate 30-250 $\mu$ m
0.15	dT Coolant	-0.17	$\rho$ @100°C	0.19	% Flow Rate >250 $\mu$ m
-0.22	Obscuration	-0.15	% Flow Rate <250 $\mu$ m	0.18	Mean d (d) <250 $\mu$ m
-0.22	End Obscuration	-0.18	% Flow Rate 30-250 $\mu$ m	0.18	Mean d (A) <250 $\mu$ m
-0.22	End Obscuration/min	0.16	% Flow Rate >250 $\mu$ m	0.18	Mean d (V) <250 $\mu$ m
-0.21	Oil : Air Ratio	-0.22	Mean d (smd) <250 $\mu$ m	0.15	Mean d (V) <30 $\mu$ m
-0.20	Mist Flow /min	-0.17	Mean d (smd) 30-250 $\mu$ m	0.19	Mean d (smd) <30 $\mu$ m
-0.21	Mist Flow /cycle	0.25	Mean d (d) >250 $\mu$ m	-0.25	Mean d (d) 30-250 $\mu$ m
-0.21	Oil : Air Ratio <250 $\mu$ m	0.25	Mean d (A) >250 $\mu$ m	-0.24	Mean d (A) 30-250 $\mu$ m
-0.21	Mist Flow <250 $\mu$ m /min	0.25	Mean d (V) >250 $\mu$ m	-0.23	Mean d (V) 30-250 $\mu$ m
-0.20	Mist Flow <250 $\mu$ m /cycle	0.25	Mean d (smd) >250 $\mu$ m	-0.21	Mean d (smd) 30-250 $\mu$ m
0.15	Mean d (d) <30 $\mu$ m				
0.15	Mean d (a) <30 $\mu$ m				
0.15	Mean d (v) <30 $\mu$ m				

**Table 6.4: Principal Components for Engine Misting Data**

- An increase in engine speed reduces the upper limit of gas gauge pressure in the crankcase and decreases, in terms of magnitude, the lower limit. This can be explained by either the reduced cycle duration allowing the flow less time to stabilise in response to the cyclic conditions, a forced damping, or a poor measurement resolution on the pressure sensor. Both are likely to be significant factors.
- These engine parameters are linked to several oil flow rate parameters. The flow properties pertaining to droplet flow rate, i.e. obscuration, oil : air ratio, oil flow rates per minute and per cycle, correlate closely with each other and with speed and temperature. When the engine runs faster and hotter, it

produces more mist. That oil flow rates in terms of both time and cycles are correlated indicates that a faster and hotter engine increases the flow rate of mist produced in a cycle, as well as the increase in oil flow rate arising from there being more cycles per minute.

- More significantly for the objectives of this study, the flow rate of oil as mist from the piston assembly, i.e. with droplet diameter smaller than  $250\mu\text{m}$ , also increases with speed. The effective oil : air ratio of droplets from the piston assembly varies similarly. Again, flow rate per minute and per cycle of these droplets are well correlated.
- An increase in speed and temperature appears to decrease the mean droplet size in the minor misting region i.e. droplet diameters smaller than  $30\mu\text{m}$ . This applies for diameter, area and volume weighted mean diameters only. It is thought that this may be the result of the higher running temperatures reducing the condensation of oil vapour, or affecting the breakup mechanisms of droplets e.g. the Weber number is dependent on density which decreases with temperature. It is likely that both mechanisms occur to some degree.

The second component, which accounts for 22.6% of the variation in the data, appears to link the viscometric properties of the oil with the nature of the droplet size distribution:

- Understandably, an increase in the viscosity modifier content of the oil increases the dynamic and kinematic viscosities, and the density. The increase in viscosity appears to produce an increase in the coolant inlet and outlet temperatures, and the crankcase oil temperature. This may be due to the greater friction power loss produced by the more viscous lubricant. Variation in these bulk properties does not affect the cylinder head oil temperature as this oil is run on a different lubricant circuit and its composition does not vary.
- An increase in viscosity modifier content increases the proportion of the total volume found as a mist ( $<250\mu\text{m}$ ) and, obviously, decreases the proportion formed from throw-off ( $>250\mu\text{m}$ ). The bulk of the variation in the proportion of mist ( $<250\mu\text{m}$ ) is caused by variation in the proportion of droplets in the major misting region ( $30\text{-}250\mu\text{m}$ ).



- An increase in viscosity modifier content tends to an increase in the Sauter Mean Diameter of mist droplets (<250 $\mu\text{m}$ ) and, by extension, those in the major misting region (30-250 $\mu\text{m}$ ). This, theoretically, will decrease the reaction rate of any chemical and physical processes the droplet experiences.
- An increase in viscosity modifier content tends to decrease the mean droplet size of droplets found in throw-off (>250 $\mu\text{m}$ ). This applies for diameter, area, volume weighted, and Sauter Mean Diameter values. This is different to what theory and previous experiment predicts. This, therefore, suggests that the increase in viscosity modifier content produces either a change in the mechanism of throw-off, or that a local change in lubricant properties can occur, or that the higher operating temperatures seen reduce the viscosity, thus the nature of throw-off, significantly.

The third component, which accounts for 17.0% of the variation in the data, also appears to link the viscometric properties of the oil with the nature of the droplet sized distribution:

- An increase in viscosity and viscosity modifier content produces an increase in the mean droplet size of the mist (<250 $\mu\text{m}$ ). This applies to diameter, area and volume weighted averages. This is in keeping with the findings of other studies (Dasch et al., 2008). However, examining the relationships between viscosity and diameter weighted mean droplet diameter, it can be seen that no significant trend appears to exist, and it may be outliers that contribute to the apparent increase, Figure 6.13.
- The increase in the droplet size of the mist with viscosity modifier content is reflected in an increase in droplet diameter for small mist droplets (<30 $\mu\text{m}$ ). The volume weighted mean and Sauter Mean Diameter are those that correlate most strongly, as these are the most sensitive diameter measurements in small droplets.
- However, perhaps surprisingly, the mean droplet diameter for mist (30-250 $\mu\text{m}$ ) appears to decrease with an increase in viscosity modifier content and, thus, with an increase in the overall mist (<250 $\mu\text{m}$ ) mean diameter.

Looking at the data for this relationship, Figure 6.14, it can be seen that this trend is not significant.

- Interestingly, the correlations between the viscosity modifier content and the proportions of volume as mist and throw-off are the inverse of that seen in the component 2. This may be a result of this analysis being limited to linear variables. Thus, a non-linear relationship between viscosity and viscosity modifier content and the proportions of mist and throw-off may well be described through the cumulative effect of these two linear relationships.
- As previously described, an increase in viscosity modifier results in an increase in dynamic and kinematic viscosity, and density. In terms of operating temperatures, this component differs from the second in that only the difference in temperature between the cylinder head oil and the crankcase is found to correlate well. This difference decreases with increasing viscosity modifier content, a phenomenon discussed in Component 1 as typical of higher engine operating temperatures.

In order to further highlight the dominant trends in the dataset, the data from each test is fed into each principal component and plotted: This is termed a score plot. Such plots can differentiate characteristic behaviour in the data. Data points, i.e. test conditions, exhibiting similar behaviour tend to cluster on the plot. The similarity of the behaviour to the exact behaviour described by the principal component is shown by the proximity of the point or cluster of points to the origin. The points furthest from the origin behave most similarly to the principal component.

Figure 6.15 and Figure 6.16 show the score plot for principal components 1 and 2, coded by oil and engine condition. The clustering of points is far more profound when considered in terms of engine condition. Conditions with the same speed group tightly but there is little differentiation with load. Therefore, it appears that engine speed most significantly differentiated misting behaviour. Higher speeds, as they cluster further from the origin, conform more closely to the relationships seen in the principal components than conditions at low speeds. As both components 2 and 3 address the relationships between oil properties and droplet behaviour. The score plots for

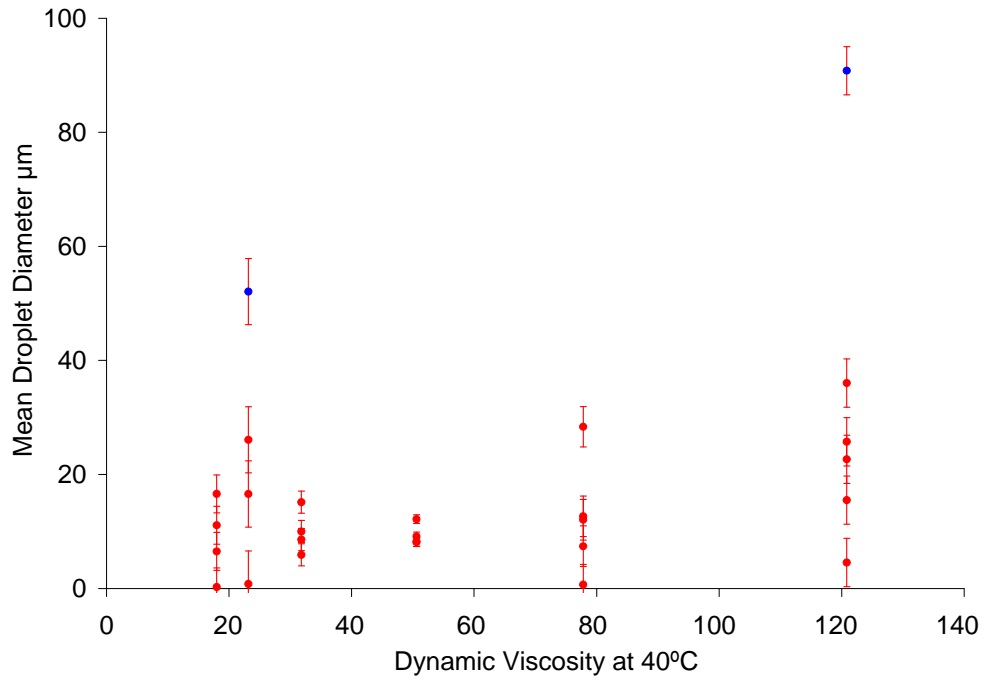


**Figure 6.13: Variation of the Diameter-Weighted Droplet Diameter of Mist with Viscosity**

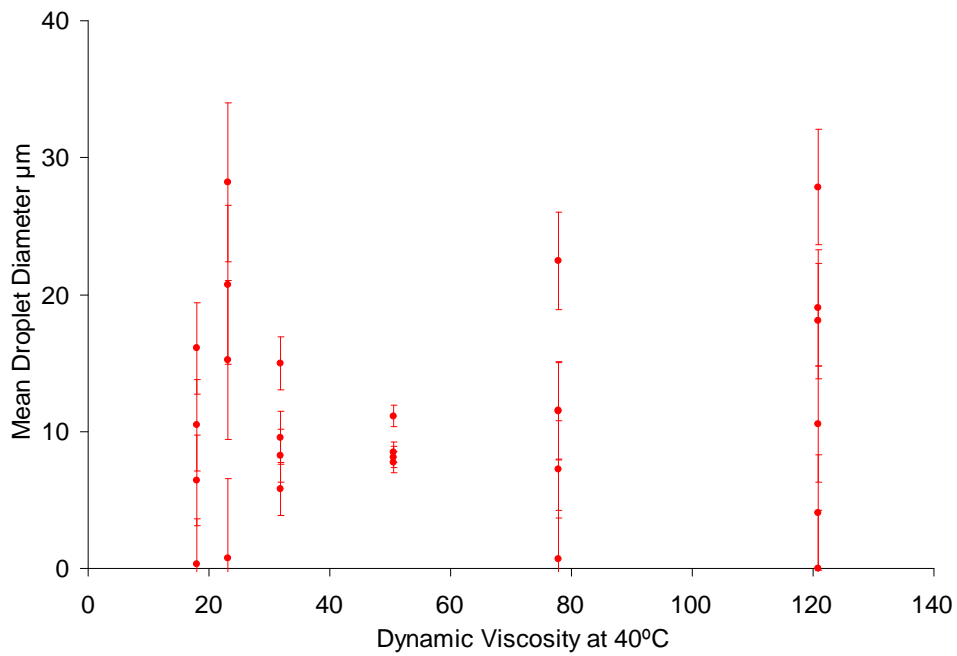


**Figure 6.14: Variation of the Diameter-Weighted Droplet Diameter of the Minor Misting Region with Viscosity**

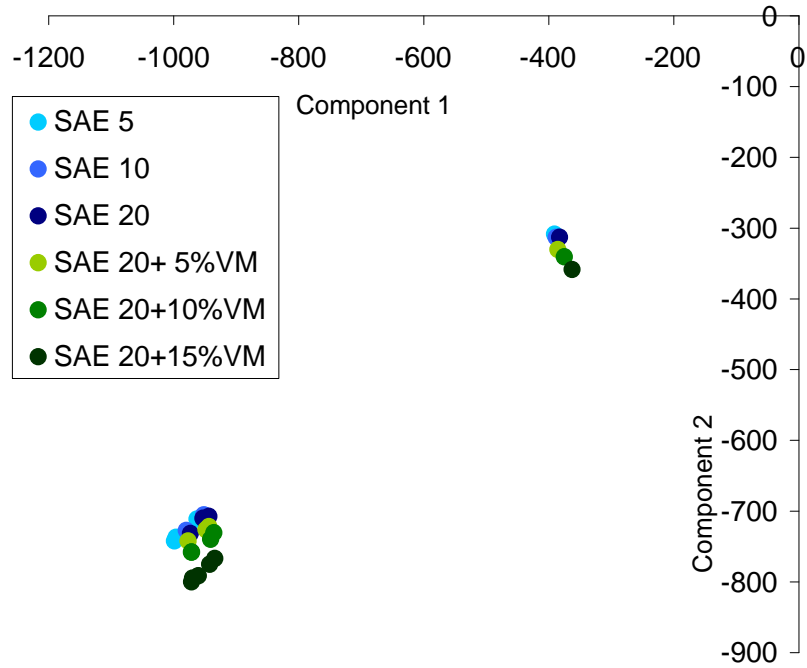


Figure 6.15: Score Plot of Principal Components 1 and 2, by Oil

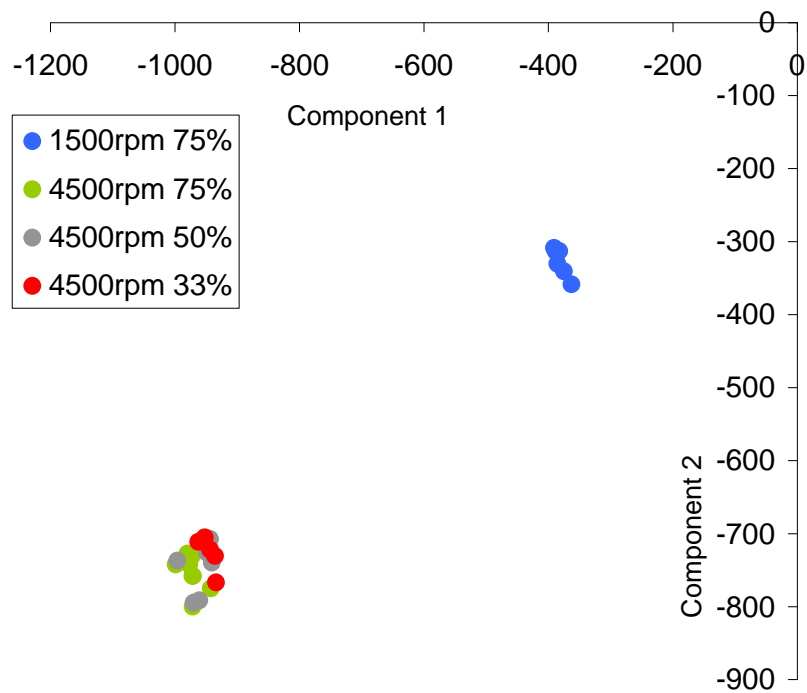


Figure 6.16: Score Plot of Principal Components 1 and 2, by Engine Condition

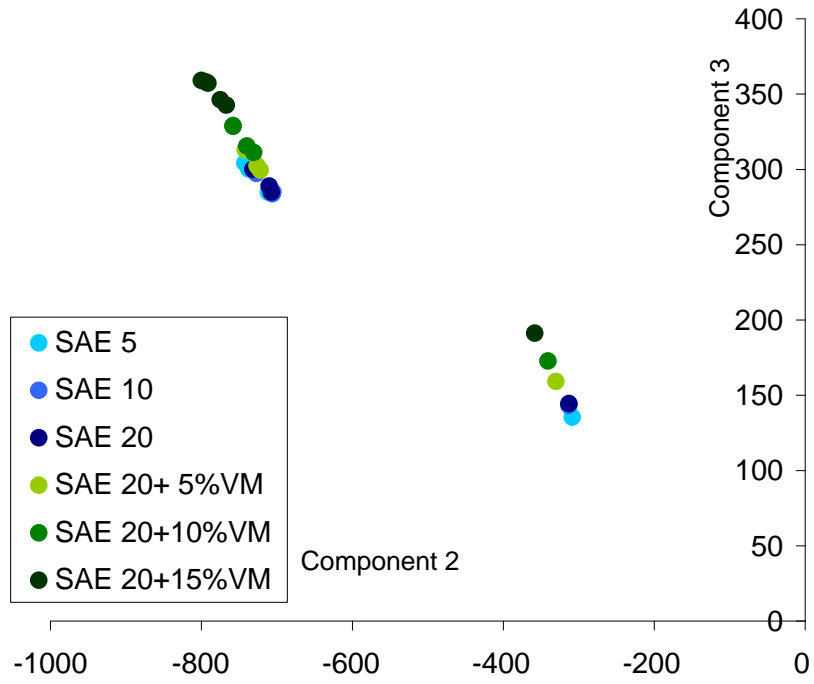


Figure 6.17: Score Plot of Principal Components 2 and 3, by Oil

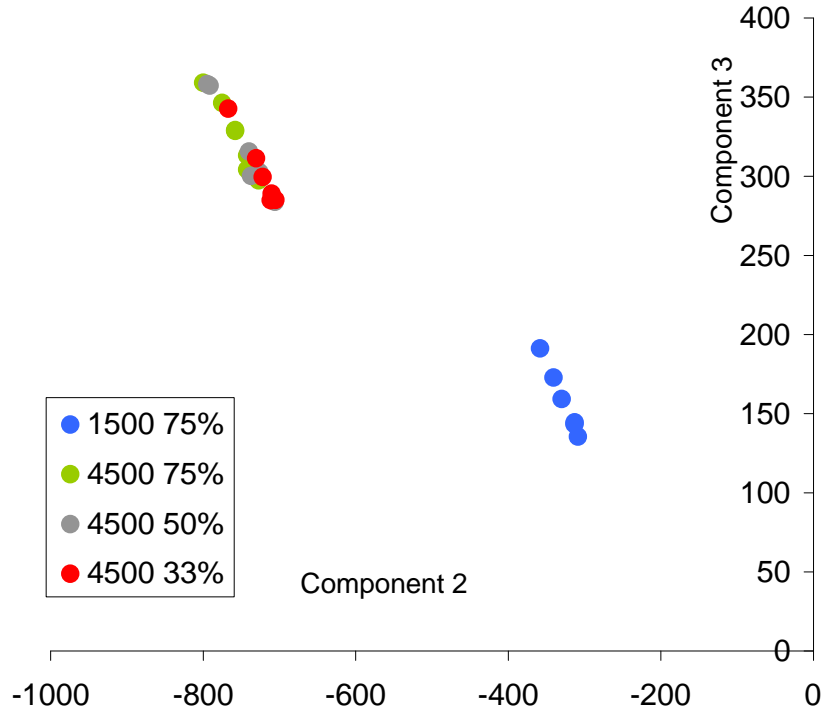


Figure 6.18: Score Plot of Principal Components 2 and 3, by Engine Condition

components 2 and 3, Figure 6.17 and Figure 6.18, also show that overall behaviour is most clearly defined by engine speed, rather than oil properties.

The most relevant relationships observed show that higher engine speed and operating temperature produces an increase in flow rate of mist from the piston assembly. As this includes temporal and cyclical flow rates, this indicates that an increase in speed and temperature increases the formation of mist droplets. The change in viscometric properties caused by an increase in viscosity modifier concentration produces variation in the relative proportion of the various mist components, particularly between the major misting region and throw-off. The lack of correlation between throw-off and misting, despite their common variation with viscosity, indicates that they are distinct mechanisms, as understood by their droplet size ranges. This confirms that the droplets formed in the piston assembly have diameters  $<250\mu\text{m}$ , primarily with diameters 30-250 $\mu\text{m}$ . The most significant observation is that, within the range of parameters tested here, that misting is most significantly affected by engine speed and temperature, rather than lubricant properties.

## 6.7 Summary

- A system to measure the nature of mist produced in the crankcase was designed, built and used. Changes in engine speed, load, oil viscosity and viscosity modifier content were considered.
- Spray from resonating ducts limited the range of speeds studied. Oil splash restricted the accuracy of oil flow rate data to relative comparison only.
- Droplet size distributions show, as in the simulation studies, three characteristic droplet sizes: A major misting region, and minor misting region and a region of large droplets attributed to throw-off from components.
- The characteristic droplet sizes in each region, and hence the bounds of each region, exhibited larger droplet diameters than in the simulation work: This is attributed to the higher viscosity base oils used in these tests.
- The droplet size distributions show that an increase in oil viscosity and viscosity modifier content produces an increase in droplet size, particularly in the misting regions. A reduction in mist flow rate can be inferred from the reduced proportion of mist droplets in the flow.
- Statistical analysis by principal component analysis links increasing engine speed with an increase in mist flow rate. Links are established between increasing viscosity modifier content, viscosity, and increasing droplet size in the throw-off. Similar links are established between viscosity modifier content, viscosity, and droplet size in the mist. However, this latter trend is not seen to be statistically significant.
- The nature of droplets in the misting region and the throw-off, though they share common input variables in viscosity and viscosity modifier content, do not correlate well with each other, confirming that they are distinct mechanisms.
- The droplet sizes in the minor misting region are more strongly linked to engine speed and temperature. This links their formation to either droplet breakup or vapour condensation, or both.





## **Chapter 7: Measurement of Lubricant Degradation in a Fired Engine with Varying Viscosity Modifier Structure**

### **7.1 Introduction**

The tendency of a lubricant to mist is thought to affect its degradation rate in the engine. This is because it influences the flow of lubricant through the piston assembly, thus the residence time, and the variation in droplet size and concentration will increase the surface to volume ratio, thus the reaction rates of chemical and physical processes. Therefore, lubricants containing different polymeric additives and varying misting tendency were used in an engine for an extended run and the degradation and flow of lubricant and its additives was analysed.

### **7.2 Method**

The Ricardo Hydra test engine discussed in Chapter 6 was used in this study. The crankcase gas extraction system and the particle sizer were removed and lubricant sample collection systems were installed. These samples were analysed to characterise the degradation of the lubricant and variations in its composition through the engine.

#### **7.2.1 Apparatus**

The specification of the Ricardo Hydra engine is discussed in Section 6.2.1. Three sampling systems were installed. The first samples lubricant from the top ring zone, TRZ, shown in Figure 7.1. This system is a development of work by Saville (1988), Gamble (2002) and Lee (2006). In these systems, gas and lubricant from the piston assembly is driven by gas pressure down a tube attached to the piston and out of the engine where it is collected.

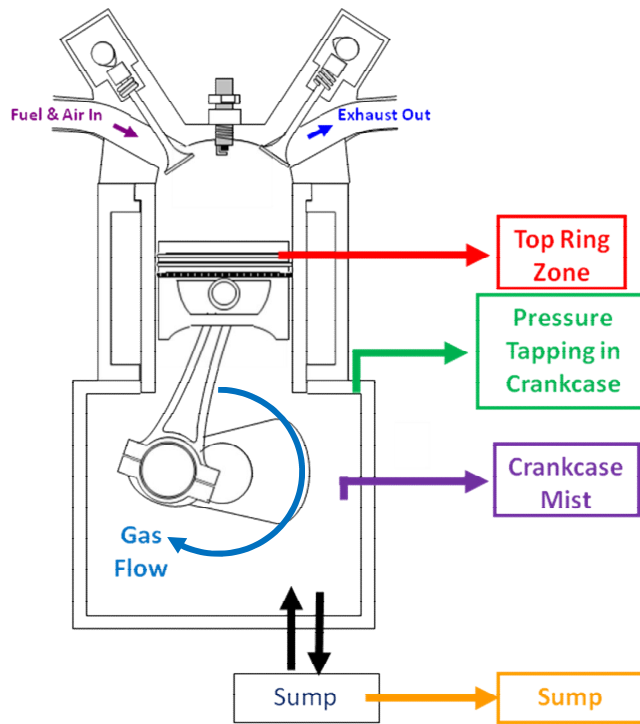


Figure 7.1: Sample Locations in the Ricardo Hydra Engine

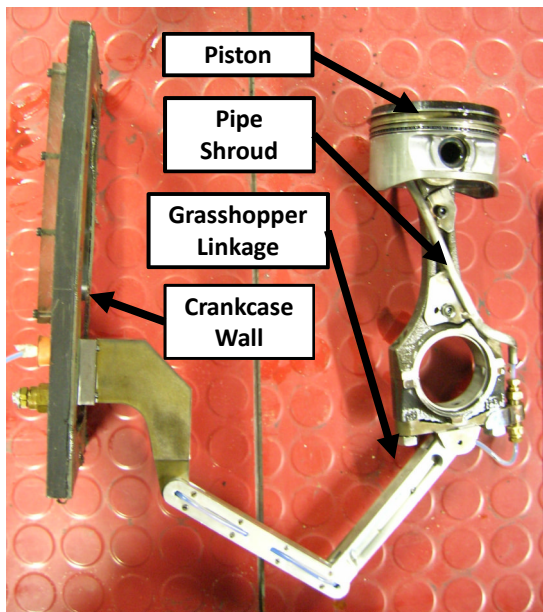


Figure 7.2: Top Ring Zone Sampling System

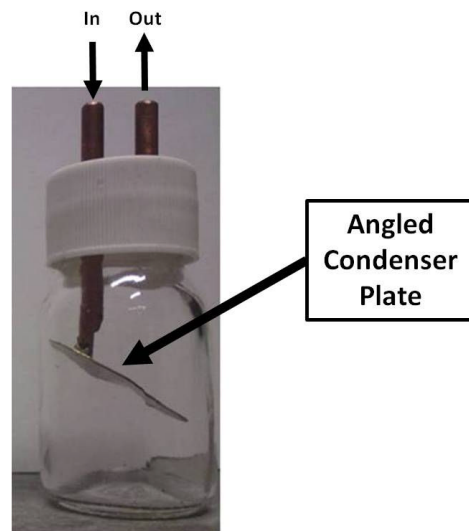


Figure 7.3: Sample Bottle, after Notay (2009)

Lubricant is collected from the top ring groove, the region of highest lubricant degradation, through a 0.5mm diameter hole in the anti-thrust side. The pressure difference drives a gas flow which entrains lubricant as, it is thought, a mist and as a sheared film. This flows down a PTFE pipe from the back of this hole, in a shroud down the con-rod, through a grasshopper linkage between the bearing cap and the crankcase wall, Figure 7.2, where it exits the engine and enters a sample vial with a condenser plate Figure 7.3

The current system is an incremental development of that described by Gamble (2002) and Lee (2006). The tube carrying linkage enables higher speeds to be run. Previous systems where the tube was left loose were limited to 2000rpm. The condenser plate in the sample bottle was designed to minimise oil loss and, thus, maximise sample size.

In such systems, it is crucial that samples are representative of the normal running conditions of the engine. Therefore, it is necessary to ensure that the lubricant sampling rate is not so high as to cause significantly diminished lubrication performance. According to Stark (2005), the lubricant volume in the piston assembly above the oil control ring in this engine is approximately 6ml and has a residence time of approximately 60 seconds, thus has a flow rate of approximately 6ml/minute and 360ml/hr at 1500rpm, full load and 50% throttle. Notay (2009), whilst developing this system, collected samples at 67g/hr, or approximately 54ml/hr. Whilst it should be noted that this data was collected during warm-up where significant amounts of fuel and water will increase the sample size, sometimes by a factor of 2, and that some evaporation will occur, reducing the sample size, it can be seen that the TRZ sampling rate is in the order of 15% of the total oil flow rate through this region. This is not seen to have a significant effect of lubrication, from observed wear patterns and running temperatures (Gamble et al., 2002; Lee, 2006).

The second sampling system is designed to sample the mist from the crankcase. In this, a 20mm diameter pipe was attached to crankcase and routed to the room extraction, Figure 7.4. This flow path contained a Norgren F74-4GD-QPO 0.1 $\mu$ m

coalescing filter to capture as many droplets from the flow as possible. This filter is passive and contains no cooling mechanism; therefore it is not thought that it induces any condensation of fuel or water vapour in the gas flow. Following the discussions in Section 6.5, it was important to sample the mist-sized droplets rather than any larger droplets including those from the con-rod throw-off. This is important as it is the mist-sized droplets only that are hypothesised to be sourced in the piston assembly. Therefore a 90° fitting was attached to the tube inlet, Figure 7.5. Thus, the opening faced downwards and, more importantly, away from the natural direction of gas flow in the crankcase at this point. Thus, only droplets that are stably entrained in the gas flow will be allowed to flow up the tube, as large diameter droplets i.e. those from the throw-off, will not be able to follow this path due to their large inertia preventing their entrainment in the gas flow. Initial studies found that the sample flow rate was excessive and would have led to significant reduction in sump size during a test. Therefore, a ball valve was installed upstream of the filter. The valve was kept closed to cut off the flow but opened for 30 minutes before each sample time, allowing samples of 8-10ml to be collected.

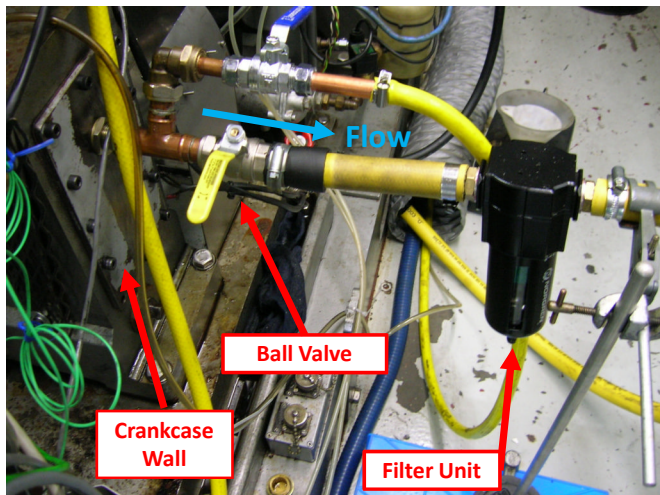


Figure 7.4: Crankcase Mist Sampling System

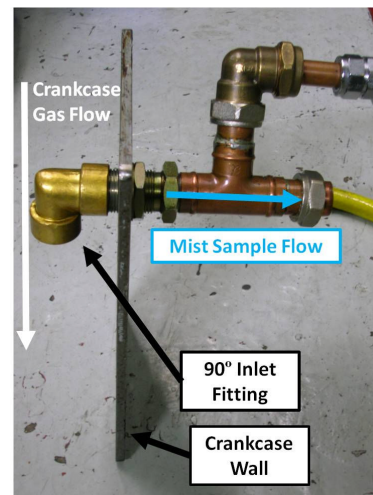
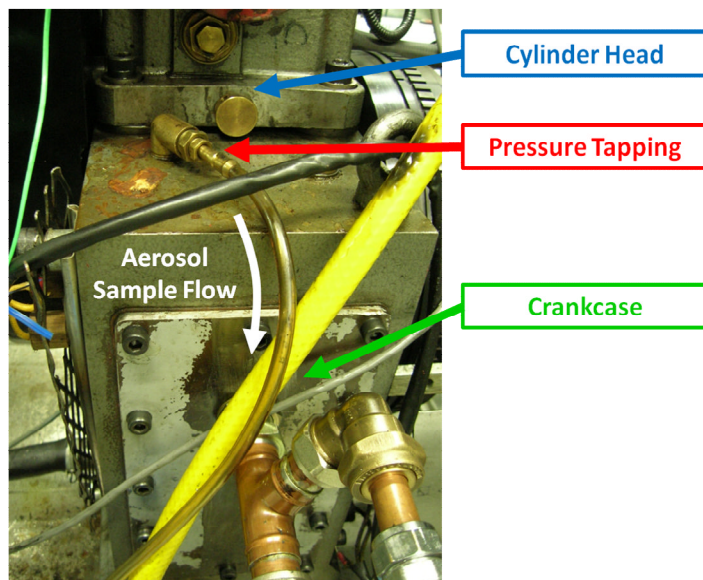


Figure 7.5: Mist Sampling System Inlet

The third sampling system was a chance observation of oil accumulating in the outlet pipe from a pressure tapping on the top of the crankcase, see Section 6.2.1, Figure 7.6. This is termed the aerosol sample. This is a 6mm diameter hole facing upwards in the crankcase, approximately normal to the gas flow in the crankcase at this position. Immediately after leaving the crankcase, the pipe makes a 90° turn. The sample tube is routed into a sample bottle, Figure 7.7, similar to the previous TRZ system without a condenser plate. The outlet tube from the sample bottle is, similarly, connected to the room extraction. This flow is driven by the pressure difference between the crankcase and the room. This pressure difference is in the order of 0.01MPa rather than the order of 0.5MPa for the TRZ system. Thus, the flow rate is much lower. Therefore, considering the low flow rate, the small diameter and tortuous path, it is hypothesised that only aerosol droplets, whose entrainment is dictated by Brownian motion (Seinfeld et al., 2006; Ghiaasiaan, 2008), are able to follow this path. Thus, this system is a suitable way to sample aerosol-sized droplets. As the sample flow rates were extremely low, in the order of 0.15-0.20ml/hr, a sample was only taken every 20 hours of engine running.



**Figure 7.6: Aerosol Sampling System**



**Figure 7.7: Aerosol Sample Bottle**

As the lubricant sump on this engine is external, sampling from the sump is easy. Therefore, a 7ml sample from the sump was taken with a syringe every time a sample was taken from any other location in the engine, except during warm-up, where changes in sump oil composition are not likely to be affected by the condensation effects seen in this period.

### 7.2.2 Procedure

The same procedure was used for all tests in this study. Engine conditions were kept uniform, as oil composition was the main variable in these tests. Tests were run as shown in Table 7.1.

Parameter	Condition
Speed	2500rpm
Load	75%
Throttle	50%
Test Duration	20 Hours
Fuel	Reference ULG95 Gasoline
Ignition Timing	12° Before TDC
Sump Volume	1.5 Litres

Table 7.1: Engine Test Conditions

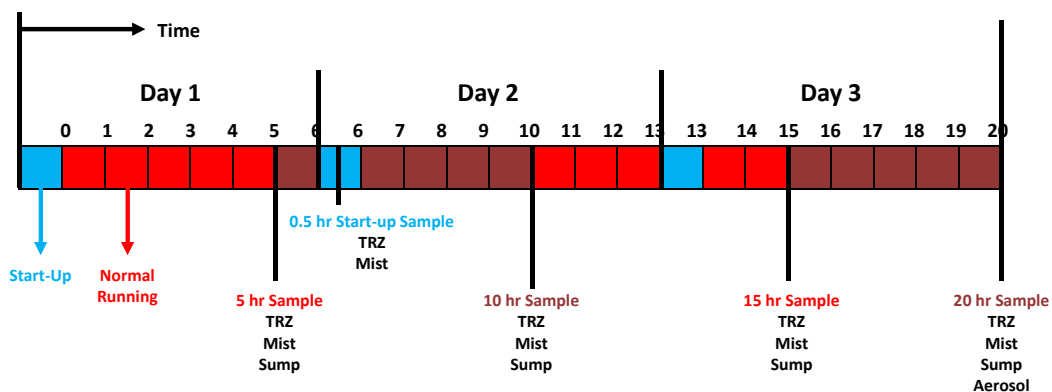


Figure 7.8: Engine Test Procedure and Sample Intervals

The engine was run for 20 hours with lubricant samples from the engine taken every 5 hours of normal running. In order to ensure that the engine had reached thermal equilibrium, the engine was run for 1 hour each time it was started before normal running was considered to have begun. TRZ and mist samples were taken half an hour after start-up, i.e. during warm-up, to give some indication of behaviour under these conditions. During start-up, the TRZ, mist and aerosol sample bottles were changed to avoid sample contamination. This test procedure is shown schematically in Figure 7.8. Values for engine component, coolant and exhaust temperatures were recorded at each sample point and at the beginning of each period of normal running. These were recorded from the engine control system. Emissions data was recorded from the exhaust system by a Horiba Mexa-544 JE which measured CO, hydrocarbon, CO<sub>2</sub>, O<sub>2</sub>, and recorded predicted air:fuel ratio and lambda ratio i.e. the air fuel ratio relative to perfect combustion conditions. These values were recorded, again, every time a sample was taken and when normal running began.

Sample bottles were not kept on the engine overnight, in order to prevent contamination and chemical reaction. Instead, all samples from the engine were kept in a refrigerator to prevent further oxidation (Notay, 2009). The following procedures were followed when taking a sample from each location:

- TRZ – As the sample was collected in a standard sample bottle, the sample bottle was collected from the engine, sealed and placed in the fridge. A fresh bottle was then attached to the engine to collect the subsequent sample.
- Mist – The mist sample was collected in the filter module. Thus, when a sample was taken, the module was removed and replaced with a fresh and clean equivalent. The original was then emptied into a sample bottle and thoroughly rinsed and wiped and then used as the next replacement.
- Sump – The sample was collected in a syringe and placed in a sample bottle. A fresh syringe was used for each sample to prevent contamination.
- Aerosol – As the sample was only collected once, the same bottle was used throughout.

To avoid contamination between tests, the sump was flushed with fresh lubricant using the same procedure as described in Section 6.2.3. The sump was changed for a fresh 1.5 litre of the lubricant for the next test and the engine motored at 1500rpm and 50% throttle for half an hour. The sump was changed again and motored for a further half an hour under the same conditions. The sump was then changed again, the oil filter and the filter cartridge on the mist sampling system changed. Separate sample bottles were used for each sampling system during this period to prevent both leakage and contamination.

### **7.3 Chemical and Physical Analysis**

The samples collected were analysed in several ways, all with reference to their fresh equivalents. Viscosity and viscoelastic measurements were taken of the degraded sump oil after 20 hours. These were measured on the Malvern Kinexus rheometer, as described in Section 5.5. Viscosity was measured using a parallel plate at 100 $\mu$ m gap, at 20°C and at a constant shear stress of 100 Pa, i.e. in the Newtonian region before shear thinning occurs, see Section 3.7. Viscoelastic measurements were taken

A viscoelastic analysis was performed, similarly to Section 5.5. In this, the linear viscoelastic regions of both polymer blends were measured in an amplitude sweep at a constant frequency of 43 Hz and a temperature of 20°C. In light of this, analysis of the viscoelastic crossover was undertaken. In this, the variation in viscoelastic response with oscillation frequency is measured, at a constant maximum shear rate of 5% and a temperature of 20°C. Key parameters, such as frequency, stress, strain, complex modulus and complex viscosity are recorded for the crossover point.

#### **7.3.1 Chemical Degradation**

The thermal and chemical degradation of the lubricant samples was measured using Fourier Transform Infrared Spectrometry, FTIR. This apparatus, as described by Van der Maas (1969) and Griffiths (1986), measures the spectrum emitted when the sample is illuminated with laser light. When illuminated with light, energy is



transferred into the material and the molecules are excited. Different chemical bonds resonate at different frequencies, thus emitting light with a different wavelength. Convention dictates that wavelength is reported as different wavenumber, the reciprocal of wavelength:

$$\text{wavenumber (cm}^{-1}\text{)} = \frac{1}{\text{wavelength (cm)}} \quad [7.1]$$

Thus, a detector measures the light emitted at a range of wavelengths, reporting measurements as percentage absorbance where:

$$\% \text{ Absorbance} = 100 \times \frac{I_{in} - I_{emitted}}{I_{in}} \quad [7.2]$$

Where  $I_{in}$  is the intensity of light when no sample is present, this is often measured in a parallel path simultaneously to the sample measurements, and  $I_{emitted}$  is the intensity of light that is received from the sample.

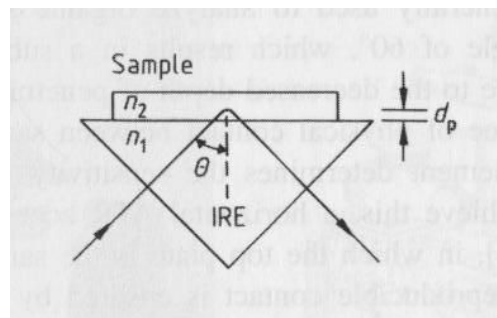


**Figure 7.9: Schematic of ATR Element, from Gunzler (2002),  $n_1$  and  $n_2$  are the refractive indices,  $n_1 > n_2$ ,  $d_p$  is the penetration depth,  $\theta$  is the angle of incidence**

In this study, the attenuated total reflectance, ATR, method was used (Gunzler, 2002). The machine is a Perkin Elmer Spectrum 2000 with a Specac Golden Gate Diamond ATR. In this, the sample is placed on a crystal and is illuminated by laser light from

below. Light that is absorbed and re-emitted from the surface of the sample is measured from below, see Figure 7.9.

The laser light is of a single wavelength and is received back from the sample at a range of wavelengths simultaneously. Thus, the received signal must be separated. This is done using an interferometer. In this, the light is split into two identical beams and sent through two paths of slightly different lengths. When the two paths are recombined, the different wavelengths present in the beams cause interference patterns to be produced. Slight changes in the difference between the path lengths are used to produce different interference patterns. These various patterns are deciphered using a Fourier Transform, which gives the intensity of the light of a particular wavenumber.

Where a particular chemical bond resonates with the exciting laser light, energy is absorbed, reducing the intensity of light emitted at the wavenumber that corresponds to this molecule. Thus, an increase in absorbance at a particular wavenumber can be correlated to the presence of a particular chemical species. For oil degradation, the carbonyl bond, C=O, which absorbs at around 1690-1750  $\text{cm}^{-1}$ , is seen as a key indicator of oxidative degradation. The oxidation of hydrocarbons by the following schematic reaction produces carbonyl species, Figure 7.10:

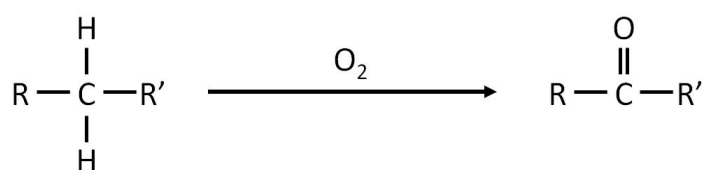


**Figure 7.10: Schematic of Hydrocarbon Oxidation Leading to Carbonyl Formation, after Emanuel (1997) and Gamble (2002)**

To indicate the degree of oxidation, the area of the carbonyl absorbance peak on the FTIR peak was integrated i.e. the area bounded by the trace curve and a straight line that connects the curve points at 1690 and 1750  $\text{cm}^{-1}$ , Figure 7.11. The latter boundary

represents a base line that prevents the distortion of peak area measurements by the vertical shifting of a curve because a particular sample is optically darker than another, absorbing more light at all wavenumbers.

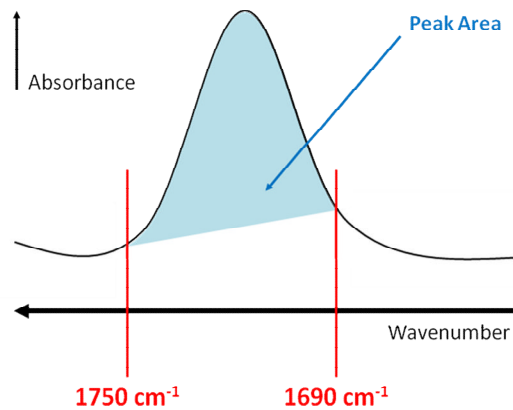


**Figure 7.11: FTIR Peak Area Schematic**

The peak at  $1600\text{ cm}^{-1}$ , integrated between  $1550$  and  $1650\text{ cm}^{-1}$ , is also seen as an indicator of oil degradation. This can represent the reaction of the oil with the nitrogen in the combustion gas i.e. nitration, producing a C=N bond (Van-Der-Maas, 1969). It may also indicate the oxidation or thermal degradation of the oil producing unsaturation of the hydrocarbon chain, a C=C bond (Van-Der-Maas, 1969). This latter bond is formed when there are insufficient hydrogen atoms, requiring carbon atoms to bond to each other twice and to one hydrogen atom for stability, rather than to two hydrogen atoms, which is the original state of a quality hydrocarbon lubricant. Both mechanisms occur, and the peak will certainly contain contributions from each mechanism.

In this study, the FTIR traces were measured by technicians at BP Technology Centre, Pangbourne and analysis of the traces was done in the labs at the University of Leeds.

### 7.3.2 Fuel Dilution

The dilution of fuel into the lubricant oil cannot be detected using FTIR because the chemical species in the fuel and the lubricant oil are identical and, thus, cannot be

differentiated on a trace. Therefore, the presence of fuel is typically measured by differentiating hydrocarbon species by length and molecular weight. In this investigation, this was done using gas chromatography, GC. As described by Firfield (2000), this technique involves the vaporising of a sample into a carrier gas, in this case Helium, which then is allowed to flow through a long column packed with material. Inversely to GPC, the lighter fractions leave the column first and the heavier fractions later. This is because a GC column is designed that the mobility of smaller species increases their flow through the column rather than enhancing their diffusion into the column material, as in GPC. The machine used for this analysis was an Agilent 6890 GC with a HP-5M5 column.

The GC trace shows the measure concentration of the sample emerging at a certain time. This time axis can be, for chemically similar materials, correlated with the number of carbons in the molecule chain. The fuel fractions of a typical lubricant sample are taken to be species with between 6 and 16 carbons (Lee et al., 2006). Thus, the integrated area of the GC trace in this range will give the concentration of fuel fractions in the sample. The material was measured using a flame ionisation detector, FID. This apparatus mixes the column outlet gases with hydrogen and oxygen where it is burnt in a small jet. The jet body is wired as a cathode and an anode wire is placed above the flame. A potential difference of 200V is applied across the flame and the electrical conductivity measured. It is assumed that the electrical conductivity of the gas is directly proportional to the concentration of charged particles in it. Thus, the electrical conductivity of the flame will increase when more hydrocarbons leave the column.

GC analysis was performed by technicians at BP Technology Centre, Pangbourne.

### **7.3.3 Polymer Degradation**

The degradation of the viscosity modifiers in the lubricants was investigated using GPC, as described in Section 5.3. The effect of polymer degradation is similar whether the degradation is thermal or shear-induced. The polymer chain will break

into sections, normally two, with the break close to the centre of the molecule, as this is where the stress on the bonds is greatest. Thus, the degradation of polymers will show on a GPC trace as a tail forming on the original polymer peak, with a corresponding reduction in peak height, and secondary species appearing where chain scission reduces chain length. These changes are most clearly seen in light scattering, LS, traces, though such traces cannot be used to quantify the concentrations of species. Refractive index, RI, measurements can indicate whether any change in polymer concentration occurs, a possible indicator of evaporation or misting-induced composition changes. However, as polymer concentrations are low, changes are often hard to resolve. GPC traces can also show the effects of other processes:

- Fuel dilution will show a peak below the base oil peak
- Sludge formation will produce a peak above the base oil peak and below the polymer peak
- The agglomeration of polymer molecules will produce a peak above the original polymer peak
- The polymer tails of detergent and dispersant molecules can be seen in the region of  $M_n \approx 3000$

## 7.4 Oil Matrix

It was decided that lubricants with different misting tendencies would be tested in this study. Therefore, the lubricants tested would be a base oil, and two lubricants of the same base oil containing viscosity modifiers exhibiting different misting tendencies. A 6cSt Group III base oil was chosen as the reference base oil, Table 7.2. To this was added 1% neutral calcium sulphonate detergent and 1% calcium succinimide dispersant to reduce deposits and potential damage to the engine components. The base oil test was repeated to indicate the statistical accuracy of the test procedure. Arising from the findings of Chapter 5, polymer 1 and polymer 5 were chosen for viscosity modifiers. These are high molecular weight linear olefin copolymer and high molecular weight isoprene-co-styrene fixed star polymer, respectively. The blends containing polymer were blended to a nominal 10cSt, which meant a polymer concentration of 1% by weight in both blends. The viscosity modifier was top treated

onto the base oil blend i.e. added to an existing blend; thus meaning that the detergent and dispersant concentrations will be slightly less than 1% in these blends. The dynamic viscosity of these blends was measured using the Malvern Rheometer, as described in Section 4.3.1.

Blend	Base Oil	Additives	Polymer	% Wt	Kinematic Viscosity @100°C cSt	Dynamic Viscosity @20°C mPa.s
Base Oil	6cSt Group III	1% Detergent 1% Dispersant	-	-	6	56.9
Polymer 1			Olefin Copolymer Linear, $M_n = 51945$	1%	10	152.6
Polymer 5			Isoprene-co-Styrene Star, $M_n = 146499$	1%	10	157.5

Table 7.2: Lubricant Blends for Engine Tests

Using the equations described in Section 3.7.2, the entanglement properties of the blends were calculated. These are shown in Table 7.3. As before, the entanglement parameters for the star polymer are calculated for single arms rather than the whole molecule. It can be seen that the linear polymer blend has a higher degree of entanglement. Whilst both blends are considered dilute, an intermolecular interaction that exists will be much more prevalent in the linear polymer blend.

Blend	Entanglement Parameters					
	$M_n$	Chain Length	$M_e$	$M_e$ Blend	$E$	$E_{blend}$
Polymer 1	51945	3028	1660	606852	31.3	0.086
Polymer 5	146499	703.2 (1 arm)	8572	820027	1.71	0.018

Table 7.3: Entanglement Parameters of Polymer Blends

Using the relationships described in Section 5.5 and the Mark-Houwink plots for these polymers in Section 5.3, the molecular coiling parameters were derived and calculated. As expected, the star polymer, 5, has a larger hydrodynamic volume and

self concentration, so is a larger and denser molecular structure. However, as discussed previously, the fixed star structure prevents significant entanglement-induced viscoelasticity.

Blend	Molecular Parameters			
	$R_G$ nm	$HDV$ $m^3 \times 10^{-24}$	$C_{molecule}$ $\times 10^{-5}$	$l_p$ pm
Polymer 1	8.2	2.3	4.8	1.65
Polymer 5	11.2	5.9	15.2	7.13

Table 7.4: Molecular Parameters of Polymer Blends

## 7.5 Results

The results of the analyses on the engine samples are presented in this section. Some general observations were made:

- The engine control system had a malfunction in the speed sensor circuit whereby the engine would occasionally trip the emergency stop. Thus, constant monitoring was required. A quick resetting of this sensor would enable the engine to return to the test speed in 3-4 seconds. The component temperatures did not vary significantly in this period. However, the transient loads through the engine will have affected the gas flows through the piston assembly during this period. This malfunction was rectified after the base oil tests, thus was not experienced during the tests of the polymer blends.
- The TRZ sampling system was run for approximately 120 hours without issue from the start of initial commissioning up to the end of the base oil tests. During the first polymer blend test, the sample tube became blocked after approximately 15 hours by deposits forming where the pipe joined the piston behind the top ring groove. This test was not considered completed and its results are not shown here. The engine was stripped and the deposits removed from the sample pipe. However the pipe would block in a similar manner after

approximately 20 hours running with a polymer blend. Thus, though the rest of the tests proceeded without issue, the engine was stripped, deposits removed and the engine rebuilt. The implications of this are twofold: Firstly, the minor changes in operating parameters associated with rebuilding an engine had to be considered but the measured engine parameters indicated that this effect was not significant. Secondly, it appears that the presence of polymer in the lubricant blend may cause an increase in deposit formation in the piston assembly. Further testing would be needed to substantiate this.

### 7.5.1 FTIR Analysis

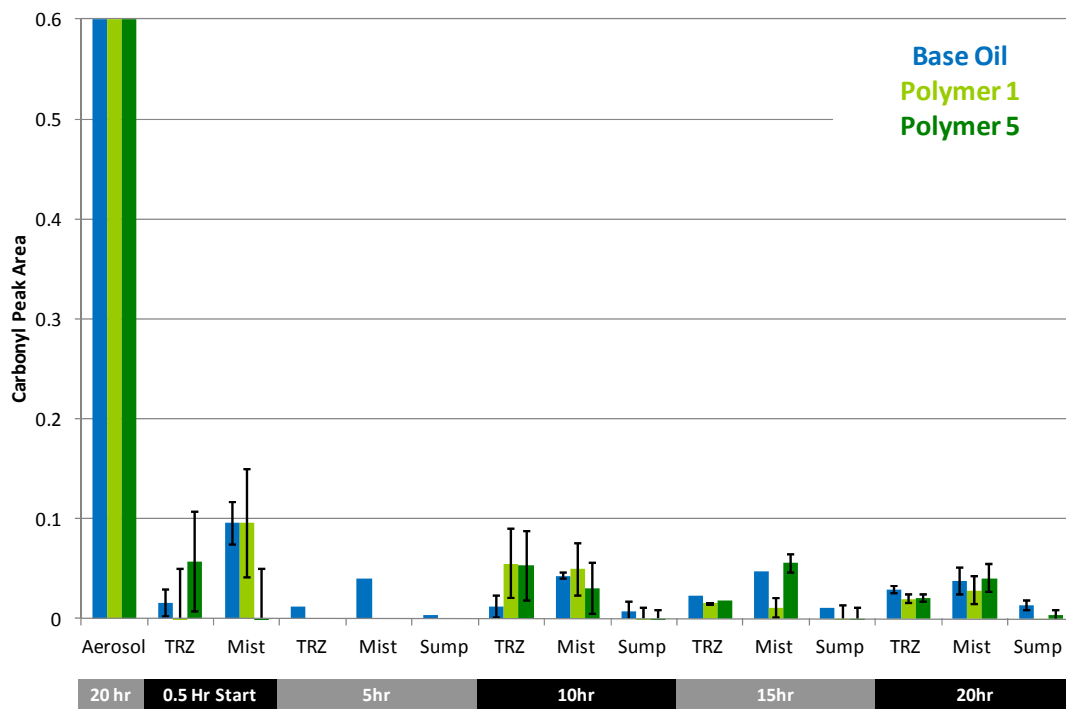
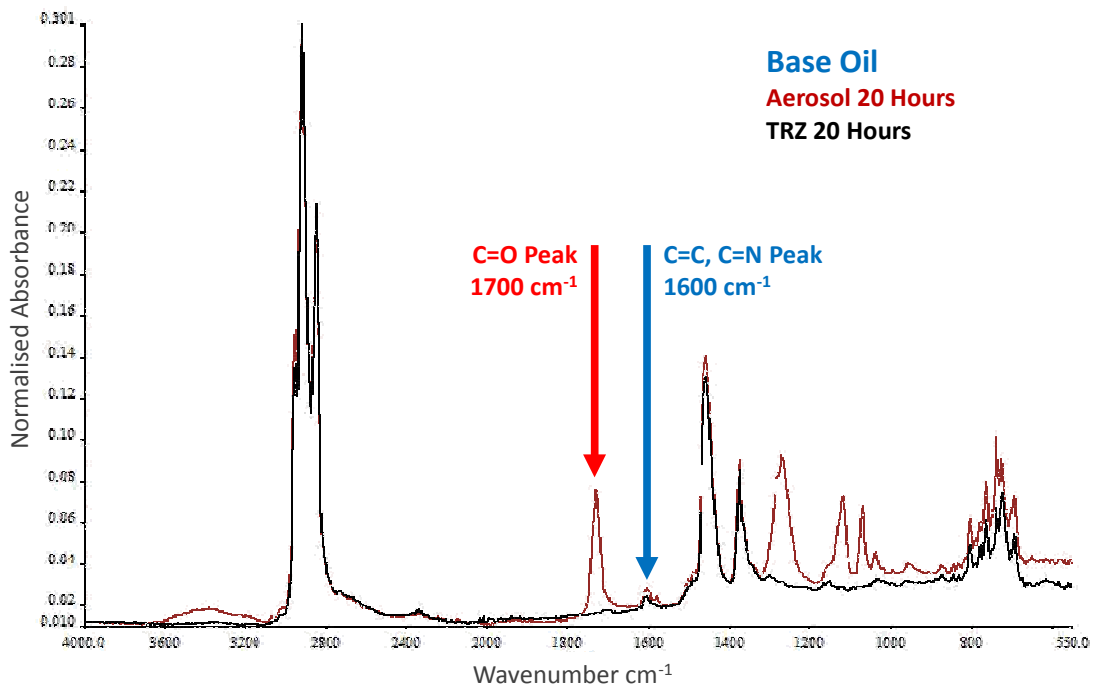


Figure 7.12: FTIR Carbonyl Peak Areas for Engine Test Samples

Figure 7.12 shows the integrated carbonyl peak areas to indicate oxidative degradation of the lubricant in all the tests and in all positions in the engine. Analyses for polymer tests after 5 hours were not performed to reduce processing time. It is



clear that only the aerosol sample is significantly degraded. Figure 7.13, showing the FTIR traces for the first base oil test after 20 hours, confirms this, as the carbonyl peak for the TRZ oil is insignificant when compared to the aerosol sample. This appears to stand against established theory and measurement (Yasutomi et al., 1981; Lee et al., 2006) that indicate that the TRZ oil should be highly degraded based on carbonyl concentration. The reason why this is not more degraded than the sump oil has not been fully explained. It is thought that this may be either a function of the upgraded TRZ sampling system, particularly the condenser plate in the sample bottle, which captures more sample from the gas stream, or that the FTIR analysis used the ATR method when previous experiments used a transmittance cell.



**Figure 7.13: FTIR Trace for Base Oils after 20 Hours, where the Absorbance Axis is scaled to make the Largest Peaks Equal in Magnitude**

It can be seen in Figure 7.13 that the nitration and unsaturation peak at  $1600\text{cm}^{-1}$  is more pronounced in these samples, though still small. Therefore, the characterisation

of degradation from these mechanisms is shown in Figure 7.14. It can be seen that this data is clearer and more statistically reliable.

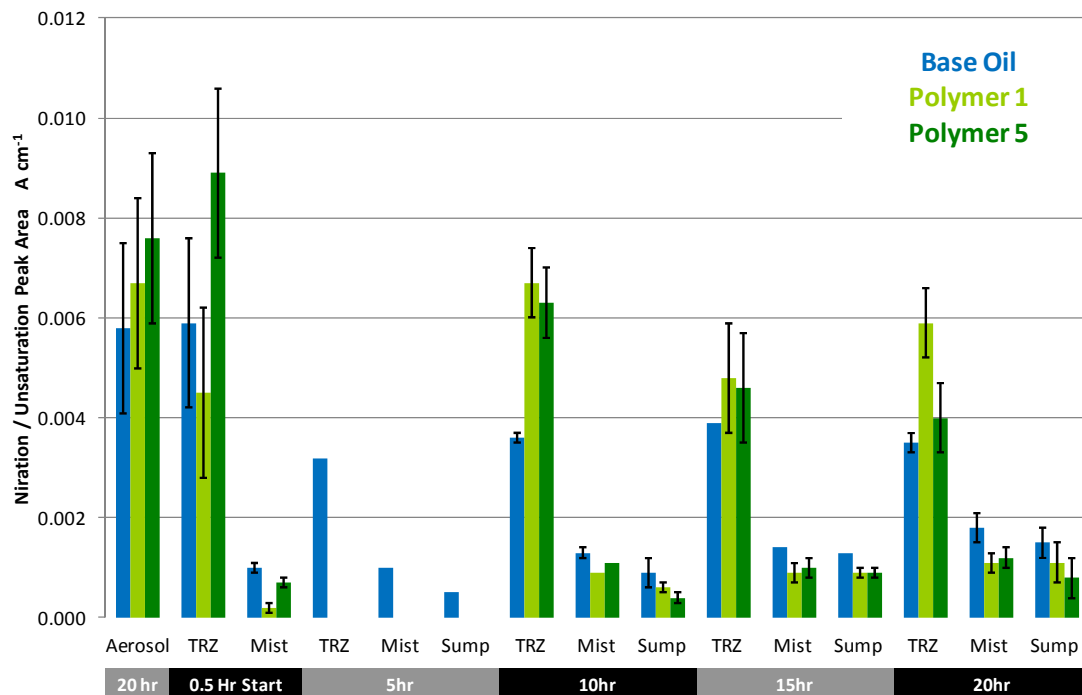


**Figure 7.14: FTIR Nitration and Unsaturation Peak Areas for Engine Test Samples**

The TRZ lubricant is significantly more degraded than that in the sump on this basis. This is anticipated by the higher temperatures, chemical, thermal and mechanical stresses on the lubricant in this region. The level of degradation in the TRZ does not change through the test. This is also anticipated, as the TRZ is the greatest region of lubricant degradation. The degradation levels in the sump increase through the test. This fits with the assumption that the small volume of highly degraded lubricant returning to the sump from the piston assembly are initially well diluted by the sump volume, but cause sump degradation levels to rise over time as the quantity of oil in the sump that has passed through the piston assembly increases.

TRZ degradation levels are higher for the polymer blends than for the base oils. It is hypothesised that this is caused by their increased viscosity producing a higher

residence time in the piston assembly, causing it to be more highly degraded. As the viscosity of the sump oil decreases over time, the difference between polymer blends and base oil decreases, implying, possibly, a reduced residence time.

The mist samples indicate levels of degradation slightly higher than the sump, but significantly lower than the TRZ. It is hypothesised, therefore, that the mist oil has passed through the piston assembly, but had a lower residence time than the TRZ oil, or, perhaps, did not reach the upper piston assembly where temperatures are higher. The apparent increase in degradation level in mist oil during the test indicates that the mist oil is not so degraded that the variation in sump degradation with time is insignificant. There does not appear to be a significant variation in mist degradation between oil blends. This, again, reflects the same lack of resolvable difference in sump degradation levels.

Aerosol samples are comparable in degradation to TRZ samples i.e. significantly more degraded than mist samples. This appears to confirm the theory that fine droplets will degrade more rapidly than larger droplets and bulk oil. This increased degradation level may also be a result of a longer residence time in the engine due to the slow deposition rate of diffusion-controlled aerosols. It should be noted that, whilst degradation is significantly higher for small droplets, their tiny volume relative to the  $\approx 6\text{ml}$  typically in the piston assembly, much more the  $1500\text{ml}$  in the sump, means that the increased degradation has an insignificant effect on the overall system.

There is no significant difference in aerosol degradation between the different oil blends tested here. The simulation work in Chapter 5 indicates that the presence of large polymers suppresses the formation of aerosol-sized droplets by the mechanical mechanisms observed therein. Thus, that there is aerosol sized droplets to sample in the engine implies that there are other mechanisms at work. These aerosol droplets are likely to be formed from either the condensation of oil vapour, or from the breakup of mist-sized droplets, or, more likely, both mechanisms concurrently.

## 7.5.2 Fuel Dilution

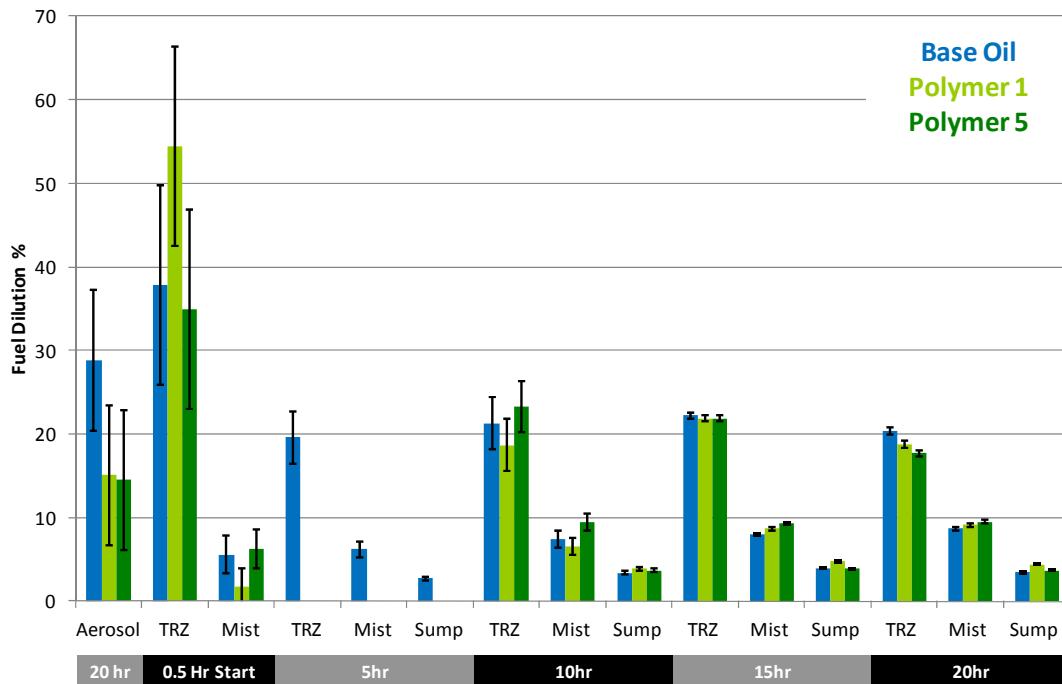


**Figure 7.15: GC Fuel Dilution Concentrations for Engine Test Samples**

Figure 7.15 shows the measured fuel dilution concentration in the samples taken during the tests. As expected, the TRZ oil contains approximately 20-22% fuel. This is due to the close proximity of this lubricant to the combustion chamber, where fuel impinging on the liner is retained in the oil film on the liner surface. This oil can flow round the piston assembly and, ultimately, into the sump. Hence, the sump contains approximately 3-4% fuel. The mist sample contains approximately 6-10% fuel, intermediate between the sump and TRZ. This seems to confirm that the mist is sourced in the piston assembly, as sump oil could not accumulate fuel concentrations of this magnitude. The reduced quantity of fuel in the mist, when compared to the TRZ, can be attributed to continuous supply of fuel to the TRZ whereas no fresh fuel can enter the mist sample when it has left the piston assembly other than by more mist sample accumulating. Thus, when evaporation of the fuel from the oil equilibrates

with the supply of fuel to the oil, the fuel dilution in the TRZ will be much higher. It is thought that there may also be a higher evaporation rate of fuel from mist droplets when compared to oil in the TRZ, where the surface area of the oil volume is relatively low. The levels of fuel dilution in each region of the engine do not change significantly with time.

As expected, the fuel dilutions in the TRZ samples after start-up are very high, up to 54%. This is a result of the lower engine temperatures reducing the evaporation rate from the oil, and the over-fuelling required to run a cold engine increasing the supply of fuel to the TRZ oil. The mist sample from the start-up period does not contain a significantly different concentration of fuel to mist samples at thermal equilibrium. This reflects the smaller change in temperatures undergone during warming up in this region: Both the TRZ and the crankcase gas are at ambient conditions,  $\sim 15^{\circ}\text{C}$ , when the engine is started, but the TRZ exceeds  $200^{\circ}\text{C}$  when the engine is fired and the crankcase gas finds equilibrium at  $\approx 50\text{-}60^{\circ}\text{C}$ . Hence, there will be a smaller difference in fuel evaporation rate from the oil in the crankcase during start-up.

The aerosol sample shows widely varying levels of fuel dilution, from  $\approx 15\text{-}37\%$ . The fuel dilution in the piston assembly i.e. the source of the aerosol droplets, is intermediate in this range. Thus, under some conditions, more fuel accumulates in the sample, and, under others, fuel is lost from the sample. This could be caused by a variation in droplet size and surface area affecting evaporation rates. The increase in fuel dilution could be a result of colder ambient temperatures causing a condensation of fuel vapour from the gas flow. This latter effect would become much more significant than for other samples as: firstly, the sample volume is lower and, secondly, the 20 hour sample period would allow a greater volume of blow-by gas to interact with the sample.

As might be expected, there is no significant change in fuel dilution levels between the lubricant blends, other than for aerosol sized droplets. However, the latter is more likely to be an environmental effect rather than compositional.

### 7.5.3 Polymer Degradation

Figures 7.16 to 7.24 show the GPC traces for the various samples. Figure 7.16 shows the fresh polymer blends. The different viscosity modifiers show distinct behaviour. The star polymer has a much sharper peak, indicating a narrow distribution of molecular weights. The linear polymer has a broader peak, indicating a wider molecular weight distribution than the star. The higher retention time indicates that the linear polymer has a lower molecular weight. As this is a light scattering trace, the magnitude of the peaks cannot be used quantitatively. The base oil peak for both lubricants is seen at 34-35 minutes.

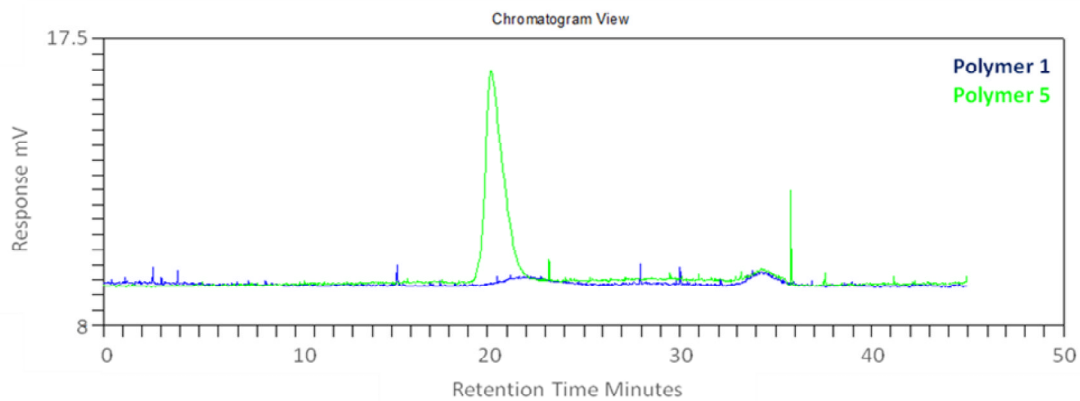


Figure 7.16: GPC Trace for Fresh Polymer Blends

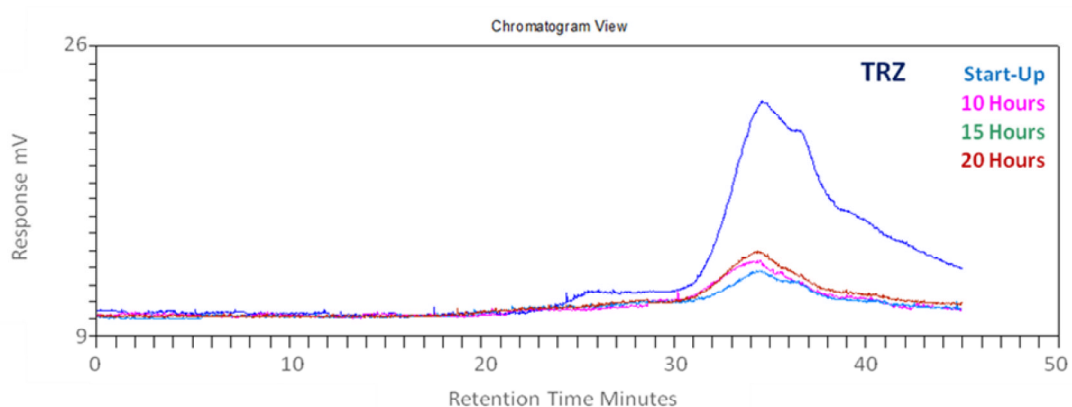
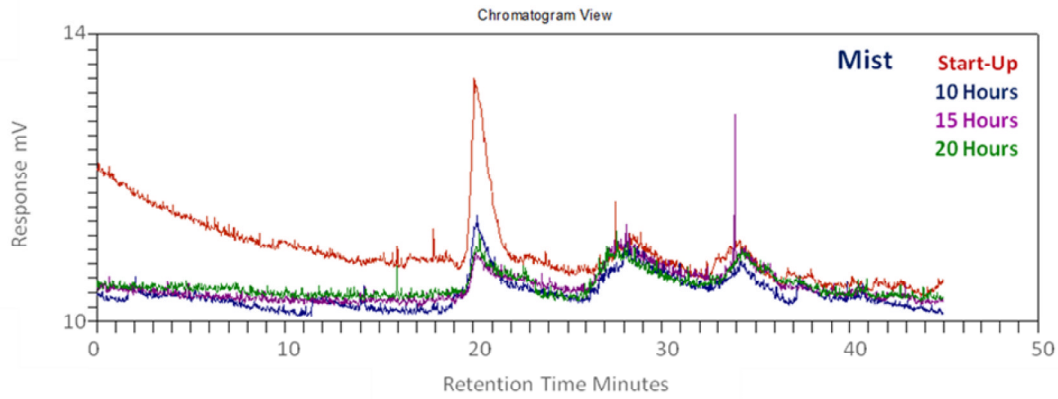
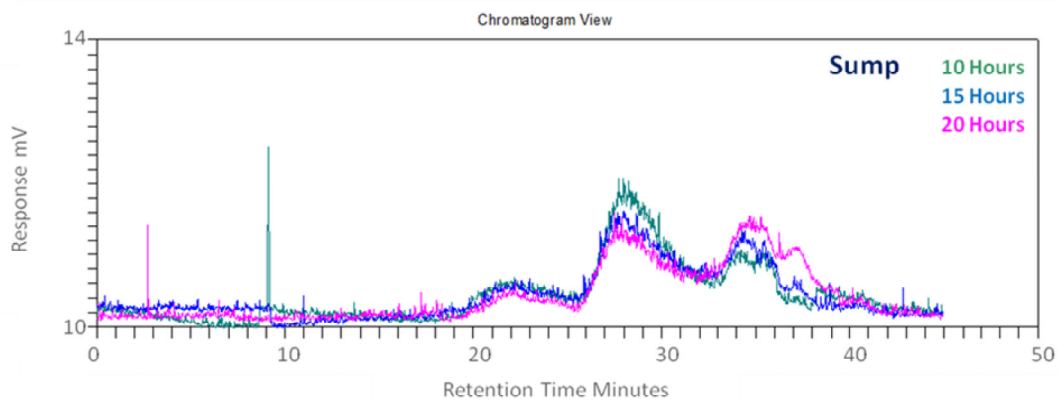


Figure 7.17: TRZ Samples of Polymer 1 by GPC



**Figure 7.18: Mist Samples of Polymer 1 by GPC**



**Figure 7.19: Sump Samples of Polymer 1 by GPC**

Figures 7.17, 7.18 and 7.19 show light scattering traces for TRZ, mist, and sump sample, respectively, for the blend of polymer 1, the linear OCP. The mist samples show the characteristic peak of polymer 5, implying that there was some contamination of the mist sample. The source of this is not known, but it is presumed that some oil was retained in the mist sampling system after cleaning and flushing. The linear polymer peak is still visible at 22 minutes, as a shoulder of the polymer 1 peak. This indicates that there was no significant degradation of the linear polymer during this test. The TRZ samples do not show as distinct a polymer peak at 22 minutes, implying degradation of the polymer. Other peaks appear on these traces at approximately 27-30 minutes. This is hypothesised to be sludge precursors, caused by the degradation of the base oil. The wide molecular weight distribution of this peak is

more likely to result from the polymerising of a base oil under degradation than the scission of a polymer.

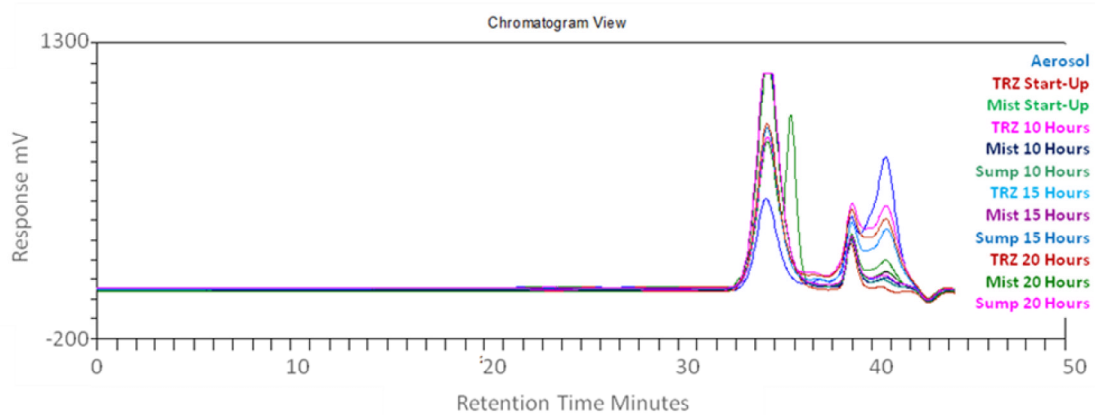


**Figure 7.20: RI GPC Trace of Polymer 1 Engine Test Samples**

The refractive index traces for these blends are shown in Figure 7.20. These do not show any visible change in the polymer concentration. The potential sludge precursor peak at 27-30 minutes is shown to be extremely small and other peaks not seen clearly on the LS traces to be significant e.g. the fuel dilution peak at 41 minutes reflecting the higher fuel concentration in TRZ and mist samples. An unusual shoulder peak to the base oil peak is visible at 36 minutes in the aerosol sample. This is also seen for the equivalent sample in the polymer 5 test, Figure 7.24, so is apparently repeatable. There is, currently, no explanation for this peak.

Figures 7.21, 7.22 and 7.23 show light scattering traces for TRZ, mist, and sump samples, respectively, for the blend of polymer 5, the star polymer. It can be seen that the position and shape of the polymer peak has not changed significantly in any of these locations in the engine, nor with time. Thus, during this test, there appears to have been no significant degradation of the star polymer. The refractive index traces for these blends are shown in Figure 7.24. These indicate that there is little change in polymer concentration in these blends. Small changes are observed in TRZ blends but these are thought to be a result of fuel dilution rather than degradation.



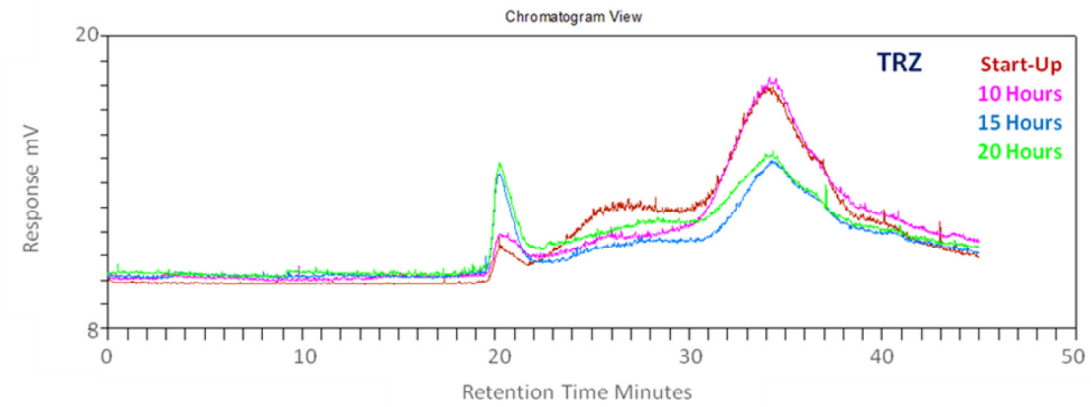


Figure 7.21: TRZ Samples for Polymer 5 by GPC

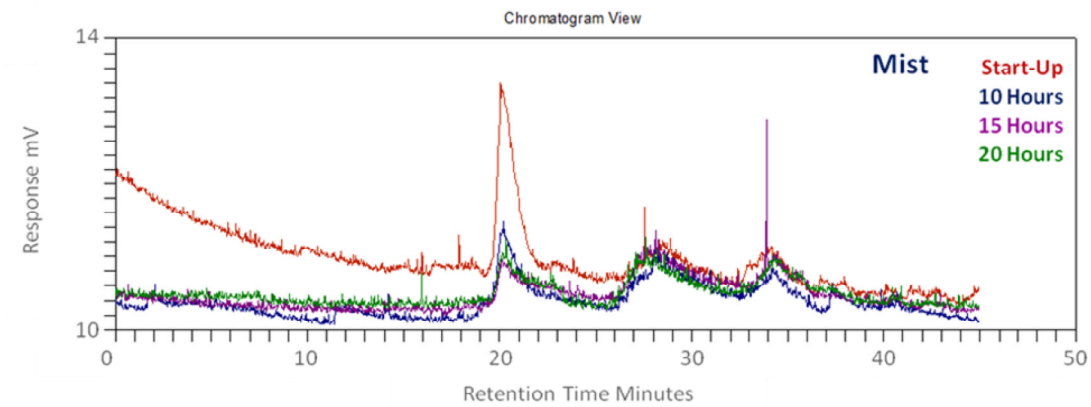


Figure 7.22: Mist Samples for Polymer by GPC

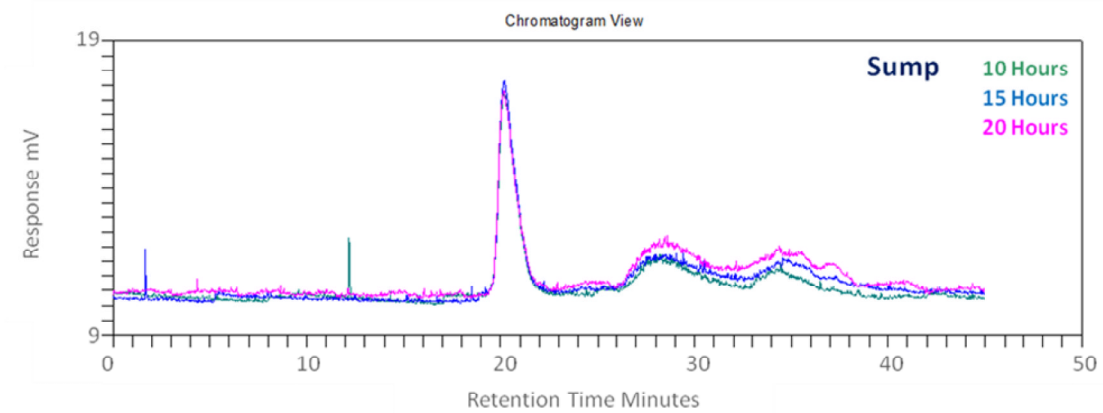
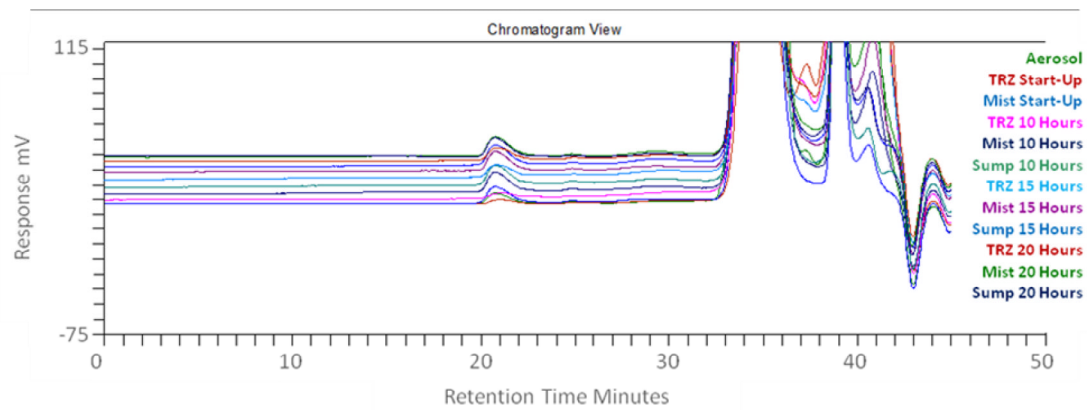


Figure 7.23: Sump Samples for Polymer 5 by GPC



**Figure 7.24: RI GPC Trace for Polymer 5 Engine Test Samples**

Overall, degradation of the polymers is low. However, the linear polymer is more degraded when found in the TRZ. In the period of a typical engine oil change in a modern engine i.e. in the extreme long term, this degradation may significantly affect the sump oil composition. Further testing would be required to confirm this.

#### 7.5.4 Rheological Analysis

Table 7.5 shows the shear viscosity of the fresh and 20 hour sump oil for both blends. This was measured on the Malvern Kinexus Rheometer at 20°C using a parallel plate with a 100µm gap. This data represents an average of the data in the Newtonian region at shear rates of  $10^1$ - $10^2$ s<sup>-1</sup>. It can be seen that significant viscosity reduction has occurred through the test. This is a result of the fuel dilution seen in the sump oil and any degradation of the polymer viscosity modifiers.

Blend	Dynamic Viscosity at 20°C mPa.s
Polymer 1 Fresh	157.5
Polymer 1 Used	82.6
Polymer 5 Fresh	152.6
Polymer 5 Used	79.4

**Table 7.5: Viscosity Measurements of Fresh and Used Polymer Blends**

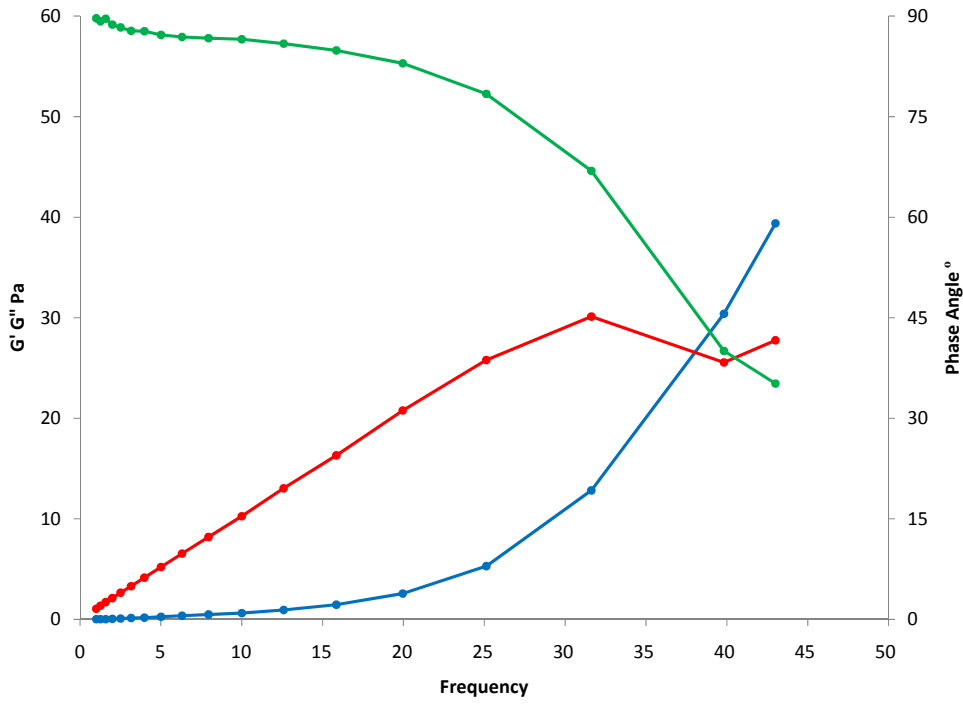


Figure 7.25: Crossover Data for Fresh Polymer 1 Blend

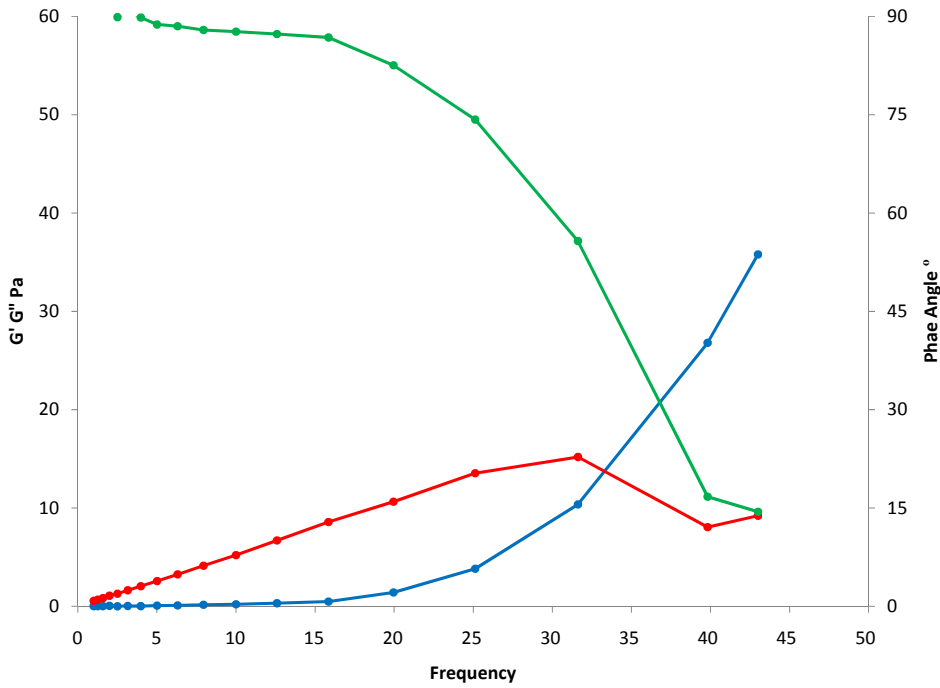


Figure 7.26: Crossover Data for Used Polymer 1 Blend

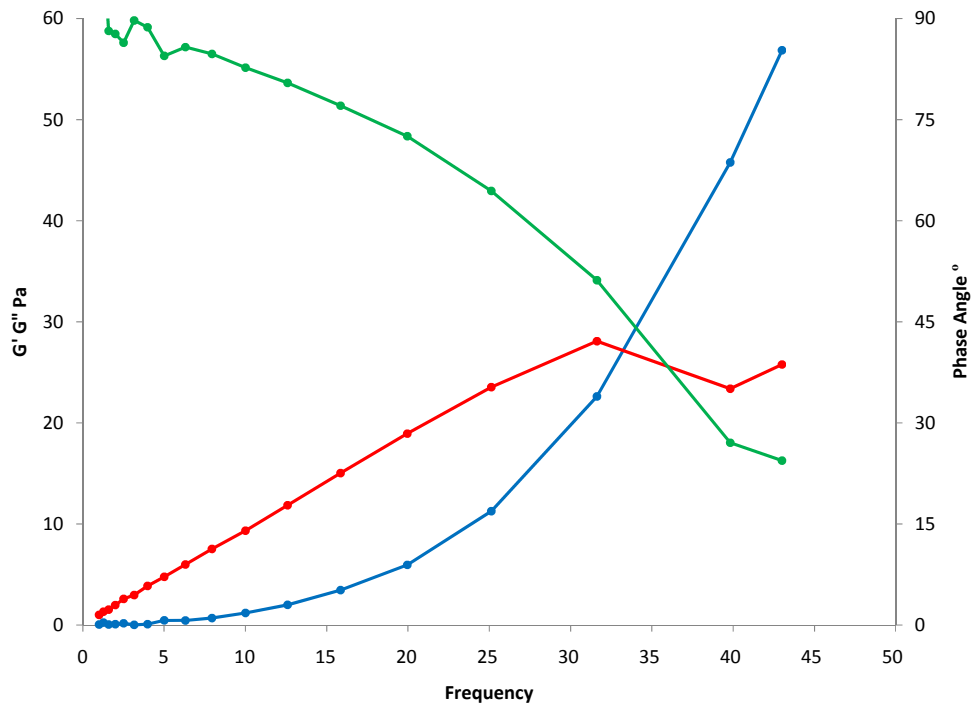


Figure 7.27: Crossover Data for Fresh Polymer 5 Blend

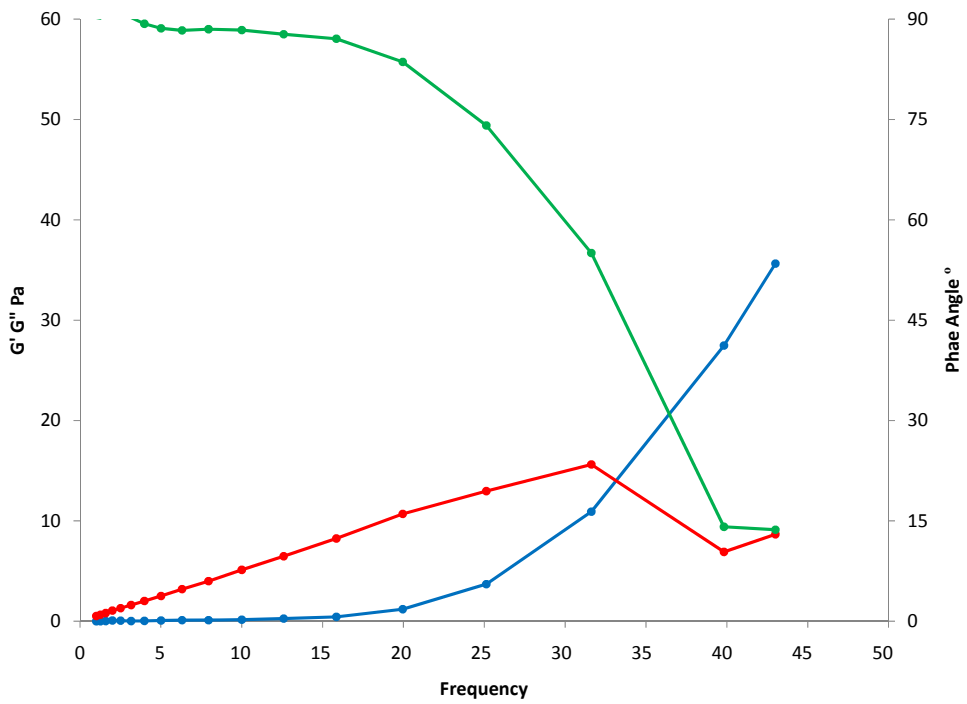


Figure 7.28: Crossover Data for Used Polymer 5 Blend

Figures 7.25 to 7.28 show the crossover test data for the polymer blend, both fresh and used. These show that the viscoelastic behaviour under these conditions is extremely similar. As discussed in Chapter 5, these blends show highly viscoelastic behaviour at very low shear stresses. Table 7.6, showing the relevant parameters for the nearest data point to crossover for each blend, confirms these relationships. When comparing the fresh blends to the sump oil after 20 hours, significant reductions in the shear stress and complex modulus at crossover are seen. This is a result of the viscosity loss discussed previously. What is clear from these tests is that the blends, both fresh and degraded, are significantly viscoelastic. This indicates that polymer degradation has not taken place to the extent that the viscoelastic properties of the lubricant are significantly altered. The small reduction in the frequency of crossover seen for used oils relative to fresh is not significant.

Blend	Crossover Parameters			
	Frequency Hz	Maximum Strain $\gamma^*$ %	Maximum Stress $\sigma^*$ Pa	Complex Modulus $G^*$ Pa
Polymer 1 Fresh	31.6	3.63	1.19	32.7
Polymer 1 Used	31.6	3.63	0.67	18.4
Polymer 5 Fresh	31.6	3.64	1.31	36.1
Polymer 5 Used	31.6	3.63	0.69	19.1

**Table 7.6: Crossover Parameters for Fresh and Used Polymer Blends**

## 7.6 Polymer Concentration Change

It has been considered that high shear stresses encountered during the misting process may produce some change in the lubricant. It is thought that might be seen in two ways. Firstly, high local shear stresses may cause the mechanical degradation of the polymer molecules. Secondly, the differing response to shear of the individual components of a lubricant may cause some fraction of the lubricant to mist more readily than others. This would lead to a higher concentration of certain components or fractions in either the misted or unmisted lubricant. In terms of the piston assembly, as misting is a significant oil transport mechanism, this phenomenon could lead to a

built-up or deficiency of certain lubricant components in the piston assembly in the long term.

The analyses described previously, particularly the GPC analysis, indicate that these mechanisms do not occur in the engine. It was therefore considered worthwhile to investigate whether this behaviour was representative of the misting mechanism hypothesised to occur in the piston ring gaps. Therefore, to investigate this, the mist measuring apparatus described in Section 4.2 was modified so that samples of the misted lubricant could be generated. The particle sizer was removed and a condenser plate installed that drained into a sample jar, Figure 7.29. The unmisted oil was collected as before.

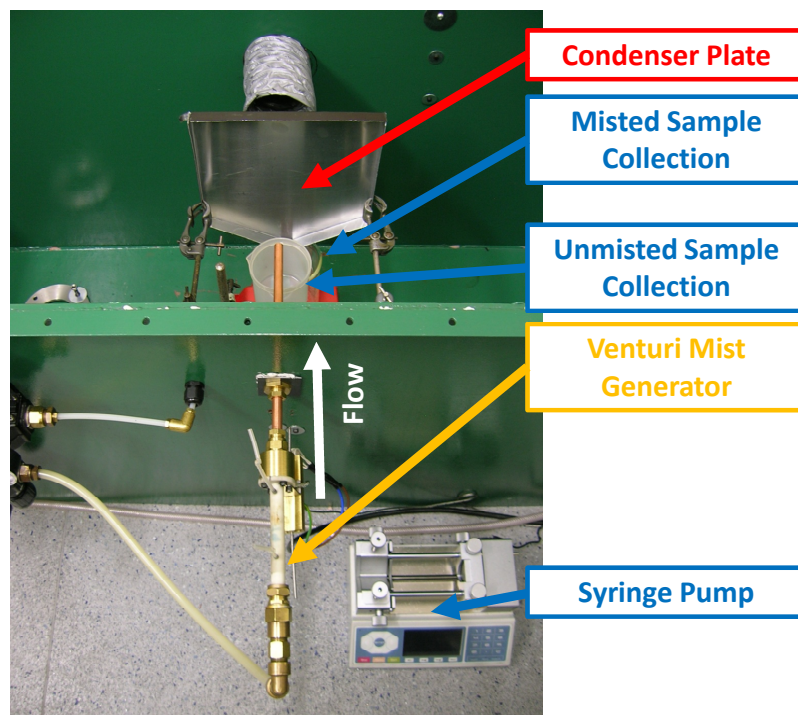


**Figure 7.29: Simulator Mist Sampling Apparatus**

The test conditions were chosen to produce mist rather than spray, thus the inlet flow rate into the syringe pump was 3ml/min. Under these conditions, as shown in Figure

6.7, the misting tendency is 4-8%. Thus, a sample of unmisted lubricant would be approximately 10-25 times greater in volume than the misted lubricant sample collected in the same time. Thus, the test was run for 20 minutes, using 60ml of lubricant. GPC traces of fresh, misted and unmisted lubricant samples were taken with a RI detector, as described in Section 5.3.

The lubricants analysed were the 12 cSt blends produced from 4 cSt i.e. nominally with the greatest polymer concentration, for polymer 1 and polymer 5, Section 5.4. The fully formulated lubricant tested in Section 4.5 was also tested. These are shown in Table 7.7.

Blend	Type	Polymer Concentration (wt)	Kinematic Viscosity at 100°C (cSt or mm <sup>2</sup> s <sup>-1</sup> )	Dynamic Viscosity at 20°C (Pa.s)
Polymer 1	OCP Linear	1.90%	13.0	129.0
Polymer 5	Star Isoprene-co-Styrene	1.30%	12.1	127.1
Fully Formulated	?	?	9.6	115.4

**Table 7.7: Blend Properties for Mist Separation Study**

The results from the GPC analysis are shown in Figures 7.30 to 7.32. These show that there is no significant change in the polymer peak height, indicating that the misting process does not change the polymer concentration. There is also no significant change in the polymer molecular weight, the distribution of molecular weights about the mean, and no new peaks appear on the traces. Thus, it can be seen that misting process does not indicate any mechanical degradation of the polymer. It is noted that there are two secondary polymer peaks at 29 and 32.5 minutes in the fully formulated lubricant. These peaks are the hydrocarbon tails of the detergent and dispersant molecules in the formulation. The misting process does not affect these additives noticeably.

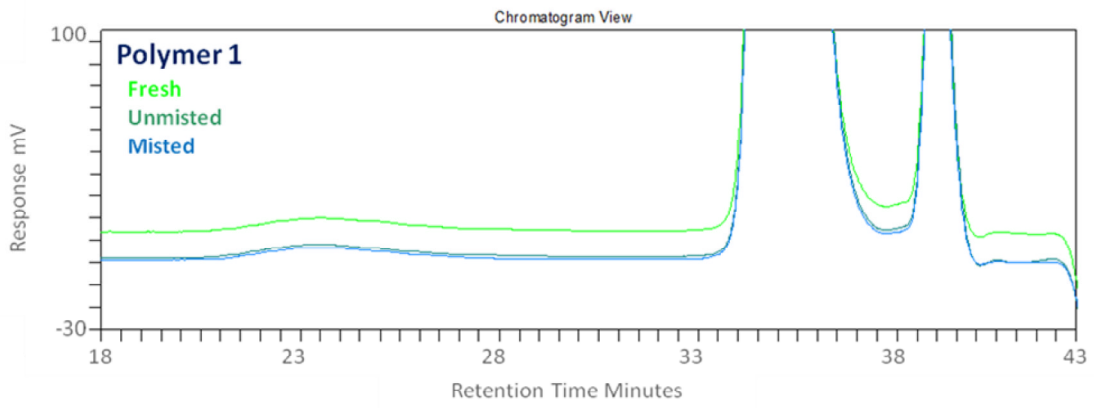


Figure 7.30: RI Trace of Polymer 1 Blend

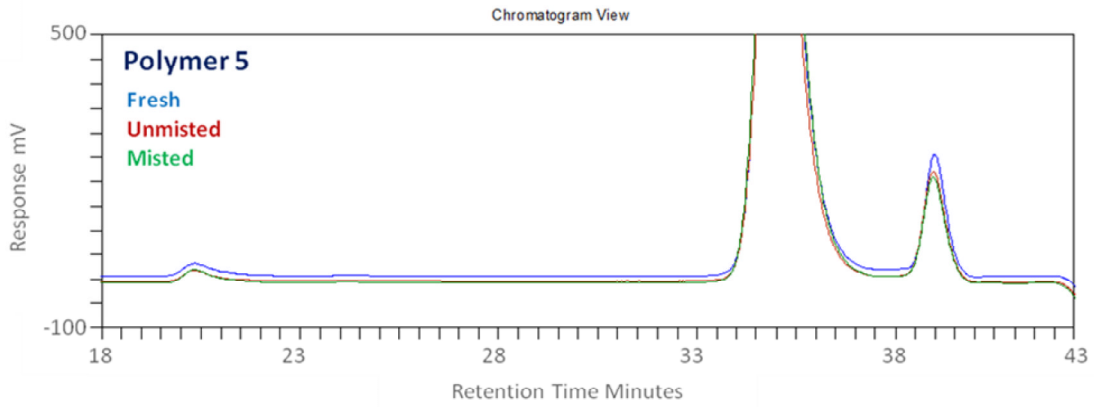


Figure 7.31: RI Trace of Polymer 5 Blend

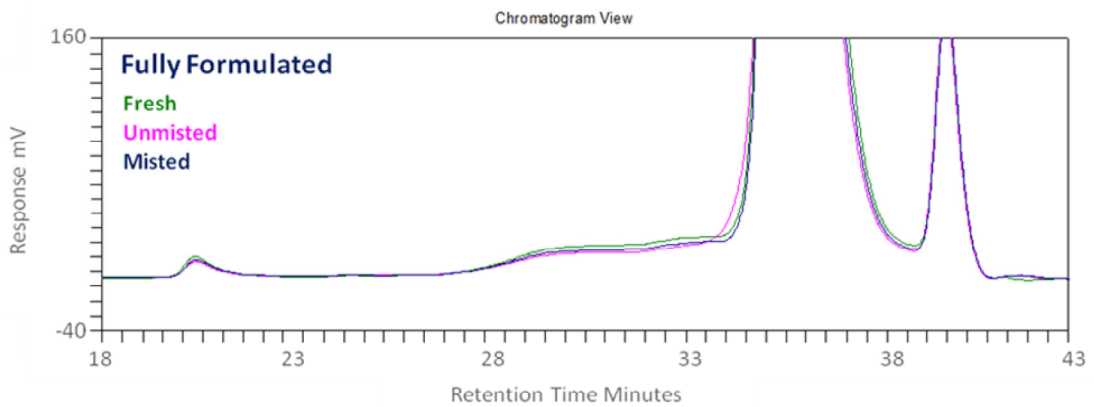


Figure 7.32: RI Trace for Fully Formulated Lubricant



These observations indicate that the misted, unmisted and fresh lubricant have the same composition i.e. the misting process does not change the composition of the lubricant. Thus, this confirms that the mist sampled in the engine tests is formed by a similar mechanical interaction between the lubricant, gas flows and component edges. This also gives further credence to the theory that the mist found in the crankcase is sourced in the piston assembly.

## 7.7 Summary

- Samples of lubricant were sampled from a fired engine during a 20 hour test program. Samples were taken of top ring zone, crankcase mist, crankcase aerosol, and sump oil. Lubricants with varying misting tendencies were tested: a base oil blend, and two blends containing polymer viscosity modifiers. A linear OCP and an isoprene-co-styrene star were used as viscosity modifiers.
- FTIR measurement of nitration and unsaturation peaks was found to produce more robust results than for the carbonyl peak for this test.
- Crankcase mist was found to be more chemically and thermally degraded than the sump oil, though less than the TRZ oil. Similarly, fuel dilutions of mist oil were intermediate between the sump and TRZ. This indicates that the mist was sourced in the piston assembly. This oil potentially has a lower residence time in the piston assembly than the oil sampled directly from the TRZ region.
- Aerosol droplets are still found in the engine, even when polymer viscosity modifiers are present. Thus, other aerosol formation mechanisms must occur. The aerosol is shown to be significantly more degraded than samples at other locations.
- Degradation levels in the TRZ remain constant throughout the test, as this is the region where most degradation occurs. The degradation levels in the sump increase with time as more TRZ oil is fed back into the. Fuel dilution levels in the sampling locations remain constant throughout the test, implying equilibrium at steady state engine conditions.

- GPC analysis showed that polymer degradation is not significant in the sump or mist oil. Linear polymers were seen to degrade in the TRZ, but star polymers were not, indicating greater thermal, chemical and shear stability.
- No significant difference in polymer concentration was seen between the sump, mist, aerosol and TRZ oils, other than by fuel dilution. Thus, it appears that the lubricant remains a continuum when misted and transported by other mechanisms.
- Comparison of fresh, misted and unmisted samples generated in the simulation rig used in Chapters 4 and 5 show that misting by the hypothesised mechanical mechanism does not produce polymer degradation or any change in polymer concentration. This confirms that the mist in the crankcase is sourced in the piston assembly by a similar mechanism.
- Viscoelastic analysis of fresh and degraded sump oil shows no significant reduction in viscoelastic tendency, even though the modulus of the blends reduces significantly. This suggests that the polymer degradation seen is not sufficient to significantly affect the viscoelastic properties of the oils.

## Chapter 8: Conclusions

### 8.1 Introduction

In chapter, the previous chapters are summarised, the most important conclusions stated, and areas thought worthy of further investigation are described.

The aims of this study were:

- To investigate the nature of misting in the piston assembly. The determination of its source, quantity, stability and end point were of chief importance.
- To determine the factors that affect the nature of the mist produced. Lubricant properties engine conditions and flow parameters were the focus of this.
- To determine and quantify any link between misting and long-term lubricant performance. The degradation rate of the lubricant was of particular interest in this regard.

The subsequent investigation produced the following significant findings:

- A laboratory rig has been developed that reproduces the flow conditions and lubricant misting mechanisms in the piston gaps. Measurement of mist in an engine has shown that the mists produced by this rig are representative of those produced by the hypothesised mechanisms in the piston assembly.
- The misting of lubricant in the piston assembly has been shown to occur by measurement of droplets in the crankcase.
- The mechanical mechanism of droplet formation in the piston ring gaps has been shown, through observation and simulation, to occur in a fired engine.
- Other effects of other droplet formation mechanisms were seen: Vapour condensation, droplet breakup, inertial throw-off.
- The nature of mist in the engine is dependent on engine conditions. It is also dependent on the viscosity and polymer content of the lubricant.
- The viscosity and molecular weight of a base oil greatly affects its tendency to produce mist.

- The misting of lubricant is strongly affected by the inclusion of polymeric viscosity modifiers. Thus, the misting process is shown to be dependent on lubricant viscoelasticity, molecular entanglement.
- Aerosol-sized droplets in the engine were seen to degrade more quickly than mist, spray and bulk oil. However, as their volume is very small, this effect was not significant in the duration of testing.
- No significant variation in the degradation of lubricants with varying misting properties was resolved in the tests performed.

These conclusions are discussed in more detail in the following sections, followed by recommendations for future research to further develop this work.

## **8.2 Review of Relevant Studies on Two Phase Flow and Hydrocarbon Misting**

In Chapter 2, it was shown that there was a fundamental lack of understanding and detailed investigation of the misting of lubricant in the piston assembly. It was, however, demonstrated that this was a significant area for engine tribology as it influences oil consumption, oil transport to the upper piston assembly, and the degradation of the lubricant.

Therefore, a detailed study was made of relevant literature on the subjects of two-phase flows, particularly those of hydrocarbons, polymeric liquids, rheology and entanglement. This research indicated that:

- Lubricant mist flows in the piston can be simplistically described as annular mist flow.
- The mist in the piston assembly is likely to contain aerosol, mist and spray-sized droplets. All of these have different source mechanisms and different behaviours.
- Adding long chain polymers to a fluid can greatly reduce its tendency to form droplets. This is attributed to an increase in viscoelastic behaviour.

- Viscoelastic behaviour can be attributed to the stretching and deformation of polymer molecules, and is increased when the molecules are entangled.

### **8.3 Simulation of Misting in the Piston Ring Gap**

In Chapter 4, a method was described to simulate the formation of lubricant mist in the piston ring gap of an engine. A test rig was designed and built, based around a venturi mist generator and a laser diffraction particle sizer. The misting properties of a range of lubricants were tested.

#### **8.3.1 Considering the Components of a Commercial Lubricant**

Initially, a commercial lubricant was considered in its component parts. The following conclusions were found:

- The misting tendency of a base oil decreases linear with an increase in molecular weight, and by a third order polynomial with an increase in viscosity.
- Equiviscous oils of different API oil groups did not show significant variation in misting tendencies, except synthetic PAO, Group IV, which tended to mist more readily.
- The contribution of several additives was measured. Some surface-active additives were found to increase misting tendency, others had no significant effect.
- Polymeric viscosity modifiers reduced the misting tendency of a lubricant very significantly, and to a greater degree than any other additive.

#### **8.3.2 Considering the Effects of Viscosity Modifying Polymers**

Arising from the conclusions of Chapter 4, the effect of viscosity modifiers on misting properties was investigated in detail in Chapter 5. Several linear and star polymers of varying molecular weight and chemistry were blended and compared. These blends

were described in detail in terms of their viscoelasticity, molecular coiling and entanglement. This investigation found that:

- All the blends containing polymers were found to have significant viscoelasticity.
- Blends with a higher degree of molecular entanglement were found to reduce misting tendency most dramatically. These were exclusively linear polymers, as the entanglement behaviour of star polymers is better defined by the entanglement of their individual arms.
- Linear polymers were seen to vary more greatly in their properties than the star polymers tested.
- Small linear polymers had little effect on misting tendency. Micellar star polymers were found to come apart under shear. Thus, their behaviour was as for a small linear polymer.
- Blends hypothesised to have a higher viscoelastic response tended to have a lower tendency to form droplets.
- The shear properties of the blends predicted the misting response well, but not perfectly. Differences in molecular structure produce differences in molecular mobility which were seen to cause these apparent discrepancies. It is thought that the extensional properties of the blends would be a better predictive tool for misting properties.

#### **8.4 Measurement of the Lubricant Mist Formed in a Fired Engine**

In Chapter 6, using the same laser diffraction particle sizer as Chapters 4 and 5, the mist present in the crankcase of a fired engine was extracted and measured. It was hypothesised that most of this mist was formed in the piston assembly. Lubricants of varying viscosity and polymer content were tested and compared. The following observations were made:

- As predicted, aerosol, mist and spray-sized droplets were found in the crankcase gas flows. The behaviour of the spray was found to be inertially thrown off the con-rod and crankshaft assembly. The aerosol and mist behaved

as though it was formed in the piston assembly, though this could not be proven.

- The distributions of droplet sizes reflected those produced in the simulation rig, implying similar mechanisms. Generally, larger droplets were produced than in the simulator. Higher lubricant viscosity or engine conditions may cause this.
- An increase in the base oil viscosity, or the blend viscosity when polymers were included, produced larger mist droplets and reduced the proportion of fine mist and aerosol. This was as predicted in the simulator work.
- Engine conditions had a greater effect on the nature of the droplets than the lubricant chemistry. An increase in engine speed and, to a slightly lesser extent, an increase in load, produced smaller droplets. It is thought that this is a result of higher engine temperatures and, thus, lower lubricant viscosity, or reduced condensation of vapour fractions onto the droplets.

## **8.5 Measurement of Lubricant Degradation in a Fired Engine with Varying Viscosity Modifier Structure**

In Chapter 7, the lubricants with varying misting properties were used in extended engine runs, and the effect of misting properties on degradation was investigated. Lubricant was sampled from several locations in the engine, the crankcase mist, crankcase aerosol, the top ring zone and sump lubricant. These were analysed chemically and rheologically to determine degradation. A linear and a star polymer were added to the same base oil to produce three comparative blends with different misting properties. The following observations were made:

- The aerosol in the crankcase is significantly more degraded than lubricant in other systems. This is a result of its high surface area to volume ratio.
- The crankcase mist is significantly more degraded and contains more fuel fractions than the sump oil, but less so than the top ring zone. This shows that the mist is sourced in the piston assembly.
- No significant difference in oxidation or nitration was seen between the different lubricants tested.

- The linear polymer showed some degradation in the top ring zone. The star polymer, however, showed no measurable degradation in the engine during this test.
- Comparison with sampled lubricant from the simulator indicates that lubricant in both systems shows no variation in polymer concentration or degradation during the misting process. This implies that the crankcase mist had formed by a similar mechanism.
- It was deduced that crankcase aerosol forms from either droplet breakup or from vapour condensation, crankcase mist forms by mechanical mechanisms in the piston assembly, and spray forms inertially from the con-rod and crankcase assembly.
- The polymer-containing blends were still significantly viscoelastic when degraded for 20 hours in the sump.

## **8.6 Suggestions for Future Work**

Arising from the conclusions of these studies, several areas were recognised as requiring more detailed or alternative investigation.

The viscoelastic and rheological properties measured gave a good prediction and explanation of the misting behaviour of the polymer blends. However, these tests were less able to predict behaviour when comparing molecules of significantly different molecular structure. It is thought that, as the hypothesised droplet formation mechanisms involved extensional shear of the lubricant, the extensional properties of lubricants would allow more accurate prediction of misting behaviour. Thus, it is suggested that any further investigation measures the extensional properties of polymer-containing lubricants and establish any correlations that exist.

The developed top ring zone sampling system and mist sampling system have produced good results. However, there is still some understanding to be made of the heat and mass transfer between the liquid, gas and oil vapour phases of the samples gases, and how this affects the sample that is collected. It was noticed that the top ring



zone samples were not as heavily degraded as predicted, and no explanation can currently be offered for this.

The 20 hour engine tests were not sufficiently long to resolve any difference between the oils tested. However, apparent differences in depositing were observed with polymer-containing lubricants. Therefore, longer engine tests are thought to be important. With the improved resolution of the lubricant sampling apparatus, a thorough understanding of the degradation process could be developed by using a longer test. It is thought that this would allow lubricants to be better differentiated in their long term performance. The polymer-containing blends tested in the engine were rheologically similar. Tests with lubricants with greater variation in viscoelasticity or entanglement, whilst keeping similar viscometric behaviour, would be of great interest.

## **8.7 Recommendations for Future Research**

This study has identified areas that are worthy of new research, and other research areas for which the findings of this study have significant implications. These are described here.

The viscoelastic analysis supporting the simulation measurements showed that these parameters are important under the conditions in the lab. However, the viscoelastic properties of polymer-containing lubricants at piston temperatures and pressures are not known. Study of the polymer molecules indicated that they are relatively well coiled under lab conditions. However, the molecules will be well extended at engine temperatures. This latter effect will have a significant effect on parameters such as entanglement and the stretching of the molecule under shear. Therefore, further investigation into the rheology of polymer-containing lubricants at elevated temperatures and pressure would give better understanding. Producing a misting simulation rig that could approach these conditions would increase its representation of the engine conditions.

Whilst a large range of polymers was tested, the comparative relationships that were drawn from the investigation in Chapter 5 are generalistic at this stage. It was established that molecular entanglement and viscoelasticity have a large effect on the misting properties of a lubricant and that, to some degree, these parameters can be altered independently. Therefore further investigation to develop and quantify these parameters and their relationship to misting tendency is important. The possibility of producing blends with similar viscoelastic response but greatly varying entanglement, and vice versa, is theoretically possible, and has potential to produce more tailored rheology of lubricants. The effect of polydispersity of polymer blends on misting would also be useful as most commercial lubricants contain more than one polymer.

Several detailed lubrication models exist, such as that of Gamble (2002). Therefore, the quantifiable findings of this study should be incorporated into these models to improve their accuracy. The knowledge of droplet sizes in the engine will allow the passage of mist through the piston assembly to be better predicted. Also, the viscoelastic properties observed to be important in the lubricants should be incorporated into these models. The incorporation of the hypothesised misting mechanism in the piston ring gaps into models is seen as an important development.

The polymer-containing blends were seen to have some effect on the flow of lubricant in the simulation rig and were deduced to have had an effect on the flow of lubricant through the piston assembly. Therefore, an investigation into the residence time of lubricant in the piston assembly when viscometric and rheological properties are altered would be of great use to understanding degradation and would inform oil transport models. Techniques and apparatus for this measurement have been developed and used previously by Stark (2006).

## Chapter 9: References

- Akagawa, K, Fujii, T, Ito, J, Hamano, Y and Horiuchi, T (1985). "Horizontal Liquid Film-Mist Two-Phase Flow, 2nd Report: Droplet Deposition and Entrainment Rates." *Bulletin of the Japanese Society of Mechanical Engineers* 28(236): 301-308.
- Al-Hadithi, T S R, Barnes, H A and Walters, K (1992). "The Relationship between the Linear (Oscillatory) and Nonlinear (Steady-State) Flow Properties of a Series of Polymer and Colloidal Systems." *Colloid and Polymer Science* 270: 40-46.
- Alemite LCC (2011). *Alemite Oil Mist Application Manual*. Alemite, Charlotte, NC, USA.
- Arcoumanis, C, Khezzar, L, Whitelaw, D S and Warren, B C H (1994). "Breakup of Newtonian and Non-Newtonian Fluids in Air Jets." *Experiments in Fluids* 17: 405-414.
- ASTM (1986). *Standard Test Method for Misting Properties of Lubricating Fluids*. ASTM Standard D3705-86(2003).
- ASTM (2003). *Standard Test Method for Fuel Injector Shear Stability Test (FISST) for Polymer Containing Fluids*. ASTM Standard D5275-03.
- ASTM (2005). *Standard Test Method for Evaluation of Automotive Engine Oils for Inhibition of Deposit Formation in a Spark-Ignition Internal Combustion Engine Fuelled with Gasoline and Operated Under Low-Temperature, Light-Duty Conditions*. ASTM Standard D6593-05.
- ASTM (2005). *Standard Test Method for Evaporation Loss of Lubricating Oils by the Noack Method*. ASTM Standard D5800-05.
- ASTM (2007). *Test Method for Shear Stability of Polymer Containing Fluids Using a European Diesel Injector Apparatus*. ASTM Standard D6278-07.
- Audette, W A and Wong, V (2000). *Oil Transport Along the Engine Cylinder Liner: Coupling Vaporization and Film-Thickness Analysis*. 12th International Colloquium Tribology 2000-Plus, Technische Akademie Esslingen, Ostfildern, Germany, January 11-13, 2000.
- Bailey, B K and Ariga, S (1990). "On-Line Diesel Engine Oil Consumption Measurement." *SAE Technical Paper* 902113.
- Bair, S, Lockwood, F E, Anderson, W B, Zhang, Z and Dotson, D (2007). "Measurements of Elasticity in Multigrade Motor Oil at Elevated Pressure." *Tribology Transactions* 50(3): 407-414.
- Bair, S and Qureshi, F (2003). "The High Pressure Rheology of Polymer-Oil Solutions." *Tribology International* 36: 637-645.
- Barth, H G (1984). *Modern Methods of Particle Size Analysis*, Wiley.
- Benvenuti, L H, Coelho, E, Possuelo, R, Filho, A S, De-Campos, J F L, Ribeiro, E and Elias, A L (2002). "Fuel Economy Performance Evaluation of 5W30 Low Friction Oil." *SAE Technical Paper* 2002-01-3530.

- Bezot, P, Hesse-Bezot, C, Constans, B, Faure, D and Hoornaert, P (1993). "A Microscopic Study by Dynamic Light Scattering of Four Viscosity Index Improvers in Two Model Solvents and a Mineral Base Oil." SAE Technical Paper 932835.
- Bloch, H P (1987). Oil Mist Lubrication Handbook: Systems and Applications, Gulf Publishing Company.
- Bolander, N W, Steenwyk, B D, Sadeghi, F and Gerber, G R (2005). "Lubrication Regime Transitions at the Piston Ring-Cylinder Liner Interface." Proceedings of the IMechE: J Journal of Engineering Tribology 219: 19-31.
- Brown, M A, McCann, H and Thompson, D M (1993). Characterization of the Oil Film Behaviour Between the Liner and Piston of a Heavy Duty Diesel Engine. SAE Technical Paper 932784.
- Brown, S R and Hamilton, G M (1978). "Negative Pressure Under a Lubricated Piston Ring." Journal of Mechanical Engineering Science 20(1): 49-57.
- Burnett, P J (1992). Relationship Between Oil Consumption, Deposit Formation and and Piston Ring Motion for Single-Cylinder Diesel Engines. SAE Technical Paper 920089.
- Cadle, R D (1965). Particle Size: Theory and Industrial Applications, Reinhold Publishing Corporation.
- Caress, P G (1992). "A Study of Lubricant Effects on Inlet Valve Deposits using a Specially Adapted Test Vehicle." SAE Technical Paper 922300.
- Cecil, R (1973). "High Temperature Thickening of Motor Oils." Journal of the Institute of Petroleum 59(569): 201-210.
- Charles, P, Elfassi, M and Lubrecht, A A (2010). "Double-Newtonian Rheology in a Model Piston-Ring Cylinder-Wall Contact." Tribology International 43: 1902-1907.
- Chen, C I, Wu, P, Duda, J L and Klaus, E E (1994). Predicting Viscosity-Shear Relationships of VI-Improved Lubricants. SAE Technical Paper 942025.
- Cheng, K Y, Shayler, P J and Murphy, M (2004). "The Influence of Blow-By on Indicated Work Output from a Diesel Engine under Cold Start Conditions." Proceedings of the IMechE: D Journal of Automobile Engineering 218: 333-340.
- Cho, M-R, Choi, J-K and Han, D-C (2001). "Calculation of Mixed Lubrication at Piston Ring and Cylinder Liner Interface." KSME International Journal 15(7): 859-865.
- Choi, J-K, Min, B-S and Han, D-C (1993). Effect of Oil Aeration Rate on the Minimum Oil Film Thickness and Reliability of Engine Bearing. SAE Technical Paper 932785.
- Chu, B (1991). Laser Light Diffraction, Academic Press Inc, Harcourt Brace Jovanovich.
- Clark, N N, Tatli, E, Barnett, R, Wayne, W S and McKain, D L (2006). "Characterization and Abatement of Diesel Crankcase Emissions." SAE Technical Paper 2006-01-3372.
- Covitch, M J (1988). "Oil Thickening in the MACK T-7 Engine Test, II - Effects of Fuel Composition on Soot Composition." SAE Technical Paper 880259.
- Covitch, M J (2003). Olefin Copolymer Viscosity Modifiers. Lubricant Additives: Chemistry and Applications. L. R. Rudnick, CRC Press.

- Coy, R C (1998). "Practical Applications of Lubrication Models in Engines." *Tribology International* 31(10): 563-571.
- Cross, M M (1965). "Rheology of Non-Newtonian Fluids: A New Flow Equation for Pseudoplastic Systems." *Journal of Colloid Science* 20: 417-437.
- Crowe, C, Sommerfeld, M and Tsuji, Y (1998). *Multiphase Flows with Droplets and Particles*, CRC Press.
- Dasch, J M, D'Arcy, J B, Kinare, S S, Yin, Y, Kopple, R G and Salmon, S C (2008). "Mist Generation from High-Speed Grinding with Straight Oils." *Tribology Transactions* 51: 381-388.
- Dasch, J M, D'Arcy, J B, Kinare, S S, Yin, Y, Kopple, R G and Salmon, S C (2008). *Mist Generation from High-Speed Grinding with Straight Oils*. STLE - *Tribology and Lubrication Technology*. October 2008: 40-47.
- Daskivich, R A (1980). *Sensitivity of New-Engine Oil Economy to Cylinder Bore Characteristics*. ASME Winter Annual Meeting, Chicago 1980.
- David, R L A (2008). *Associative Polymers as Antimisting Agents and other Functional Materials via Thiol-ene Coupling*, PhD Thesis, California Institute of Technology.
- Davies, C N (1973). "Diffusion and Sedimentation of Aerosol Particles from Poiseuille Flow in Pipes." *Aerosol Science* 4: 117-128.
- Davis, E J and Schweiger, G (2002). *The Airborne Microparticle: Its Physics, Chemistry, Optics and Transport Phenomena*, Springer.
- Day, L, Dunaevsky, V and McCormick, H (2008). *Critical Factors Affecting Oil Consumption and Deposit Formation in Engines and Compressors Come to Lights From Research in Two Disciplines*. *Tribology and Lubrication Technology*, STLE. September 2008: 31-39.
- De-Silva, P, Priest, M, Lee, P M, Taylor, R I and Kruchinin, D (2010). *The Effect of Biofuel Components and Gasoline Administered Friction Modifiers on Engine Lubricant Performance*. STLE Annual Meeting 2010. Las Vegas, USA.
- Della-Valle, D, Tanguy, P A and Carreau, P J (2000). "Characterization of the Extensional Properties of Complex Fluids Using an Orifice Flowmeter." *Journal of Non-Newtonian Fluid Mechanics* 94: 1-13.
- Delvigne, T (2010). "Oil Consumption Sources in a Modern Gasoline Engine Including Contribution of Blow-By Separator and Turbocharger: An Experimental Study Based on the Use of Radiotracers." SAE Technical paper 2010-01-2256.
- DePetris, C, Giglio, V and Police, G (1996). *Some Insights on Mechanisms of Oil Consumption*. SAE Technical Paper 961216.
- Diaby, M, Sablier, M, Le-Negrate, A, El-Fassi, M and Bouquet, J (2009). "Understanding Carbonaceous Deposit Formation Resulting from Engine Oil Degradation." *Carbon* 47: 355-366.
- Dowson, D, Economou, P N, Ruddy, B L, Strachan, P J and Baker, A J S (1979). *Piston Ring Lubrication: Part II, Theoretical Analysis of a Single Ring and a Complete Ring Pack*. *Energy Conservation through Fluid Film Lubrication Technology: Frontiers in Research and Design*. S. M. Rohde, ASME.
- Ebner, H W and Jaschek, A O (1998). *The Importance of Blow-By Measurements, Measuring Equipment Required and Implementation*. SAE Technical Paper 981081.

- Edwards, C F (1995). Application of Ideal Spray Concepts to Understanding the Stochastic Dynamics of Sprays. Mechanics and Combustion of Droplets and Sprays. H. H. Chiuet al, Begell House Inc.
- Ejakov, M A, Schock, H J and Brombolich, L J (1998). "Modeling of Ring Twist for an IC Engine." SAE Technical Paper 982693.
- Ellermann, J, Rohrle, M D and Schelling, H (1981). "Oil Consumption and Blowby of Truck Diesel Engines - Test Bench Results." SAE Technical Paper 810937.
- Emanuel, N M, Denisov, E T and Maizus, Z K (1997). Liquid Phase Oxidation of Hydrocarbons, Plenum Press.
- Ergungor, Z, Smolinski, J M, Manke, C W and Gulari, E (2006). "Effect of Polymer-Surfactant Interactions on Elongational Viscosity and Atomization of PEO Solutions." Journal of Non-Newtonian Fluid Mechanics 138: 1-6.
- Fan, K, Li, J, Ma, H, Wu, H, Ren, T, Kasrai, M and Bancroft, G M (2008). "Tribological Characteristics of Ashless Dithiocarbamate Derivatives and their Combinations with ZDDP as Additives in Mineral Oil." Tribology International 41: 1226-1231.
- Ferguson, J, Hudson, N E and Odriozola, M A (1997). "The Interpretation of Transient Extensional Viscosity Data." Journal of Non-Newtonian Fluid Mechanics 68: 241-257.
- Fernando, R H and Glass, J E (1988). "Dynamic Uniaxial Extensional Viscosity (DUEV) Effects in Roll Application II: Polymer Blend Studies." Journal of Rheology 32(2): 199-213.
- Fernando, R H, Xing, L-L and Glass, J E (2000). "Rheology Parameters Controlling Spray Atomization and Roll Misting Behaviour of Waterborne Coatings." Progress in Organic Coatings 40: 35-38.
- Ferry, J D (1980). Viscoelastic Properties of Polymers, John Wiley and Sons.
- Ferry, J D (1980). Viscoelastic Properties of Polymers, 3rd Edition, Wiley.
- Fetters, L J, Kiss, A D, Pearson, D S, Quack, G F and Vitus, F J (1993). "Rheological Behaviour of Star-Shaped Polymers." Macromolecules 26(647-654).
- Fifield, F W and Kealey, D (2000). Principles and Practice of Analytical Chemistry, 3rd Edition, Blackwell Science.
- Fischer, R (1995). "Calculation of the Discharge Characteristic of an Orifice for Gas-Liquid Annular-Mist Flow." International Journal of Multiphase Flow 21(5): 817-835.
- Flamberg, A, Koller, R D, Herbeaux, J-L and Van-Arsdale, W E (1994). Mechanical Degradation of Multigrade Oils in Laboratory Engine Tests. SAE Technical Paper 942024.
- Fry, M, Nightingale, C and Richardson, S (1995). High-Speed Photography and Image Analysis Techniques Applied to Study Droplet Motion within the Porting and Cylinder of a 4-Valve SI Engine. SAE Technical Paper 952525.
- Furuhama, S, Hiruma, M and Tsuzita, M (1979). "Piston Ring Motion and its Influence on Engine Tribology." SAE Technical Paper 790806.
- Furuhama, S, Hiruma, M and Yoshida, H (1981). An Increase of Engine Oil Consumption at High Temperature of Piston and Cylinder. SAE Technical Paper 810976.
- Furuhama, S and Sumi, T (1961). "A Dynamic Theory of Piston-Ring Lubrication." Bulletin of the Japanese Society of Mechanical Engineers 4(16): 744-752.

- Furuhama, S and Tada, T (1961). "On the Flow of Gas Through the Piston-Rings: 1st Report, The Discharge Coefficient and Temperature of Leakage Gas." *Bulletin of the Japanese Society of Mechanical Engineers* 4(16): 684-690.
- Furuhama, S and Tada, T (1961). "On the Flow of Gas Through the Piston-Rings: 2nd Report, The Character of Gas Leakage." *Bulletin of the Japanese Society of Mechanical Engineers* 4(16): 691-698.
- Furuhama, S, Takiguchi, M and Tomizawa, K (1981). "Effect of Piston and Piston Ring Designs on the Piston Friction Forces in Diesel Engines." SAE Technical Paper 810977.
- Gallopoulos, N E (1970). Engine Oil Thickening in High-Speed Passenger Car Service. SAE Technical Paper 700506.
- Gamble, R J (2003). PhD Thesis, University of Leeds.
- Gamble, R J, Priest, M and Taylor, C M (2002). "Detailed Analysis of Oil Transport in the Piston Assembly of a Gasoline Engine." *Tribology Letters* 14(2): 147-156.
- Gell, C B, Graessley, W W, Efstratiadis, V, Pitsikalis, M and Hadjichristidis, N (1997). "Viscoelasticity and Self-Diffusion in Melts of Entangled Asymmetric Star Polymers." *Journal of Polymer Science: Part B: Polymer Physics* 35: 1943-1954.
- George, H F and Hedrick, D P (1993). Comparative Rheology of Commercial Viscosity Modifier Concentrates. SAE Technical Paper 932834.
- Ghiaasiaan, S M (2008). Two-Phase Flow, Boiling, and Condensing: In Conventional and Miniature Systems, Cambridge University Press.
- Glass, J E, Schulz, D N and Zukoski, C F (1991). Polymers as Rheology Modifiers: An Overview. *Polymers as Rheology Modifiers*. D. N. Schulz et al, ACS Symposium Series 462.
- Graessley, W W (2008). *Polymeric Liquids and Networks: Dynamics and Rheology*, Garland Science.
- Graessley, W W and Edwards, S F (1981). "Entanglement Interactions in Polymers and the Chain Contour Concentration." *Polymer* 22: 1329-1334.
- Griffiths, P R and Haseth, J A D (1986). *Fourier Transform Infrared Spectrometry*, John Wiley & Sons.
- Guenther, M, DeWaard, D, LaPan, M, Jensen, T, Seigl, W, Baldus, S and Loo, J (1998). "Comparison of Vehicle Running Loss Evaporative Emissions using Point Source and Enclosure Measurement Techniques." SAE Technical Paper 980403.
- Gulari, E, Manke, C W, Smolinski, J M, Marano, R S and Toth, L (1995). *Polymer Additives and Mist Suppressants in Metalworking Fluids: Laboratory and Plant Studies*. The Industrial Metalworking Environment: Assessment and Control.
- Gulwadi, S D (1998). "A Mixed Lubrication and Oil Transport Model for Piston Rings using a Mass-Conserving Algorithm." *Transactions of the ASME - Journal of Engineering for Gas Turbines and Power* 120: 199-208.
- Gunsel, S (2009). *Lubricant Design: Impacts on Energy Efficiency*. Additives 2009, York, UK.
- Gunzler, H (2002). *IR Spectroscopy: An Introduction*, Wiley VCH.
- Hadsburg, T (2003). *Lubricant Base Stocks*. Royal Society of Chemistry: Additives 2003.

- Harigaya, Y, Suzuki, M and Takiguchi, M (2003). "Analysis of Oil Film Thickness on a Piston Ring of Diesel Engine: Effect of Oil Film Temperature." Transactions of the ASME - Journal of Engineering for Gas Turbines and Power 125: 596-603.
- Harigaya, Y, Suzuki, M, Toda, F and Takiguchi, M (2006). "Analysis of Oil Film Thickness and Heat Transfer on a Piston Ring of a Diesel Engine: Effect of Lubricant Viscosity." Transactions of the ASME - Journal of Engineering for Gas Turbines and Power 128: 685-693.
- Hennesy, M and Barber, G C (1995). "The Effects of Cylinder Wall Surface Roughness and Bore Distortion on Blow-By in Automotive Engines." Tribology Transactions 38(4): 966-972.
- Hewitt, G F and Hall-Taylor, N S (1970). Annular Two-Phase Flow, Pergamon Press.
- Holness, M H (1995). "Oil Mist and Machinery Space Fires." distributed by QMI Ltd [www.oilmist.com](http://www.oilmist.com).
- Holowach, M J, Hochreiter, L E and Cheung, F B (2002). "A Model for Droplet Entrainment in Heated Annular Flow." International Journal of Heat and Fluid Flow 23: 807-822.
- Hoult, D P and Azzola, J H (1993). The Possible Role of Surface Tension in the Reduction of Top Ring Drag. SAE Technical Paper 932781.
- Houser, K R and Crosby, T A (1992). "The Impact of Intake Valve Deposits on Exhaust Emissions." SAE Technical Paper 922259.
- Hronza, J and Bell, D (2007). "A Lubrication and Oil Transport Model for Piston Rings using a Navier-Stokes Equation with Surface Tension." SAE Technical Paper 2007-01-1053.
- HSE (1997). Measurement of Oil Mist from Mineral Oil-Based Metalworking Fluids. Methods for Determination of Hazardous Substances Procedure 84, Health and Safety Executive.
- Hung, D L S, Harrington, D L, Gandhi, A H, Markle, L E, Parrish, S E, Shakal, J S, Sayar, H, Cummings, S D and Kramer, J L (2008). Gasoline Fuel Injector Spray Measurement and Characterization: A New SAE J2715 Recommended Practice. SAE Technical Paper 2008-01-1068.
- Hunt, T A and Todd, B D (2009). "A Comparison of Model Linear Chain Molecules with Constrained and Flexible Bond Lengths under Planar Couette and Extensional Flows." Molecular Simulation 35(14): 1153-1167.
- Inagaki, H, Saito, A, Murakami, M and Konomi, T (1997). "Measurement of Oil Film Thickness Distribution on Piston Surface Using the Fluorescence Method: Development of Measurement System." JSME International Journal 40(3): 487-493.
- Ishihara, S, Nakashima, K, Urano, K and Murata, K (1999). The Designs of Piston and Piston Ring to Reduce Lubricating Oils Flow into the Combustion Chamber. SAE Technical Paper 1999-01-3316.
- Ishii, M and Mishima, K (1989). "Droplet Entrainment Correlation in Annular Two-Phase Flow." International Journal of Heat and Mass Transfer 32(10): 1835-1846.
- Ito, A, Tsuchihashi, K and Nakamura, M (2006). "A Study on the Mechanism of Lubricating Oil Consumption of Diesel Engines - 4th Report: The measurement of Oil Pressure Under the Piston Oil Ring." SAE Technical Paper 2006-01-3440.



- Iwakata, K, Onodera, Y, Mihara, K and Ohkawa, S (1993). Nitro-Oxidation of Lubricating Oil in Heavy-Duty Diesel Engine. SAE Technical Paper 932839.
- Jain, S, Dalal, I, Orichella, N, Shum, J and Larson, R G (2009). "Doi Bending and Torsional Potentials Affect the Unravelling Dynamics of Flexible Polymer Chains in Extensional or Shear Flows?" *Chemical Engineering Science* 64: 4566-4571.
- Jakubik, T, Lawes, M, Woolley, R and Jicha, M (2006). "Study of Ambient Turbulence Effects on Diesel Sprays in a Fan-Stirred Vessel." *Atomization and Sprays* 16: 687-703.
- Jeng, Y-R (1992). "Theoretical Analysis of Piston-Ring Lubrication, Part I: Fully Flooded Lubrication." *Tribology Transactions* 35(4): 696-706.
- Jeng, Y-R (1992). "Theoretical Analysis of Piston-Ring Lubrication, Part II: Starved Lubrication and its Application to a Complete Ring Pack." *Tribology Transactions* 35(4): 707-714.
- Johansson, P and Andersson, S (2010). "Variations in Piston Second Land Pressure as a Function of Rings Gap Position." *International Journal of Engine Research* 11: 153-161.
- Kabanemi, K K and Hetu, J-F (2009). "Nonequilibrium Stretching Dynamics of Dilute and Entangled Linear Polymers in Extensional Flow." *Journal of Non-Newtonian Fluid Mechanics* 160: 113-121.
- Karyappa, R B and Natarajan, U (2008). "Monte Carlo Simulations of Chain Dimensions and Conformational Properties of Various Poly(n-alkly methacrylates) in Solution." *Journal of Macromolecular Science: Part B, Physics* 47: 1075-1086.
- Kato, M, Fujita, K, Suzuki, H, Baba, Y, Ishima, T and Obokata, T (2009). "Analysis of Lubricant Oil Film Behaviour on the Piston Surface According with Piston Shapes by Means of LIF and PIV." SAE Technical Paper 2009-01-0003.
- Keenan, J H, Chao, J and Kaye, J (1983). *Gas Tables: Thermodynamic Properties of Air, Products of Combustion, and Component Gases: Compressible Flow Functions*, 2nd Edition, Wiley-Interscience.
- Kemp, W H (2007). *Zero Carbon Car: Building the Car the Auto Industry can't get Right*, Azttext.
- Keribar, R, Dursunkaya, Z and Fleming, M F (1991). "An Integrated Model of Ring Pack Performance." *Transactions of the ASME - Journal of Engineering for Gas Turbines and Power* 113: 382-389.
- Khonsari, M M and Booser, E R (2005). "Guidelines for Oil Mist Lubrication." *Machinery Lubrication Magazine*.
- Kim, C, Bae, C and Choi, S (1999). *Gas Flows Through the Inter-Ring Crevice and Their Influence on UHC Emissions*. SAE Technical Paper 1999-01-1533.
- Kim, H-D, Kim, J-H, Park, K-A, Setoguchi, T and Matsuo, S (2003). "Computational Study of the Gas Flow Through a Critical Nozzle." *Proceedings of the IMechE: C Journal of Mechanical Engineering Science* 217: 1179-1189.
- Kinsey, J S, Mitchell, W A, Squier, W C, Linna, K, King, F G, Logan, R, Dong, Y, Thompson, G J and Clark, N N (2006). "Evaluation of Methods for the Determination of Diesel-Generated Fine Particulate Matter: Physical Characterization Results." *Aerosol Science* 37: 63-87.

- Klaus, E E, Duda, J L and Bala, V (1991). Prediction of High Temperature Viscosities of Polymer Solutions up to  $10^7 \text{sec}^{-1}$  Shear Rates. SAE Technical Paper 912411.
- Korcek, S, Sorab, J, Johnson, M D and Jensen, R K (2000). "Automotive Lubricants for the Next Millennium." *Industrial Lubrication and Tribology* 52(5): 209-220.
- Kumar, P and Khonsari, M M (2009). "On the Role of Lubricant Rheology and Piezo-Viscous Properties in Line and Point Contact EHL." *Tribology International* 42: 1522-1530.
- Lansdown, A R (1994). High Temperature Lubrication, Mechanical Engineering Publications Ltd.
- Lawes, M, Lee, Y and Marquez, N (2006). "Comparison of Iso-Octane Burning Rates Between Single-Phase and Two-Phase Combustion for Small Droplets." *Combustion and Flame* 114: 513-525.
- Lee, H-S, Wang, S S, Smolenski, D J, Viola, M B and Klusendorf, E E (1994). "In Situ Monitoring of High-Temperature Degraded Engine Oil Condition with Microsensors." *Sensors and Actuators B* 20: 49-54.
- Lee, P M (2006). PhD Thesis, University of Leeds.
- Lee, P M, Priest, M, Stark, M S, Wilkinson, J J, Lindsay-Smith, J R, Taylor, R I and Chung, S (2006). "Extraction and Tribological Investigation of Top Piston Ring Zone Oil from a Gasoline Engine." *Proceedings of the IMechE: J Journal of Engineering Tribology* 220: 171-180.
- Lefebvre, A H (1989). *Atomization and Sprays*, Taylor and Francis.
- Ligier, J-L and Ragot, P (2007). "Mixed Lubrication and Roughness Surface Effects Application to Piston Rings." SAE Technical Paper 2007-01-1246.
- Liu, Z and Reitz, R D (1997). "An Analysis of the Distortion and Breakup Mechanisms of High Speed Liquid Drops." *International Journal of Multiphase Flow* 23(4): 631-650.
- Ma, M-T, Sherrington, I and Smith, E H (1996). "Implementation of an Algorithm to Model the Starved Lubrication of a Piston Ring in Distorted Bores: Prediction of Oil Flow and Onset of Gas Blow-By." *Proceedings of the IMechE: J Journal of Engineering Tribology* 210: 29-44.
- Ma, Z (2010). "Oil Transport Analysis of a Cylinder Deactivation Engine." SAE Technical Paper 2010-01-1098.
- Ma, Z, Henein, N A and Bryzik, W (2006). "A Model for Wear and Friction in Cylinder Liners and Piston Rings." *Tribology Transactions* 49: 315-327.
- Maekawa, K, Mitsutake, S and Morohoshi, S (1986). "A Study on Engine Lubricating Oil Consumption by Computer Simulation." SAE Technical Paper 860546.
- Malvern Instruments Ltd (2008). Malvern Instruments Ltd. [www.malvern.co.uk](http://www.malvern.co.uk).
- Mang, T and Diesel, W (2001). *Lubricants and Lubrication*, Wiley.
- Mang, T and Dresel, W (2001). *Lubricants and Lubrication*, Wiley-VCH.
- Manly, B F J (1994). *Multivariate Statistical Methods: A Primer*, Chapman & Hall.
- Marano, R S, Messick, R L, Smolinold, J M and Toth, L (1995). *Polymer Additives as Mist Suppressants in Metalworking Fluids Part 1: Laboratory and Plant Studies - Straight Mineral Oil*. SAE Technical Paper 950245.
- Massey, B and Ward-Smith, J (1998). *Mechanics of Fluids*, 7th Edition, Stanley Thornes.

- Masuko, M, Ohkido, T, Suzuki, A, Ueno, T, Okuda, S and Sagawa, T (2007). "Effect of Ashless Dispersant on Deterioration of Antiwear Characteristics of ZnDTP due to Decomposition during the Oxidation Inhibition Process." *Tribology Transactions* 50: 310-318.
- McGeehan, J A (1979). "A Survey of the Mechanical Design Factors Affecting Engine Oil Consumption." SAE Technical Paper 790864.
- McGeehan, J A, Alexander-III, W, Ziemer, J N, Roby, S H and Graham, J P (1999). "The Pivotal Role of Crankcase Oil in Preventing Soot Wear and Extending Filter Life in Low Emission Diesel Engines." SAE Technical Paper 1999-01-1525.
- McGrogan, S and Tian, T (2010). "Numerical Simulation of Combustion-Driven Oil Transport on the Top Land of an Internal Combustion Engine." *International Journal of Engine Research* 11: 243-256.
- McKinley, G H (2005). "Dimensionless Groups for Understanding Free Surface Flows of Complex Fluids." *SOR Rheology Bulletin*.
- Miltsios, G K, Patterson, D J and Papanastasiou, T C (1989). "Solution of the Lubrication Problem and Calculation of the Friction Force on the Piston Rings." *Transactions of the ASME - Journal of Tribology* 111: 635-641.
- Min, B-S, Kim, J-S, Oh, D-Y, Choi, J-K and Jin, J-H (1998). Dynamic Characteristics of Oil Consumption: Relationship Between the Instantaneous Oil Consumption and the Location of Piston Ring Gap. SAE Technical Paper 982442.
- Mishra, P C, Balakrishnan, S and Rahnejat, H (2008). "Tribology of Compression Ring-to-Cylinder Contact at Reversal." *Proceedings of the IMechE: J Journal of Engineering Tribology* 222: 815-826.
- Mistry, K K, Neville, A, Morina, A and Webster, M N (2008). "Lubricant/Surface Interactions under Extreme Pressure Conditions: Corrosion Inhibitor Interacting Extreme Pressure/Anti-Wear Additives on Steel Surfaces." *Proceedings of the IMechE: J Journal of Engineering Tribology* 222: 315-323.
- Miyachika, M, Hirota, T and Kashiyama, K (1984). "A Consideration on Piston Second Land Pressure and Oil Consumption of Internal Combustion Engines." SAE Technical Paper 840099.
- Mori, S and Barth, H G (1999). *Size Exclusion Chromatography*, Springer.
- Moritani, H and Nozawa, Y (2003). "Oil Degradation in Second-Land Region of Gasoline Engine Pistons." *R&D Review of the Toyota CRDL* 38(3): 36-43.
- Mortier, R M and Orszulik, S T (2010). *Chemistry and Technology of Lubricants*, 3rd Edition, Blackie Academic and Professional.
- Mufti, R and Priest, M (2005). "Experimental Evaluation of Piston-Assembly Friction Under Motored and Fired Conditions in a Gasoline Engine." *ASME Transactions - Journal of Tribology* 127: 826-836.
- Mufti, R A and Priest, M (2009). "Effect of Engine Operating Conditions and Lubricant Rheology on the Distribution of Losses in an Internal Combustion Engine." *Transactions of the ASME - Journal of Tribology* 131: 041101:041101-041109.
- Muller, M, Topolovec-Miklozic, K, Dardin, A and Spikes, H A (2006). "The Design of Boundary Film-Forming PMA Viscosity Modifiers." *Tribology Transactions* 49: 225-232.

- Munro, R (1981). "Blow-By in relation to Piston and Ring Features." SAE Technical Paper 810932.
- Nakamura, M, Hayashi, H and Ito, A (2005). A Study on the Mechanism of Lubricating Oil Consumption of Diesel Engines: 2nd Report, Mechanism of Oil Film Generation on the Piston Skirt. SAE Technical Paper 2005-01-2167.
- Nakashima, K, Ishihara, S and Urano, K (1995). Influence of Piston Ring Gaps on Lubricating Oil Flow into the Combustion Chamber. SAE Technical Paper 952546.
- Nasr, G G, Yule, A J and Bendig, L (2002). *Industrial Sprays and Atomization*, Springer.
- Natgrass, S R, Thompson, D M and McCann, H (1994). First In-Situ Measurement of Lubricant Degradation in the Ring Pack of a Running Engine. SAE Technical Paper 942026.
- Nepomnyashchy, A A, Velarde, M G and Colinet, P (2002). *Interfacial Phenomena and Convection*, Chapman & Hall/CRC.
- Nguyen, T Q and Kausch, H-H (1999). *Flexible Polymer Chain Dynamics in Elongational Flow: Theory and Experiments*, Springer.
- Nicholls, M A, Do, T, Norton, P R, Kasrai, M and Bancroft, G M (2005). "Review of the Lubrication of Metallic Surfaces by Zinc Dialkyl-Dithiophosphates." *Tribology International* 38: 15-39.
- Noorman, M T, Assanis, D N, Patterson, D J, Tung, S C and Tseregounis, S I (2000). Overview of Techniques for Measuring Friction using Bench Tests and Fired Engines. SAE Technical Paper 2000-01-1780.
- Notay, R B R S (2009). Development and Understanding of Gasoline Engine In-Situ Piston Assembly Oil Sampling, MEng Dissertation. University of Leeds.
- Obokata, T, Ishima, T, Koyama, T, Uehara, K, Kobayashi, K and Mashimo, T (1995). Characterization of Spray Flows Initiated from Air Assisted Injector using Phase Doppler Anemometry. The 1995 ASME/JSME Fluids Engineering and Laser Anemometry Conference and Exhibition, August 13-18th, 1995, South Carolina, USA.
- OSHA (2008). Occupational Safety and Health Guideline for Oil Mist, Mineral Oil.
- Paschall, T W and Gaynor, P A (2003). "Application of and Improvements in Motors Using Oil Mist Lubricated Bearings." *IEEE Paper PCIC-2003-18*: 169-177.
- Peter-Wu, C S, Melodick, T, Lin, S C, Duda, J L and Klaus, E E (1990). "The Viscous Behaviour of Polymer Modified Lubricating Oils over a Broad Range of Temperature and Shear Rate." *Transactions of the ASME - Journal of Tribology* 112: 417-425.
- Phen, R V, Richardson, D and Borman, G (1993). Measurements of Cylinder Liner Oil Film Thickness in a Motored Diesel Engine. SAE Technical Paper 932789.
- Powell, J R and Compton, D A C (1992). "Automated FTIR Spectrometry for Monitoring Hydrocarbon-Based Engine Oils." *Lubrication Engineering - STLE* 49(3): 233-239.
- Priest, M (2002). Optimisation of Piston Assembly Tribology for Automotive Applications. *Tribological Research and Design for Engineering Systems: Proceedings of the 29th Leeds-Lyon Symposium on Tribology*, University of Leeds, Elsevier Science Publications.
- Priest, M and Taylor, C M (2000). "Automotive Engine Tribology - Approaching the Surface." *Wear* 241: 193-203.

- Przesmitzki, S and Tian, T (2007). "Oil Transport Inside the Power Cylinder During Transient Load Changes." SAE Technical Paper 2007-01-1054.
- Przesmitzki, S, Vokac, A and Tian, T (2005). "An Experimental Study of Oil Transport between the Piston Ring Pack and Cylinder Liner." SAE Technical Paper 2005-01-3823.
- Quillen, K, Stanglmaier, R H, Moughon, L, Takata, R, Wong, V, Reinbold, E and Donahue, R (2007). "Friction Reductions by Piston Ring Pack Modifications of a Lean-Burn Four-Stroke Natural Gas Engine: Experimental Results." Transactions of the ASME - Journal of Engineering for Gas Turbines and Power 129: 1088-1094.
- Rakopoulos, C D, Rakopoulos, D C, Mavropoulos, G C and Giakoumis, E G (2004). "Experimental and Theoretical Study of the Short Term Response Temperature Transients in the Cylinder Walls of a Diesel Engine at Various Operating Conditions." Applied Thermal Engineering 24: 679-702.
- Rhodes, R B (1999). Star Polymer Viscosity Index Improver for Oil Compositions. Shell Oil Company, Houston, TX. US Patent Number H1,799.
- Riande, E, Diaz-Calleja, R, Prolongo, M, Masegosa, R and Salom, C (2000). Polymer Viscoelasticity: Stress and Strain in Practice, Marcel Dekker.
- Richardson, D E (2000). "Review of Power Cylinder Friction for Diesel Engines." Transactions of the ASME - Journal of Engineering for Gas Turbines and Power 122: 506-519.
- Rizzo, J E (1975). "A Laser Doppler Interferometer." Journal of Physics Part E: Scientific Instruments 8: 47-52.
- Rohde, S M (1980). "A Mixed Friction Model for Dynamically Loaded Contacts with Application to Piston Ring Lubrication." Proceedings of Leeds-Lyon Symposium 7 - Friction and Traction.
- Rohde, S M, Whitaker, K W and McAllister, G T (1979). A Study of the Effects of Piston Ring and Engine Design Variables on Piston Ring Friction. Energy Conservation through Fluids Film Lubrication Technology: Frontiers in Research and Design. S. M. Rohde, ASME.
- Rotondi, R, Bella, G, Grimaldi, C and Postriotti, L (2001). "Atomization of High-Pressure Diesel Spray: Experimental Validation of a New Breakup Model." SAE Technical Paper 2001-01-1070.
- Rottenkolber, G, Dullenkopf, K, Wittig, S, Kolmel, A, Feng, B and Spicher, U (1999). Influence of Mixture Preparation on Combustion and Emissions Inside an SI Engine by Means of Visualization, PIV and IR Thermography during Cold Operating Conditions. SAE Technical Paper 1999-01-3644.
- Ruddy, B, Dowson, D and Economou, P (1981). "A Theoretical Analysis of the Twin-Land Type of Oil-Control Piston Ring." Proceedings of the IMechE: Journal of Mechanical Engineering Science 23(2): 51-62.
- Ruddy, B L, Dowson, D and Economou, P N (1981). "The Prediction of Gas Pressures within the Ring Packs of Large Bore Diesel Engines." Journal of Mechanical Engineering Science 23(6): 295-304.
- Rycroft, J E, Taylor, R I and Scales, L E (1997). "Elastohydrodynamic Effects in Piston Lubrication in Modern Gasoline and Diesel Engines." Proceedings of Leeds-Lyon Symposium 32 - Elastohydrodynamics '96: 49-54.

- Saito, K, Igashira, T and Nakada, M (1989). "Analysis of Oil Consumption by Observing Oil Behaviour Around Piston Ring Using a Glass Cylinder Engine." SAE Technical Paper 892107.
- Saville, S B, Gainey, F D, Cupples, S D, Fox, M F and Picken, D J (1988). A Study of Lubricant Condition in the Piston Ring Zone of Single Cylinder Diesel Engines Under Typical Operating Conditions. SAE Technical Paper 881586.
- Schaller, W, Durr, M, Albers, A, Burger, W, Fritz, M and Groth, K (2001). "Measures to Limit the Latent Operational Danger of Large Marine Diesel Engines (Above 2.25 MW)." MTZ Motortechnische Zeitschrift (Offprinted by Schaller Automation) 62(7/8, 12).
- Schulz, D N and Glass, J E (1991). Polymers as Rheology Modifiers, ACS Symposium Series.
- Schwartz, S E and Mettrick, C S (1994). Mechanisms of Engine Wear and Engine Oil Degradation in Vehicles using M85 or Gasoline. SAE Technical Paper 942027.
- Seinfeld, J H and Pandis, S N (2006). Atmospheric Chemistry and Physics: From Air Pollution to Climate Change, Wiley-Interscience.
- Shell International (1995). Technical Specification: Oil Mist Lubrication Systems. Shell International.
- Shrimpton, J S, Yule, A J, Watkins, A P and Balachandran, W (1995). Size and Velocity Measurements in an Electrostatically Produced Hydrocarbon Spray. The 1995 ASME/JSME Fluids Engineering and Laser Anemometry Conference and Exhibition, August 13-18th, 1995, South Carolina, USA.
- Simmons, M J H and Azzopardi, B J (2001). "Drop Size Distributions in Dispersed Liquid-Liquid Pipe Flow." International Journal of Multiphase Flow 27: 843-859.
- Sliwicki, E and Mikielwicz, J (1988). "Analysis of an Annular-Mist Flow Model in a T-Junction." International Journal of Multiphase Flow 14(3): 321-331.
- Smith, B J (2001). Oil Mist Detection as an Aid to Monitoring an Engine's Condition, Article redistributed through QMI, [www.oilmist.com](http://www.oilmist.com).
- Smith, B J and Holness, M H (2005). "Oil Mist Detection in the Atmosphere of the Machine Rooms: New Regulations for Atmospheric Oil Mist Detection." Power Engineer 9(1): 27-32.
- Smolinski, J M, Gulari, E and Manke, C W (1996). "Atomization of Dilute Polyisobutylene/Mineral Oil Solutions." AIChE Journal 42(5): 1201-1212.
- Sochting, S J and Sherrington, I (2009). "The Effect of Load and Viscosity on the Minimum Operating Oil Film Thickness of Piston-Rings in Internal Combustion Engines." Proceedings of the IMechE: J Journal of Engineering Tribology 223(383-391).
- Sorab, J, Holdeman, H A and Chui, G K (1993). Viscosity Prediction for Multigrade Oils. SAE Technical Paper 932833.
- Springer, K J (1991). "Global What? Control possibilities of CO<sub>2</sub> and Other Greenhouse Gases." Transactions of the ASME: Journal of Engineering for Gas Turbines and Power 113: 440-447.
- Stachowiak, G W and Batchelor, A W (2001). Engineering Tribology, Butterworth Heinemann.

- Stanciu, I (2009). "Physico-Chemical Analysis of Two Copolymers used as Viscosity Improvers for SAE 10W Mineral Oil." *Ovidius University Annals of Chemistry* 20(1): 72-75.
- Stark, M S, Gamble, R J, Hammond, C J, Gillespie, H M, Lindsay-Smith, J R, Nagatomi, E, Priest, M, Taylor, R I and Waddington, D J (2005). "Measurement of Lubricant Flow in a Gasoline Engine." *Tribology Letters* 19(3): 163-168.
- Szydlo, Z A (2007). "Effective Air/Oil Ratio in Industrial Oil Mist Lubricating Systems." *Industrial Lubrication and Tribology* 59(1): 4-11.
- Tamminen, J, Sandstrom, C-E and Nurmi, H (2005). "Influence of the Piston-Ring Inter-Ring Pressure on the Ring Pack Behaviour in a Medium Speed Diesel Engine." *SAE Technical Paper* 2005-01-3847.
- Tatli, E and Clark, N N (2008). "Crankcase Particulate Emissions from Diesel Engines." *SAE Technical Paper* 2008-01-1751.
- Taylor, C M (1993). *Engine Tribology*, Elsevier.
- Taylor, C M (1994). "Fluid Film Lubrication in Automobile Valve Trains." *Proceedings of the IMechE: J Journal of Engineering Tribology* 208(221-234).
- Taylor, R I and Evans, P G (2004). "In-Situ Piston Measurements." *Proceedings of the IMechE: J Journal of Engineering Tribology* 218: 185-200.
- Teclemariam, Z, Soliman, H M, Sims, G E and Kowalski, J E (2003). "Experimental Investigation of the Two-Phase Flow Distribution in the Outlets of a Multi-Branch Header." *Nuclear Engineering and Design* 222: 29-39.
- Texaco Inc (1968). *Mist Lubrication*. Texaco Inc, Lubrication Series, 54, 10: 117-128.
- Thirouard, B and Tian, T (2003). "Oil Transport in the Piston Ring Pack (Part I): Identification and Characterization of the Main Oil Transport Routes and Mechanisms." *SAE Technical Paper* 2003-01-1952.
- Thirouard, B and Tian, T (2003). "Oil Transport in the Piston Ring Pack (Part II): Zone Analysis and Macro Oil Transport Model." *SAE Technical Paper* 2003-01-1953.
- Thirouard, B, Tian, T and Hart, D P (1998). *Investigation of Oil Transport Mechanisms in the Piston Ring Pack of a Single Cylinder Diesel Engine, Using Two Dimensional Laser Induced Fluorescence*. *SAE Technical Paper* 982658.
- Thomson, A (1996). *The Tribological Performance of Piston Ring Packs Designed for Low Emissions*. PhD Thesis, University of Leeds.
- Tian, T (2002). "Dynamic Behaviours of Piston Rings and their Practical Impact: Part 1, Ring Flutter and Ring Collapse and their Effects on Gas Flow and Oil Transport." *Proceedings of the IMechE Part J: Journal of Engineering Tribology* 216: 209-227.
- Tian, T (2002). "Dynamic Behaviours of Piston Rings and their Practical Impact: Part 2, Oil Transport, Friction and Wear of Ring/Liner Interface and the Effects of Piston and Ring Dynamics." *Proceedings of the IMechE Part J: Journal of Engineering Tribology* 216: 229-247.
- Tian, T, Noordzij, L B, Wong, V W and Heywood, J B (1998). "Modeling Piston-Ring Dynamics, Blow-By and Ring-Twist Effects." *Transactions of the ASME - Journal of Engineering for Gas Turbines and Power* 120: 843-854.

- Ting, L L and Mayer, J E (1974). "Piston Ring Lubrication and Cylinder Bore Wear Analysis: Part I, Theory." *Transactions of the ASME - Journal of Lubrication Technology* 96: 305-314.
- Tirtaatmadja, V and Sridhar, T (1993). "A Filament Stretching Device for Measurement of Extensional Viscosity." *Journal of Rheology* 37(6): 1081-1101.
- Tissera, C A, Swartz, M M, Tatli, E, Vellaisamy, R, Clark, N N, Thompson, G J and Atkinson, R J (2005). "NO<sub>x</sub> Deomposition in Natural Gas, Diesel and Gasoline Engines for Selective NO<sub>x</sub> Recirculation." *SAE Technical Paper* 2005-01-2144.
- Todsén, U and Niethus, K U (2006). "Optical Ways to Improve the Tribological System Piston-Ring-Liner." *SAE Technical Paper* 2006-01-0527.
- Toploveć-Miklozić, K, Forbus, T R and Spikes, H A (2007). "Performance of Friction Modifiers on ZDDP-Generated Surfaces." *Tribology Transactions* 50: 328-335.
- Trabold, T A and Kumar, R (2000). "High Pressure Annular Two-Phase Flow in a Narrow Duct: Part I - Local Measurements in the Droplet Field." *Transactions of the ASME - Journal of Fluids Engineering* 122: 364-374.
- Triballier, K, Dumouchel, C and Cousin, J (2003). "A Technical Study on the Spraytec Performances: Influence of Multiple Light Scattering and Multi-Modal Drop-Size Distribution Measurements." *Experiments in Fluids* 35: 347-356.
- Truscott, R and Reid, T (1983). "Ring Dynamics in a Diesel Engine and its Effect on Oil Consumption and Blowby." *SAE Technical Paper* 831282.
- Tuladhar, T R and Mackley, M R (2008). "Filament Stretching Rheometry and Break-Up Behaviour of Low Viscosity Polymer Solutions and Inkjet Fluids." *Journal of Non-Newtonian Fluid Mechanics* 148: 97-108.
- Tung, S C and McMillan, M (2004). "Automotive Tribology Overview of Current Advances and Challenges for the Future." *Tribology International* 37: 517-536.
- Usui, M, Murayama, K, Oogake, K and Yoshida, H (2008). Study of Oil Flow Surrounding Piston Rings and Visualization Observation. *SAE Technical Paper* 2008-01-0795.
- Van-De-Voort, F R, Sedman, J, Cocciardi, R A and Pinchuk, D (2006). "FTIR Condition Monitoring of In-Service Lubricants: Ongoing Developments and Future Perspectives." *Tribology Transactions* 49(3): 410-418.
- Van-Der-Maas, J H (1969). *Basic Infrared Spectroscopy*, Heyden & Son Ltd.
- Wakabayashi, R and Kawanishi, M (2007). "The Effects of Piston Rings and Liner Break-In on Lubricating Condition." *SAE Technical Paper* 2007-01-1250.
- Wakabayashi, R, Mochiduki, K and Yoshida, H (2009). "Lubricating Condition of Piston Ring and Cylinder for Significantly Reducing Piston Friction Loss." *SAE Technical Paper* 2009-01-0188.
- Wakuri, Y, Ono, S, Soejima, M and Masuda, K (1981). "Oil-Film Behaviour of Reciprocating Slider with Circular Profile." *Bulletin of the Japanese Society of Mechanical Engineers* 24(194): 1462-1469.
- Wakuri, Y, Soejima, M, Kitahara, T, Nunotani, M and Kabe, Y (1995). "Characteristics of Piston Ring Friction: Influences of Lubricating Oil Properties." *JSME International Journal: Series C* 38(3): 593-600.



- Wannatong, K, Chanchaona, S and Sanitjai, S (2008). "Simulation Algorithm for Piston Ring Dynamics." *Simulation Modelling Theory and Practice* 16: 127-146.
- Ward-Smith, A J (1971). *Pressure Losses in Ducted Flows*, Butterworths.
- Watkins, R C (1973). "An Improved Foam Test for Lubricating Oils." *Journal of the Institute of Petroleum* 59(567): 106-113.
- Willauer, H D, Ananth, R, Hoover, J B, Foote, A B, Whitehurst, C L, Williams, F W and Mushrush, G W (2007). "Flammability of Aerosols Generated by a Rotary Atomizer." *Combustion Science and Technology* 179(7): 1303-1326.
- Williams, J (2005). *Engineering Tribology*, Cambridge.
- Williamson, B P, Walters, K, Bates, T W, Coy, R C and Milton, A L (1997). "The Viscoelastic Properties of Multigrade Oils and their Effect on Journal-Bearing Characteristics." *Journal of Non-Newtonian Fluid Mechanics* 73: 115-126.
- Winborn, L D and Shayler, P J (2001). "Fuel Losses to the Crankcase and Hydrocarbon Return with Recirculated Oil and Ventilation Flow." *Proceedings of the IMechE: D Journal of Automobile Engineering* 215(10): 1117-1130.
- Wong, V W, Thomas, B C and Watson, S A G (2007). "Bridging Macroscopic Lubricant Transport and Surface Tribochemical Investigations in Reciprocating Engines." *Proceedings of the IMechE: J Journal of Engineering Tribology* 221: 183-193.
- World Bank Open Data Initiative (2008). *Development Indicators*. <http://data.worldbank.org>.
- Yang, Q and Keith Jr, T G (1995). "An Elastohydrodynamic Cavitation Algorithm for Piston Lubrication." *Tribology Transactions* 38(1): 97-107.
- Yasutomi, S, Maeda, Y and Maeda, T (1981). "Kinetic Approach to Engine Oil: 1, Analysis of Lubricant Transport and Degradation in Engine System." *Industrial and Engineering Chemistry: Product Research and Development* 20: 530-536.
- Yilmaz, E, Thirouard, B, Tian, T, Wong, V W and Heywood, J B (2001). "Analysis of Oil Consumption Behaviour During Ramp Transients in a Production Spark Ignition Engine." *SAE Technical Paper* 2001-01-3544.
- Yilmaz, E, Tian, T, Wong, V W and Heywood, J B (2002). *An Experimental and Theoretical Study of the Contribution of Oil Evaporation to Oil Consumption*. *SAE Technical Paper* 2002-01-2684.
- Yilmaz, E, Tian, T, Wong, V W and Heywood, J B (2004). *The Contribution of Different Oil Consumption Sources to Total Oil Consumption in a Spark Ignition Engine*. *SAE Technical Paper* 2004-01-2909.
- Yule, A J and Salters, D G (1995). "On the Distance Required to Atomize Diesel Sprays Injected from Orifice-Type Nozzles." *Proceedings of the IMechE: D Journal of Automobile Engineering* 209: 217-226.
- Zuidema, H H (1945). "Oxidation of Lubricating Oils." *Chemical Reviews* 38(2).



## **Appendix 1:**

### **Report of the GPC Analysis of Viscosity Modifiers and Tested Blends at BP Technology Centre, Pangbourne**



## Investigational Analysis Global Lubricants Technology



<b>Report Number:</b>	IAR466
<b>Report Title:</b>	SEC analysis of Polymeric lubricant additives
<b>Date:</b>	12-05-11
<b>Customer/Department:</b>	IA
<b>Request Aim:</b>	Calculate MW values for samples and comment on the chromatograms obtained.

**Report Prepared by:**  
Sam Whitmarsh  
Technology Centre  
Pangbourne  
RG8 7QR  
Tel +44 (0) 118 9765480  
[samuel.whitmarsh@bp.com](mailto:samuel.whitmarsh@bp.com)

**Aim:**

To analyse polymeric samples from Leeds collaboration, obtain molecular weight information and comment on any differences between samples in the same request.

**Samples**

All samples were obtained as solids and assumed to be 100% pure.

SV150  
SV200  
SV260  
LZ7067  
Lucant 2000  
LZ05115848L  
Paratone 8900

**Calibration:**

System column calibration was performed using Varian EasiVial PS-H polystyrene standards accurately prepared at recommended concentrations.



calibration report.pdf

**Detector Calibration settings**

System detector calibration was performed using a single polymerlabs PMMA standard with an Mp of 107kD prepared at 2.53 mg/ml in THF. Batch # 20235-1.

**Detector Calibration Settings**

IDD (Viscosity) [mins]	IDD (Light Scattering) [mins]	K (Concentration)	K (LS 45)	K (LS 90)	K (Diff Pressure)
-0.216667	0.15	12220.6	43066.7	61028.5	0.550207

**Workbook Configuration Details**

Conc Detector	LS Detector	Wavelength (nm)	Low Angle (deg)	High Angle (deg)	Visc Detector	DP Sensitivity (mv/Pa)	IP Sensitivity (mv/Pa)	Inlet Pressure (kPa)
		650	45	90		1	0	10.8

**Method:**

LC Method:	
Eluent:	THF
Flow Rate:	1ml/min
Inj Vol:	200 $\mu$ l
Column Set:	2x PL Gel Mixed D + 5 $\mu$ m guard
Column Dimensions:	300mm x 7.5 mm x 5 $\mu$ m
Temperature:	40 $^{\circ}$ C
Run Time	45 mins

Integration of peaks was carried out manually with baseline adjustment where necessary. Lines of best fit (which parts of peak to count towards the molecular weight calculations) were modified by eye so that a fair and consistent representation of the peak was achieved.

Data was produced calculating dn/dc from the accurately known weights.

**Sample and system suitability preparation:**

System suitability samples and calibration standards were prepared as follows:

System suitability samples (broad MW polymer standards) were not available at the time of analysis.

Samples were prepared as follows:

c.a. 25 mg of sample was accurately weighed into a sample vial. To this was added 10 ml of THF so that a nominal 2.5 mg/ml solution was produced. Accurate concentrations are recorded below. The vials were capped and the suspensions dissolved by a combination of vortex mixing, ultrasonication and time. Most materials had dissolved after 4 x 15 minute intervals of ultrasonication interspersed with 15 minute cool down time followed by overnight standing at room temperature and vortex mixing the following day. Paratone 8900 required a further batch of ultrasonication and 24 hour stand followed by vortex mixing. Following complete dissolution the clear colourless solutions were transferred to HPLC vials (with filtration if required) and queued on the SEC for analysis.

Sample concentrations:

Sample	weight (mg)	volume (ml)	concentration (mg/ml)
PMMA	10.1	4	2.5
SV150	26.2	10	2.6
SV200	25.5	10	2.6
SV260	27.7	10	2.8
LZ7067	24.1	10	2.4
Lucant 2000	29.1	10	2.9
LZ05115848L	22.2	10	2.2
Paratone 8900	25.2	10	2.5

**System suitability.**

Blank: - no peaks observed in any detectors. (Residual solvent peak observed in RI at 30 minutes – i.e. column volume). No system peaks to interfere with sample analysis.

Calibration successfully completed

Analysis of PMMA detector calibration yielded an Mp of 109kDa (c.f. 107kDa quoted)

System is suitable for use



## Results and Discussion:

Sample molecular weight data is presented in table 1.

Sample Name	Results File	Mp	Mn	Mw	PD	Alpha	Bulk IV
PMMA (std)	110510-0005.rst	109859	103600	107316	1.0359	0.4550	0.2522
SV150	110510-0006.rst	88633	65039	89669	1.3787	-0.2627	0.5878
SV200	110510-0007.rst	658609	80003	583791	7.2971	-0.2338	0.6712
SV260	110510-0008.rst	664254	146499	547840	3.7395	-0.2049	0.9093
Lucant 2000	110510-0010-Repeat (01).rst	5347	2997	5690	1.8981	0.5914	0.1653
LZ7067	110510-0009-Repeat (01).rst	108469	42359	106146	2.5059	0.4778	0.7514
LZ05115848L	110510-0011.rst	163777	75412	177289	2.3509	0.5403	0.8919
paratone 8900	110510-0012.rst	102936	51945	153190	2.9490	0.5221	0.6916

**Table 1:** Molecular weight data for samples analysed.

If only the larger peak in the SV series compounds is analysed then SV200 – PD goes to 1.80 SV260 goes to 1.88 with a corresponding increase in Mn. See discussion below.

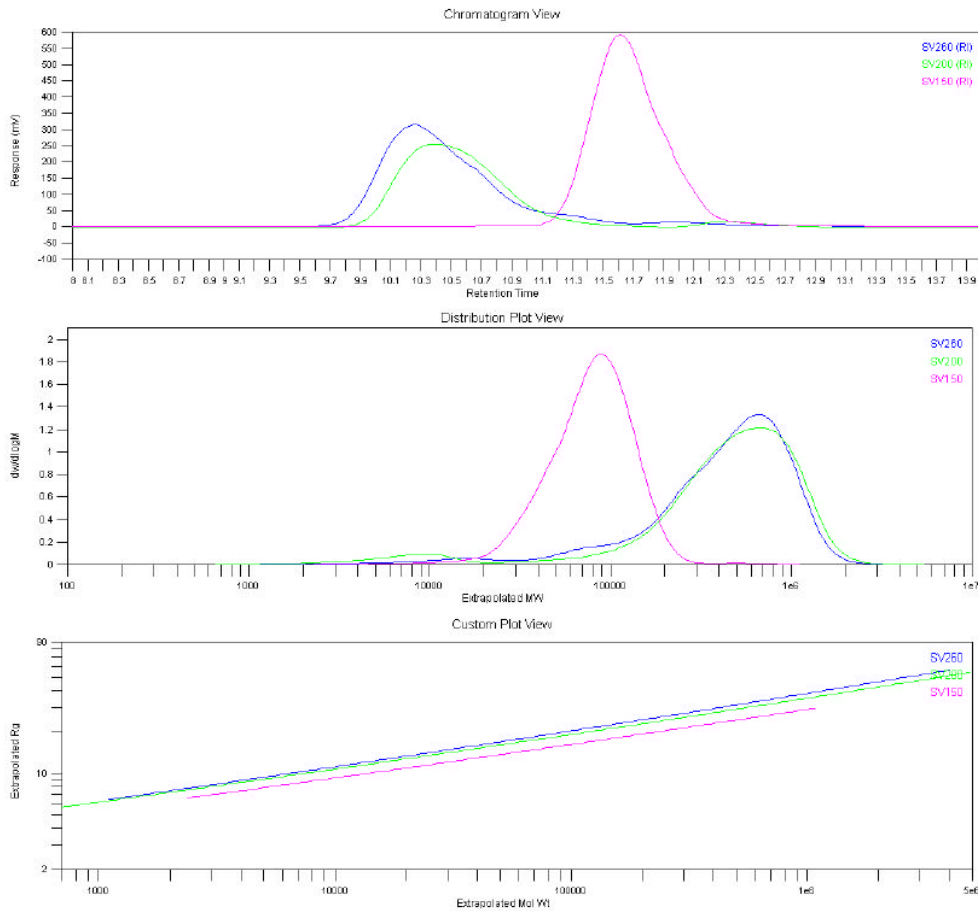


**Figure 1:** Top: RI chromatograms  
Middle: Distribution plots  
Bottom: Mark Houwink Plot for the SV series polymers.

Figure 1 shows GPC molecular weight plots for the SV series polymers. The high poly dispersity of SV200 and SV260 can be observed by the low MW peaks in the distribution plot at around 10k. In contrast SV150 does not show the presence of such material and has a correspondingly lower PD. Light Scattering data for the peak at 12.4 minutes in the SV 200 chromatogram contains low PD material (1.02) with an Mn of c.a. 60 kDa. LS data for the higher molecular weight peak at 10.5 contains a higher molecular weight fraction with a higher poly dispersity 400 kDa Mn PD 1.22 respectively. This may indicate either a broad range of molecular weight polymer, agglomeration of the smaller material to produce the larger peak or fragmentation of the larger material to lower molecular weight species. Of interest is the close matching of species in the Mark Houwink plot all with very low alpha values indicating a hard sphere polymer architecture.

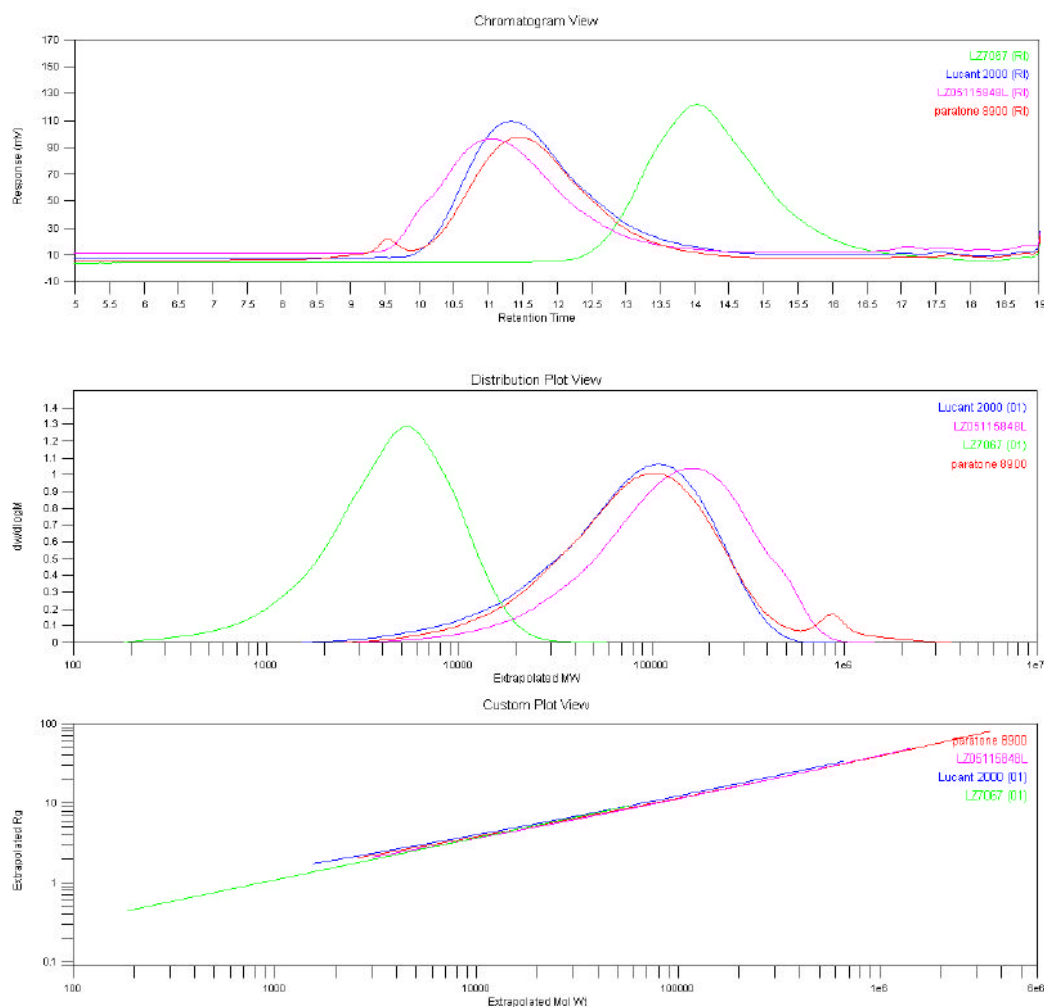


**Figure 2:** Top: RI chromatograms for the polymer analytes shown  
 Middle: Distribution plots for the polymer analytes shown.  
 Bottom: Mark Houwink Plot for the polymer analytes shown.  
 NB LZ7067 and Lucant 2000 are mislabelled (misplaced vials)  
 and should be green = Lucant, Blue = LZ7067

Figure 2 shows the GPC molecular weight plots for polymers LZ7067, Lucant 2000, LZ05115849L and Paratone 8900.

Lucant 2000 (green in Figure 2) is of significantly lower molecular weight than the other materials analysed with a  $M_n$  value around 3 kDa. Paratone 8900 and LZ7067 are of similar molecular weights though paratone has a larger polydispersity and a distinct peak at higher molecular weights at c.a. 9.5 minutes in the RI chromatogram. LZ05115849L has the largest molecular weight. Alpha values from the mark houwink plot are all tightly grouped for these materials with values that suggest polymer architecture such as a linear random coil. LZ7067 may have some random branching character.

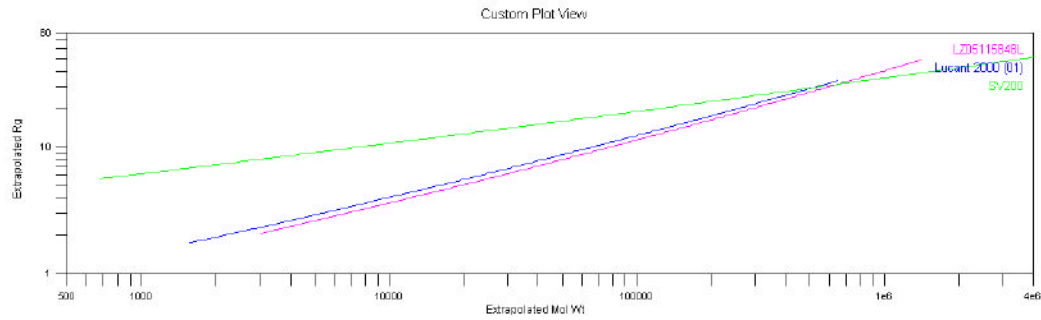


**Figure 3:** Mark-Houwink plot of SV200, LZ05115848L and LZ7067  
 NB LZ7067 and Lucant 2000 are mislabelled (misplaced vials)  
 Blue = LZ7067

Figure 3 shows the different polymer architectures observed in this experiment. SV200 – hard sphere (green) LZ7067 – linear random coil with some random branching character (Blue) LZ05115848L – linear random coil.

### Conclusion:

Molecular weights and Mark-houwink plots for the samples analysed are presented. The SV series of compounds appear to be of significantly different polymer architecture (hard sphere) to the other materials (linear random coil). Molecular weights range from Mn 3 kDa to 146kDa.